NEW MEXICO DEPARTMENT OF TRANSPORTATION

RESEARCH BUREAU

Innovation in Transportation

Characterization of Unknown Bridge Foundations

Prepared by:
Department of Civil Engineering
1 University of New Mexico
Albuquerque, NM 87131

Prepared for:
New Mexico Department of Transportation
Research Bureau
7500B Pan American Freeway NE
Albuquerque, NM 87109

In Cooperation with:
The US Department of Transportation
Federal Highway Administration

Report NM13STR-02
May 2017

THIS PAGE LEFT BLANK INTENTIONALLY

SUMMARY PAGE

1. Report No. NM13STR-02	2. Recipient's Catalog No.
3. Title and Subtitle Characterization of Unknown Bridge Foundations	4. Report Date May 6, 2017
5. Author(s): Tang-Tat Ng, Arup Maji, Saman Rashidyan, and Ali F. Jwary	6. Performing Organization Report No.
7. Performing Organization Name and Address University of New Mexico Department of Civil Engineering MSC01 1070 1 University of New Mexico Albuquerque, NM 87131	8. Performing Organization Code 9. Contract/Grant No. C05626
10. Sponsoring Agency Name and Address NMDOT Research Bureau 7500B Pan American Freeway PO Box 94690 Albuquerque, NM 87199-4690	11. Type of Report and Period Covered Final Report 5/2013-5/2017 12. Sponsoring Agency Code
13. Supplementary Notes	

14. Abstract

The Federal Highway Administration has reported 85,000 bridges nationwide that have no design or as-built plans identifying the type, depth, geometry, and materials of the foundations. It is evident that an unknown percentage of these bridges with missing foundation data could also be highly vulnerable to scouring that is induced by water flow coupled with erodible soils. Currently, NMDOT has identified more than 300 bridges with unknown foundations. It is crucial to identify the bridge foundation characteristics, particularly the type and depth of foundations, in order to determine the susceptibility to scour. Characterization of these unknown foundations is also necessary for planning retrofitting of each bridge substructure. Based on the most comprehensive study of various nondestructive testing methods in National Cooperative Highway Research Program project 21-5 and other case studies, the low cost nondestructive testing methods such as Sonic Echo/Impulse Response, Parallel Seismic, and Induction Field can be used to determine the unknown foundation depth. Field tests on bridges in New Mexico and numerical simulations were performed to identify the best practice for conducting these nondestructive tests. Guidelines on evaluation of unknown foundations and on conducting nondestructive tests are provided.

15. Key Words Nondestructive testing, Unknown Bridge Foundations, Sonic Echo, Parallel Seismic, Induction Field		16. Distribution Statement Available from NMDOT Research Bureau	
17. Security Classi. of the Report	18. Security Classi. of this page	19. Number of Pages 211	20. Price

THIS PAGE LEFT BLANK INTENTIONALLY

Project No. NM13STR-02

Characterization of Unknown Bridge Foundations

Final Report

By
Tang-Tat Ng, Ph.D., P.E.
Arup Maji, Ph.D., P.E.
Saman Rashidyan, Graduate Research Assistant
Ali F. Jwary, Graduate Research Assistant

Department of Civil Engineering
MSC01 1070, Albuquerque, NM 87131
University of New Mexico

Report NM13STR-02

A Report on Research Sponsored by
New Mexico Department of Transportation
Research Bureau

in Cooperation with
The U.S. Department of Transportation
Federal Highway Administration
May 2017

NMDOT Research Bureau
7500B Pan American Freeway NE
PO Box 94690
Albuquerque, NM 87199-4690
(505) 798-6730

research.bureau@state.nm.us
http://www.dot.state.nm.us/content/nmdot/en/Research.html

PREFACE

The research reported herein the finding of the effectiveness of nondestructive testing methods to characterize unknown bridge foundations. An in-depth literature search, laboratory and field tests, and numerical simulations were performed to establish the best procedures of carrying out nondestructive testing on unknown bridge foundations.

NOTICE

DISCLAIMER

ABSTRACT

The National Bridge Inventory (NBI) recognized 86,133 bridges in the United States have no foundation data on record in 2003. It is evident that an unknown percentage of the 86,133 bridges identified by NBI with missing foundation data could also be highly vulnerable to scouring induced by water flow coupled with erodible soils. Currently, NMDOT has identified more than 300 bridges with unknown foundations. It is vital to identify the unknown bridge foundation characteristics, particularly the type and depth of foundations, in order to determine the susceptibility to scour.

Conventional excavation, coring and boring excavations to identify unknown bridge foundation depths and types are deemed to be expensive, destructive, and limited in their application to the unknown foundation problem. Many surface and borehole nondestructive testing (NDT) technologies have been developed for this purpose. Three economical proven technique (Sonic Echo/Impulse Response (SE/IR), Parallel Seismic (PS) methods, and Induction Field (IF)) were selected for this project. The project focused more on SE/IR method since it is the most inexpensive and quick method.

Equipment for conducting these three NDT tests was purchased. Preliminary tests under controlled environmental conditions were performed to study the applicability and limitations of these NDT methods. Then, numerous NDT tests were performed on six bridges and one partially dismantled bridge. The foundation depths of two bridges are known in order to validate the NDT results.

SE/IR results show that the obtained signal was affected by various factors such as hammer tip type, striking method, pile and superstructure conditions and environmental conditions. The effectiveness of various striking methods was studied. Sensors locations and other pertinent factors were examined. Recommendation of striking method and sensor location is provided that has been validated by SE/IR tests in the field on piles and pier walls. Unfavorable reflections from discontinuities along the pile such as cracks, voids, variations in foundation material and quality of surrounding soils could influence the SE/IR results. SE/IR tests led to successful identification of the depths of timber and concrete foundations but did not work for steel piles. Therefore, SE/IR tests are not recommended for steel piles.

PS tests are able to identify the foundation depths of timber and steel piles. Determination of the arrival time of the first P-wave was found to be difficult at shallow depth due to ambient noise level. There is no effect on the characteristics of source (vertical, horizontal and even inclined striking on any appropriate parts of the structure). They all produced acceptable signals.

No IF field tests could be carried out due to the difficulty of placing boreholes close enough to the test piles. The preliminary result of conducting IF tests in two testbeds confirmed the maximum distance between the borehole and the test pile. Soil types and soil moistures did not affect the performance of IF tests. Also, IF method could be used to detect reinforced concrete foundations.

Various factors that affect the success of SE/IR tests were also investigated by finite element simulations. The full-waveform inversion method was carried out and the results have been compared against the observed field records. The comparison provides a means of better understanding and conducting the SE/IR tests and interpreting the results.

Finally, the selection of appropriate NDT methods and the guidelines for conducting these nondestructive tests were given in the Implementation Plan and Procedures Manual documents.

ACKNOWLEDGMENTS

This research is financially sponsored by the New Mexico Department of Transportation and the Federal Highway Administration. The UNM research team would like to thank the project technical panel (Dr. Thiet Nguyen, Mr. James Castillo, Ms. Michelle Mann, and Mr. Jeff Vigil) for their valuable suggestions during the technical meetings, and the valuable service and stewardship of project managers Dr. David Hadwiger and Ms. Keli Daniell. The authors would like to thank the Administrator, Ms. Dee Billingsley for her fine accounting and reimbursements. A special gratitude is given to the Bridge Inspection Unit of NMDOT District 4 for providing the manpower and the mobile scaffold for a field test and to Mr. Mark Strzelczyk and his crews of NMDOT for drilling boreholes for PS tests. Editing help of Ms. Dana Garcia is greatly appreciated. Thanks to the help of Ms. April Eckhardt in conducting field experiments. Special thanks go to Ms. Rebekah Lucero, UNM Civil Engineering accountant.

TABLE OF CONTENTS

LIST OF TABLES

LIST OF FIGURES

LIST OF APPENDICES

THIS PAGE LEFT BLANK INTENTIONALLY

1. INTRODUCTION

1.1 PROBLEM STATEMENT

According to the Federal Highway Administration (*1*), there are about 85,000 bridges nationwide that do not have any design or as-built plans identifying the type, depth, geometry and materials of their foundations. The National Bridge Inventory (NBI) has identified 86,133 bridges in the United States that have no foundation data on record. It is evident that an unknown percentage of these 86,133 bridges, identified by NBI as missing foundation data, could also be highly vulnerable to scouring that is induced by water flow coupled with erodible soils. Currently, NMDOT has identified about 266 bridges with unknown foundations. Figure 1 shows a bridge over the Gila River. Unknown bridge foundations potentially give rise to scour safety risks (see Figure 2). Therefore, it is crucial to identify the bridge foundation characteristics of bridges for which the information is missing, particularly the type and depth of foundations, in order to determine the susceptibility to scour for each of these. Characterization of unknown foundations is also necessary for planning and retrofitting of each bridge's substructure.

FIGURE 1 A Bridge over the Gila River

Conventional excavation, coring and boring excavations to determine unknown bridge foundation depths and types are deemed to be expensive, destructive and limited in their application to the unknown foundation problem (*2*). There is therefore a real need to research and develop lower cost nondestructive testing (NDT) methods to provide foundation depth and type data on unknown bridge foundations to aid in evaluating scour safety.

FIGURE 2 Complete Loss of Support under a Bridge Pier (*3*)

1.2 SPECIFIC OBJECTIVES OF THIS RESEARCH PROJECT

The research reported herein has the overall goal of providing guidance for performing future NDT inspections in New Mexico. The specific objectives are:

1. To develop NDT procedures that can be used to determine foundation characteristics. These can then be used for all bridges coded as unknown foundations in the NMDOT bridge inventory using timely and economical testing methods.
2. To identify the most efficient and timely non-destructive approach for determining the subsurface bridge foundation characteristics for which information is unavailable or limited.

To achieve the goals, we have performed extensive literature review on various NDT methods and collected DOT's experience of applying NDT methods in other states. Field tests and numerical simulations were carried out to obtain the comparison between field data and numerical response. The results were used to identify the best practice of conducting NDT tests in New Mexico. Based on the project findings, we have developed procedures for NMDOT engineers to identify and characterize unknown bridge foundations and guidelines for use by NMDOT engineers to characterize the type, depth, and geometry of unknown bridge foundations.

1.3 LITERATURE REVIEW

1.3.1 Deep Foundations and Common Nondestructive Techniques

1.3.1.1 Deep Foundations

Highway bridges are commonly supported on deep foundations. Shallow foundations are used occasionally. The deep foundations are structural members that are made of timber, concrete, steel, composite (combination of two materials out of timber, steel, and concrete). There are four common basic deep foundation construction methods. Deep foundations are based on one of the following techniques:

- Driven piles - Piles are driven into the ground by mechanical force. The prefabricated timber, steel, or concrete piles are banged into the ground by a hammer, pushed by shear brute force, or vibrated by a shaker.
- Driven cast-in-place piles – a hollow steel casing is driven into the ground first. The cavity is subsequently filled with concrete.
- Drilled shafts – a cylindrical hole of the required depth is excavated. Reinforcement cage is placed in the excavated hole and subsequently filled with concrete.
- Augercast (Continuous-flight auger) piles – a hollow stem auger is drilled into the ground. Concrete is pumped through the hollow stem of the auger while the auger is pulled up. Reinforcement, if necessary, is pushed into the concrete manually.

Preliminary information on the type of unknown foundation is essential to the selection of NDT methods and to the interpretation of the experimental results. The site characteristics and access limitation need to be considered. NDT testing methods have varying degrees of site access requirements. Surface NDT will generally require access to the substructure of a bridge. On larger bridges or in difficult terrain access may require some form of crane or scaffold from the superstructure. Borehole NDT methods will require a soil boring or probe and therefore will be more limited at each site. The access requirements should be reviewed prior to the selection of the NDT method.

Bridge Deck A bridge deck may have several variables that may impact the quality of the test data. The clearance below the bridge deck is very important especially for borehole methods. Special drilling equipment may be required for low clearance bridges. Connections between the superstructure and the substructure determine the extent of traffic noise that is transmitted through the structure itself to the foundation, affecting the NDT tests that use wave transmission principles.

Automotive Traffic Traffic on bridges may pose a substantial problem for some NDT methods. One factor to consider is the number of traffic lanes on the bridge relative to the volume of traffic and time of day. This relationship between traffic flow and existing lanes will greatly influence maintenance of traffic (MOT) plans and schedule. For most of the NDT methods, testing during non-peak hours (i.e. at night) may be preferable (i.e. less noise and vibrations at night). If daytime lane closure is required on a highly traveled bridge, then some lane capacity analysis may be necessary to ensure minimal impact to traffic flow.

Season Seasonal weather fluctuations may affect the access of substructure. These impacts could be associated with variations in the water levels and flow velocities under a bridge.

Subsurface Conditions Highly variable soil strata may be reflected in the data resulting from NDT testing and should be considered while making predictions about foundation depth. Many of the NDT methods utilize wave transmission principles based on wave velocities through soil strata. Wave velocities vary differently from one material to the next; therefore, some basic understanding of the subsurface conditions is helpful. The data interpretation from the NDT methods should be analyzed in conjunction with known or estimated rock depths as they apply to the area.

1.3.1.2 Common Nondestructive Techniques

Surface methods such as Sonic Echo/Impulse Response, Bending Wave, Ultra-seismic, and Spectral Analysis of Surface Wave require accelerometers or geophones that are mounted on the top or the side of the bridge substructure. These methods require access to the top and the side of bridge substructures. Parallel Seismic, Borehole Radar, Borehole Sonic, Cross-hole sonic and Induction Field methods are common borehole NDT methods. A brief overview of these nine common NDT methods and their capabilities and limitations is described here. (*4*).

The cost and the time delay of borehole installation before testing are the major disadvantage of the borehole methods. If testing of every pile is desired, a borehole may be needed for each pile which can be very expensive. In addition, an estimated pile length is required to determine the boring depth. However, borehole methods are more versatile and reliable than surface methods.

Sonic Echo/Impulse Response (SE/IR) The source and a receiver are typically placed on the top and/or sides of an exposed foundation. A longitudinal wave is generated by a hammer and the depth of the foundation is calculated by the time difference between the source (impulse) and the echo for SE analysis, or from the resonant peaks for IR analysis. The Sonic Echo and Impulse Response methods are similar to Low Strain Pulse Echo and Low Strain Transient Response methods in Pile Integrity Testing respectively.

Capabilities The method is quick and inexpensive. The method has shown good performance for determining the depths of timber piles, concrete piles, and drilled shafts that extend up above the ground or water surface. The method can be used to determine the depths of pier walls.

Limitations. The echoes from pile bottom will likely not be measured for embedded length to diameter ratios much greater than 30:1 due to attenuation of waves. This limitation may decrease to 10:1 in stiff soils (high elastic modulus). No echo can be detected if the impedance of foundation soils (rock) is similar to that of the pile. Also, piles cannot be detected below a buried pile cap. Furthermore, the method does not work on steel piles (H-piles and pipe-piles) due to energy dissipation.

Bending Wave The Bending Wave method is based on the dispersion characteristics and echoes of bending waves traveling along very slender member like piles. The method has been applied to timber and concrete piles. The method involves mounting a minimum of two horizontal receivers a few feet apart on one side of an exposed pile, and then impacting the pile horizontally on the opposite side of the pile a few feet above the topmost receiver. The raw data is filtered

based on the selected frequencies. For each selected frequency, the depth is calculated by identifying the initial wave arrival and subsequent reflection (echo).

Capabilities It does not require access to a pile's top surface since bending (flexural) waves are generated by striking horizontally on the side of a pile. Successful testing of timber piles of up to 60 ft in length has been reported.

Limitations. An accessible vertical surface of at least 4-5 ft or more in length is needed. Layers of stiff soils can result in apparent short pile lengths. There are difficulties in identifying flexural wave reflections from more massive, deep foundations. Data processing is more complicated than SE/IR tests. Piles cannot be detected below a buried pile cap. Also, the method will not work on steel piles (H-piles and pipe-piles) due to energy dissipation.

Ultra-Seismic (US) The Ultra-Seismic method is a sonic reflection technique that uses three or more sensors. The principle is similar to that of SE/IR method.

Capabilities Data reliability is typically increased since it does not require the knowledge of the wave velocity of the pile. The method was found to be less affected by the presence of large beams on top of columnar substructure than the SE/IR method. The data of multiple sensors are processed to distinguish waves travelling down and up and to minimize the noise from attached substructure reflections.

Limitations. An accessible vertical surface of at least 4-5 ft or more in length is needed. Piles cannot be detected below a buried pile cap. Other limitations are similar to those of SE/IR method.

Spectral Analysis of Surface Waves (SASW) The SASW test involves determining the variation of surface wave velocity versus depth in layered systems. The bottom depths of exposed substructures or footings are indicated by slower velocities of surface wave travel in underlying soils.

Capabilities Capable of determining the depths of shallow abutments, pier walls, and other solid substructures with a flat surface.

Limitations Requirement of a flat surface for generating surface waves. Not suitable for deep foundation since the maximum foundation depth that can be determined is limited by the longest horizontal dimension of tested foundation.

Parallel Seismic (PS) A Parallel Seismic test consists of impacting an exposed foundation substructure either vertically or horizontally with a hammer to generate either compressional or flexural waves which travel down the foundation and are transmitted to the surrounding soil. The arrival of transmitted compressional wave is tracked at regular intervals by either hydrophone receiver suspended in a water-filled cased borehole or by a clamped three-component geophone receiver in a cased or uncased borehole (if it stands open without caving).

Capabilities The method has the widest range of application of any of the methods for determining unknown foundation bottom depths regardless of depth, substructure type, geology,

and materials. Both compressional and shear waves can be used with the method as generated by vertical and horizontal impacts. The data interpretation is simple.

Limitations The method is more expensive than surface methods since a borehole must be drilled. Highly variable soil velocity conditions complicate the data interpretation. Larger impact force must be generated for long piles.

Borehole Radar The Borehole Radar test uses a transmitter/receiver radar antenna to measure the reflection of radar echoes from the side of the bridge substructure foundation. It works well with soils with low conductivity (sands). The use of a directional, focused radar antenna could potentially improve the results; however, it is quite expensive.

Capabilities The test is quick. Radar also works well at detecting steel and reinforced concrete because the steel reflects the signal strongly. It can be used to estimate the thicknesses of toes and heels of footings, as well as to indicate depths of unknown foundations.

Limitations Cost is higher than surface methods since a borehole must be drilled and cased with a 4-in. diameter PVC casing. The result is significantly affected by soil conditions and moisture in the ground since radar is severely attenuated in conductive soils (clays).

Borehole Sonic The Borehole Sonic test involves lowering a source and a receiver unit in a borehole and measuring the reflections of compressional or shear waves from the side of the bridge substructure foundation using essentially horizontal ray paths.

Capabilities Fair potential reflections have been reported in the process of determining the piles' lengths.

Limitations More expensive than surface methods since a borehole must be drilled. It may be difficult to obtain reflections of small targets without generating higher frequency waves in soils.

Cross-Hole Sonic Similar to the standard Cross-Hole Sonic Logging test for checking the integrity of drilled shafts, the Cross-Hole Sonic test involves lowering a source and a receiver unit in two separate boreholes simultaneously and measuring the wave transmitted time between the source and the receiver.

Capabilities The interpretation is simple. The method is applicable for any foundation type and material and NMDOT engineers have experience.

Limitations It is more expensive than single borehole methods. Well-aligned tube installation may be difficult.

Induction Field (IF) In Induction Field method an electro-magnetic field is induced through a soil-foundation system and the change of the field due to the nearby metal objects is detected. The testing is implemented by passing a DC current through a polarized magnetic field sensor which is lowered into a PVC cased borehole adjacent to the test pile. A magnetic field is consequently induced in the pile's metal which can be detected by the probe. The depth of the

foundation is determined by measuring the magnetic field strength at various depths, and noting the changes in magnetic field strength.

Capabilities The IF is a proven technology for the determination of the depth of steel piles and reinforced concrete piles. IF is not affected by background vibration noise. The method could be performed in conjunction with the PS method or the Borehole Sonic method to improve reliability with minimal additional cost.

Limitations The method does not work on timber piles or unreinforced concrete piles. The boring must be drilled within 0.5 m (18 in) of the foundation. Interpretation of data from the IF method may be complicated by the existence of ferrous materials in soils.

1.3.2 Drilling Equipment

All the borehole methods mentioned above require the drilling of a borehole (or two boreholes) parallel to the existing foundation. In order to be successful in determining the existing bridge pier depth the borehole must be located within 18 inches of the existing pier's location for the IF method and within six feet for the PS method. In either case a borehole of at least 3-in diameter needs to be drilled ten to fifteen feet below the estimated foundation bottom elevation. In some cases, the bridge superstructure might not provide enough clearance for the drilling rig to be located underneath the bridge deck. Specialized low headroom drilling equipment may be needed. The service can be contracted out to a drilling company that has the capability. However, scheduling and the accumulative cost in order to complete the testing of all required bridges can be a concern. Therefore, a low headroom drilling rig (Geoprobe Model 7822DT) was purchased for this project.

1.3.3 Nondestructive Testing Implementation in Other States

A comprehensive literature search was conducted on information available from national organizations (Transportation Research Board and American Association of State Highway and Transportation Officials), State DOTs (Alabama, Arizona, Colorado, Florida, Illinois, Indiana, Louisiana, and North Carolina), journal and conference publications. A search of the International Transport Research Document database did not provide information pertinent to NDT of unknown bridge foundations (UBF); all other sources provided valuable insights into both the technologies involved and the field applications. No information was found on application of NDT on UBF in Arizona. It may be due to the low number of UBF in Arizona. Also, these bridges are located on local and minor roads (*5*). The Federal Highway Administration (FHWA) presented guidelines on the methods of evaluation of bridges with unknown foundations, including a method of determining the embedment (*1*). A series of FHWA Webinars (*6-9*) outlined a road map on how to tackle the issue of unknown bridge foundations.

The policies implemented by the FHWA regarding how to reduce the number of bridges with unknown foundations led state DOTs to explore various methods to determine the foundation characteristics for these bridges, either directly through field testing or indirectly by implementing

other methods. Risk-based approaches have been implemented by several states to establish priorities for their investigations, based on the results of National Cooperative Highway Research Program (NCHRP) Project 24-25 (*5*). Artificial Neural Networks (ANN) methods have been used in Florida, North Carolina, and Texas to predict foundation depths of bridges with unknown foundations. ANN consist of applying a mathematical model with capabilities similar to biological neural networks (e.g. central nervous system). The model creates a series of interconnected nodes, each capable of processing information in parallel with the other nodes. The network is trained with data examples from which to "learn" the complex relationships relating the inputs and outputs of a system. McLemore et al. (*1*) describes the development of ANN for bridges in Florida. Two models were developed to predict the length of concrete and steel piles.

A comprehensive evaluation was made of potential NDT technologies that could be relevant to this problem in the NCHRP 21-5 project, as outlined in 'Determination of Unknown Subsurface Bridge Foundations' (*2*). This report presents the test results of a research study on the applicability of using borehole-based nondestructive testing techniques to disclose the characteristics of unknown subsurface bridge foundations. The results included in this report are from the three borehole-based NDT techniques of PS test, borehole sonic test, and borehole radar test. The field testing was performed at multiple bridges with known foundations in Alabama, Colorado, and Texas, using all methods that were considered state-of-the-practice at the time. Phase 2 consisted of multiple "blind" field tests at 21 bridge sites in Colorado, Massachusetts, Michigan, Minnesota, New Jersey, and Oregon. While this research did not create new NDT methods or technologies, it greatly enhanced the understanding of the nuances relevant for field applications and the successful transfer of various NDT technologies to the field engineer. The PS method has the broadest application to the investigations of concrete, timber and steel bridge substructures.

Nondestructive methods are increasingly being used in the determination of conditions of unknown bridge foundations. As per Olson et al. (*2*), the foremost need is to determine the foundation depth, followed by foundation type, geometry and subsurface conditions.

FHWA/Florida DOT (*1*) conducted a detailed evaluation of bridge foundation, including NDT, scour evaluation, and risk analyses. This investigation included summaries of activities in the DOTs of various states. Several surface and borehole NDT technologies were implemented in investigating unknown foundations (*10-13*). Both SE/IR and PS methods were found to work best in Louisiana (*14*). US and PS tests were carried out in Alabama (*15*). The finding indicated that the US method worked well to assess "short" pile and PS method was recommended for use when the result was inconclusive.

Successful IF tests were reported on determination of the embedment depth of H-piles in North Carolina and Pennsylvania (*16*).

Figure 3 shows the unknown foundation process developed at North Carolina DOT for UBF in their bridge management system in 2005. The use of the risk-based management guidelines for scour was suggested in 2010 to evaluate remaining low-risk bridges with unknown foundation in North Carolina. The review of all unknown foundation bridges was completed in 2012.

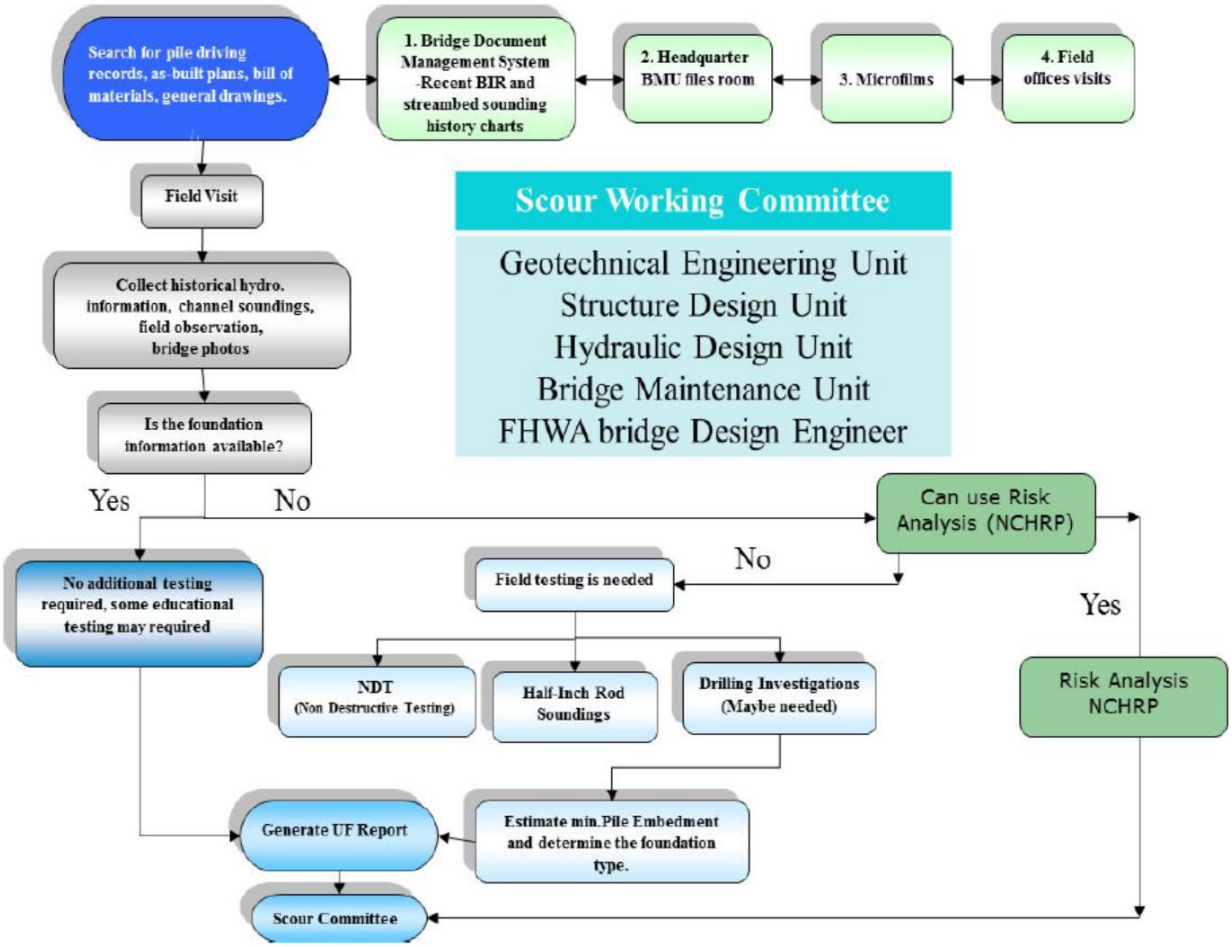

FIGURE 3 Flowchart for North Carolina Unknown Bridge Foundation Process (*17*)

Figure 4 illustrates the appropriate application of the NDT method as suggested by Florida DOT. Here, SE/IR tests are not recommended since other methods provide much better results.

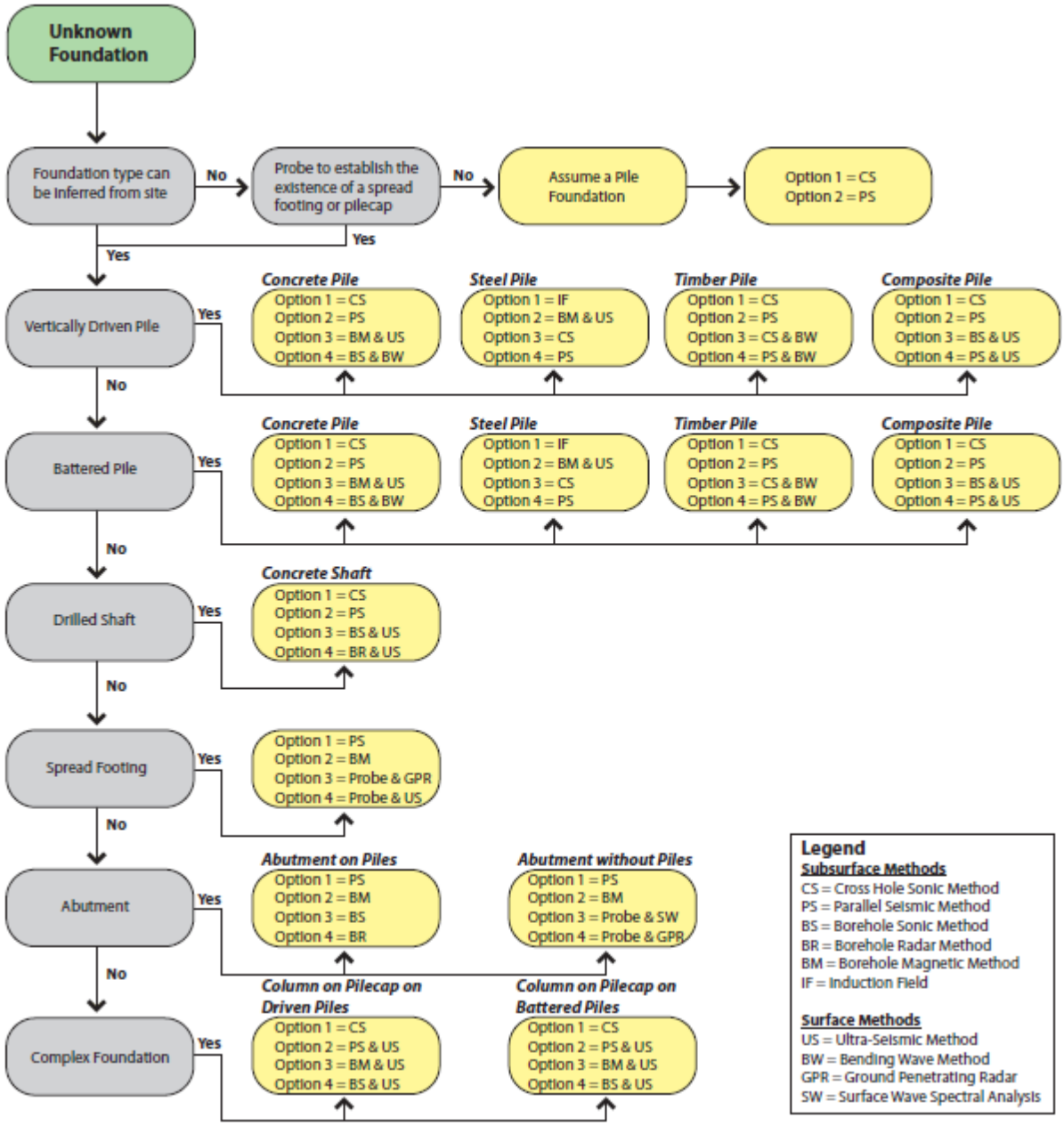

FIGURE 4 Various NDT Methods and Their Appropriate Use (*1*)

Strategic Highway Research Program (SHRP) led to the development of the NDT Toolbox for highway applications which allows DOT engineers to select appropriate NDT tools *(18)*. According to this joint FHWA/AASHTO/TRB product, "many NDT technologies are available to owner agencies; however, each has its own set of applications, strengths and weaknesses, and practitioners need clear information to help them select the best NDT method to evaluate the condition of a specific feature. The NDToolbox provides an independent assessment to allow owner agencies to be confident in their choice of technology and method. The NDToolbox enables owners to:

- Provide information, quickly and reliably, about the under-the-surface conditions of bridge decks without causing undue additional wear to the bridges themselves.
- Yield faster measurements in the field by using hand-held stereoscopic "fingerprinting" equipment for testing the quality assurance of materials.
- Use automated thermal profiling systems and other technologies to reliably prevent deterioration and segregation of hot-mix asphalt construction.
- Detect easily and efficiently the extent, depth and severity of de-lamination in hot-mix asphalt pavements.
- Meet smoothness requirements for Portland cement concrete pavements, more easily and less expensively, by detecting surface irregularities in real-time before the cement hardens.
- Use continuous deflection measuring devices to determine the structural capacity of pavement with better spatial coverage and less impact on traffic.
- Monitor more thoroughly the condition and deterioration of tunnel linings while providing less disruption of traffic.

Hossain et al. (*19*) presented research on the determination of the depth of the foundation of a previously unknown bridge foundation at Fort Worth, Texas. The bridge was supported by driven steel H-piles. Three NDT techniques were utilized: (1) PS method, (2) SE/IR method, and (3) resistivity imaging (RI). The main objective of this study was to compare the suitability of these three different NDT techniques to determine the unknown bridge foundation depth. Based on the field test results, both PS and RI methods provided foundation depth close to actual foundation depth. However, the SE/IR method was determined to be unsuitable for determining the unknown steel H-pile depth.

In one such case (*20*), a construction project was delayed by a state inspector after it was noted that a field inspector was not present during shaft construction. In order to resume construction, the state required that SE/IR testing be performed on the 12 shafts to verify their integrity. It was determined that all 12 shafts had bulbs (or widening) between approximately 8 and 13 ft. Several of the shafts were partially uncovered by the contractor, and the bulbs were confirmed. After testing and approval by the design engineer, the state allowed construction to continue.

In addition to the abovementioned literature search, emails have been sent to various state DOTs including Alabama, Arizona, Colorado, Florida, Illinois, Louisiana, North Carolina, Minnesota and Texas to determine the current state of practice of NDT testing for UBF. The questionnaire together with the responses can be found in Appendix B. A summary of the responses is listed below:

- **Arizona DOT** No information on nondestructive testing on bridge piles in Arizona
- **Colorado DOT** used consultants to work on the unknown foundation bridges. NDT tests have been carried out on eleven bridges the type of NDT tests were not disclosed.
- **Florida DOT** hired consultants to evaluate 2,500 unknown foundation bridges. The consultants developed the methodology and carried out the production work. Structures Maintenance Office is responsible for NDT testing of bridges with unknown foundations. For a large majority of the bridges, the consultants used a statistically based evaluation method instead of performing NDT. Only PS method has been used on 3 bridges which had a high importance.

- **Illinois DOT** did not use NDT testing on unknown bridge foundations. They have bridge plans for most of the bridges in Illinois which specify which type of foundation is used. Only 7 bridges were found with unknown foundations out of 7500 state owned structures. For those structures in a water environment subject to scour an unknown foundation would be assumed to be scour critical and either monitored during significant hydraulic events or remediated with stone rip-rap. The responsible unit for unknown bridge foundations is the bridge management unit. They would use a consultant to do the NDT if necessary.
- **Minnesota DOT** has just started the investigation on the unknown bridge foundations. Some preliminary PS tests were performed to determine the unknown pile lengths by using a special cone in the cone penetration testing as the receiver.
- **North Carolina DOT** has completed their unknown bridge foundations program. 6,000 bridges have been identified as having unknown foundations. They have tried almost all of the NDT methods in the past to estimate the minimum depth of piles. The most often used two methods are the Bending Wave method and the Low Strain Pulse Echo method (SE method). They tried to stay away from any borehole methods due to additional drilling cost, time consuming, and sometimes require specialty equipment to perform the drilling. The Geotechnical Engineering Unit was responsible for NDT testing of bridges with unknown foundations. The NDT was performed by both the consultants and the Geotechnical Engineering Unit staff. Low Strain Pulse Echo was performed by trained staff members. The average cost of unknown bridge foundation evaluation by consultants is $800 to $1600 per bridge. The half-inch sounding rod was used to provide some information concerning the subsurface conditions (rock depth) as addition method to clarify the estimation of the minimum depth prediction from the NDT.
- **Texas DOT** has 111 bridges on-system and 7637 off-system bridges that have unknown foundations. However, they do not currently use nondestructive testing methods to estimate the depth and/or other characteristics of bridge foundations with unknown foundations.

1.4 SELECTION OF THE THREE NDT METHODS

Based on information provided by NMDOT, there are 266 bridges in New Mexico that have insufficient information regarding bridge substructure and can be considered scour critical. NMDOT and FHWA prioritized these bridges by placing them into 3 categories (high risk, moderate risk, and low risk). They are categorized based on available information and visual assessments with the criteria defined by NMDOT. The complete list can be found in Appendix A. The database has been updated with the results of this project and the work of a consultant. Tables 1 and 2 summarize the inventory of the bridges with unknown foundations in terms of their priority and the superstructure material in New Mexico.

TABLE 1 Inventory of Bridges with Unknown Foundations in New Mexico.

	High Risk	Moderate Risk	Low Risk	Total
State	2	14	46	62
Local	20	22	162	204
Total	22	36	208	266

TABLE 2 Superstructure Materials of Bridges with Unknown Foundations in New Mexico.

	Steel	Timber	Concrete	Aluminum	Masonry	Total
State	14	38	10	0	0	62
Local	71	24	103	5	1	204
Total	85	62	113	5	1	266

Since these bridge foundations are made of concrete, timber, or steel, the selected NDT methods should work properly on these materials. Considering the advantages and limitations of the aforementioned NDT methods, three methods (SE/IR, PS, and IF) were selected. All selected methods are proven techniques (*2*). The surface SE/IR method and two borehole methods (PS and IF) are easy to operate compared to other NDT methods. The equipment of these three NDT methods are inexpensive. Although these NDT tests can be performed by one person, it is more efficient with two persons. The pros and cons of the methods can be found in previous section. In addition, NMDOT engineers already have experience on the equipment for SE/IR tests. It has been used on determining the length and integrity of the drilled shaft foundations placed at the I-40-Coors interchange in Albuquerque, NM. The existing equipment can be used to perform SE/IR tests without modification and it can be upgraded easily to perform PS tests. The detailed reasons for selecting these three methods (SE/IR, PS, and IF) are described first. Then, the principles and important facts of each method are explained in detail.

The SE/IR method was selected because it is the most economical NDT method and can be used for timber and concrete foundations. Moreover, the SE/IR method was selected because the setup is quick and straightforward. The setup time for each test takes only 15 minutes. Each test can then be conducted in minutes. Every pile at a bridge site can be tested within a reasonable time. In addition, The SE/IR method has less requirement for the exposed length of the pile. Bending Wave and Ultra-seismic methods need a 4-5 ft of accessible exposed part of the pile. The SASW method requires a flat access to generate the surface wave.

The two borehole methods (PS and IF) were selected because of the limitations of SE/IR method. The SE/IR method does not work on steel piles (H-piles or steel pipe piles without concrete filling). It cannot detect the pile toe reflection for complex foundations (the pile is fully embedded underneath a massive pier wall). The result of SE/IR method is doubtful for long piles (embedded length to diameter ratios greater than 30:1).

Among the borehole methods, the PS method not only is a proven technique but also has the widest range of application for determining the depth of unknown foundation regardless of depth, substructure type, geology, and materials. The test is also quick. The number of data points needed

to be obtained in each PS test depends on the depth of the borehole. Each data point can be obtained in less than 2 minutes. Although the method imposes an additional cost of drilling a borehole, soil exploration can be conducted during the excavation to obtain valuable geotechnical information. It should be noted that the newly purchased equipment from Olson for this project is able to conduct both PS and SE/IR tests.

Although PS method can work on steel piles, IF method is the best proven technology for determining the depth of steel piles. IF tests are quicker than PS tests. Unlike PS method, IF method is not affected by traffic vibration. The data interpretation is very straightforward. In addition, the equipment is inexpensive. A device has been purchased for this project. Reliability of the result can be improved by performing an additional PS test in conjunction with the IF test. The major challenge of this method is that the borehole must be within 1.5 ft from the pile edge. This may be accomplished by the newly purchased Geoprobe Model 7822DT drilling rig for low clearance bridges.

1.4.1 Sonic Echo/Impulse Response Method

Figure 5 shows the SE/IR test setup underneath a bridge. A small hammer equipped with an electronic trigger is utilized to generate the impact (source). The impact can be applied at the top of the pile (pile top striking), on the striking block that attached on the pile surface, or at the pile cap (Point A, Point B, or Point C). The generated stress wave travels down the pile and reflects (or echoes) back at the interface of the pile toe and foundation soil. The wave is recorded through a sensor (a geophone or an accelerometer) mounted on the side of the pile (*13*). More than one sensor can be attached to improve the reliability of the test if the length of the exposed pile is long enough to accommodate the sensors. Figure 6 shows a typical velocity amplitude-time graph obtained from a sensor. This type of presentation will be called as velocity graph from here on. In this figure, the indicated impulse and echo points show the moments of the waves passing through the sensor location while traveling down and returning respectively. Once the propagated wave velocity is known, the total pile length (L_t) and buried length (L_b) shown in Figure 5 can be calculated using following equations.

L_{tr}: Distance between the sensor location and pile toe ($= \frac{v \times \Delta t}{2}$) (1)

Where Δt: Time difference between the impulse and first echo
v: Propagated wave velocity

L_t: Total pile length = $L_{tr} + L_a$ (2)

L_b: Buried pile length = $L_t - L_e$ (3)

L_e: Exposed pile length between the pile cap and ground surface

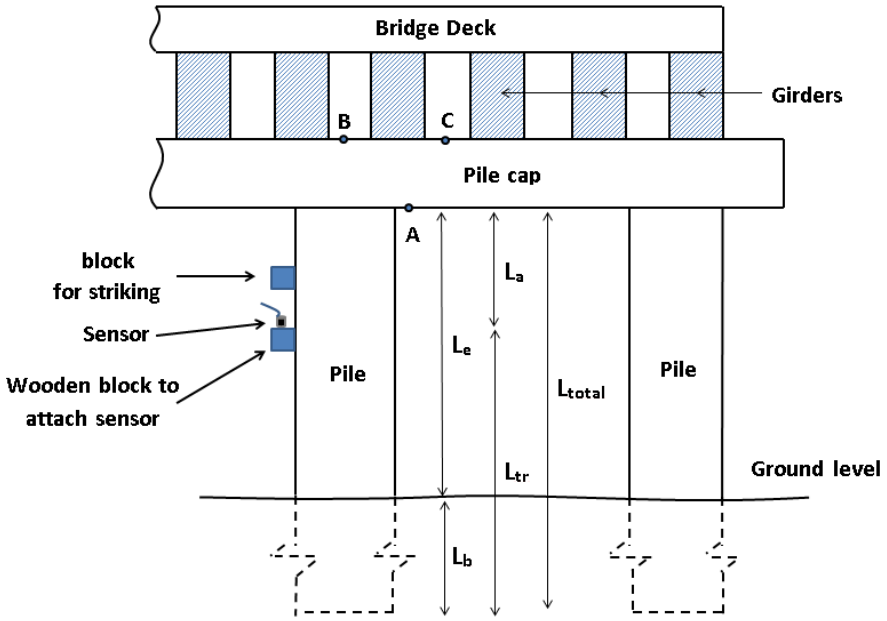

FIGURE 5 SE/IR Test Setup for Piles Underneath a Bridge

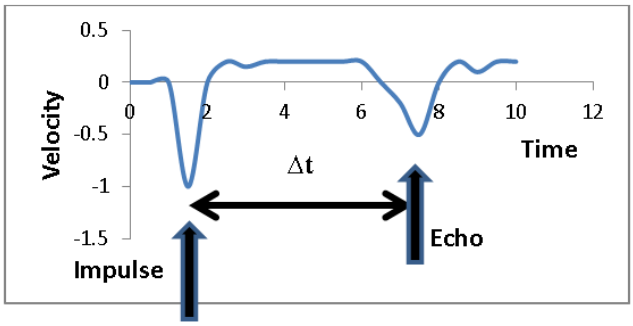

FIGURE 6 A Typical Velocity Amplitude-time Graph

The signals obtained from sensors can also be investigated by Impulse Response (IR) analysis. The force and velocity time history signals are converted into frequency domain using the Fast Fourier Transform. Mobility is then defined as the ratio between the converted frequency-base velocity and the frequency-base force. The result is commonly presented as a plot of mobility versus frequency as shown in Figure 7. For the generated wave lengths greater than the diameter of a prismatic pile, there are resonant frequencies that depend on the pile length and the propagated wave velocity as shown in Figure 7 (*21*). The length of the pile can be estimated from the difference of successive resonant frequencies (Δf) as:

$$L_{total} = \frac{v}{2 \times \Delta f} \quad (4)$$

The Δf is the difference between consecutive *resonant* frequencies.

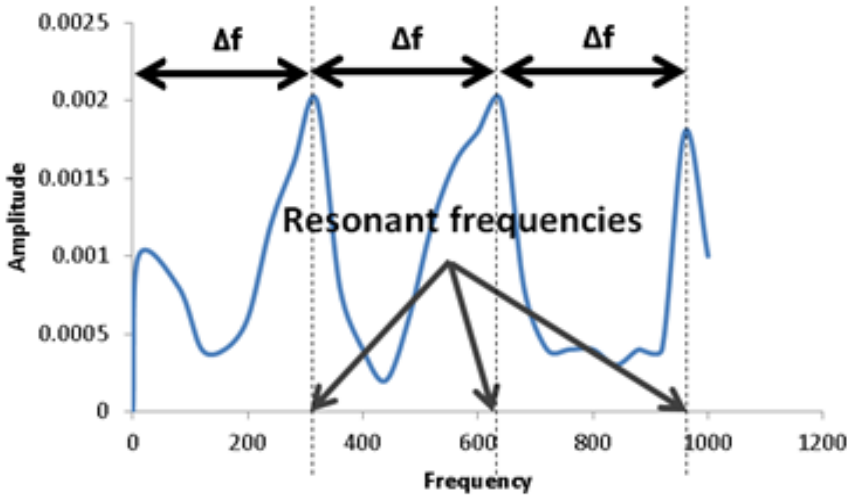

FIGURE 7 Resonant Frequencies on a Typical Mobility Graph

Factors affecting SE/IR testing are listed in Table 3 (*22*). Although the SE/IR method is easy to conduct in the field, some precautions regarding its applicability are listed in the table (*22*). The pile-to-soil stiffness ratio and length-to-diameter ratio of the pile are two major factors affecting the success of the SE/IR test (*23*). Since the impact force energy is radiated from the pile shaft into the surrounding soil. It is difficult to determine the length of a long pile with a high slenderness ratio (*24*). The surrounding soil absorbs energy and dampens the measured response (echo). The maximum detectable pile length-to-diameter ratio reported in literature varies from 10 to 30, depending on the stiffness ratio of the pile and the surrounding soil (*25*). It was found that the SE/IR method can be applied on drilled shafts if the shaft to soil stiffness ratio is more than 77 (*23*).

TABLE 3 Factors Affecting SE/IR Testing (*22*).

Factors	Consequences	Proposed Corrective measures
Incorrect hammering	Generation of poor longitudinal waves.	Striking perpendicular to the top surface of pile head.
Incorrect hammers	Too small a hammer with a stiff head generates high frequency waves which attenuates too fast and cannot reach the deeper part of the pile. Too large a hammer with a soft head generates a wave with a large contents of low frequencies and a large pulse period which may mix up with reflections from small defects in shallow depth of the pile.	Using an adequate hammer. If defects are in the shallow part of the pile, a small and very hard tipped hammer should be tried. The correct selection and use of hammers depend on the experience and judgment of the operator.
Soil resistance and damping	(a) Abrupt change in soil stiffness may induce a reflected wave. (b) Soil layers may induce secondary waves. (c) Soil's damping (radial and viscous) may reduce the strength of the wave propagation in the pile by attenuation.	Differentiating between the secondary waves from the soil layers and the reflections from pile toe and anomalies.
Wave velocity of piles assumed in analysis	Wrongly assumed wave velocity leads a wrong estimation of pile length (or defect location).	Calibrating the wave velocity on a pile (known length) of the same material as the pile under testing.
Large diameter pile	On a large diameter pile, there is a problem in generating plane waves propagating longitudinally along the pile's axis.	The wave length should be larger than the pile's diameter. If the pile diameter is too large, use other alternative methods.
Long pile	The wave reflection may be too weak or there is no reflection at all due to attenuation of the wave for a long pile.	(a) Increase the hammer impact energy. (b) Increase the resolution of sampling and signal-to-noise ratio of the measurement. (c) Use other alternative methods.
Defects near the pile head and multiple defects	(a) Defects near the pile head may lead to dispersion of the initial impact wave and a distortion of echo wave. (b) Multi-reflections reduce the wave energy transmitted to the deep part of the pile and lead to wave superposition.	(a) To overcome the effects of defects near the pile head and to detect defects in the deep part of the pile, try to use heavy and less stiff tipped hammer. (b) Experienced interpretation is needed. (c) Development of more sophisticated programs for modeling and interpretation.
Instrument	Poor resolution cannot differentiate the reflections from two close reflectors. Low signal-to-noise ratio may not pick up week signals from the toe of a long pile.	The instrument shall have adequate resolution (minimum 50(s) and signal-to-noise ratio and other advanced features such as signal filtering, auto-ranging, auto-averaging, and auto-correlation.

The quality of the source and the location of the sensor are important for a successful SE/IR test. The source should have enough energy to produce a detectable echo from the pile's bottom in the velocity graph. A standard hammer with a hard tip usually produces desirable impulses. However, it sometimes generates unfavorable high frequency waves that make it difficult to interpret the test results. This problem is associated with the sensor location, placing the sensor at different locations may produce successful interpretation (*26*).

The propagated wave velocity depends on the quality of the material. Knowing the wave velocity accurately yields accurate results in SE/IR tests. The application of a multi-sensors array on wood timber utility poles was proposed for more reliable and accurate results (*27*).

The presence of a pile cap and superstructure can undermine the success of determination of foundation depth using SE/IR tests. Two main geometric factors were reported that limit the applicability of the SE/IR method (*21*). They are the ratio of the intervening structure tributary area above the shaft to the drilled shaft area and the pile cap thickness to shaft diameter ratio. The result of two scenarios is shown in Figure 8. The darkened curves are the results obtained while the head is inaccessible. The light-colored curves represent the result where the pile head is accessible. With inaccessible the pile head, the length of the pile is difficult to determine. Echoes from multiple cap reflection can be seen in the velocity graph (see Figure 8a) and identifying the resonance frequencies corresponding to the reflection of the toes are difficult (see Figure 8b). However, the result is very clear with an accessible head (see light colored curves).

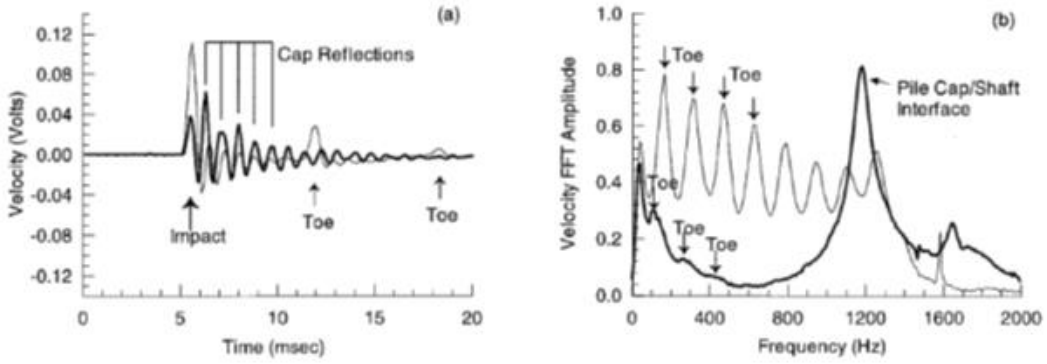

FIGURE 8 Effect of Accessible and Inaccessible Heads on Velocity Graph

The determination of the length of a pile is affected by any echo reflections from the impedance changes such as changes in pile dimensions, cracks, voids, variations in material quality and variations in the surrounding soil layers affect (*28*).

Anomalies such as consecutive bulges and necks also result in reflections between the impulse and the echo from the pile bottom on the velocity graph. Such reflections should be considered when the echo from pile bottom is sought. A study showed that the defects with sizes greater than 10–30% and 45% can be identifiable by SE and IR analyses, respectively (*29*). An example of a defective pile with a bulge and a neck and the corresponding velocity signal is indicated in Figure 9 *(30)*.

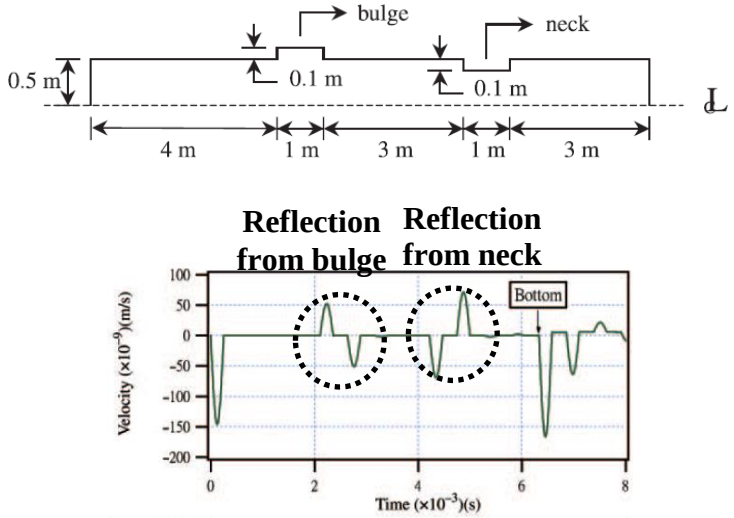

FIGURE 9 Velocity Graph of a Defective Pile with a Bulge and a Neck

The impedance change along a pile also produces oscillation on the mobility graph. An example of a mobility graph affected by impedance change along a pile is shown in Figure 10 (*31*). The Δf = 200 Hz corresponds to the reflection from the pile bottom, whereas the Δf = 980 Hz corresponds to the cross-section change at 2 m below the pile top.

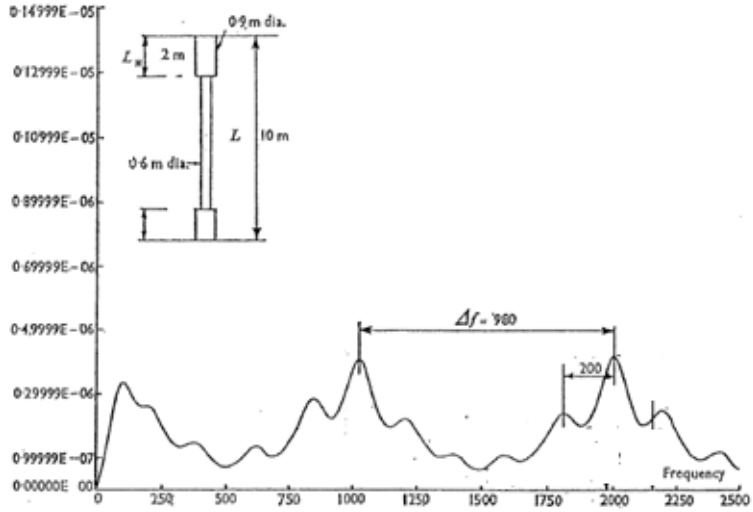

FIGURE 10 An Example of a Mobility Graph with Impedance Change in the Pile

1.4.2 Parallel Seismic Method

The PS method is one of the common low strain methods that can be used to detect the length of piles. However, this method is more expensive than the SE/IR method because it requires drilling a hole parallel to the test pile. The borehole is cased with a 2-in caped-end PVC tube and filled with clean water for better coupling with the sensor (hydrophone).

In the PS test, an instrumented hammer produces an impulse that travels downward through the pile. As the stress wave travels down the pile, a portion of the wave is transmitted into the surrounding soil. The transmitted wave is recorded by a hydrophone that is inside a nearby borehole. The hydrophone is raised or lowered in uniform increments and the test is repeated at each increment. The velocity graph is recorded at each depth. The first arrival time of the wave is defined at each velocity graph. These velocity graphs are stacked together as shown in Figure 11. A typical setup is also shown in this figure.

Since the wave velocity of the pile material is significantly higher than the wave velocities of soils, the arrival times differ between two consecutive depth increments, one tested when the hydrophone is parallel to the pile and the second when the hydrophone is below the pile. Two straight lines can be determined from these arrival times and the intersection of the two lines is then identified as the foundation depth (*32*, *33*). An additional benefit of the PS test is that the wave propagation through the soil provides information about the soil condition (such as stiffness) adjacent to the foundation (*34*).

A newly developed combined Parallel Seismic and Cone Penetration Test (PS/CPT) system allows collecting soil data and conducting a PS test simultaneously during a CPT test. The new combined technique has a great advantage over conventional PS tests since no borehole is required (*35*). Olson et al. (*36*) presented details of the principles and operations of the combined (CPT+PS) system.

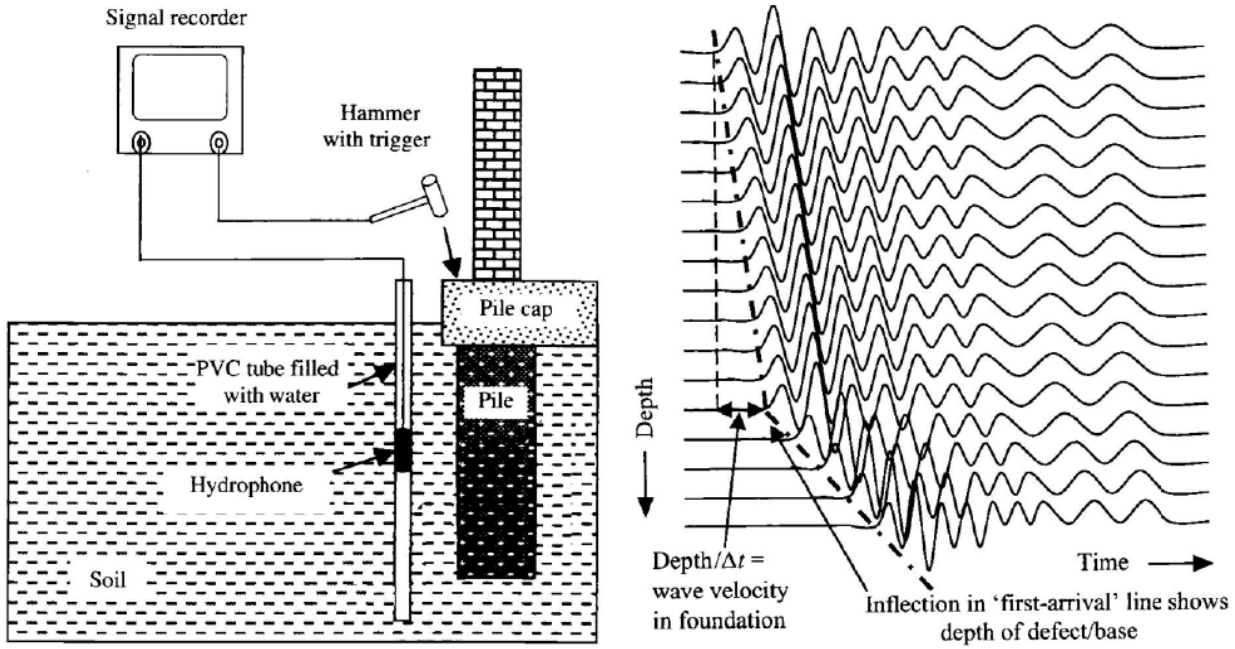

FIGURE 11 Typical Setup and Test Data of PS Test (*12*)

1.4.3 Induction Field Method

The IF method is used to measure the depth of steel foundations (H-piles or pipe piles) or concrete piles with continuous reinforcing steel. This method can be performed in conjunction with the PS method, since the installed borehole for IF tests can also be used for PS tests.

The IF method involves determining the length of the metal within the foundation by inducing an electro-magnetic field through a soil-foundation system and detecting the change of the magnetic field due to the nearby metal objects. The testing is implemented by passing a DC current through a polarized magnetic field sensor which is lowered into a PVC cased borehole adjacent to the test pile. A magnetic field is consequently induced in the pile's metal which can be detected by the probe. The depth of the foundation is determined by measuring the magnetic field strength at various depths, and identifying the changes in magnetic field strength. A typical IF setup and associated data are indicated in Figure 12.

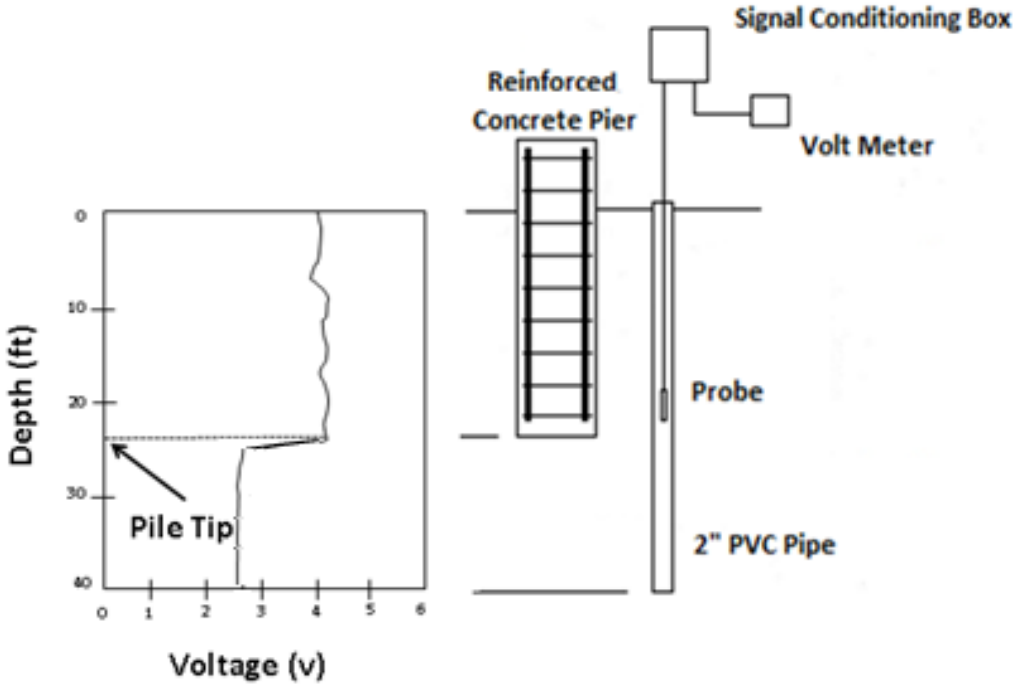

FIGURE 12 The IF Result and a Typical IF Setup

THE PAGE LEFT BLANK INTENTIONALLY

2. RESEARCH METHODOLOGY

Three NDT methods (SE/IR, PS, and IF) were used to determine the conditions of unknown bridge foundations. As mentioned before, the three NDT methods have different requirements regarding degrees of site access. SE/IR generally requires access to the substructure of a bridge. Borehole methods (PS and IF) require a soil boring that must be installed as close as possible to the test pile before conducting testing. The borehole methods require a borehole to extend at least 10 feet deeper than the expected embedment pile depth. The PS method requires a borehole to be located within 6 feet from the test pile while the IF method requires a borehole to be located within 18 inches (preferably within 12 inches). Two-inch inner diameter PVC tube with an end cap should be placed in the hole and the spacing between the PVC tube and the hole should be backfilled with compacted native soil. The tube must be filled with water before conducting PS tests.

Two devices and ancillary equipment were purchased for this project from Olson Instruments, Inc. for SE/IR and PS tests and from Pile Dynamics Inc. for IF tests. We acquired the equipment pursuant to ASTM D5882-07-2013 (*37*), ACI 228.2R-13 (*38*). Equipment purchased from Olson consists of the Freedom Data PC platform, two 100mv/g 1D accelerometers, a hydrophone, and a hammer with force transducer and 4 hammer tips. The hammer tips are hard, medium hard, medium soft, and soft. The contact time for hard tip is mainly between 1200 to 2000 milliseconds. The contact time increases with the degree of softness of the hammer tip. For IF tests, the Length Inductive Test Equipment (LITE) comprises a signal conditioner, multimeter, Probe (sensor) and battery.

Before conducting the field tests with the new equipment, preliminary tests were performed under controlled environmental conditions to study the applicability and limitations of these NDT methods. The tests were conducted in the Civil Engineering Structural Lab, on the University of New Mexico (UNM) campus, and at a test site off campus. It was expected that the knowledge obtained from these controlled tests should improve the success rate of conducting NDT tests in the field. In coordination with the NMDOT, numerous NDT field tests have been performed at each bridge location. For each bridge, the foundation was investigated in detail to determine the foundation depth as well as to reveal any possible difficulties that might be encountered. Since it was crucial to provide test procedures to conduct the SE/IR, PS and IF tests, initial test procedures were developed based on numerous sources in the literature review. However, they were regularly modified during the preliminary and field tests based on the success and failure of various tests conducted in the project. It should be noted that such procedures allow efficient collection of high quality data in the limited timeframe assigned for field testing. The tests procedures for each selected NDT method will be presented later.

The specifications of all NDT tests performed in this project are summarized in Table 4. Details of the setup of NDT tests and the results will be elaborated later. The foundations were known for Bridge Nos. 1676 and 7480 since the as-built drawings are available. Validation of SE/IR and PS tests was confirmed by conducting these two tests on Bridge No. 1676 while validation of PS tests was examined on Bridge No. 7480.

TABLE 4 Specifications of Preliminary and Field NDT Tests.

Test Type	Test Object	Foundation Material	NDT Test
Preliminary	Centennial Building Column (UNM)	Reinforced Concrete	SE
	Structural Lab Concrete Wall (UNM)	Reinforced Concrete	SE
	Centennial Library Column (UNM)	Reinforced Concrete	SE
	Biology Annex Building Column (UNM)	Wood	SE
	Buried Cylinder in Ground (Private Test Site)	Reinforced Concrete	IF, PS
	Constructed Wooden Box Test-bed (UNM)	Steel	IF
Field	Highway Bridge No. 7480 - H-pile foundation	Steel	SE, PS
	Highway Bridge No. 5899 - Pier wall foundation	Reinforced Concrete	SE
	Highway Bridge No. 6922 - Pile foundation	Wood	SE
	Highway Bridge No. 1190 - Pile foundation	Wood	SE
	Highway Bridge No. 1676 - Pile foundation	Wood	SE, PS
	Railroad Santo Domingo Bridge- Pile foundation	Wood	SE
	Partially Dismantled Bridge near Route 419 (Bridge No. 6253)	Wood	SE

The purpose of selecting the bridges is presented:

- Santo Domingo Bridge

  This railroad bridge was the first bridge recommended by Mr. Bob Meyers and Ms. Michelle Mann of NMDOT on which preliminary SE/IR tests were performed because of the bridge location and the foundation material. In addition, the bridge is far away from any automotive traffic. NMDOT has the equipment that has been used regularly for Pile Integrity Tests. It was decided to use NMDOT's equipment to start the project before the completion of the purchase of the required equipment for the research project. The new equipment has the capability for conducting PS tests and for an additional sensor. The SE/IR tests were implemented while NMDOT's engineers were the observers.

- Bridges Nos. 1190 and 6922

  It was expected that a great amount of unknown bridge foundations in New Mexico were supported by timber piles, therefore it was crucial to investigate the performance of SE/IR tests on such foundations. The communication with NMDOT revealed that performing NDT on the unknown foundations of state-owned bridge of high risk was their highest priority. Therefore, SE/IR tests were suggested for 7 high risk state-owned timber bridges from the NMDOT database including bridges Nos. 312, 1190, 1873, 1876, 4069, 5893, and 6922. Since the bridge inspection reports and pictures of Bridges No. 1190 and 6922 were available to the UNM research group, it was decided to perform the NDT tests on those two bridges.

- Bridge No. 1676

  Validation of the research results was essential, therefore the UNM research group requested NMDOT to provide a bridge with *known* foundation. Bridge No. 1676 was introduced to the research group for conducting the NDT tests (SE/IR and PS tests). The selection of the bridge was based on the following reasons:

  1. The as-built drawings of the bridge foundation were available.
  2. The bridge site was conveniently located (just 66 miles from UNM).
  3. There was no accessibility problem and the bridge had sufficient clearance to install boreholes for PS tests.
  4. The capability of Geoprobe Model 7822DT could be examined.

- Bridge No. 6253

  In 2015, the research group obtained the information that some bridges in District 4 near NM Route 419 were being replaced. Since the timber piles of these bridges was supposed to be pulled out, validation of NDT tests can be performed on these timber piles. With the help of the technical panel, SE/IR tests were able to be conducted on one bridge prior to exhumation of the timber piles.

- Bridge No. 5899

  The foundation of Bridge No. 5899 was selected due to following reasons:

  1. The bridge was categorized as state own and high risk.
  2. The material of the foundation was concrete that provides a means to examine the performance of SE/IR equipment on concrete foundations.
  3. The bridge foundations were massive pier walls. The literature review indicated that most of SE/IR studies were on foundations of slender elements. The research group did not have adequate information on the performance of the SE/IR tests on massive pier walls. Therefore, this bridge foundation could provide valuable information of SE/IR tests on pier wall foundations.

- Bridge No. 7480

  This bridge was supported by steel H-piles and the as-built drawing was available. It was a great site to examine the performance of IF tests. However, due to the difficulty of drilling boreholes close enough to the piles, only PS method could be conducted. Although SE/IR tests were not recommended for steel piles, SE/IR tests with different setups were also conducted.

In addition to the physical NDT tests, Finite Element Method (FEM) simulations were conducted in this project. The full-waveform inversion method was carried out and the results were compared against the field observation. The comparison provides a means of better understanding and conducting the SE/IR tests and better interpreting the results. In the current study, major factors, such as a foundation's bottom condition, a foundation's material damping, hammer tip type, superstructure reflections, pier geometry and characteristics of striking, were studied using FEM models of a pile and a pier wall.

2.1 SONIC ECHO/IMPULSE RESPONSE TESTS

2.1.1 Introduction to SE/IR Test Setup

In the presence of superstructure, it is crucial to identify the best locations of source and receiver to capture the intended echo from foundation bottom. For wing piles, the top surface of the pile is accessible. SE/IR tests can be conducted by placing the sensor on the pile top or attaching the sensor to the side of the pile and striking the pile top. When the top of the foundation is inaccessible due to the presence of superstructure, the sensor must be mounted on the side of a pile to record vertical vibrations. Since geophones are heavier and larger than accelerometers, it is easier to attach an accelerometer than a geophone. Therefore, accelerometers were used as the sensor. The source must be created by striking the hammer on other areas rather than the pile top.

In this section, various options for striking and sensors attachments are presented. They have been utilized in both preliminary and field tests. They are presented in detail and prioritized throughout this report.

2.1.1.1 Striking Setup

In SE/IR tests, sonic waves are generated by striking a hammer on a surface of the foundation. P waves or S waves will be generated depending on the direction of the hammer strike. If a portion of the top of a pile is accessible, the best longitudinal P-waves can be generated by striking on its top. For piles with inaccessible top, the research group examined other options such as striking on a block attached on the side of the pile. When attached blocks to the side surface of the piles are used, they must be properly secured by nails and screws to prevent any detachments during striking.

When a horizontal strike is applied on the side of a pile, S-waves are primarily generated. P-waves will be generated at any interface when the incident waves are not propagated perpendicular to the interface. The energy of the indirect P-wave is significantly smaller than that of the P-wave produced by vertical striking. However, the side strikes are very attractive since it is much easier to apply when the top of a pile is inaccessible. It is worthy to examine the velocity graphs from the horizontal and vertical strikes. This issue will be discussed later in the preliminary and field tests.

Striking Setup for Piles with Accessible Top When either the entire or a portion of the pile top is accessible, a vertical strike can be applied on the top surface of the pile as shown in Figure 13. In this case, the longitudinal P-waves travelling down the pile is generated directly.

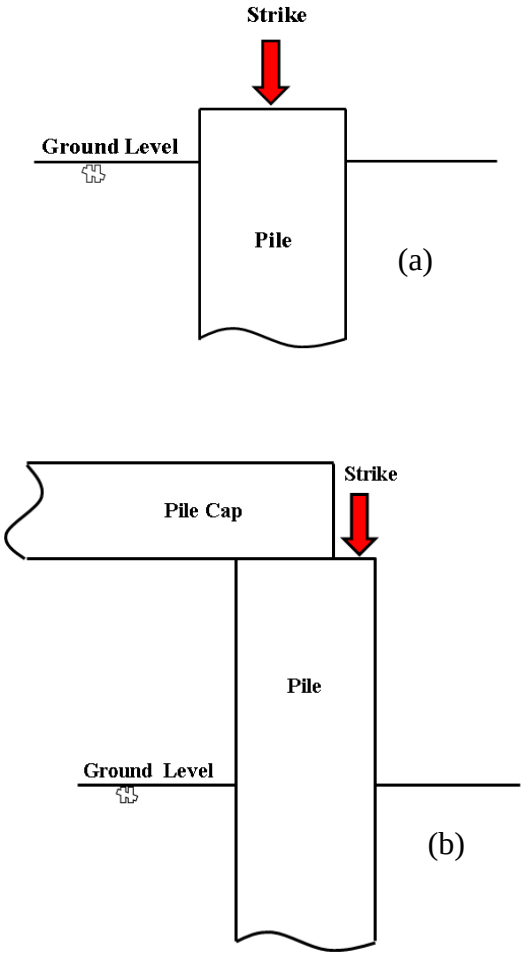

FIGURE 13 Vertical Striking on Piles with Accessible Top

Setup for Striking on Piles with Inaccessible Top For piles with inaccessible top, the longitudinal wave can be generated by striking other parts of the foundation as shown in Figures 14 to 19. When the superstructure is not placed exactly atop the pile, longitudinal waves can be produced by striking the top surface of the pile cap as indicated in Figure 14. If the presence of the girders on the top of the pile cap does not allow striking on the pile cap top surface, other options indicated in Figures 15 to 19 can be applied.

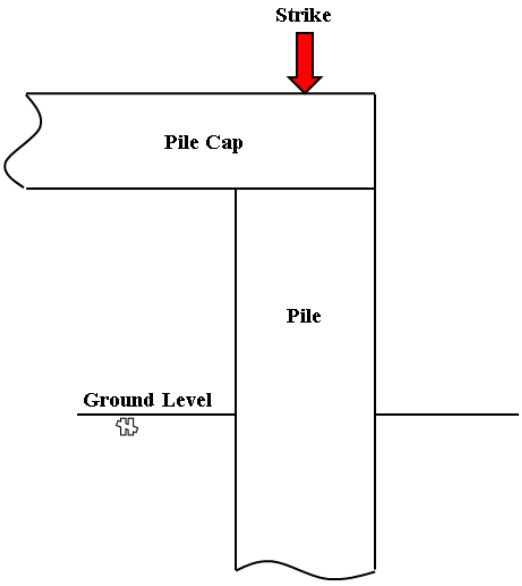

FIGURE 14 Vertical Striking on the Top Surface of Pile Cap

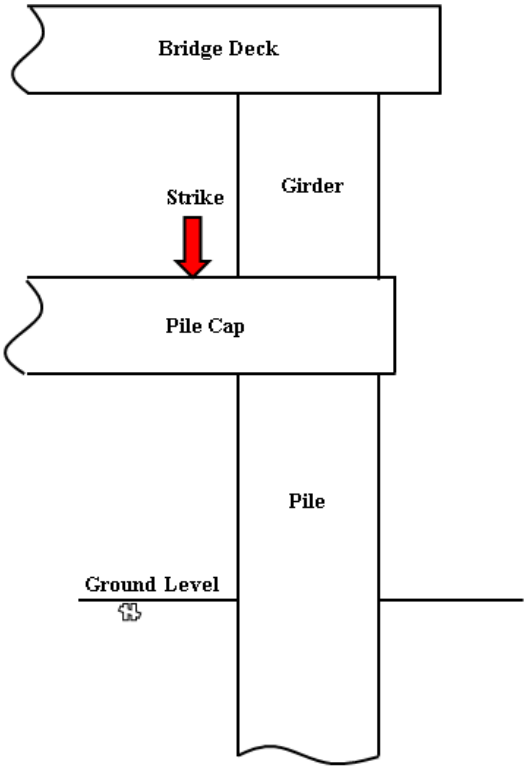

FIGURE 15 Eccentric Vertical Striking on the Top Surface of Pile Cap

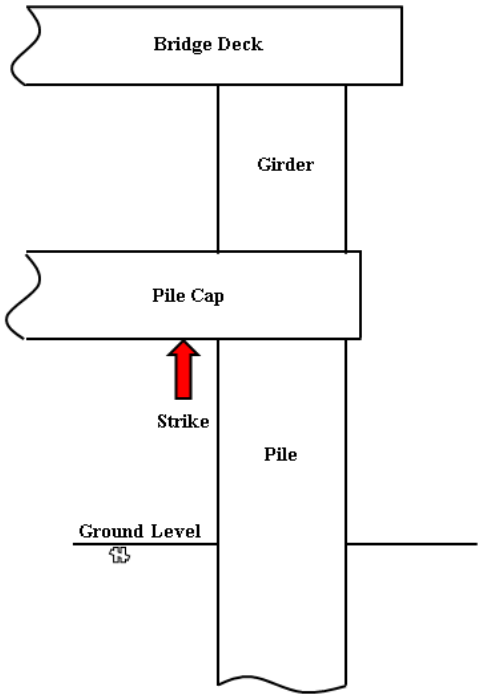

FIGURE 16 Upward Vertical Striking on the Bottom Surface of Pile Cap

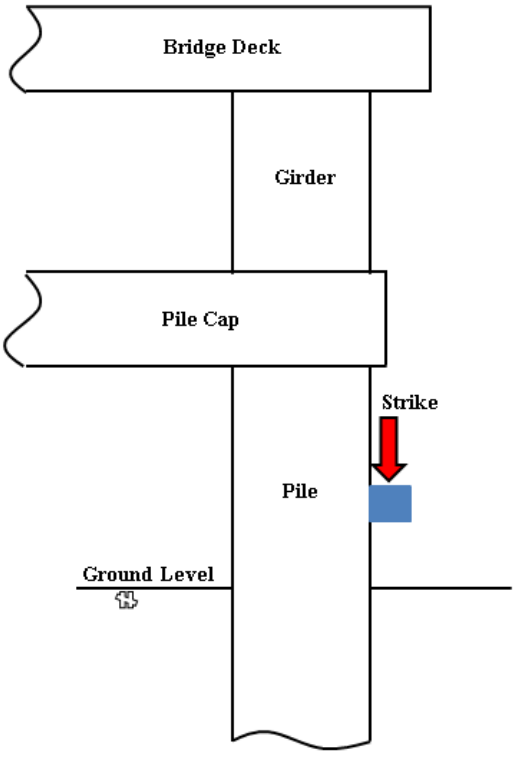

FIGURE 17 Vertical Striking on a Block Attached to the Side of a Pile

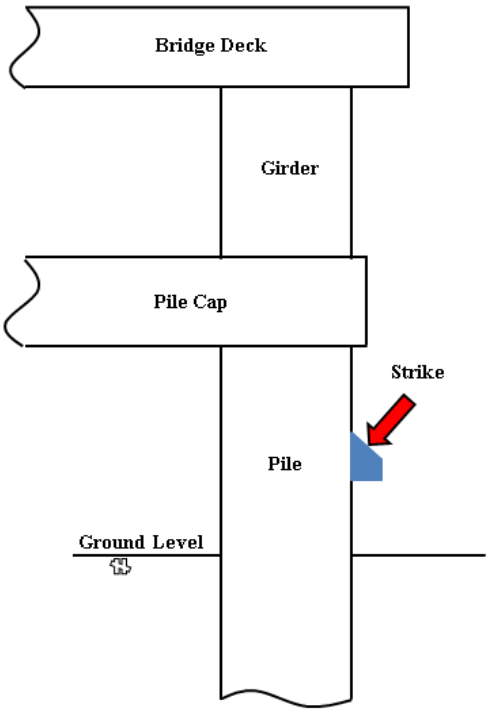

FIGURE 18 Inclined Striking on a Wedge Block Attached to the Side of a Pile

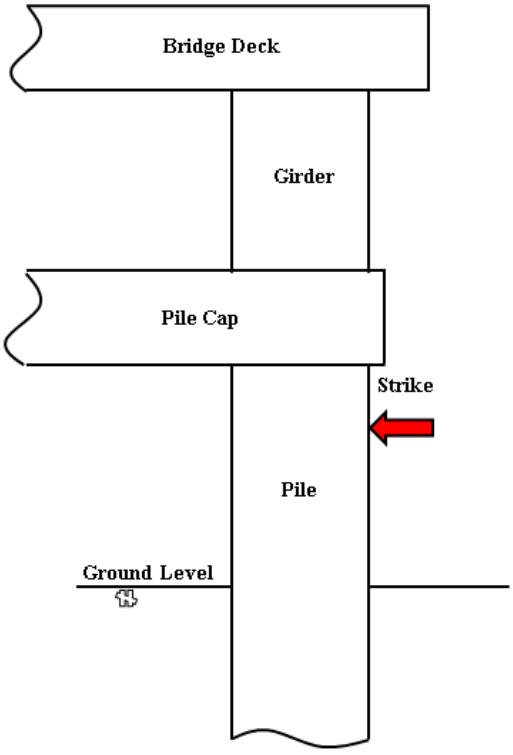

FIGURE 19 Horizontal Striking on the Side of a Pile

2.1.1.2 Sensor Setup

Accelerometer Setup on Piles with Accessible Top When the top of a pile is accessible and the size of the pile is greater than 2 ft, the accelerometer can be placed vertically to capture the longitudinal vibrations as indicated in Figure 20. Vaseline is commonly applied at the interface between the accelerometer and the pile surface for better wave transmission.

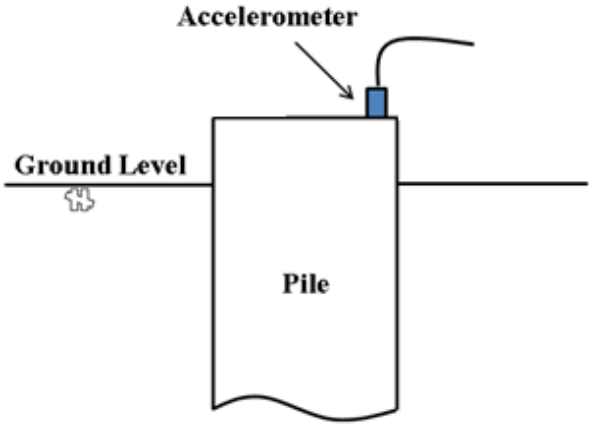

FIGURE 20 Accelerometer Setup for Piles with Accessible Top

Accelerometer Setup on Piles with Inaccessible Top When the top of a pile is inaccessible, a block is attached onto the pile's side as indicated in Figure 21. Then, the sensor is placed vertically on the mounted block to capture the vertical vibration of the pile.

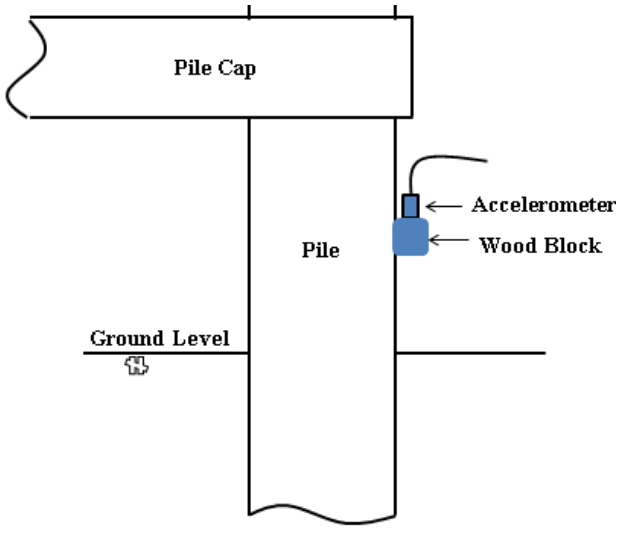

FIGURE 21 Accelerometer Setup for Piles with Inaccessible Top

Small wooden blocks (1.5" × 1.5" × 1.5") shown in Figure 22 can be used to mount the accelerometers. The dimensions of the block are noncritical as long as they are greater than the

size of the accelerometer. The blocks are attached to the side surface of the piles using nails (screws) or superglue. The accelerometer is placed vertically on the top surface of the blocks to receive longitudinal vibrations. Appropriate nuts are attached to the top surface of the blocks to ease the attachment of the accelerometer. Since the accelerometer is securely mounted on the wooden block, no Vaseline is needed between the accelerometer and the wooden block.

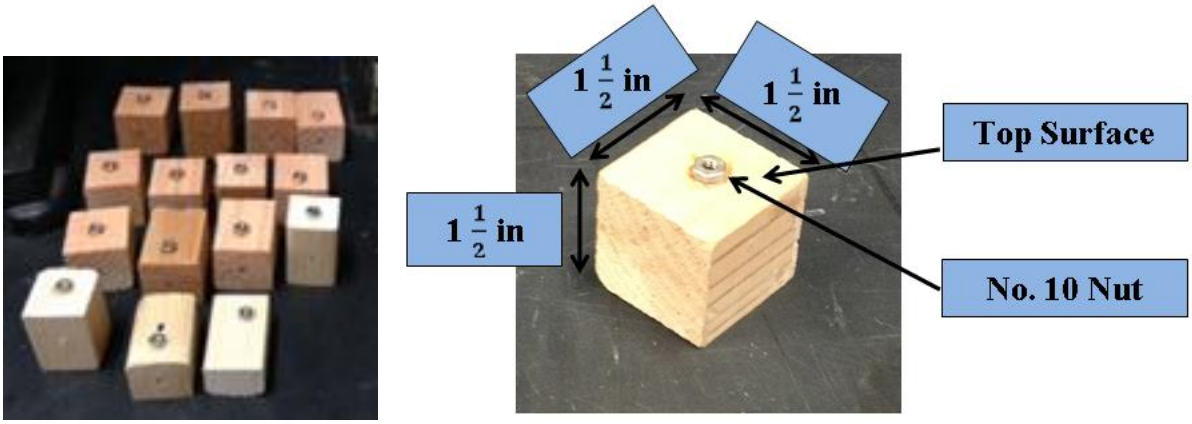

FIGURE 22 Wooden Blocks Used for Accelerometers Attachments

2.1.2 SE/IR Test Procedure

Initial SE tests procedure was developed prior to conducting the preliminary and field tests. An SE/IR test includes the selection of the method of striking, accelerometers locations, equipment assemblage, and data acquisition.

2.1.2.1 Method of Striking

A successful SE/IR test is strongly affected by the source location. Therefore, proper striking methods should be selected to obtain interpretable results. Based on the SE/IR tests setup introduction presented in the previous section, proper practical source locations are indicated in Figure 23. Such striking methods can be used depending on the accessibility of the pile top. These source locations were extensively utilized in the field. They are prioritized based on the quality of the produced data and the preferred options are discussed later.

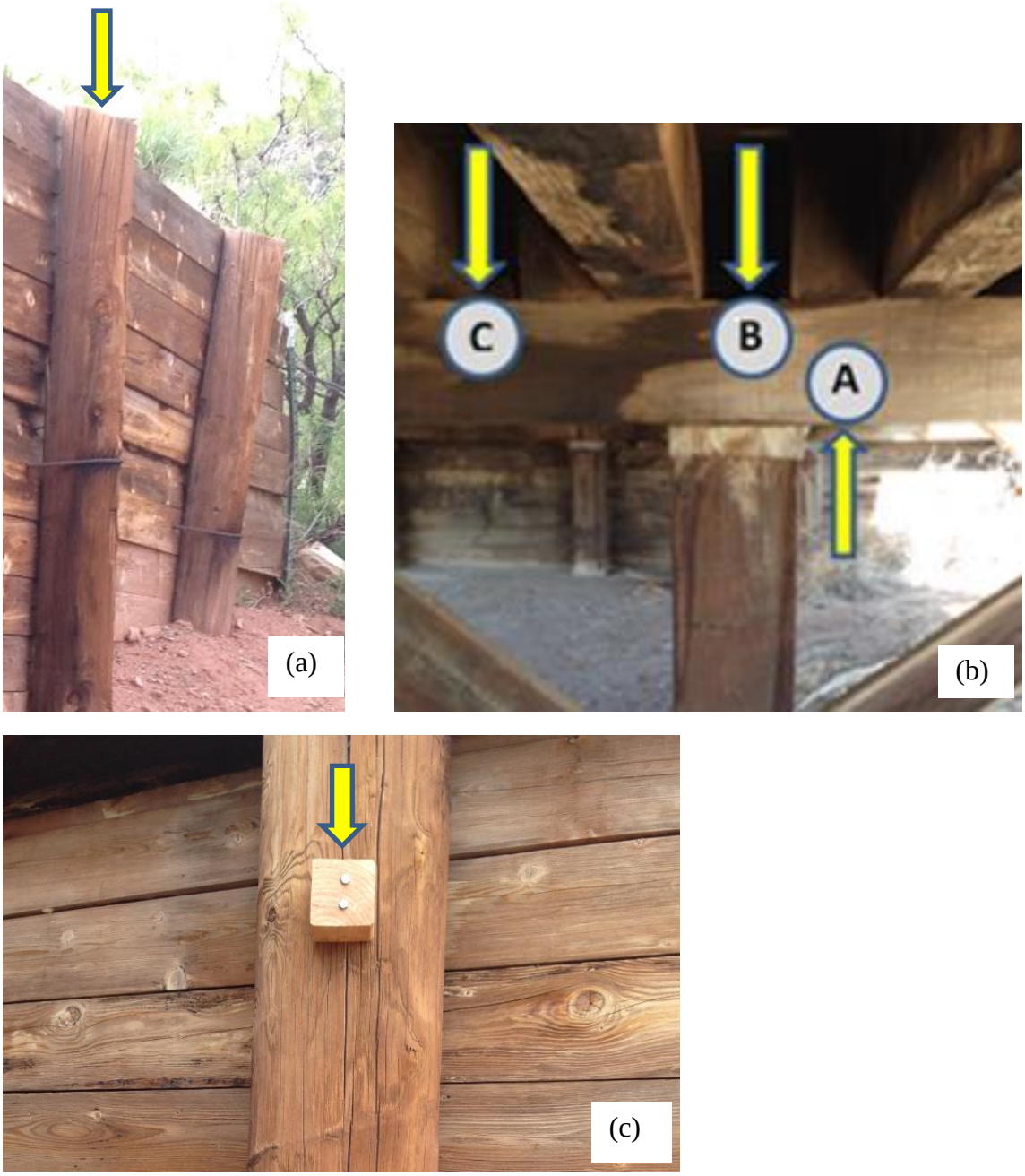

FIGURE 23 Proper Practical Source Locations, (a) Striking on top of the test pile (b), Downward striking on Point B (top of the pile cap directly above the test pile), C (top of the pile cap next to the test pile) and upward striking on Point A (bottom of the pile cap next to the test pile, (c) Striking on top surface of a block tightly attached onto the test pile

The dimensions of the wood and aluminum blocks used for striking in this project are indicated in Figure 24. The actual dimensions of the striking blocks are noncritical as long as they are larger than the size of the hammer head. The cubic aluminum block was machined with an internal curvature to provide better contact with the curved surface of the piles. The internal curve

increases the contact surface between the block and the pile's side surface. The blocks must be tightly attached onto the test pile by nails or screws as indicated in Figure 25. This method will be more difficult for concrete surface since concrete screws only have a maximum embedment of 1 ¾ inch. If more embedment depth is required, threaded holes have to be installed into the concrete which will significantly increase the cost and time.

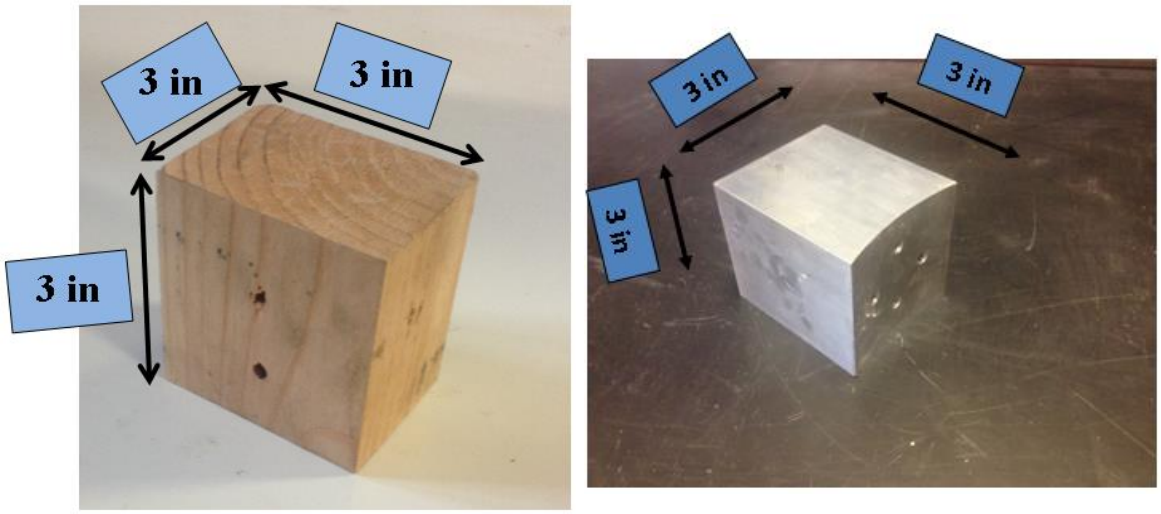

FIGURE 24 Dimentions of Wood and Aluminum Striking Blocks

FIGURE 25 Attachment of a Wooden Striking Block onto the Test Pile

2.1.2.2 Location of Receivers

The sensor (accelerometer) can be placed atop the wing piles. If the pile top is inaccessible, the accelerometers will be mounted on wooden blocks attached onto the side of the test pile with nails, screws, or glue. The dimensions of the wooden blocks used in this project can be found in Figure 22. Examples of accelerometer attachment to the pile surface is indicated in Figure 26. If two accelerometers are used, the second accelerometer should be placed far away from the first accelerometer as possible.

FIGURE 26 Accelerometers Mounted on a Pile by Wooden Blocks.

2.1.2.3. Hardware Assembly

The equipment utilized for conducting SE/IR tests should be assembled as indicated in Figure 27. Four different hammer tips are available as shown in Figure 28.

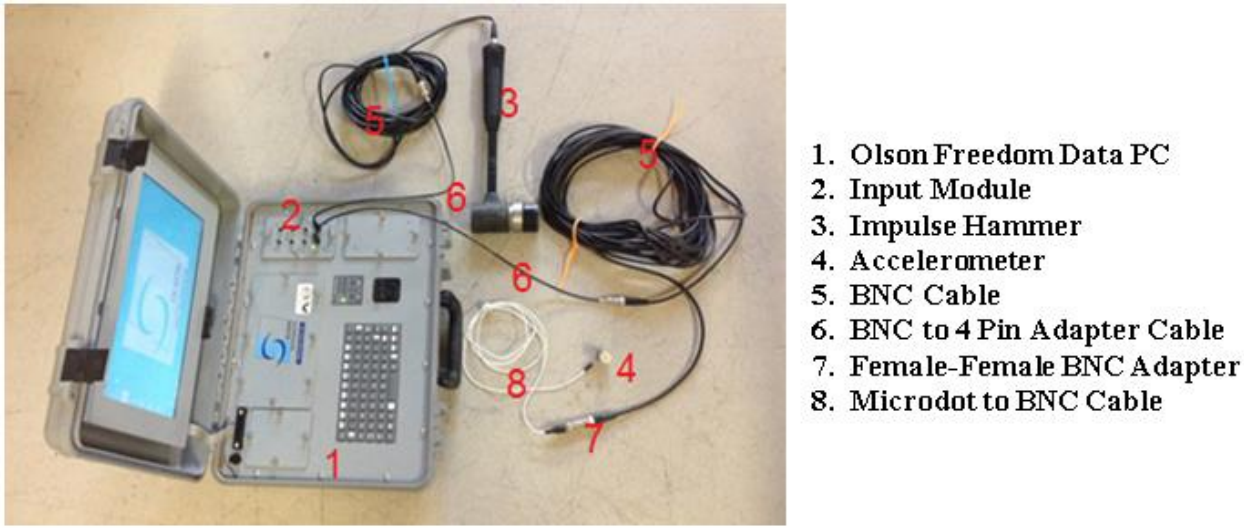

FIGURE 27 SE/IR Test Equipment

FIGURE 28 A Hammer and Four Different Tips

2.1.2.4 SE/IR Data Acquisition

The WinTFS software was used to acquire the data in this project. Figure 29 shows an example of the acquired data including raw data (top graph) and velocity graph (middle graph).

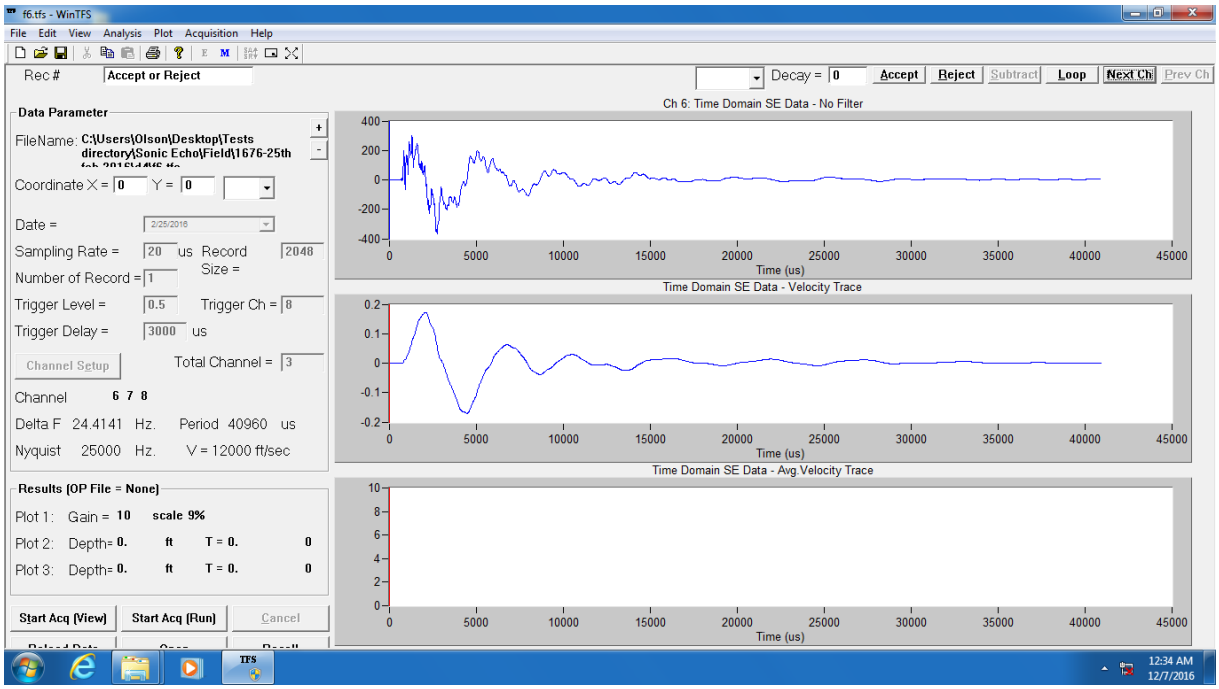

FIGURE 29 An Example of Acquired SE Data Including Raw Data (Top Graph) and Velocity Trace (Middle Graph)

The flowchart shown in Figure 30 was designed to acquire consistent SE/IR data. Based on the flowchart, each SE/IR test should be repeated adequately to achieve the desired level of reliability.

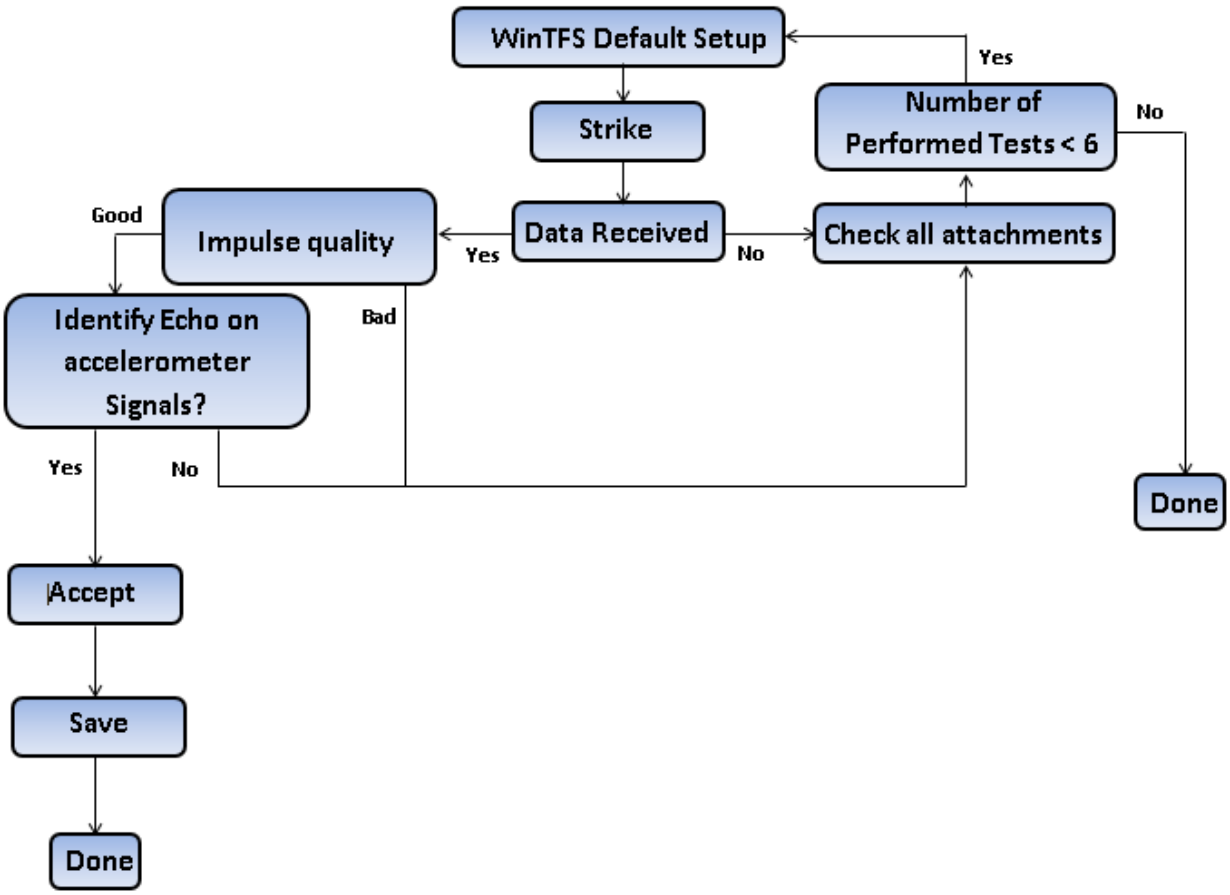

FIGURE 30 Flowchart for Conducting SE/IR Tests

2.1.2.5 SE/IR Data Processing and Length Determination

For each SE/IR test, the obtained velocity graph indicated in Figure 29 was used to determine the time difference between the impulse (source) and the echo from pile toe (Δt). Δt is used therein to represent the time difference and used to determine the pile length associated with SE analysis through Eq. 1. The software was also able to process the data and perform an IR analysis. An example of the result of an IR analysis is indicated in Figure 31. If the resonant frequencies were distinguishable in the mobility plot (bottom graph), the difference in frequency between the resonant frequencies (Δf) could be used to determine the embedment depth of a pile. Similar to Δt, Δf was used to denote the difference in frequency between the resonant frequencies in this report. Δf was used to determine the pile length associated with IR analysis through Eq. 4.

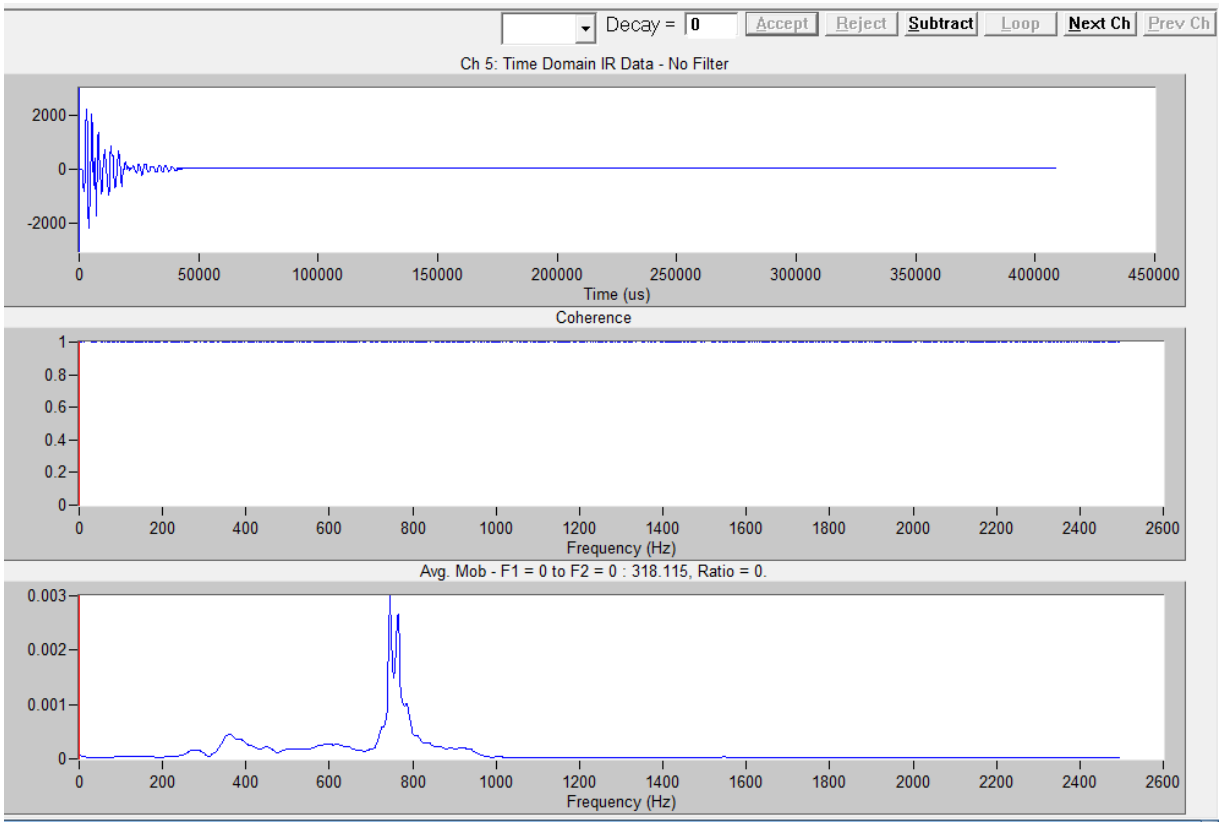

FIGURE 31 Produced Graphs from IR Analysis, Tme domain IR data (top), Coherence (middle) and Average Mobility (bottom)

In both analyses of time and frequency domains, the length measurements were based on the propagated wave velocity in the foundation material. In the current research, the utilized wave velocities were chosen based on the material quality observed in the field as well as in the literature. For example, the literature indicates the wave velocity in wood ranging from 9,900 to 12,000 ft/s that depends on the type of wood, the amount of knots, and rottenness (*39, 40*). There is no means to determine the wave velocity in the pile below ground although the wave velocity may be determined for the exposed pile. Therefore, a variation of 20% in calculated lengths is usually expected. The wave velocity in the foundation should be obtained as accurately as possible to produce more accurate results. The compressional wave velocity could be measured between two mounted receivers to improve the accuracy of the estimated length. Using two receivers can also distinguish the up-going and down-going waves.

The most important outcome of an SE test is the velocity graph. A *good* SE test should show a clear impulse and echo in the velocity graph. A *consistent* SE test should have three similar good SE tests. The measured length is considered as *"in accordance"* with the actual length when the measured length is within 90% to 110% of the actual length.

2.1.3 Preliminary SE Tests

The preliminary tests were conducted on wood and concrete elements to examine the applicability of the equipment on such materials. The elements were similar to individual piles and pier walls in real bridges. Therefore, conducting SE tests on such elements not only revealed the equipment performance but also provided guidelines to conduct tests on bridge foundation more efficiently.

2.1.3.1 SE Tests on A Wood Column

SE tests were conducted on a decorative wooden column on UNM campus. The SE test setup is shown in Figure 32. The tests were carried out only with a hard-tip hammer. The source was applied in three different ways. The impulse was produced by striking horizontally at point C, vertically on the concrete pavement next to the column, and upward on the capital. Although the hammer was not struck on the column directly, vertical striking on pavement produced a reflected longitudinal wave that traveled upward along the column and reflected from the top of column. Two accelerometers were mounted at points A and B. The accelerometers were attached on the top surface of wooden blocks glued onto the side surface of the column as shown in Figure 32.

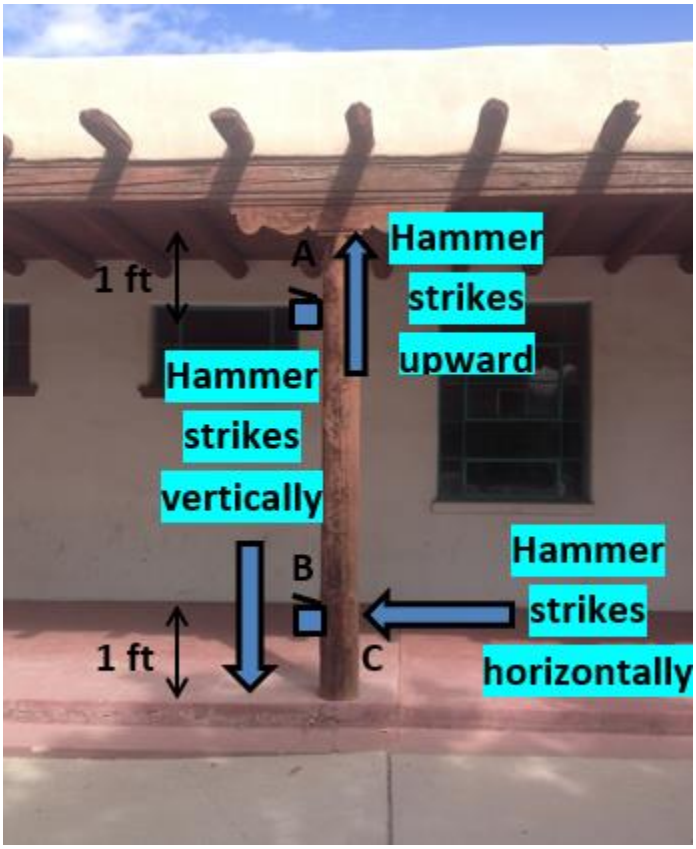

FIGURE 32 Source and Receiver Locations on a Wooden Column

As mentioned before, upon striking, three graphs including raw acceleration data, velocity graph (integrated from acceleration), and impulse signal will appear on the computer screen. The velocity graph is used to determine the length of the column.

The results showed that horizontal striking did not produce good velocity graphs that could be used to determine the length of the column. An example of velocity graphs obtained from

horizontal striking is indicated in Figure 33. Identifying the echo corresponding to the reflection from column top is difficult. Also, the signals should decay with time which is not the case here. On the other hand, the velocity graph obtained from vertical striking on pavement and upward striking on the capital were similar. The echo from the reflection of the end of the column can be identified. An example of good velocity graph is shown in Figure 34; the graph is produced by upward striking on the capital with the accelerometer at point *A*. The echo corresponding to the reflection from the bottom of the column (a part of the column is embedded in ground) is indicated on the graph. The amplitude of the signal decayed as expected. Δt can be estimated clearly as shown in the figure.

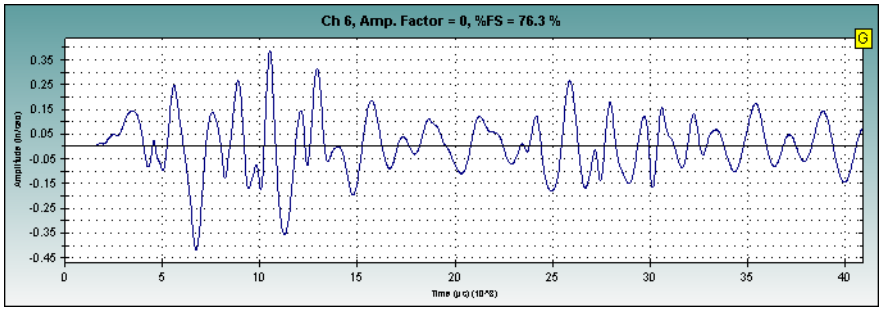

FIGURE 33 A Velocity Graph Obtained from Horizontal Striking on a Wood Column

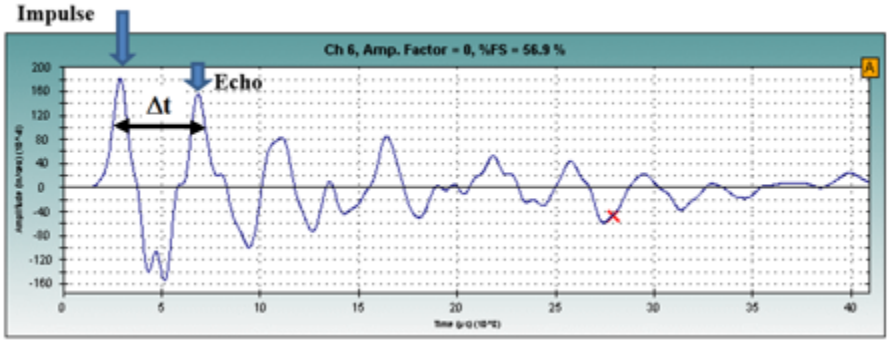

FIGURE 34 A Velocity Graph Obtained from Vertical Upward Striking

As an example, using Δt = 3920 μs in Figure 34 and the sensor location is 1 ft from the top, the column length is:

$$L_t = \frac{v \times \Delta t}{2} + 1 = \frac{10000 \times 3920 \times 10^{-6}}{2} + 1 = 20.6\, ft$$

Wave velocity in wood ν = 10,000 ft/s (based on column's material quality)

2.1.3.2 SE tests on A Concrete Column

Twelve SE tests were conducted on one of the concrete columns of the Centennial Engineering Building on UNM campus to study the behavior of SE tests on concrete material while an accelerometer was attached onto the side surface of the column. A wooden block was attached on the column surface with superglue. The accelerometer was placed vertically on the top surface of the block. In this column, it was decided to explore if horizontal striking on the capital and column

itself can produce useful velocity graphs that yields the determination of the length of concrete column. The concrete column and the test setup are shown in Figure 35. The direction and the location of the strikes are indicated in Table 5.

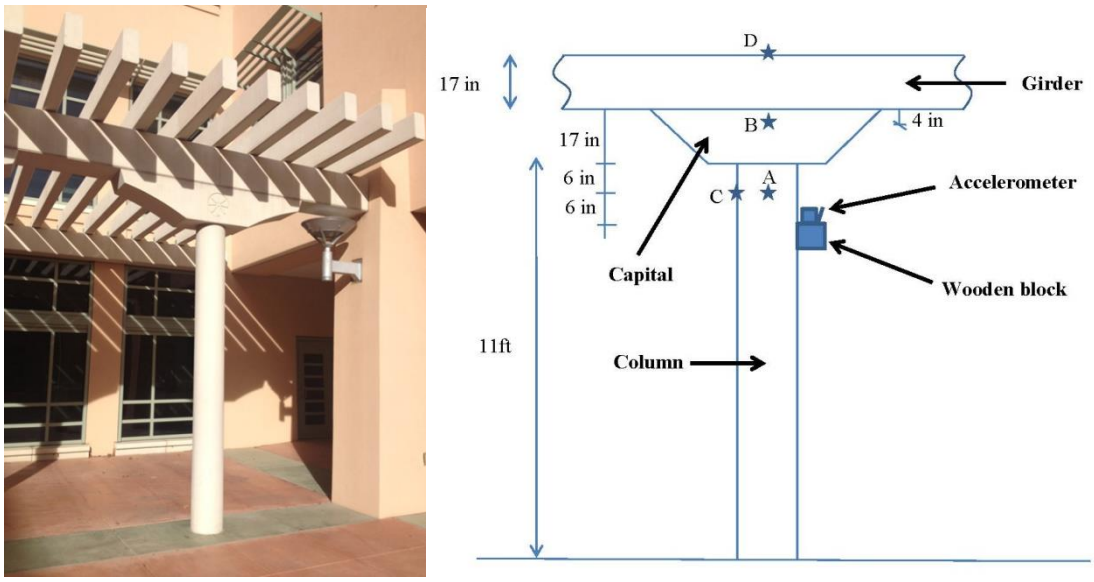

FIGURE 35 Picture and Details of Centennial Engineering Concrete Column

TABLE 5 Direction and Location of Strikes on a Concrete Column at the Centennial Engineering Center.

Test No.	Hammer Tip	Direction and Location of Strike
1	Hard	A (horizontally)
2	Hard	A (horizontally)
3	Hard	B (horizontally)
4	Hard	B (horizontally)
5	Hard	C (horizontally)
6	Hard	C (horizontally)
7	Hard	D (vertically)
8	Hard	D (vertically)
9	Medium-hard	D (vertically)
10	Medium-hard	D (vertically)
11	Medium-soft	D (vertically)
12	Medium-soft	D (vertically)

It was found that horizontal striking cannot produce good results. An example of poor velocity graphs is indicated in Figure 36. Again, the signals did not decay with time. On the other hand, the echoes were clear for the SE tests by vertical striking on the top above the column. Δt from the velocity graphs were measured and the length of the column was determined.

$$L_t = \frac{v \times \Delta t}{2} + \text{distance between accelerometer and the bottom of the capital.}$$

The wave velocity is assumed to be 10,000 ft/s. The wave velocity of concreate is very similar to the wave velocity of wood.

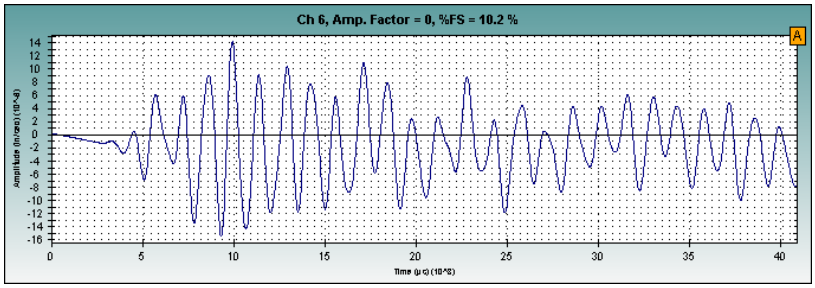

FIGURE 36 An Example of Poor Velocity Signal Produced by Horizontal Striking

The calculated lengths are summarized in Table 6. L_t is the total height of the column which is the sum of the exposed and buried part. The average calculated length (15.8 ft) is in accordance with the approximated total height of the column.

TABLE 6 Calculated Lengths of Centennial Engineering Concrete Column.

Test No.	Δt (μs)	L_t (ft)
1 ~ 6	--	--
7	2900	15.5
8	2900	15.5
9	3012	16.1
10	3020	16.1
11	3120	16.6
12	2820	15.1

2.1.3.3 SE Tests on A 3-story Concrete Column

Twelve SE tests were conducted on a reinforced concrete column on UNM campus shown in Figure 37. The column is one of the 3-story columns of the Centennial Engineering Library on UNM campus. The total length of the column is 43 ft. Only the top 7.5 ft of the column is visible as shown in the photo.

FIGURE 37 The Reinforced Concrete Column of Centennial Library on UNM Campus

SE tests were carried out with different hammer tips. Since the top of the column was accessible, the accelerometer was placed on the top surface of the column and vertical strike at top and horizontal strikes were applied as shown in Figure 38. The characteristics of all SE tests are listed in Table 7.

TABLE 7 Characteristics of SE Tests on the Concrete Column of Centennial Library on UNM Campus.

Test No	Hammer tip	Strike Direction
1	Hard	Vertically at A
2	Hard	Vertically at A
3	Medium-hard	Vertically at A
4	Medium-hard	Vertically at A
5	Medium-soft	Vertically at A
6	Medium-soft	Vertically at A
7	Hard	Horizontally at B
8	Hard	Horizontally at B
9	Medium-hard	Horizontally at B
10	Medium-hard	Horizontally at B
11	Medium-soft	Horizontally at B
12	Med-soft	Horizontally at B

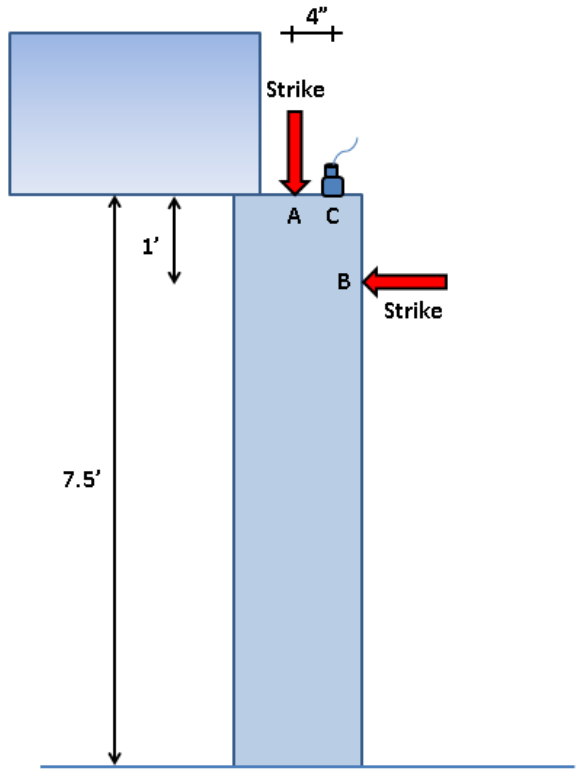

FIGURE 38 Source and Receiver Locations on the Concrete Column of Centennial Library on UNM Campus

Results of Vertical Striking with Hard Tip The velocity graphs obtained from the accelerometer in Tests 1 and 2 are depicted in Figure 39. Although high frequency noise at the beginning was clearly observed in Figure 39b, the impulse and echoes were identifiable as shown as arrows in the figure. When the accelerometer was placed at least 1 ft away from the source, the high frequencies at the beginning disappeared. Therefore, accelerometers are recommended to be placed at least 1 ft from the source.

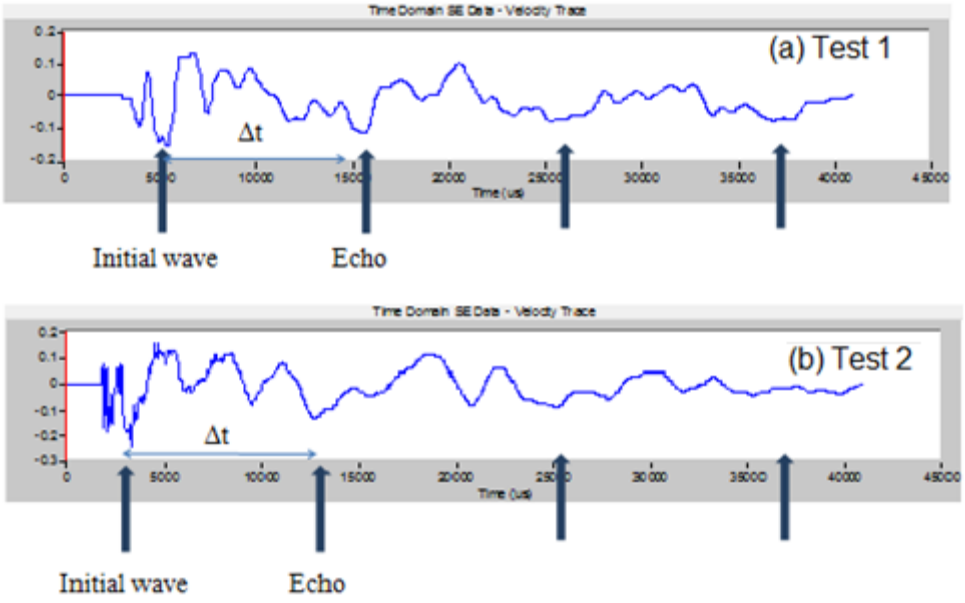

FIGURE 39 Velocity Graphs for Tests 1and 2 on the Concrete Column of Centennial Library on UNM Campus

The time differences between the initial wave and the first echo were similar for these two tests. The first and second arrows from the left are the impulse and the echo from the bottom respectively. It should be noted that the wave reflection from any change of impedance in the direction of the traveling wave along the column may be shown in the velocity graph. Valleys between marked arrows may also be due to the wave reflections at the junctions of each floor. Δt = 10 ms and the wave velocity is 10,000 ft/s, the length of the column is determined as:

$$L = \frac{v \times \Delta t}{2} = \frac{10000 \times 10 \times 10^{-3}}{2} = 50 \text{ ft}$$

The calculated length is close to the expected length of the column.

Results of Vertical Striking with Medium-hard Tip SE tests were repeated using a medium-hard tip. The velocity graphs for Tests 3 and 4 are shown in Figure 40. There are no high frequencies at the beginning of the velocity graphs. The time differences between the impulse and echo are similar to tests conducted by the hard tip (see Figure 39). Δt is still 10 ms and the calculated length is 50 ft.

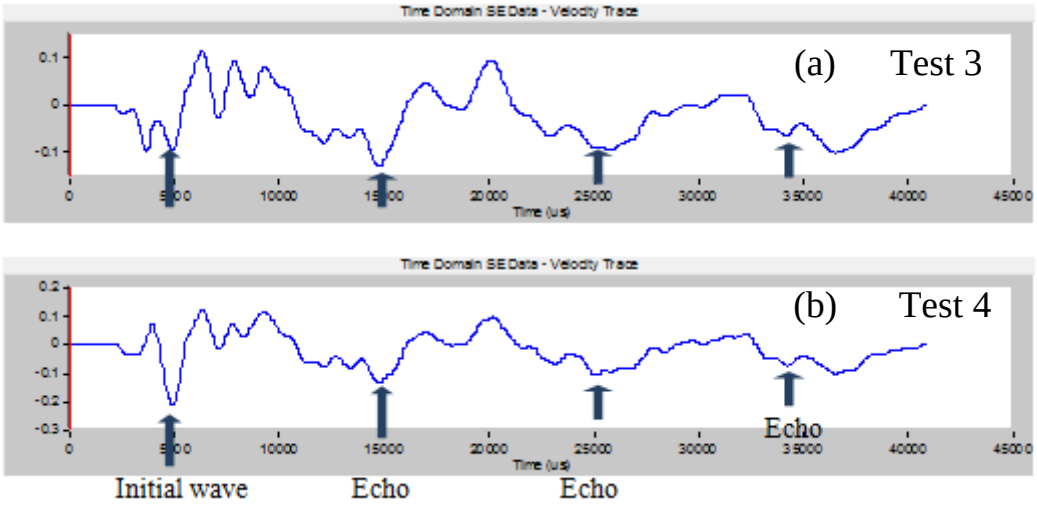

FIGURE 40 Velocity Graphs for Tests 3 and 4 on the Concrete Column of Centennial Library on UNM Campus

Results of Vertical Striking with Medium-soft Tip Medium-soft tip was used and the obtained velocity graphs are shown in Figure 41. Again, the results are similar to the velocity graphs using medium-hard tip (see Figure 40). In addition, no high frequency content can be found as seen in the velocity graph of hard tip (Figure 39b). Δt is still 10 ms and the calculated length is 50 ft.

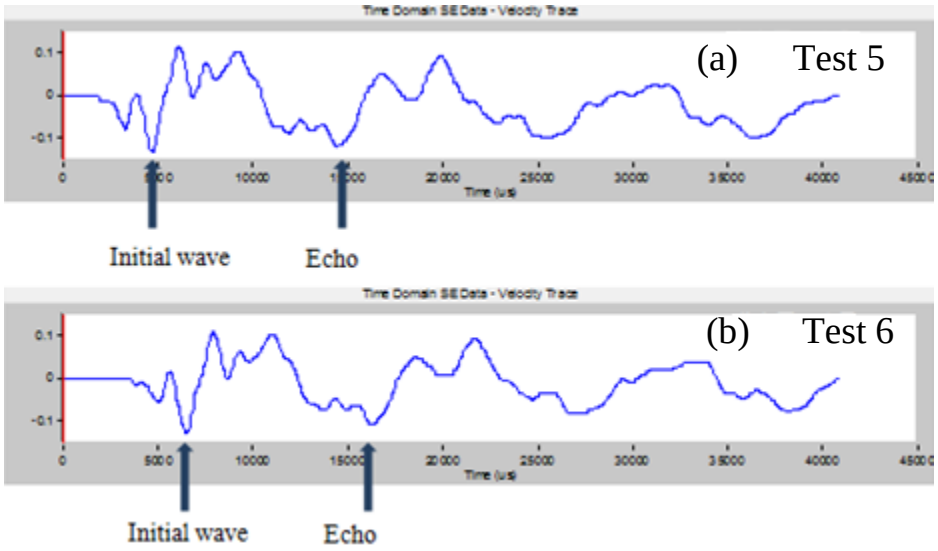

FIGURE 41 Velocity Graphs for Tests 5 and 6 on the Concrete Column of Centennial Library on UNM Campus

Results of Horizontal striking The hammer striking was applied horizontally with various hammer tips as listed in Table 6 (Tests 7 to 12). None of the results were good. A typical result is shown in Figure 42 for hard tip. There are many echoes in the graph but it is difficult to identify

the echo from the column end. Δt between echoes are too short to represent the length of the column. The reflections are due to other sources.

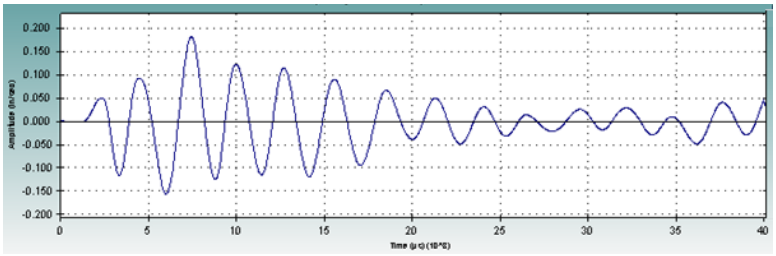

FIGURE 42 Velocity Graph for Horizontal Hammer Striking with Hard Hammer Tip on the Concrete Column of Centennial Library on UNM Campus

2.1.3.4 SE Tests on a Reinforced Concrete Wall

Since there are similarities in relative dimensions between a pier wall foundation and the reinforced concrete strong-wall at the Structural Lab of the Department of Civil Engineering at UNM (Figure 43), SE tests were conducted in the lab to study the applicability of the method on non-slender foundations. SE tests were carried out using vertical and horizontal striking with hard, medium-hard, medium-soft and soft hammer tips. Figure 44 shows the source (A~D) and the accelerometer locations (E, F and G). The accelerometer was mounted vertically on Points E, F or G. Wooden blocks were utilized to mount the accelerometers at Points F and G. Figure 49 shows the setup of one SE test.

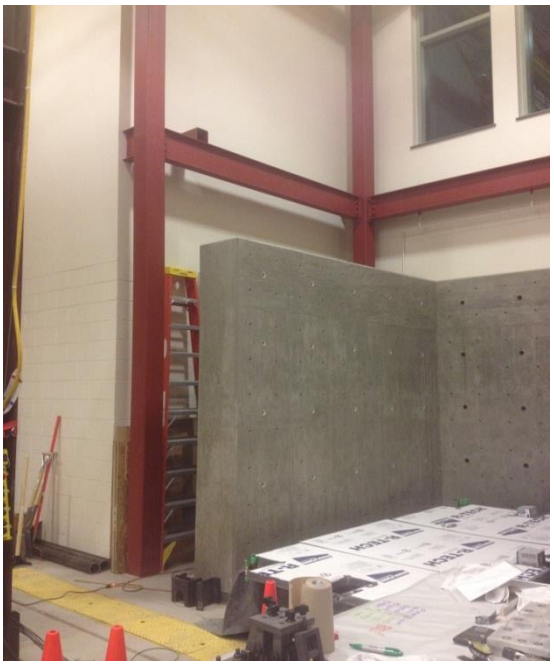

FIGURE 43 The Reinforced Concrete Wall in the Structural Lab

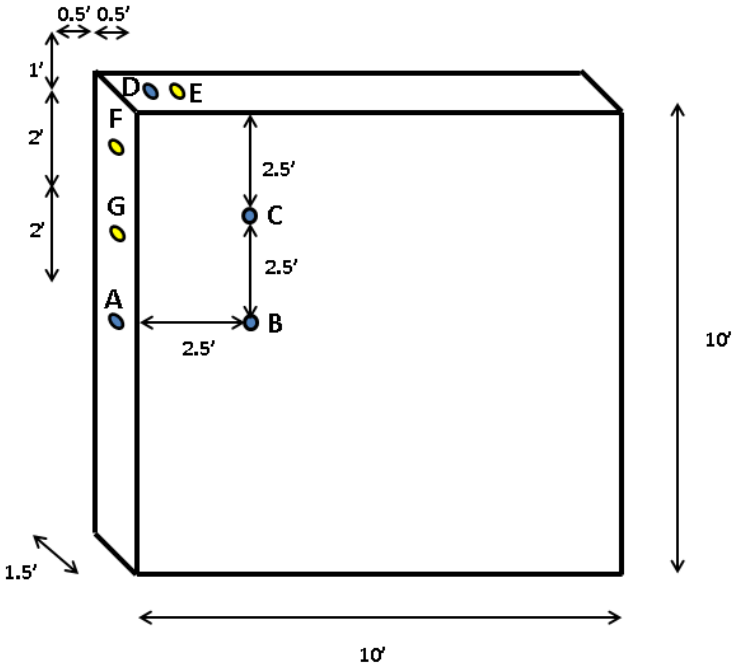

FIGURE 44 Locations of Striking Points (A to D) and Accelerometers (E, F and G) on the Reinforced Concrete Wall

FIGURE 45 An SE Setup on the Reinforced Concrete Wall

When the sources were applied by striking vertically on Point D and mounting the accelerometer at either points E, F and G, good signals were obtained with all hammer tips. We are able to determine the height of the wall. Figure 46 shows a velocity graph obtained at Point E when Point

D was stroke at with a hard-tip hammer. The Δt was determined from the time difference between impulse and echo. Δt = 2400 μs. The wave velocity of the concrete was assumed to be 10,500 ft/s. Since the sensor was mounted at the top, the wall's height with the concrete floor (L_t) was determined as follows:

$$L_t = \frac{v \times t}{2} = \frac{10500 \times 2400 \times 10^{-6}}{2} = 12.6 \text{ ft}$$

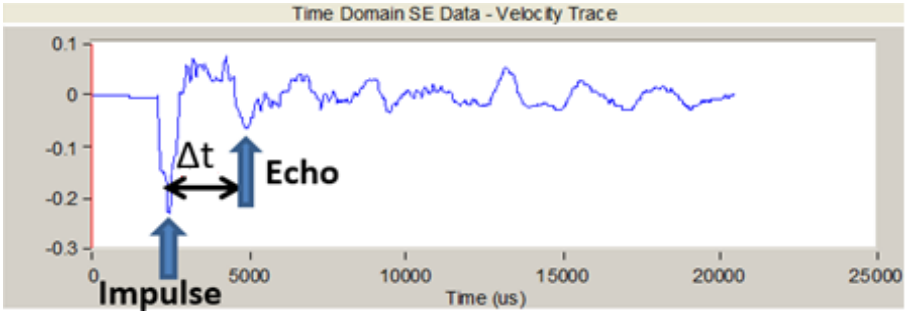

FIGURE 46 Velocity Trace of the Accelerometer at Point D with Hard Tip

On the other hand, when the source was applied by striking horizontally at Points A, B and C, the echoes from the bottom could not be determined since multiple echoes were shown near the expected echo from the bottom. This may be due to the lateral vibration of the wall. An example of poor velocity graphs is shown in Figure 47 obtained from horizontal striking at Point B.

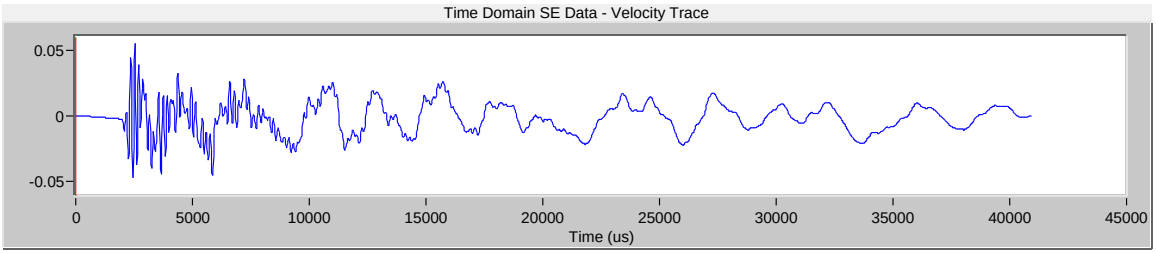

FIGURE 47 A Poor Velocity Graph Produced by Horizontal Striking

2.1.3.5 Conclusions of Preliminary SE Tests

SE tests were performed on a concrete wall and three columns composed of wood and concrete. The effect of striking direction, accelerometer location, and hammer tip type were investigated. When the top of the wall (or columns) was accessible, striking on the top surface produced the most interpretable results (highest success rate in the determination of the length). While the top of the column was inaccessible, striking on the pavement next to the column could introduce proper longitudinal waves through the column (medium success rate due to the reduction of energy). Horizontal striking produced lateral vibrations in lieu of longitudinal waves which complicated the velocity graphs. No success in SE tests performed by horizontal striking has been obtained in the preliminary SE tests.

In addition to selecting the best striking method, the sensors should be properly placed to capture the longitudinal vibration. The preliminary SE tests result indicates that vertical placement of a sensor on the side of the wall or columns produces good results. However, when the sensor was placed too close to the striking point (less than 1 ft), the noise of initial high frequency vibrations

may contaminate the velocity graph. Thus, it is recommended that the sensors be placed 1-2 ft away from the striking point to prevent the disturbing effect of the high frequency vibrations. It should be noted that using softer hammer tips decreases the high frequency content of the velocity signal which may ease the interpretation in some cases.

Based on the preliminary tests' observations, the following instructions are suggested for implementation in the field:

1) A combination of a vertical strike and vertically placed sensors is a proper way to conduct SE/IR tests.
2) Since the outcome of SE/IR tests depends on the energy (strength) of the longitudinal wave, vertical striking on the top of the foundation is the best method to use.
3) When the top of the foundation is inaccessible, the accelerometers should be placed vertically on the side of the foundation no closer than 1-2 feet from the striking point.
4) If high frequencies conceal either impulse or echo in the velocity graphs, using softer hammer tips may remove the disturbing high frequencies and consequently eases the interpretation.
5) Although the wave propagation inside a reinforced concrete wall was different from slender elements (columns or piles), applying a vertical strike at the top of the wall yielded successful tests. Placing the accelerometers vertically on the top or on wooden blocks attached to the side of the wall produced good results.

2.1.4 Field SE/IR Tests

2.1.4.1 Santo-Domingo Bridge

The Santo Domingo Railroad Bridge was selected by NMDOT for initial SE field tests. The tests were carried out with the existing SE equipment owned by NMDOT. The bridge is located 42 miles northeast of Albuquerque. The latitude and longitude coordinates of the location for this railroad bridge are: 35.488752, -106.385058. The bridge is supported by round timber piles. Figures 48 and 49 show the location and street view of the bridge, respectively.

FIGURE 48 Location of the Santo Domingo Bridge

FIGURE 49 Street View of the Santo Domingo Bridge

Sixteen SE tests were conducted on two timber piles at Bents 7 and 8. Figure 50 depicts the foundation plan and test piles.

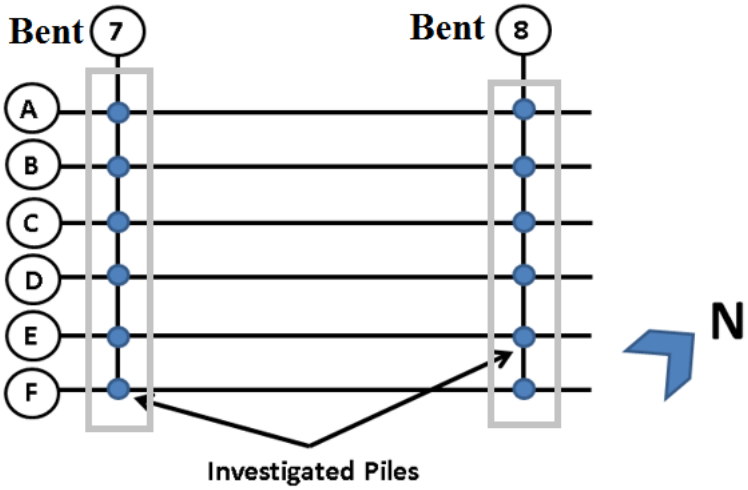

FIGURE 50 Foundation Plan and Investigated Piles of Santo Domingo Bridge

Six SE tests were performed on Pile 7-F and seven on Pile 8-E. The test setup is shown in Figure 51. Although horizontal striking did not result in interpretable velocity signals in preliminary tests, it was decided to examine if horizontal striking on the side of a pile could produce useful result in the field. Vertical striking on a metal block was used on Pile 8-E as the source. The metal block used for vertical striking was attached to the pile surface tightly. The accelerometer was attached vertically on a metal block attached to the pile. The specifications of SE tests are indicated in Table 8.

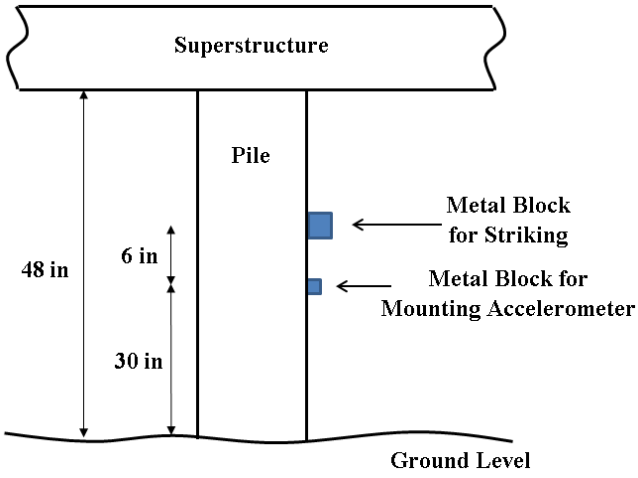

FIGURE 51 SE Tests Setup for the Santo Doming Bridge Piles (Not to Scale)

TABLE 8 Specifications of SE Tests Performed on the Santo Domingo Bridge Piles.

Pile	Test No.	Hammer Tip	Direction of Strike
7-F	1 - 4	Hard	Horizontal
7-F	5 - 6	Medium-hard	Horizontal
8-E	7 - 8	Medium-hard	Vertical
8-E	9 - 10	Medium-Soft	Vertical
8-E	11 - 13	Hard	Vertical

Tests 1 to 6 were performed on Pile 7-F with horizontal striking. The results were not useful and the length of the pile could not be determined. A typical velocity graph (Test 1) is shown in Figure 52. The arrows in the figure indicate the high frequency vibrations. These high frequencies may be due to the reflections of impedance change in the pile or may relate to the lateral vibration of the pile. Reflections from the pile toe were not found.

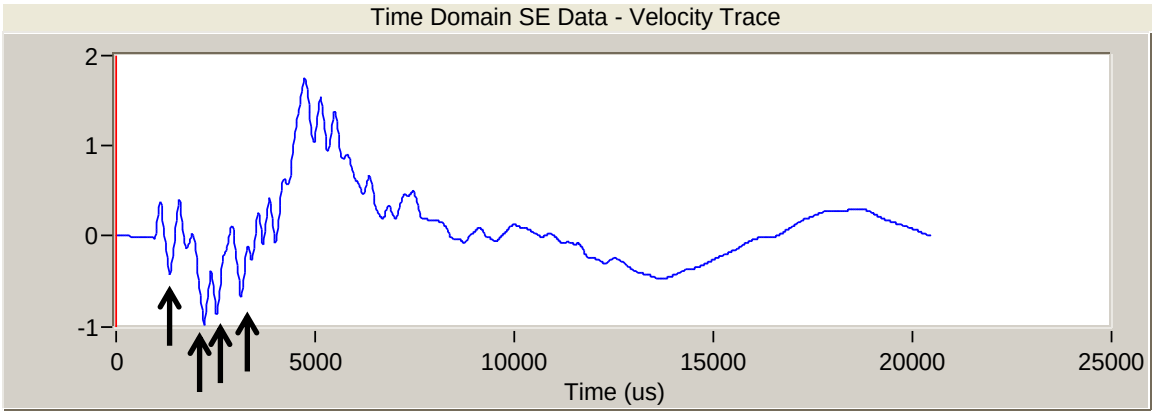

FIGURE 52 Velocity Graph from the Accelerometer (Pile 7-F)

For Pile 8-E, the accelerometer was mounted vertically on a block attached to the pile and the source was applied by vertical striking with medium-hard and medium-soft tips (Tests 7 to 10) and hard tip (Tests 11-13). The velocity graphs of medium-hard and medium-soft tips are shown in Figures 53 to 56. Poor results were obtained since the impulse was difficult to identify in the velocity graph (too many valleys at the beginning of the velocity graph). Also, we cannot pick one of valleys because the velocity magnitude of the impulse should be greater than the magnitude of the echoes. It was identified in the field that the attachment of the accelerometer was loose. The attachment was then corrected and the tests were repeated with hard tip (Tests 11 to 13). The velocity graphs of these three tests are shown in Figures 57 to 59. The impulses and echoes (shown as arrows) are clearly visible in the velocity graphs.

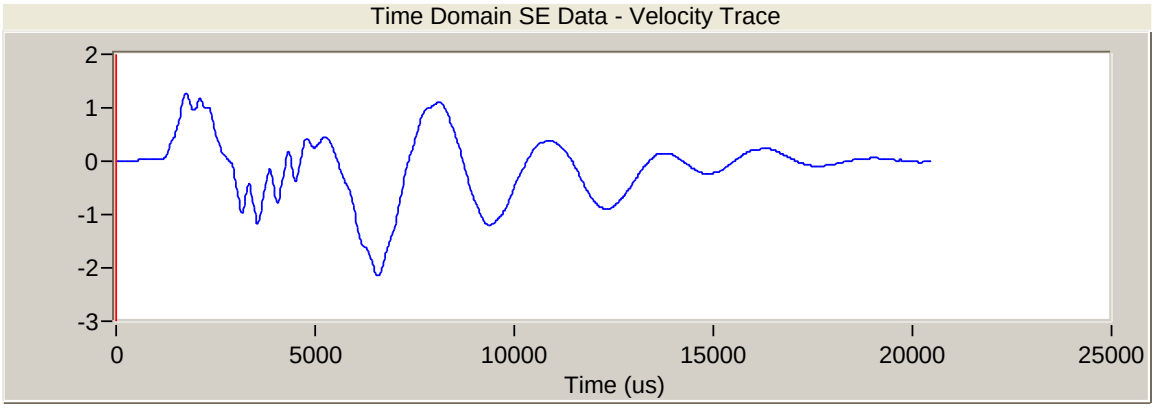

FIGURE 53 Velocity Graph of Test 7

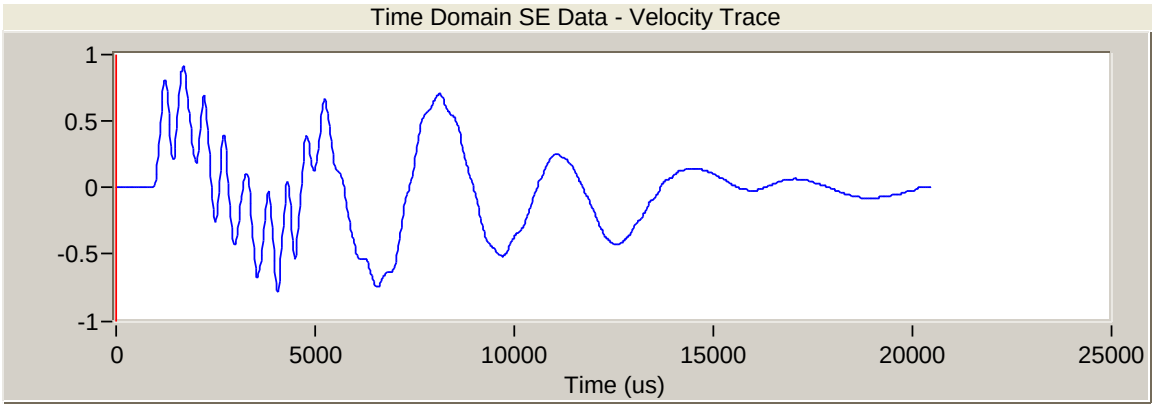

FIGURE 54 Velocity Graph of Test 8

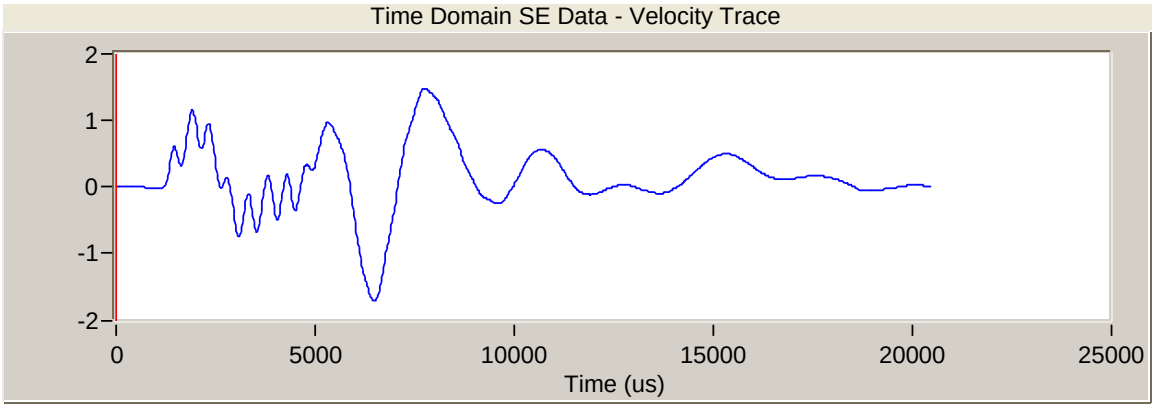

FIGURE 55 Velocity Graph of Test 9

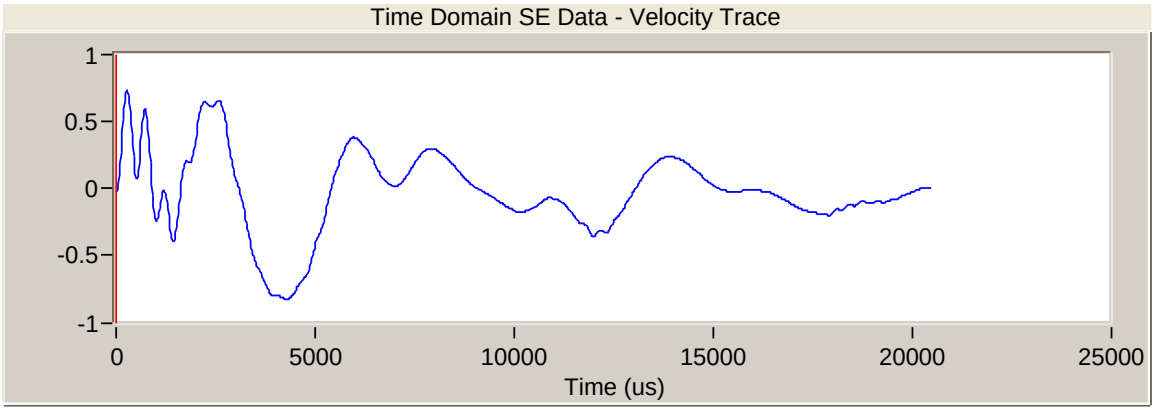

FIGURE 56 Velocity Graph of Test 10

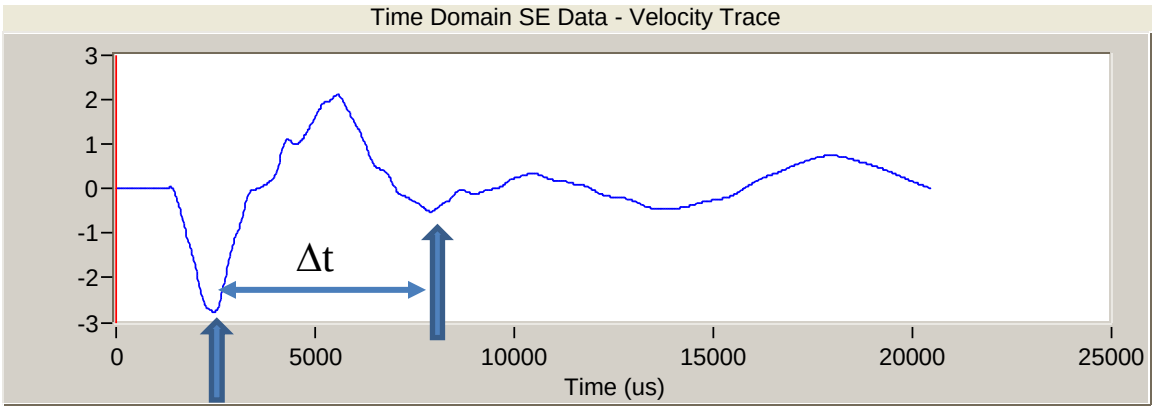

FIGURE 57 Velocity Graph of Test 11

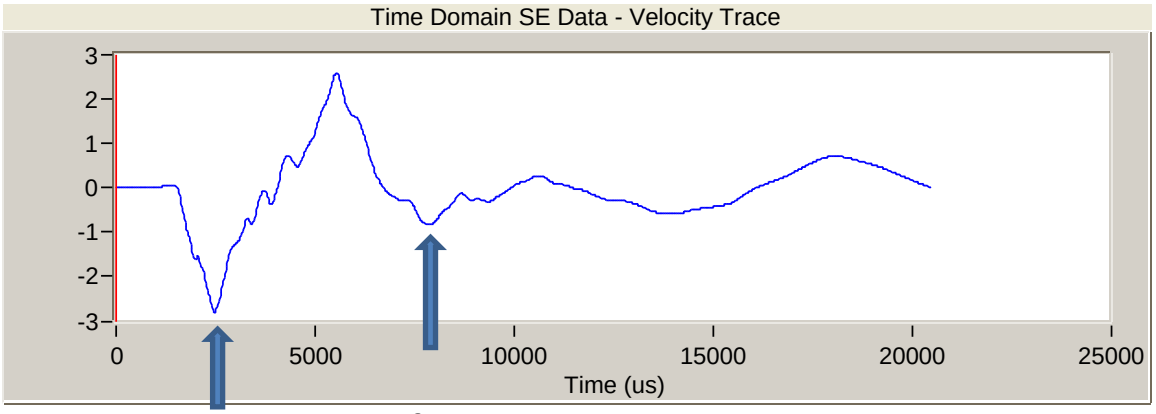

FIGURE 58 Velocity Graph of Test 12

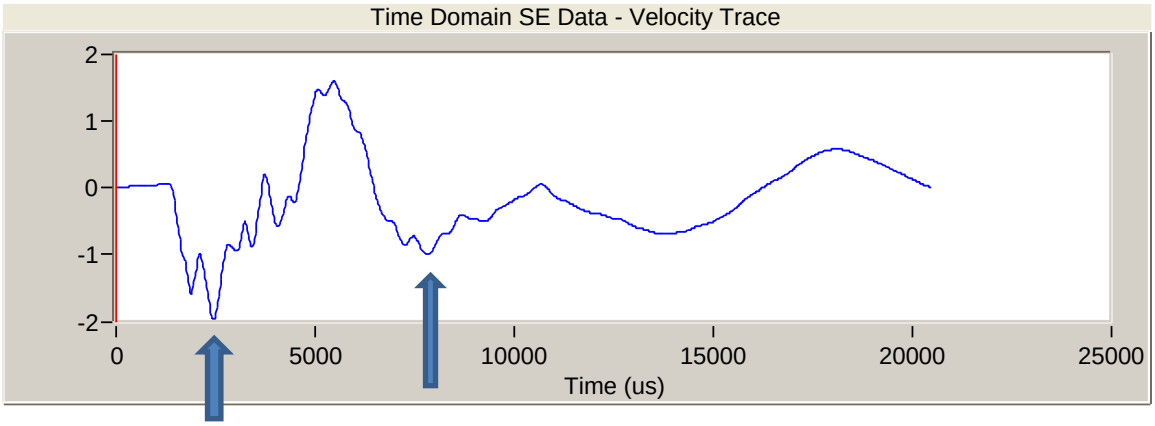

FIGURE 59 Velocity Graph of Test 13

The velocity graph of Test 11 (see Figure 57) was used to demonstrate the calculation of the total (L_t) and embedment depth (L_b) of Pile 8-E. As shown in Figure 57, Δt = 5,500 μs. The wave velocity of the pile is 11,500 ft/s and the sensor was located 1.5 ft from the top of the pile. The length of the pile was determined as:

$$L_t = \frac{v \times \Delta t}{2} + 1.5 = \frac{11500 \times 5500 \times 10^{-6}}{2} + 1.5 = 33.1 \text{ ft}$$

The embedment length is 29.1 ft since the exposed length is about 4 ft.

Table 9 shows the calculated embedment depths and the lengths of Pile 8-E.

TABLE 9 Calculated Pile Lengths of Pile 8-E.

Test No.	Δt (μs)	Embedment Depth (ft)	Total Length (ft)
11	5500	29.1	33.1
12	5420	28.7	32.7
13	5400	28.5	32.5

Summary of Results The test results for the two investigated piles are summarized in Table 10. Based on the numbers of tested piles, the success rate is 50% (1 out of 2).

TABLE 10 Estimated Lengths of Piles of Santo Domingo Bridge.

Pile	Embedment Pile Length (ft)	Exposed Pile Length (ft)	Total Pile Length (ft)
7-F	--*	4.1	--
8-E	28.8	4	32.8

Note * -- denotes unsuccessful tests

2.1.4.2 Bridge No. 6922

Bridge No. 6922 is located 40 miles east of Las Vegas on NM 104. The latitude and longitude coordinates of the bridge are 35.477197, -104.613580. The bridge location and street view of the bridge are shown in Figures 60 and 61 respectively. Numerous SE tests were conducted on 5 round timber piles. The foundation plan and investigated piles are indicated in Figure 62.

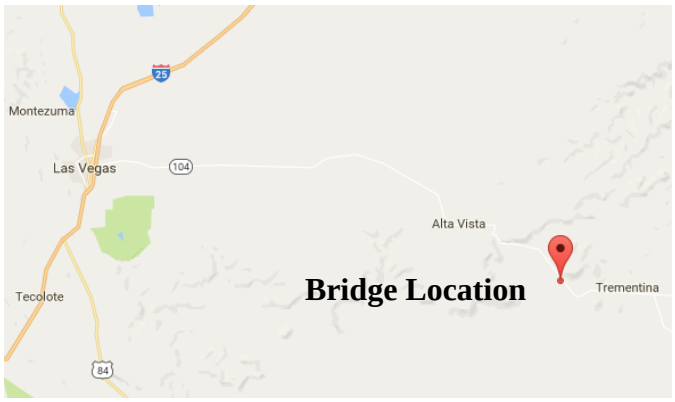

FIGURE 60 Location of Bridge No. 6922

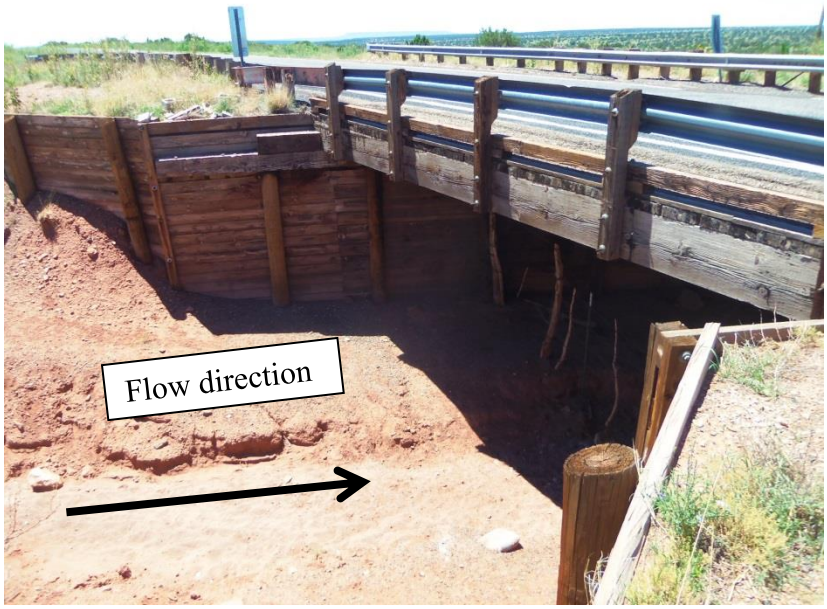

FIGURE 61 Street View of Bridge No. 6922

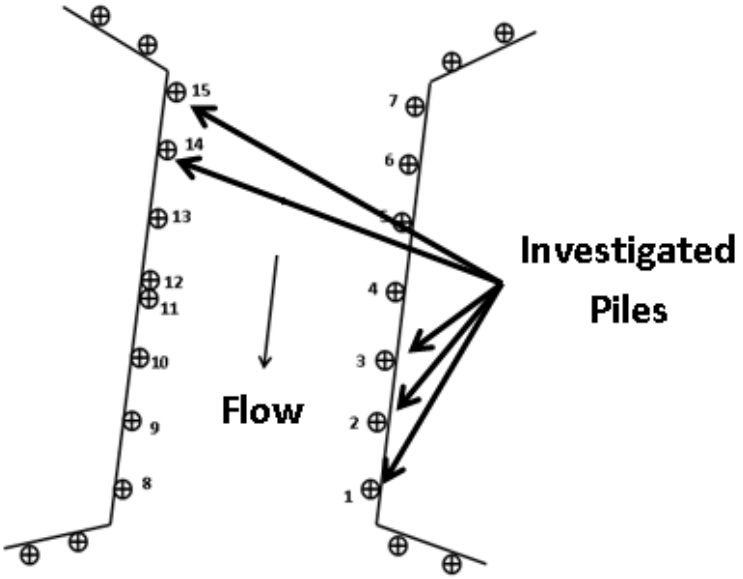

FIGURE 62 Foundation Plan and the Investigated Piles of Bridge No. 6922

The source was applied by three different hammer strikes:

- Vertical strike at the top of the pile (when the girder does not cover the entire pile's top surface such that part of the top surface of a pile is exposed)
- Vertical strike on a wooden block attached to the side of the piles
- Vertical strike on an aluminum block attached to the side of the piles

Two accelerometers were placed vertically on wooden blocks attached to the pile's side surface. The typical SE test setup is shown in Figure 63. The locations of the blocks in each tested pile are depicted in Figures 64 to 68 for Piles 1, 2, 3, 14, and 15 (see Figure 62).

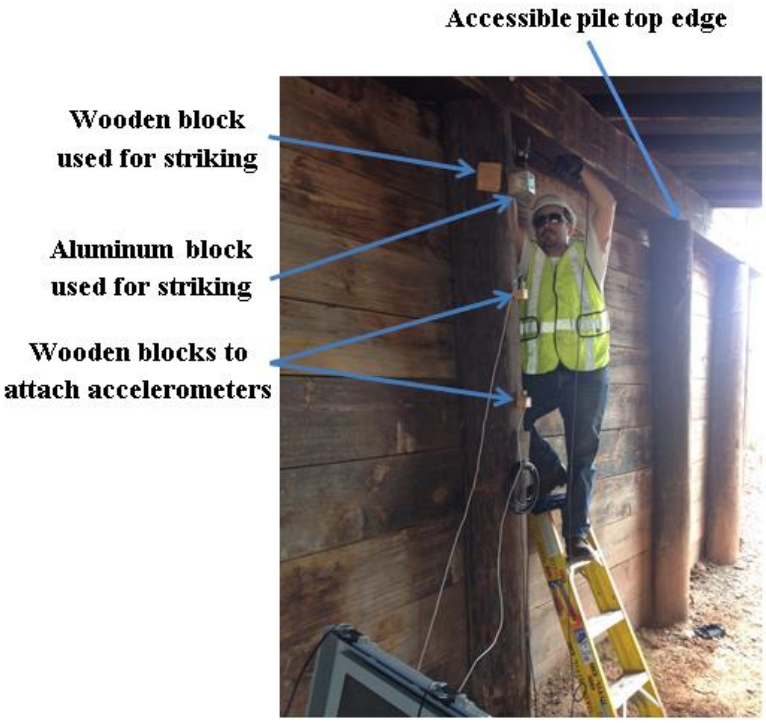

FIGURE 63 Typical SE Test Setup for Piles of Bridge No. 6922

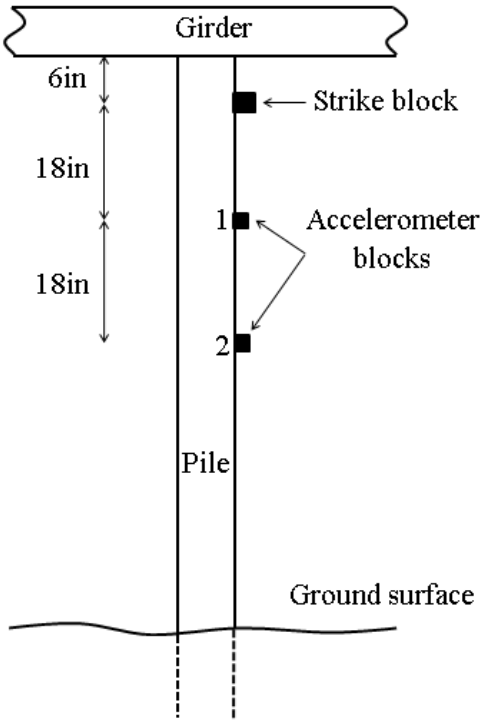

FIGURE 64 Location of Source and Accelerometers on Pile 1

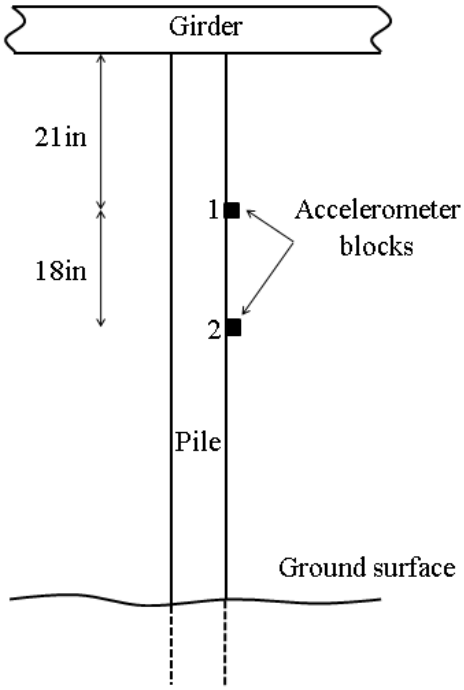

FIGURE 65 Location of Source and Accelerometers on Pile 2

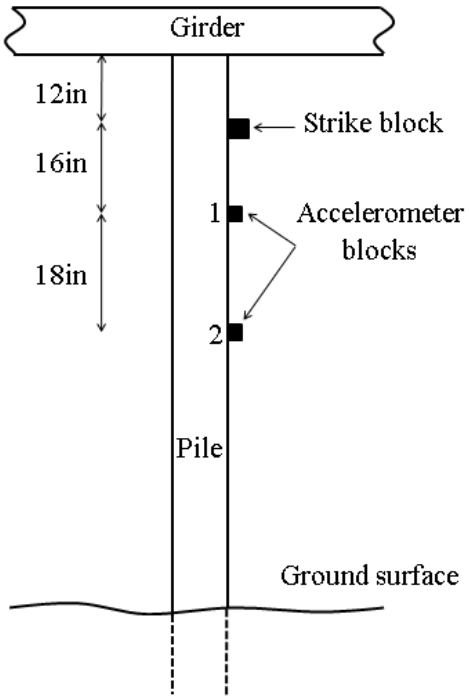

FIGURE 66 Location of Source and Accelerometers on Pile 3

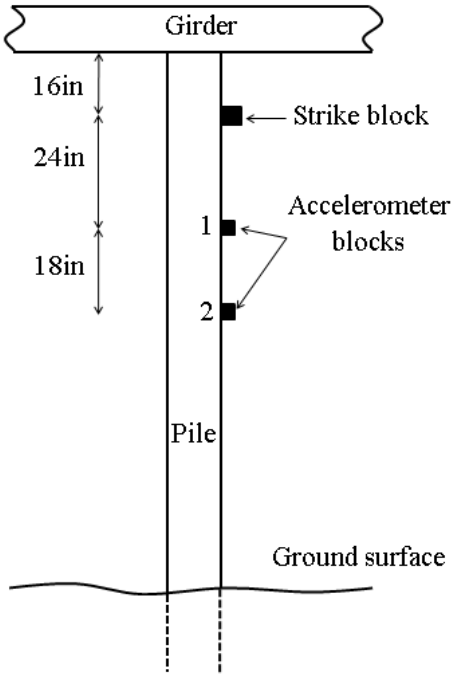

FIGURE 67 Location of Source and Accelerometers on Pile 14

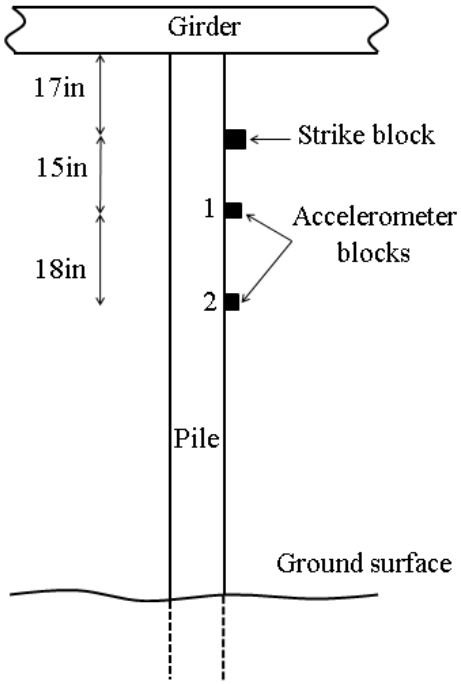

FIGURE 68 Location of Source and Accelerometers on Pile 15

Determining Propagated Wave Velocity in a Pile The propagated wave velocity was measured at Pile 2. Two accelerometers were placed far apart (79 in) so that the arrival times at these two sensors are distinguishable. Accelerometer 1 was closer to the top of the pile while accelerometer 2 was closer to the ground. This test is different from other SE tests that the distance between two accelerometers are 18 in. The time difference between the two arrival times was used to determine the wave velocity. The velocity graphs of accelerometers 1 and 2 are shown in Figure 69.

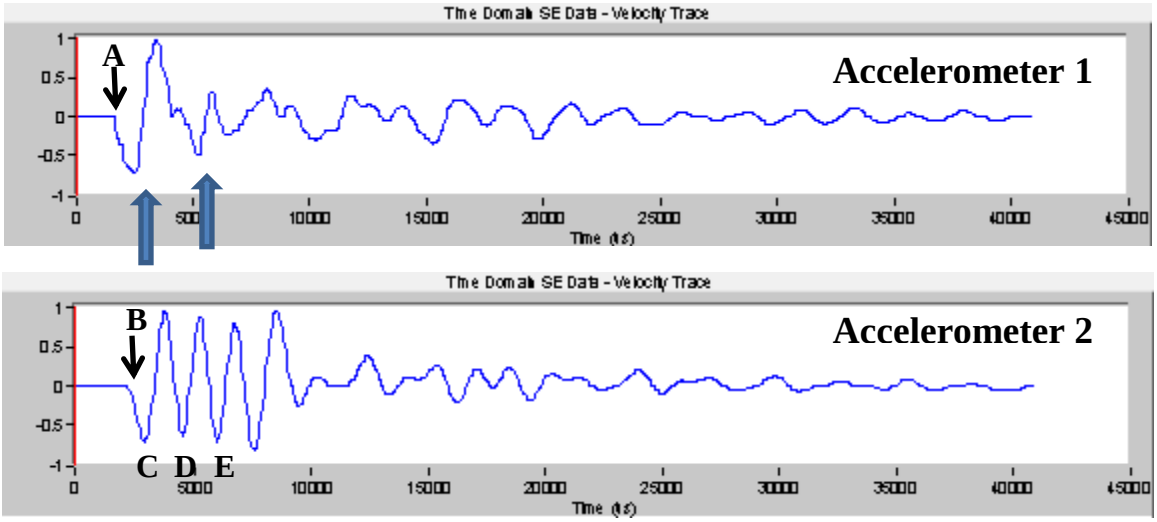

FIGURE 69 Velocity Graphs of Accelerometers 1 and 2

Points A and B show the first arrival times at accelerometers 1 and 2. The time difference (Δt) between points A and B was used to estimate the wave velocity. Since the distance between accelerometers (ΔL) is 79 in (6.58 ft) and Δt =1.96 - 1.46 = 0.5 ms, the wave velocity is estimated as:

$$v = \frac{\Delta L}{\Delta t} = \frac{6.58}{0.0005} = 13{,}160 ft/s$$

The appearance of these two velocity graphs is very different due to the locations of the two sensors. For accelerometer 1, Δt was found to be 2.76 ms and the calculated length of the pile is 19.9 ft using 13,160 ft/s as the propagated wave velocity.

Many echoes are shown in the velocity graph for accelerometer 2. The time difference between Points C (first valley) and D (second valley) is 1.62 ms. The estimated distance between the sensor and the bottom is:

$$L_{tr} = \frac{v \times \Delta t}{2} = \frac{13160 \times 1.62 \times 10^{-3}}{2} = 10.7 \text{ ft}$$

Since the distance between the accelerometer and pile top is 8.35 ft, the total pile length is estimated as L =10.7 + 8.35 = 19.05 ft. This value is very close to the estimated pile length from accelerometer 1 (19.9 ft). The reflected up-going wave continued to go upward. Then the wave was reflected at the pile top and became a down-going wave arriving at the sensor at Point E.

Since the distance between the accelerometer and pile top is 8.35 ft, the wave traveled 16.7 ft (ΔL) before returning to the accelerometer. The required time for this path is:

$$\Delta t = \frac{\Delta L}{v} = \frac{16.7}{13160} = 0.00127 \text{ sec} = 1.27ms$$

This calculated time is close to the time difference between Points D and E in Figure 69b (1.5 ms).

The above-mentioned calculations show that the multiple peaks observed at the accelerometer located far from the pile top was related to the multiple reflections from both the top and the bottom of the pile. The accelerometer closer to the top of the pile provided result that was easy to interpret. Reflections from both ends can complicate the velocity graphs. Additional discussion is presented later in the finite element analysis.

SE/IR Tests on Pile 1 Six SE/IR tests were conducted on Pile 1. A portion of the pile top surface was accessible; therefore, half of the tests were carried out by striking at the top of the pile. Table 11 indicates the specification of the six SE/IR tests conducted on Pile 1.

TABLE 11 SE Tests Conducted on Pile 1.

Test No.	Hammer Tip	Strike at
1	Hard	Top (edge)
2	Medium-hard	Top (edge)
3	Medium-soft	Top (edge)
4	Hard	Aluminum block
5	Medium-hard	Aluminum block
6	Medium-soft	Aluminum block

SE/IR Tests with Striking on Top of the Pile Results obtained from top striking showed that, hard and medium-hard hammer tips produced good data. However, poor results were found for medium-soft tip as shown in Figure 70. The impulse, the first largest magnitude, was expected to be a valley (compression down-going wave) and not a peak (tensile wave) as shown in this figure. The first valley was not related to the direct down-going compression wave. Since the impulse was difficult to identify, Δt cannot be determined.

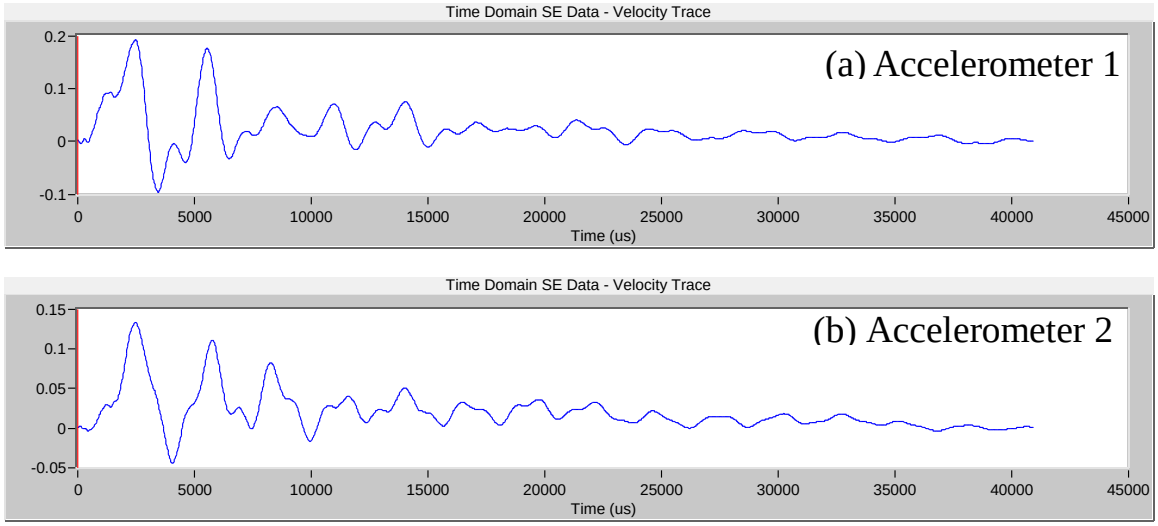

FIGURE 70 Velocity Graphs of Test 3

Table 12 shows the calculated length of Pile 1 using the Δt determined in the velocity graphs of Tests 1 and 2.

TABLE 12 Estimated Length of Pile 1 from SE Analysis.

Test No.	Accelerometer 1				Accelerometer 2			
	Δt (ms)	L_{tr} (ft)	L_a (ft)	L_t (ft)	Δt (ms)	L_{tr} (ft)	L_a (ft)	L_t (ft)
1	2.84	18.7	2	20.4	2.28	15	3.5	18.5
2	3.52	23.2	2	25.2	3.64	24	3.5	27.5

As stated before, the Impulse Response (IR) analysis based on the frequency content of the entire waveform can provide additional information to validate the results of time domain analyses in some cases. The obtained mobility graphs obtained from Tests 1 to 3 indicated clear resonant frequencies. The mobility graph obtained from accelerometer 1 in Test 1 is shown in Figure 71 as an example. The arrows indicate the resonant frequencies of the pile. The total length of the pile was calculated as:

$$L_t = \frac{v}{2\times\Delta f} = \frac{13160}{2\times 363} = 18.1 \text{ ft}$$

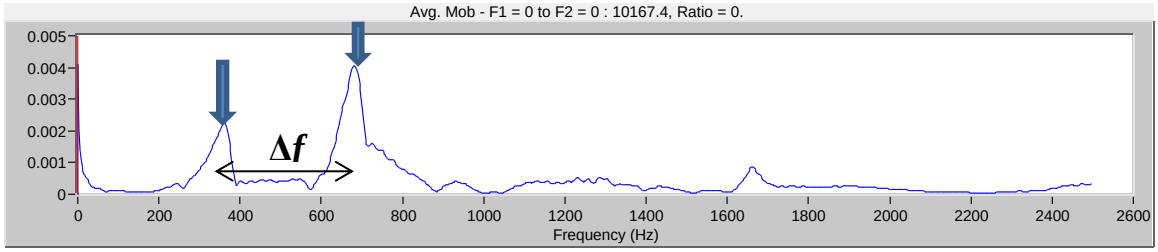

FIGURE 71 Mobility Graph Obtained from Accelerometer 1 (Test 1)

The calculated lengths of Pile 1 based on IR analysis are summarized in Table 13. Note that the variation of the calculated length is smaller than the variation calculated by SE analysis (see Table 12). Also, the IR analysis of Test 3 could estimate the length of the pile but the SE analysis was not. Therefore, IR analysis should be carried out when poor results are observed from SE analysis.

TABLE 13 Estimated Length of Pile 1 from IR Analysis.

Test No.	Accelerometer 1		Accelerometer 2	
	Δf (Hz)	L_t (ft)	Δf (Hz)	L_t (ft)
1	363	18.1	357	18.4
2	364	18.1	364	18.1
3	358	18.4	363	18.1

SE/IR Tests with Aluminum Striking Block Three SE/IR tests were conducted by striking an aluminum block with hard, medium-hard and medium-soft hammer tips (Tests 4 to 6 respectively). The force graphs of the hammer for Tests 4 and 5 are shown in Figure 72. The shapes of the impulses are different from the typical hammer impulse shown in Figure 73. Multiple peaks were shown in the graphs produced by striking on the aluminum block. The peaks may be due to the small sliding of the block on the surface of pile and occurrence of a momentary contact loss or multiple contacts between the block and pile surface.

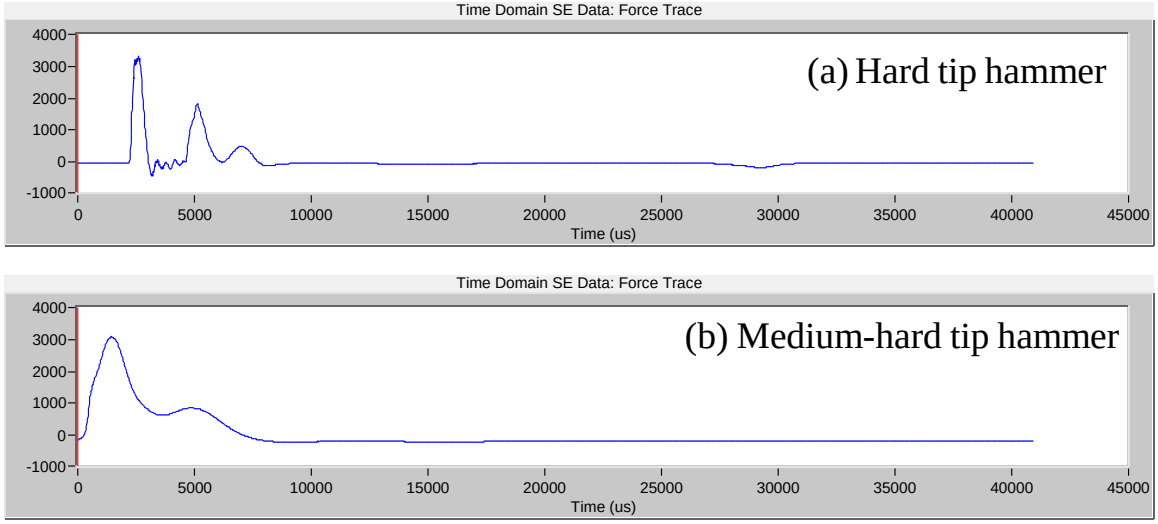

FIGURE 72 Impulse Signals of Striking on an Aluminum Block

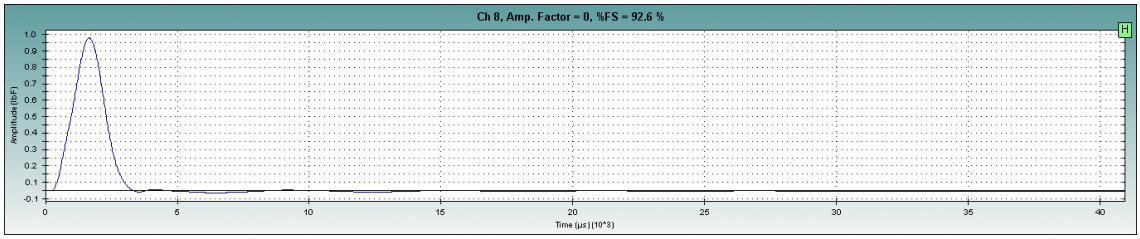

FIGURE 73 Impulse Signal of Striking on a Solid Surface

In some cases, the velocity graphs from the accelerometers showed complicated vibrations in the initial part of the graphs as shown in Figure 74. The impulse and echo could not be identified. Table 14 summaries the SE results on this pile.

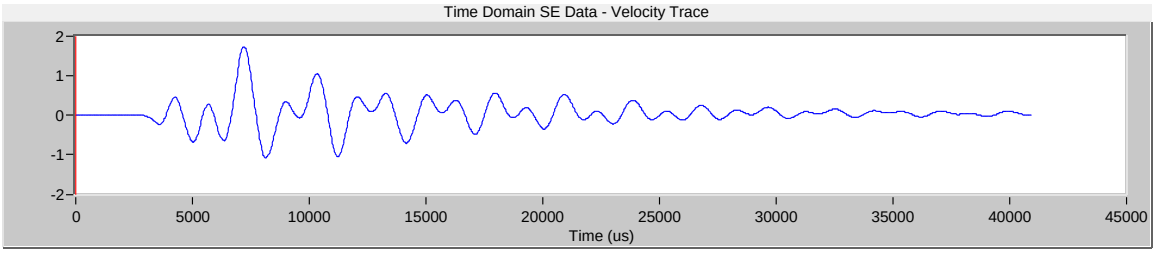

FIGURE 74 Velocity Graph Obtained from Accelerometer 1 (Test 4)

TABLE 14 Estimated Length of Pile 1 from SE Analysis (Tests 4 to 6).

Test No.	Accelerometer 1				Accelerometer 2			
	Δt (ms)	L_{tr} (ft)	L_a (ft)	L_t (ft)	Δt (ms)	L_{tr} (ft)	L_a (ft)	L_t (ft)
4	-	-	2	-	2.36	15.5	3.5	19
5	3.24	21.3	2	23.3	-	-	3.5	-
6	2.96	19.5	2	21.5	-	-	3.5	-

IR analyses were performed for Tests 4-6. A mobility graph obtained from Accelerometer 1 in Test 5 indicating clear resonant frequencies shown in Figure 75. Table 15 indicates the calculated length of the pile based on Δ*f*. Unlike the previous case (striking on the top of the pile), IR analysis did not always work. Therefore, IR analysis could determine the pile length in some cases.

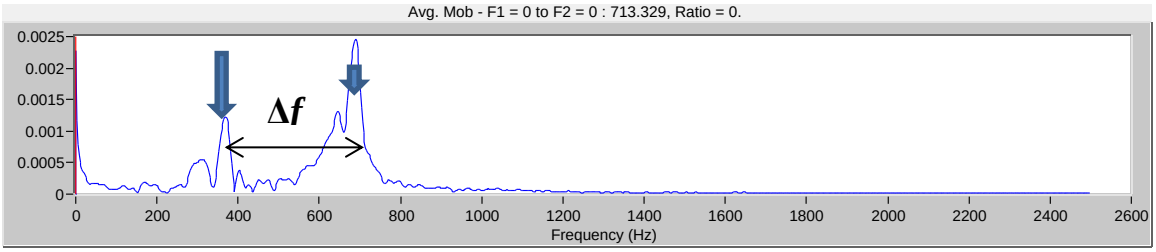

FIGURE 75 Mobility Graph of Test 6

TABLE 15 Estimated Length of Pile 1 from IR Analysis (Tests 4 to 6).

Test No.	Accelerometer 1		Accelerometer 2	
	Δf (Hz)	L_t (ft)	Δf (Hz)	L_t (ft)
4	-	-	-	-
5	354	18.6	357	18.4
6	372	17.7	-	-

SE/IR Tests Pile 2 Four SE tests were performed on Pile 2. Hard hammer tip was used for Tests 7 and 10. Medium-hard and medium-soft tips were utilized in Tests 8 and 9 respectively. The source was applied by striking the top of the pile for all tests. All results were poor except for one

velocity graph shown in Figure 76. This was for Accelerometer 1 in Test 7 and the impulse and echo were clearly identifiable in the figure. Δt is 2.76 ms and the corresponding pile length is 19.9 ft. Figure 77 shows an example of poor results. The use of softer tips did not help here.

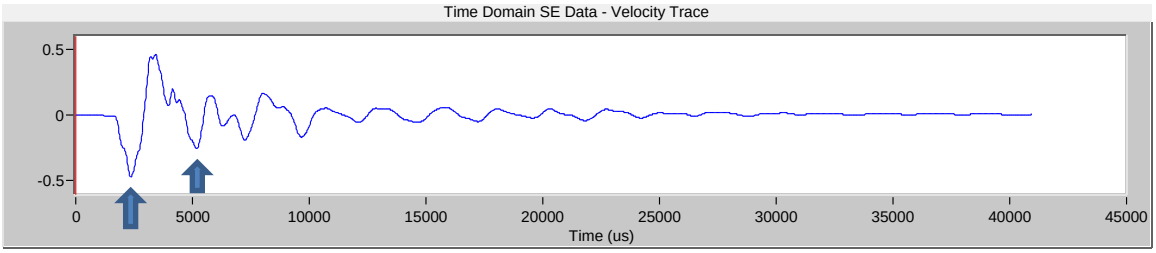

FIGURE 76 Velocity Graph of Accelerometer 1 (Test 7)

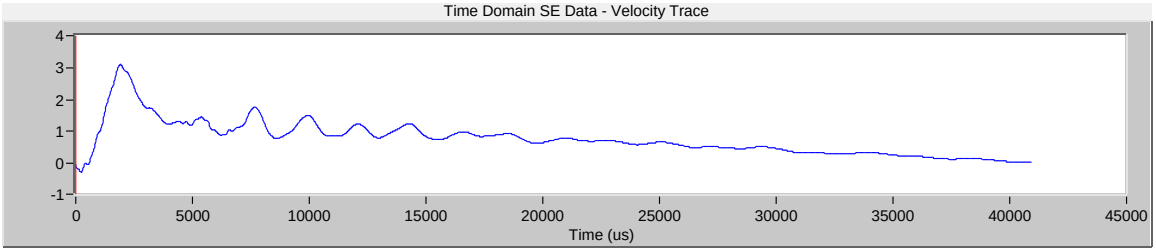

FIGURE 77 Velocity Graph of Accelerometer 1 (Test 9)

IR analysis of the data did not reveal any resonant frequencies. IR analysis could not aid the determination of pile length in this case.

SE Tests on Pile 3 Since the top of the pile was inaccessible, a wooden block and an aluminum block were attached onto the side of the pile and hard and medium-hard hammer tips were used.

SE Tests Performed with Wooden Striking Block and Hard tip Hammer SE tests were conducted by hard hammer tips in Tests 11 to 13. Since the source was applied manually, the only difference between Tests 11 to 13 was the difference between their input energies and impulse shapes (Figure 78). These source signal graphs show more regular shapes compared to sources produced by aluminum blocks (Figure 72). The corresponding velocity graphs for Tests 11 to 13 are indicated in Figures 79 to 81 respectively.

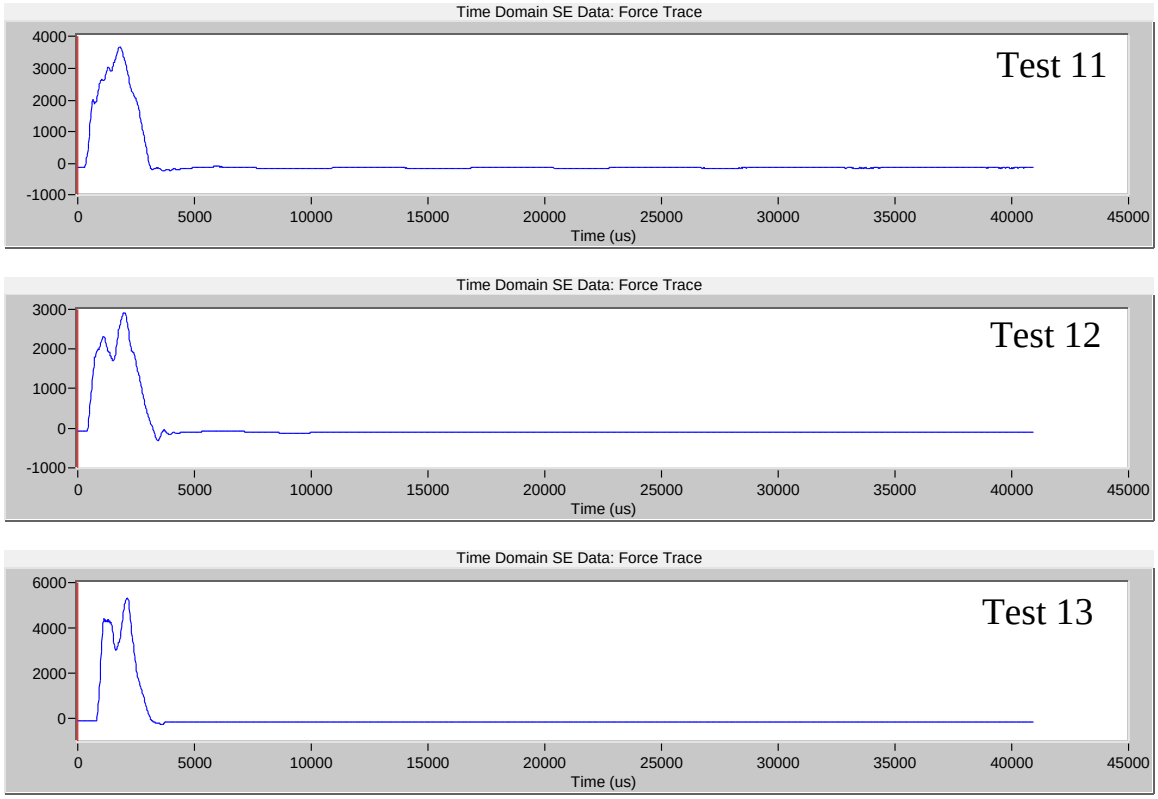

FIGURE 78 Initial Impulse from the Hammer's Force Sensor (Wooden block, Hard-tip)

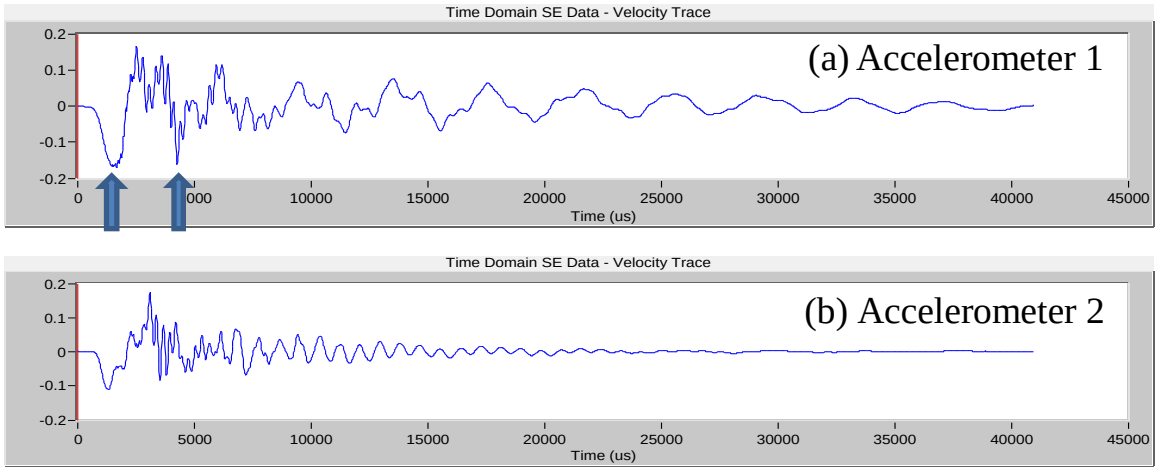

FIGURE 79 Velocity Graphs of Test 11

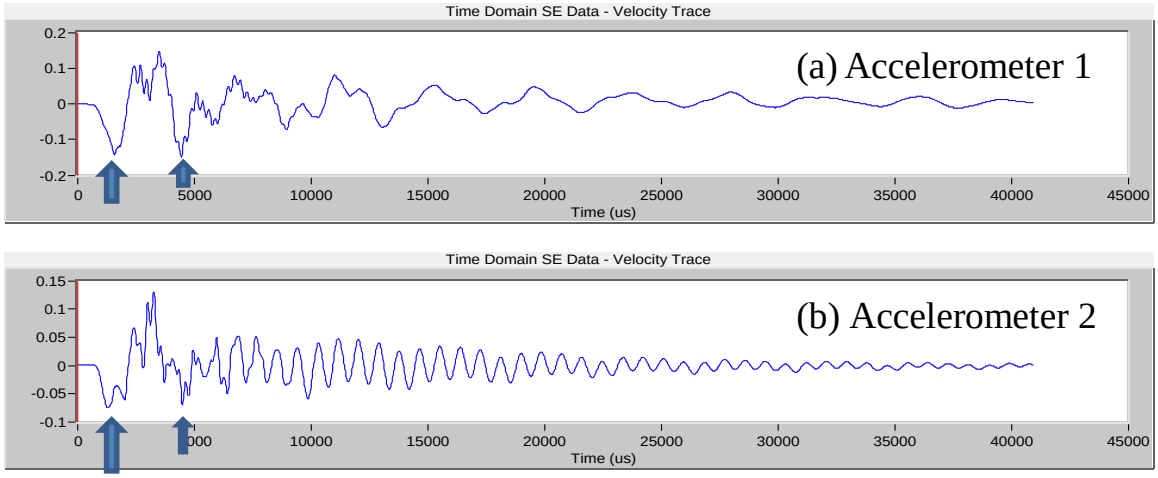

FIGURE 80 Velocity Graphs of Test 12

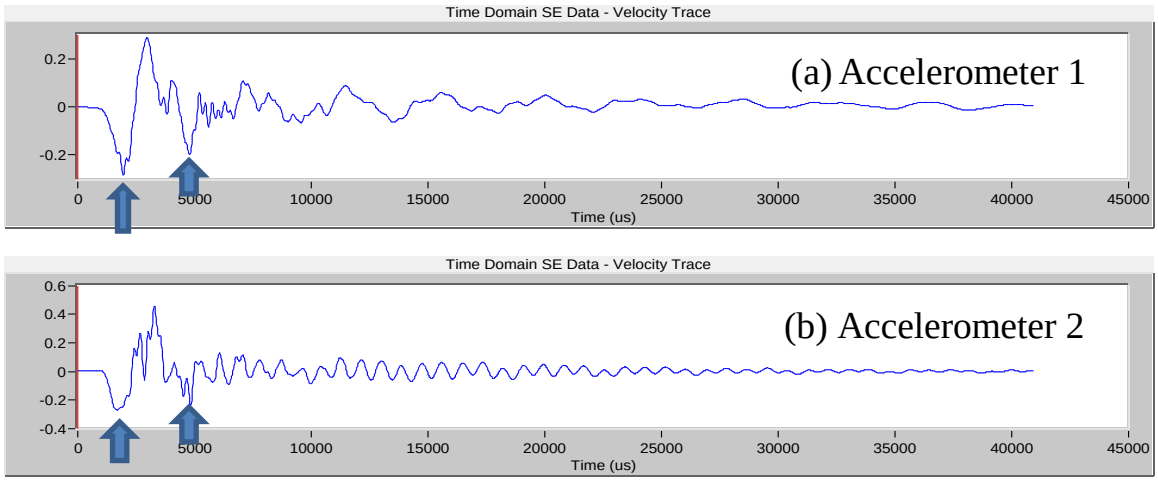

FIGURE 81 Velocity Graphs of Test 13

The result shows recognizable impulses and echoes except for Accelerometer 2 in Test 11. The clarity of these impulses and echoes implies that marginally irregular impulse shapes of the source may produce useful velocity graphs. Table 16 shows the calculated length of Pile 3 from Tests 11 to 13.

TABLE 16 Estimated Length of Pile 3 (Tests 11 to 13)

Test No.	Accelerometer 1				Accelerometer 2			
	Δt (ms)	L_{tr} (ft)	L_a (ft)	L_t (ft)	Δt (ms)	L_{tr} (ft)	L_a (ft)	L_t (ft)
11	2.8	18.4	2	20.4	-	-	3.5	-
12	2.84	18.7	2	20.7	3.22	21.2	3.5	24.7
13	2.84	18.7	2	20.7	3.16	20.8	3.5	24.3

SE/IR Tests Performed with Wooden Striking Block and Medium-hard Tip Hammer Three SE tests were conducted with medium-hard tip hammer in Tests 14 to 16. The source signals in Tests

14 to 16 are shown in Figure 82; the shape of the source signal is better that that of hard tip (see Figure 78). The corresponding velocity graphs obtained from Accelerometer 1 and 2 are shown in Figures 83 to 85 for Tests 14 to 16 respectively.

FIGURE 82 Initial Hammer Impulses (Wooden blocks, Medium-hard-tip)

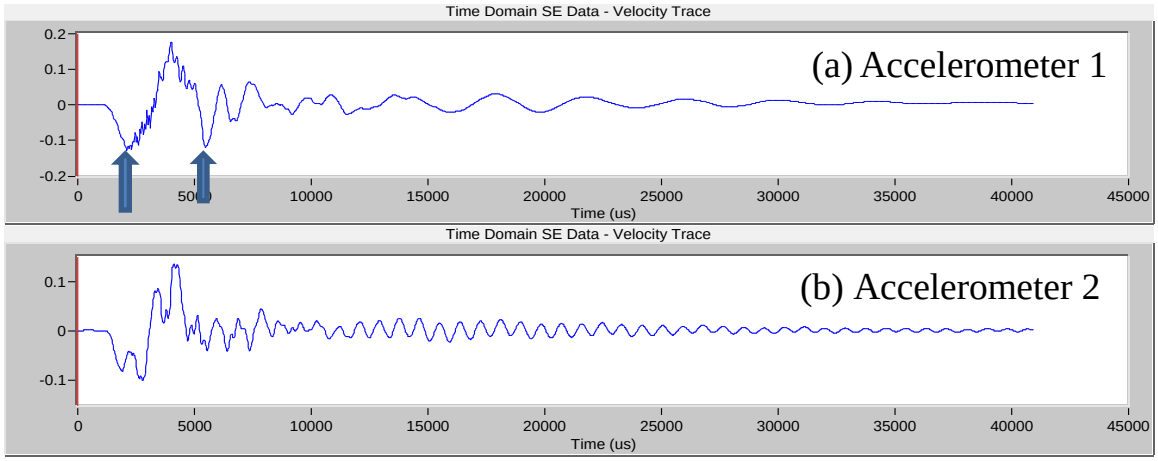

FIGURE 83 Velocity Graphs of Test 14

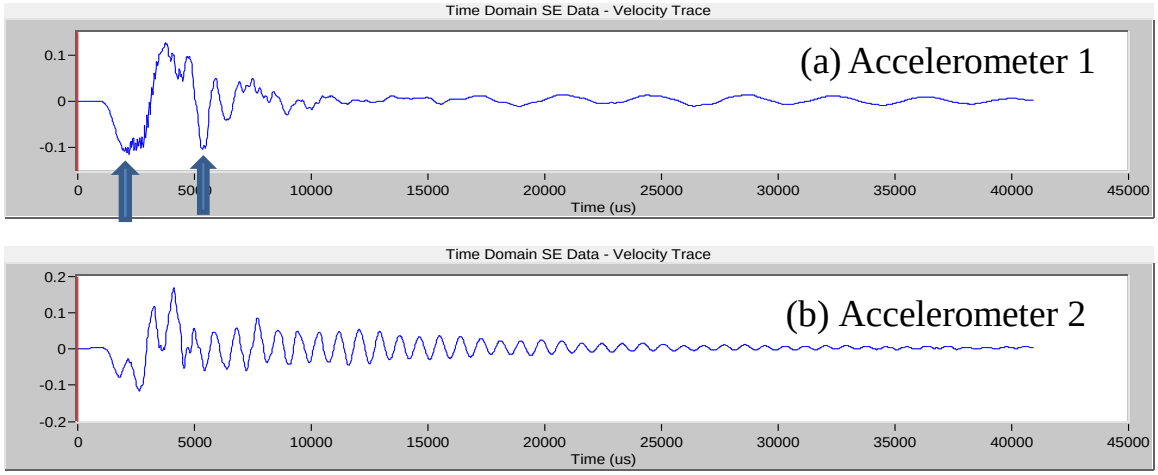

FIGURE 84 Velocity Graphs of Test 15

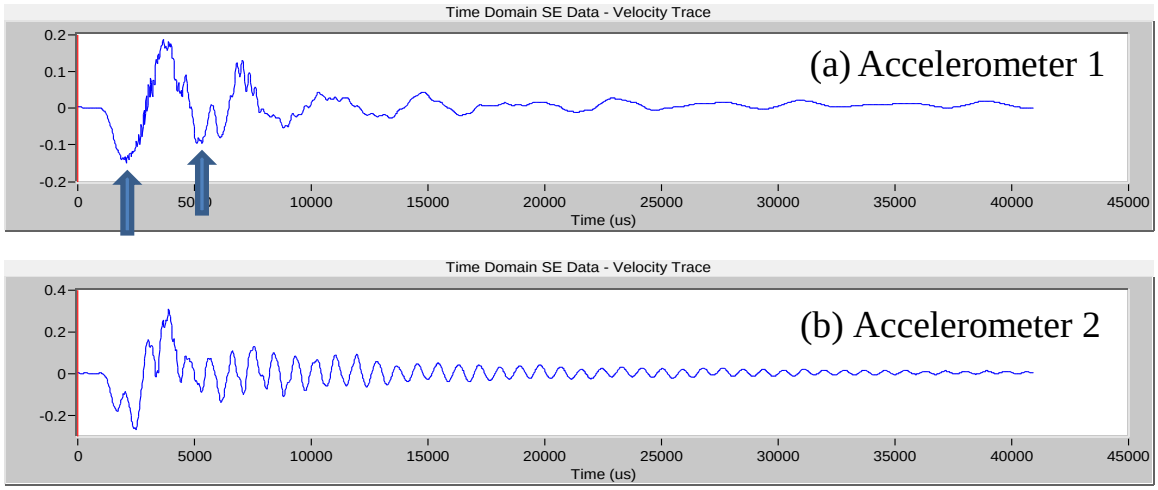

FIGURE 85 Velocity Graphs of Test 16

Results of Accelerometer 1 are much better than those obtained from Accelerometer 2. The accelerometer attachment was checked and functioned correctly. Better results of Accelerometer 1 may be due to the location of the accelerometer for this particular pile. The calculated pile lengths are summarized in Table 17.

TABLE 17 Estimated Length of Pile 3 (Tests 14 to 16).

Test No.	Accelerometer 1				Accelerometer 2			
	Δt (ms)	L_{tr} (ft)	L_a (ft)	L_t (ft)	Δt (ms)	L_{tr} (ft)	L_a (ft)	L_t (ft)
14	3.34	22.0	1.75	23.8	-	-	3.25	-
15	3.18	20.9	1.75	22.7	-	-	3.25	-
16	3.24	21.3	1.75	23.1	-	-	3.25	-

Table 18 shows the pile length determined by IR analyses (in frequency domain) for the data of Accelerometer 2. IR analyses yielded an estimated pile length around 14.5 ft although the pile

length could not be determined by the SE analysis (in time domain). This estimated pile length from IR analyses is different from the 22.7 to 23.8 ft determined from SE tests (see Table 17). Although IR analysis provides a pile length, the result may be unreliable comparing the pile length determined by SE analysis since SE analysis is more reliable in general. In addition, IR analysis on the data of Accelerometer 1 did not produce reasonable pile lengths.

TABLE 18 IR Results for Accelerometer 2 (Tests 14 to 16).

Test No.	Δf (Hz)	L_t (ft)
14	446	14.8
15	460	14.3
16	456	14.4

SE/IR Tests Performed with Aluminum Striking Block In Tests 17 to 19, different energies were imparted into the piles by striking an aluminum block attached to the side of the pile with hard hammer tip. As shown in Figure 86 the impulse graphs show multiple peaks similar to the previous observations of Pile 1 (see Figure 72).

FIGURE 86 Impulse Signals Generated by Striking the Aluminum Block with Hard Hammer Tips (Tests 17 to 19)

Poor velocity graphs were obtained for both accelerometers. Examples of poor velocity graphs are indicated in Figure 87. Only one velocity graph shown in Figure 88 (Accelerometer 2 in Test

18) could determine the length of the pile (L_t = 20.5 ft, Δt = 2.76 ms). The resonant frequencies from IR analyses did not reveal the correct pile length.

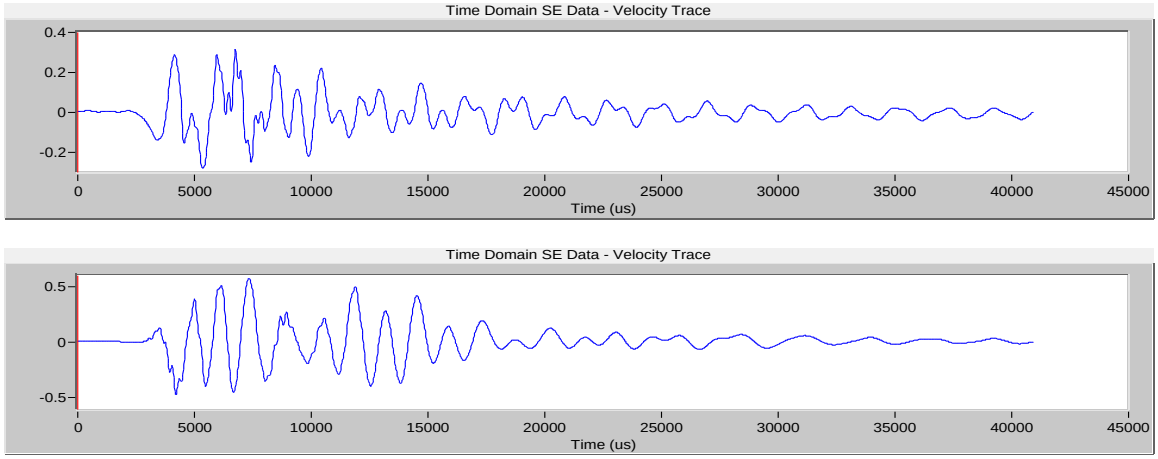

FIGURE 87 Examples of Poor Velocity Graphs Obtained by Striking the Aluminum Block

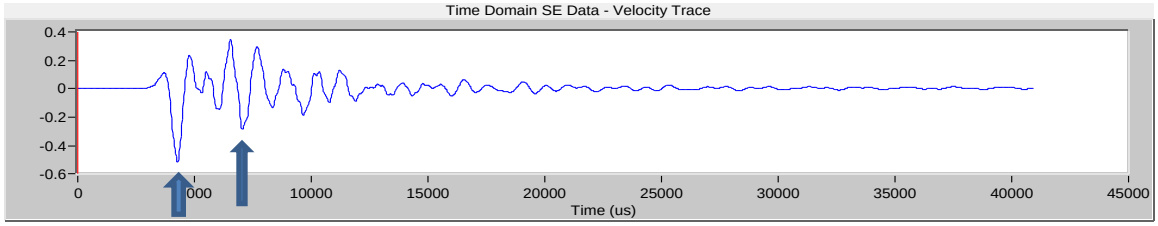

FIGURE 88 Velocity Graph Obtained from Striking the Aluminum Block (Test 18, Accelerometer 2)

Using the medium-hard tip hammer did not improve the results too. This leads to the conclusion that the aluminum block was unsuitable as the striking block for SE/IR tests. Thus, the use of aluminum block for striking is not recommended.

SE Tests on Pile 14 Three SE tests were conducted on Pile 14. The impulse and hammer tip characteristics for each test are shown in Table 19. The velocity graphs from Accelerometer 1 for Tests 20 to 22 are shown in Figure 89.

TABLE 19 Specification of Tests Conducted on Pile 14.

Test No.	Hammer tip	Strike
20	Medium-hard	Top
21	Hard	Wooden block
22	Medium-hard	Wooden block

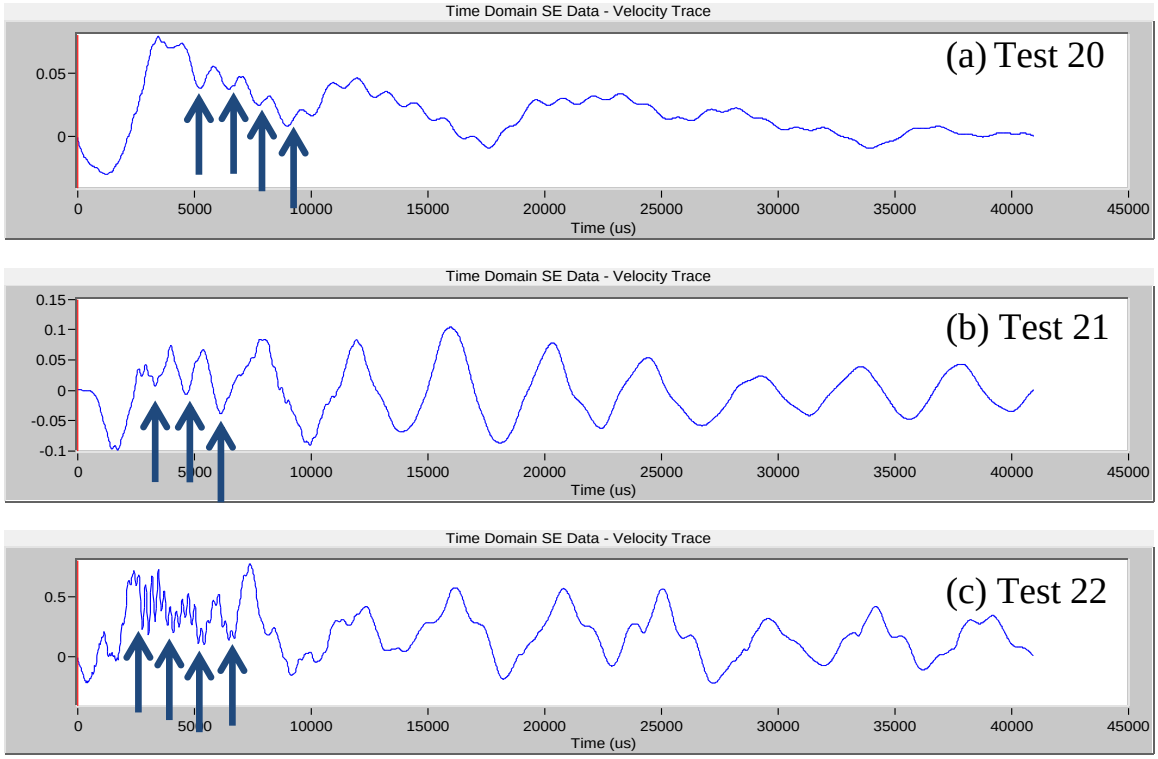

FIGURE 89 Velocity Graph Obtained from Accelerometer 1 (Tests 20 to 22)

The velocity graphs are very complicated. Closely located valleys indicated as arrows are shown in Figure 89. This is due to the presence of a huge longitudinal crack shown in Figure 90 which caused multiple internal reflections. The arrow in the figure indicates the big crack along the pile.

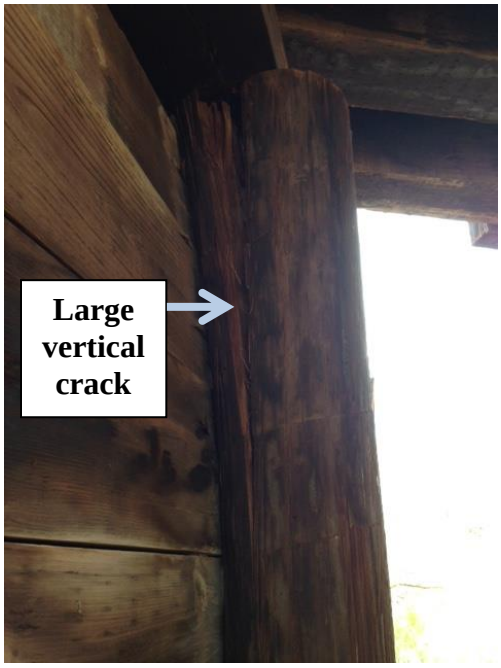

FIGURE 90 Picture of a Crack along Pile 14

SE/IR Tests on Pile 15 Six SE/IR tests were conducted on Pile 15. The characteristics of source and hammer tip for each test are shown in Table 20. Δt cannot be determined in all the velocity graphs, however, IR analysis on the data from Accelerometer 1 reveal reasonable pile length. The mobility graph of Accelerometer 1 in Test 27 is shown in Figure 91. The length of the pile was calculated from IR analysis and the results are summarized in Table 21.

TABLE 20 Specification of Tests Conducted on Pile 15.

Test No.	Hammer tip	Strike
23	Hard	Top (edge)
24	Med-hard	Top (edge)
25	Med-soft	Top (edge)
26	Hard	Wooden block
27	Med-hard	Wooden block
28	Med-soft	Wooden block

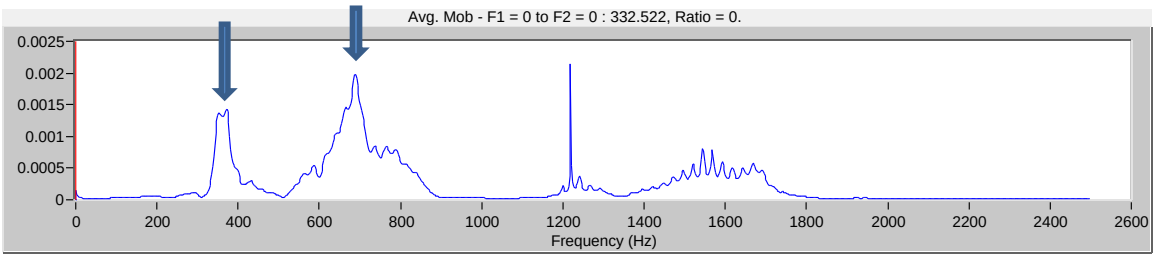

FIGURE 91 Mobility Graph of Accelerometer 1 (Test 23)

TABLE 21 Estimated Length of Pile 15 from Mobility Graphs (Tests 23 to 28).

Test No.	Δf (Hz)	L_t (ft)
23	363	18.1
24	363	18.1
25	363	18.1
26	377	17.4
27	372	17.7
28	367	17.9

Summary The inferred lengths of the five piles of Bridge No. 6922 are summarized in Table 22. Only the embedment depth of Pile 14 cannot be determined. The success rate at this site is 80%. (4 out of 5 piles)

TABLE 22 Estimated Average Length of Piles of Bridge No. 6922.

Pile	Embedment Pile Length (ft)	Exposed Pile Length (ft)	Total Pile Length (ft)
1	12.7	9	21.7
2	10.2	9.4	19.6
3	12.1	8.8	20.9
14	-	8.8	-
15	12.4	8.2	20.6

2.1.4.3 Bridge No. 1190

Bridge No. 1190 is located 23 miles west of Springer, NM on NM 21 crossing over Rayado Creek. The coordinates of the bridge are 36.368383, -104.929533. It is a 2-span bridge supported by round timber piles. The location of the bridge is shown in Figure 92. Figure 93 and 94 show the condition of the running water during the first and second visits respectively.

FIGURE 92 Location of Bridge No. 1190

FIGURE 93 Street View of Bridge No. 1190 Showing Running Water Surrounding Intermediate Bent during the First Visit

FIGURE 94 Photo of Bridge No. 1190 during the Second Visit

During the first visit, the accessibility of the intermediate bent was hindered by the running river water as indicated in Figure 93. Only the piles beneath the end bents were accessible. Due to seasonal reduction in the water level, all piles beneath the intermediate bent became accessible during the second visit as indicated in Figure 94. SE tests were conducted on the intermediate piles and the piles beneath the end bents. The investigated piles are indicated in Figure 95.

A trailer-mounted inspection platform (mobile scaffold) from NMDOT District 4 was arranged at the second visit to explore the feasibility of conducting SE tests on piles with the help of the inspection platform. Figure 96 shows the mobile scaffold that was used for attaching the blocks for accelerometer and for striking. Figure 97 shows a UNM team member performing the SE test using the scaffold.

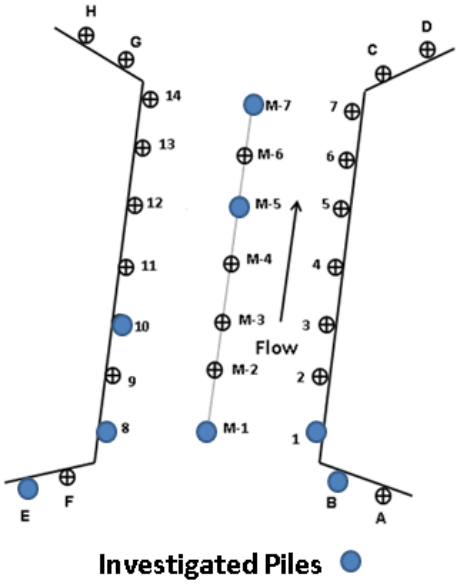

FIGURE 95 Foundation Plan and Investigated Piles of Bridge No. 1190

FIGURE 96 Mobile Scaffold from NMDOT District 4

FIGURE 97 Performing SE tests with the Aid of Mobile Scaffold

SE Tests on Pile B The accelerometer was placed at the top of the pile since the top of this wing pile was accessible, Three different hammer tips were used. The results are shown in Figure 98. As shown in this figure, Δt can be identified for medium-hard and medium-soft hammer tips but not the hard tip. This is interesting as our experience indicates that hard tip performs better than softer tips in general. The wave velocity was assumed to be 13,160 ft/s. Table 23 lists the calculated lengths of Pile B.

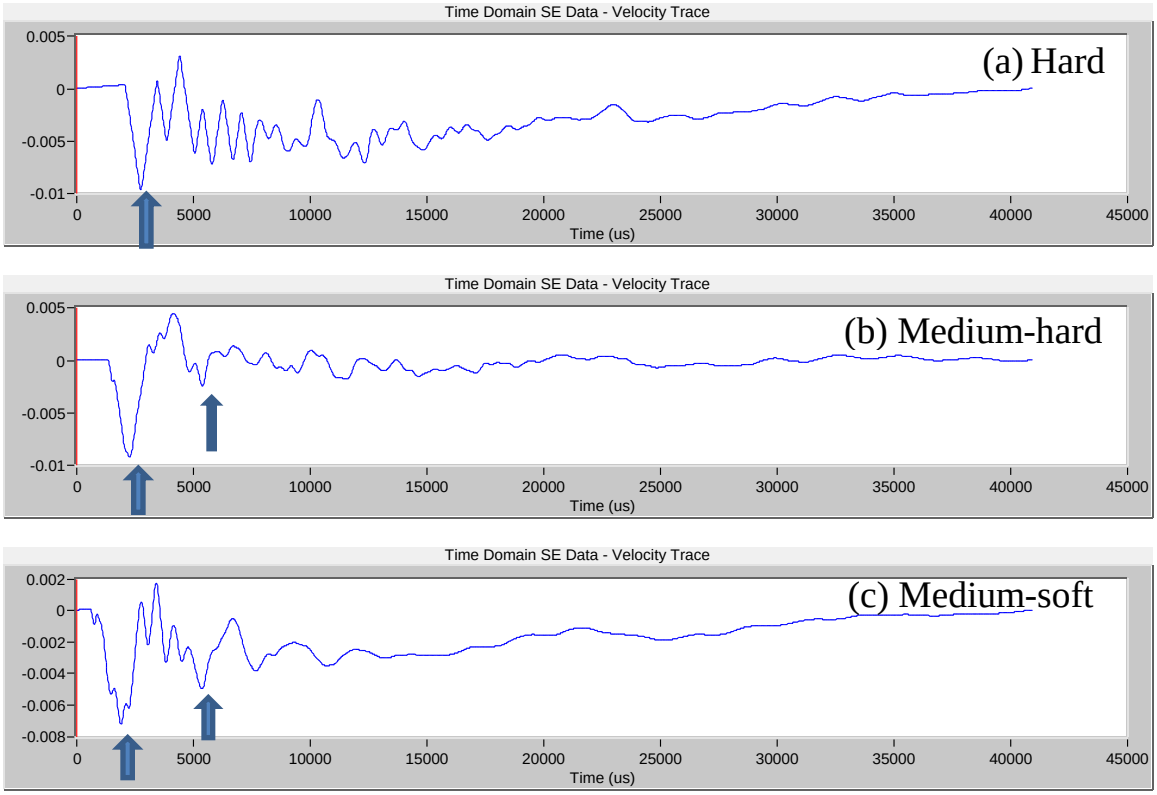

FIGURE 98 Velocity Graphs Obtained by Striking with Different Hammer Tips (Pile B)

TABLE 23 Calculated Length of Pile B.

Test No.	Hammer Tip	L_t (ft)
1	Hard	-
2	Medium-hard	20.5
3	Medium-soft	22.6

SE Tests on Pile E Three SE tests were performed on Pile E (Tests 4 to 6). Similar to Pile B, the source and receiver were placed at the top of the pile. Figure 99 shows the velocity graphs of all three tests. Distinguishable impulses and echoes can be identified in the velocity graphs for hard and medium-hard tips but not the medium soft tip. There are two echoes of similar magnitudes (shown as two arrows in Figure 99c), however, it is difficult to choose the correct one. The first one is wrong compared with the results of other SE tests. The second echo yields the pile length that is similar to those of SE tests with hard and medium-hard tips. It is suggested not to use medium-soft tip as the primary tip. Table 24 indicates the calculated pile lengths.

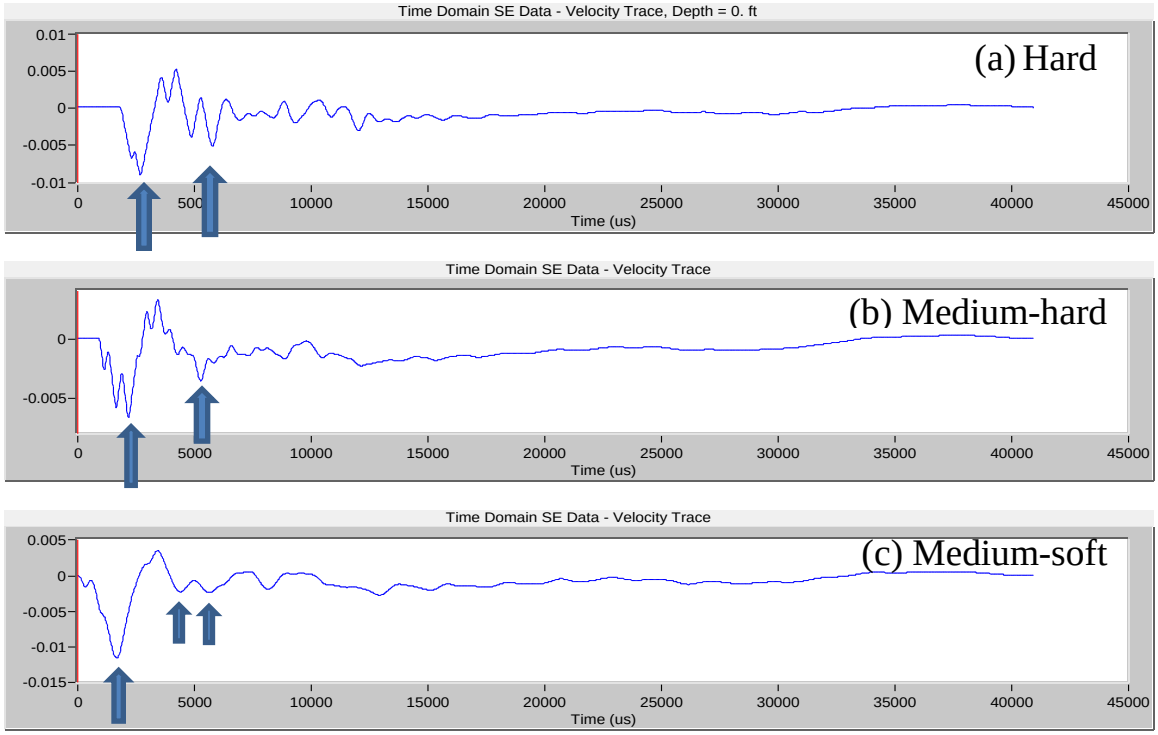

FIGURE 99 Velocity Graphs of Pile E with Different Hammer Tips (Tests 4 to 6)

TABLE 24 Calculated Length of Pile E.

Test No.	Hammer Tip	Δt (ms)	L_t (ft)
4	Hard	3.08	20.3
5	Medium-hard	3.06	20.1
6	Medium-soft	-	-

SE Tests on Pile 1 Three SE tests (7 to 9) were conducted on Pile 1 with hard, medium-hard and medium-soft hammer tips respectively. Since the top of the pile was inaccessible, a wooden block was attached with screws for striking. The accelerometer was mounted on a wooden block. Figure 100 shows the locations of the blocks for the source and receiver. The obtained velocity graphs are shown in Figure 101 for these three hammer tips. The echo is undistinguishable again when using medium-soft tip. However, the bad response was due to accelerometer's insecure attachment in this particular case. The average pile lengths are listed in Table 25.

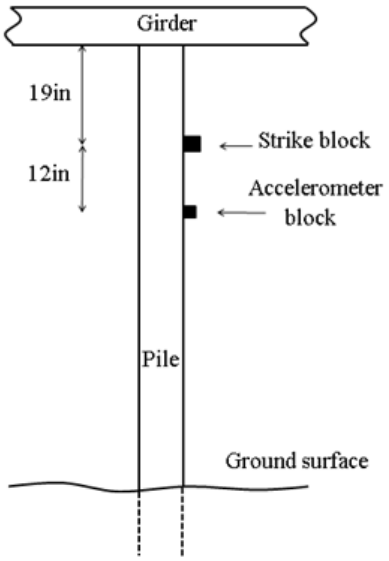

FIGURE 100 Locations of Source and Receiver for Pile 1

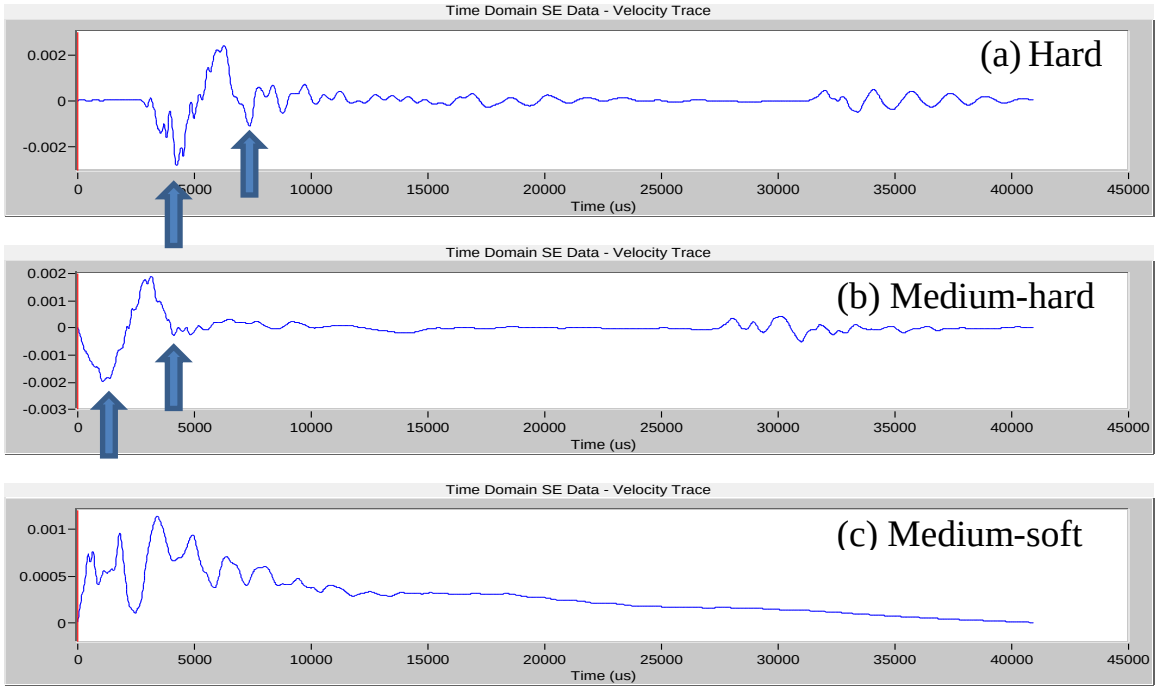

FIGURE 101 Velocity Graphs of Different Hammer Tips (Tests 7 to 9)

TABLE 25 Calculated Length of Pile 1.

Test No.	Hammer Tip	Δt (ms)	L_{tr} (ft)	L_a (ft)	L_t (ft)
7	Hard	3.08	20.3	2.6	22.9
8	Medium-hard	3.04	20	2.6	22.6
9	Medium-soft	-	-	-	-

SE Tests on Pile 8 Three SE tests (10 to 12) were conducted on Pile 8 with hard, medium-hard and medium-soft hammer tips again. The top edge of the pile was accessible; therefore, the source was applied by striking the top surface. Due to the size of the pile, the accelerometer was mounted 1 ft below the top of the pile. The velocity graphs are shown in Figure 102. Recognizable impulse and echo were found in all three velocity graphs. Unlike the SE test on Pile 1, the result of medium-soft tip was acceptable when striking at the top of the pile. The estimated pile lengths are listed in Table 26.

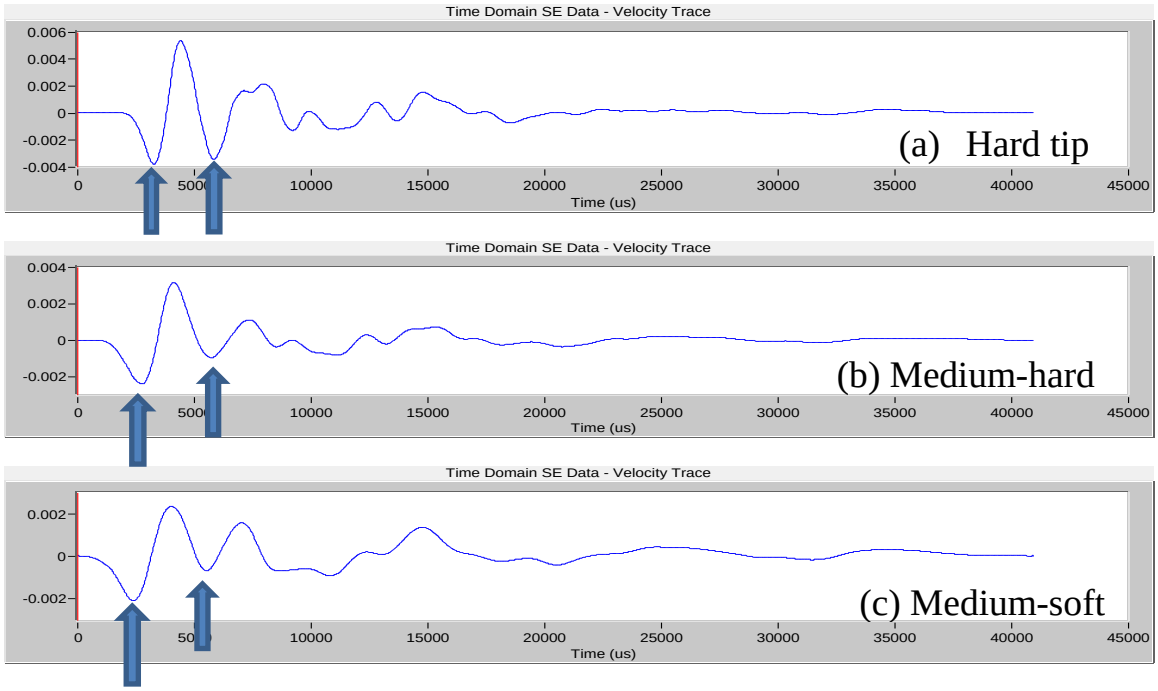

FIGURE 102 Velocity Graphs of Pile E with Different Hammer Tips (Tests 10 to 12)

TABLE 26 Calculated Length of Pile 8.

Test No.	Hammer Tip	Δt (ms)	L_{tr}(ft)	L_a(ft)	L_t(ft)
10	Hard	2.66	17.5	1	18.5
11	Medium-hard	3.02	19.9	1	20.9
12	Medium-soft	3.00	19.8	1	20.8

SE Tests on Pile 10 Two SE tests (13 and 14) were conducted on Pile 10 with hard tip. Since the top was accessible, Test 13 was performed by striking the top surface of the pile. A ½ in thick steel plate was attached on this pile as shown in Figure 103 that could be used as the striking block. The steel plate was connected to the pile with thick metal bolts but the contact was loose. There was also a gap between the steel plate and the pile. In Test 14, the source was applied by vertical striking at the edge of the steel plate. The accelerometer was mounted 40 inches below the top of the pile.

Figure 104 shows the velocity graphs of these two tests. Good result was found for vertical striking at the top (Test 13). Δt = 2.92 ms and the estimated pile length is 22.5 ft. Poor results of striking the steel plate were found which might be due to the poor coupling between the steel

plate and pile. Energy transmitted only through the steel bolts and a complex source signal was created due to the vibration of the plate. Thus, mounting the striking block on a pile tightly and securely is very essential to yield good results.

FIGURE 103 A Steel Plate Attached to Pile 10

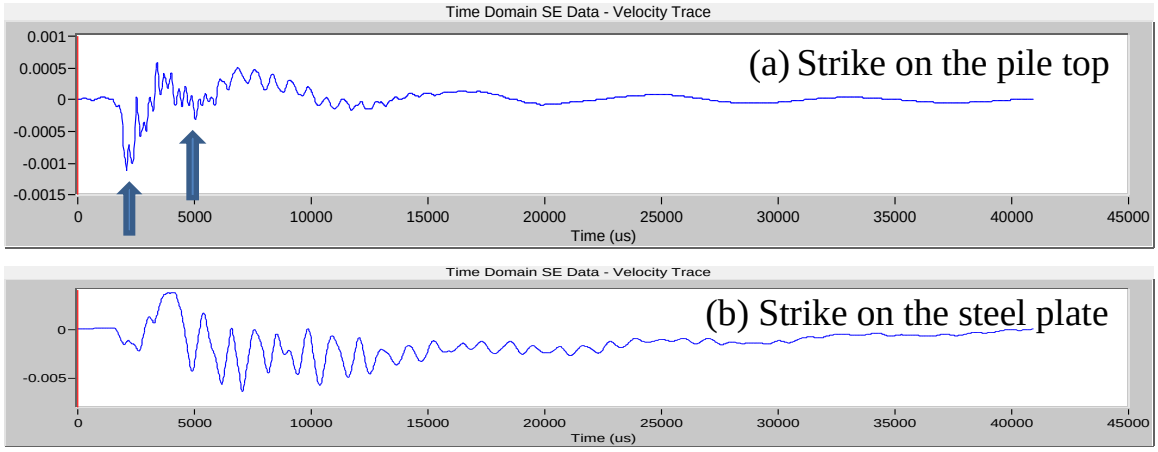

FIGURE 104 Velocity Graphs of Vertical Striking on the Pile Top and on the Steel Plate

SE Tests on Piles M-5 Twenty-one SE tests were performed on this pile. Two accelerometers were mounted on the wooden blocks attached to the side of the test pile. As mentioned before, when the top of either pile or pile cap are inaccessible, upward striking on the pile cap next to the test pile can be used as the alternative mean to produce longitudinal waves along the test pile. Figure 105 shows the locations of striking on the pile cap. Upward striking on pile cap will produce a strong tensile wave accompanied by a weak reflected compression wave. The source of some SE tests was also applied through striking block. The locations of the sensor and striking block can be found in Figure 106. Cubic and wedge wooden blocks were attached onto the pile surface with screws for striking. The striking was accomplished with four different hammer tips including hard, medium-hard, medium-soft, and soft. Table 27 lists the characteristics of all SE tests conducted on Pile M-5.

FIGURE 105 Photo of Pile M-5 and the Pile Cap

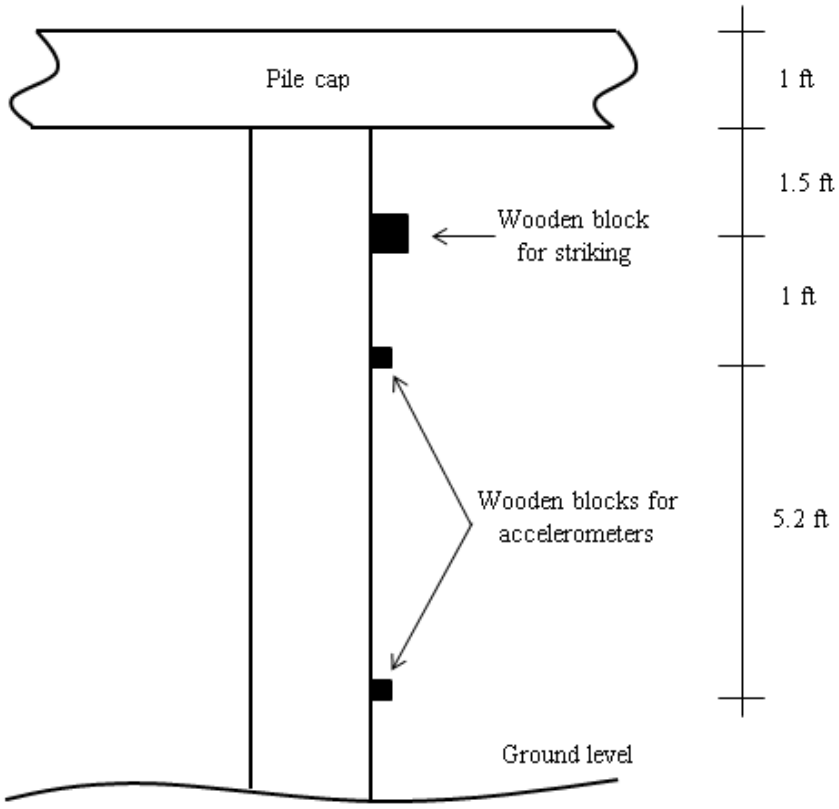

FIGURE 106 Locations of Source and Receivers Blocks for Pile M-5

TABLE 27 Specifications of SE Tests Conducted on Pile M-5.

Test No.	Hammer tip	Striking Condition
1	Hard	On block
2	Medium-soft	On block
3	Medium-soft	On block
4	Medium-soft	On block
5	Hard	Upward on pile cap
6	Hard	Upward on pile cap
7	Hard	Upward on pile cap
8	Medium-hard	Upward on pile cap
9	Medium-hard	Upward on pile cap
10	Medium-hard	Upward on pile cap
11	Medium-soft	Upward on pile cap
12	Medium-soft	Upward on pile cap
13	Medium-soft	Upward on pile cap
14	Hard	On wedge (1 screw)
15	Medium-hard	On wedge (1 screw)
16	Medium-soft	On wedge (1 screw)
17	Medium-soft	On wedge (1 screw)
18	Hard	On wedge (2 screws)
19	Medium-hard	On wedge (2 screws)
20	Medium-soft	On wedge (2 screws)
21	Soft	On wedge (2 screws)

The length of the pile was estimated from the Δt determined in the velocity graphs of both accelerometers. The specification and result of the SE tests are listed in Table 28.

TABLE 28 Results of SE Tests Conducted on Pile M-5.

Test No.	Hammer Tip	Striking Condition	Accelerometer 1		Accelerometer 2	
			Δt (ms)	L_t (ft)	Δt (ms)	L_t (ft)
1	Hard	On block	4.74	33.7	2.64	25.1
2	Medium-soft	On block	4.64	33.0	-*	-
3	Medium-soft	On block	4.54	32.4	2.78	26.0
4	Medium-soft	On block	4.72	33.6	2.84	26.4
5	Hard	Upward on pile cap	-	-	-	-
6	Hard	Upward on pile cap	4.26	30.5	2.78	26.0
7	Hard	Upward on pile cap	4.1	29.5	3.86	33.1
8	Medium-hard	Upward on pile cap	4.26	30.5	2.98	27.3
9	Medium-hard	Upward on pile cap	4.3	30.8	-	-
10	Medium-hard	Upward on pile cap	-	-	-	-
11	Medium-soft	Upward on pile cap	4.34	31.1	3.18	28.6
12	Medium-soft	Upward on pile cap	4.32	30.9	3.18	28.6
13	Medium-soft	Upward on pile cap	4.82	34.2	3.32	29.5
14	Hard	On wedge (1 screw)	3.28	24.1	2.44	23.8
15	Medium-hard	On wedge (1 screw)	3.74	27.1	3.5	30.7
16	Medium-soft	On wedge (1 screw)	-	-	-	-
17	Medium-soft	On wedge (1 screw)	-	-	-	-
18	Hard	On wedge (2 screws)	-	-	-	-
19	Medium-hard	On wedge (2 screws)	3.3	24.2	2.86	26.5
20	Medium-soft	On wedge (2 screws)	3.42	25.0	3.24	29.0
21	Soft	On wedge (2 screws)	3.94	28.4	3.56	31.1

-* : Δt cannot be determined from the velocity graph

Following observations were inferred based on the hammer and velocity graphs of the SE tests conducted on Pile M-5:

- The data from Accelerometer 1 (mounted close to the end of the pile) were slightly more consistent than the results from Accelerometer 2 mounted closer to the ground. It may be due to the interference of the natural waves existing in the ground (strong water current). The river is running on one side (see Figure 97)
- The results of the upward striking on the pile cap were consistent. The calculated buried lengths were similar to those calculated by striking on the blocks. The finding indicates that the accompanied transmitted compression wave did not affect the SE result. Therefore, upward striking on pile cap next to the test pile is acceptable as the input source.
- Care must be taken on mounting the striking block onto the test pile. Clean and clear source signal may not be generated due to imperfect coupling between the block and pile surface. The result also depends on the hammer tip as shown in Figures 107 and 108 Multiple peaks in the impact signal were found while using a hard tip (see Figure 107a). These peaks interfered with the determination of the echo in the velocity graph (see

Figures 107b and 107c). When a softer hammer tip was used, the multiple peaks disappeared for the accelerometer mounted farther from the source (see Figure 108a).

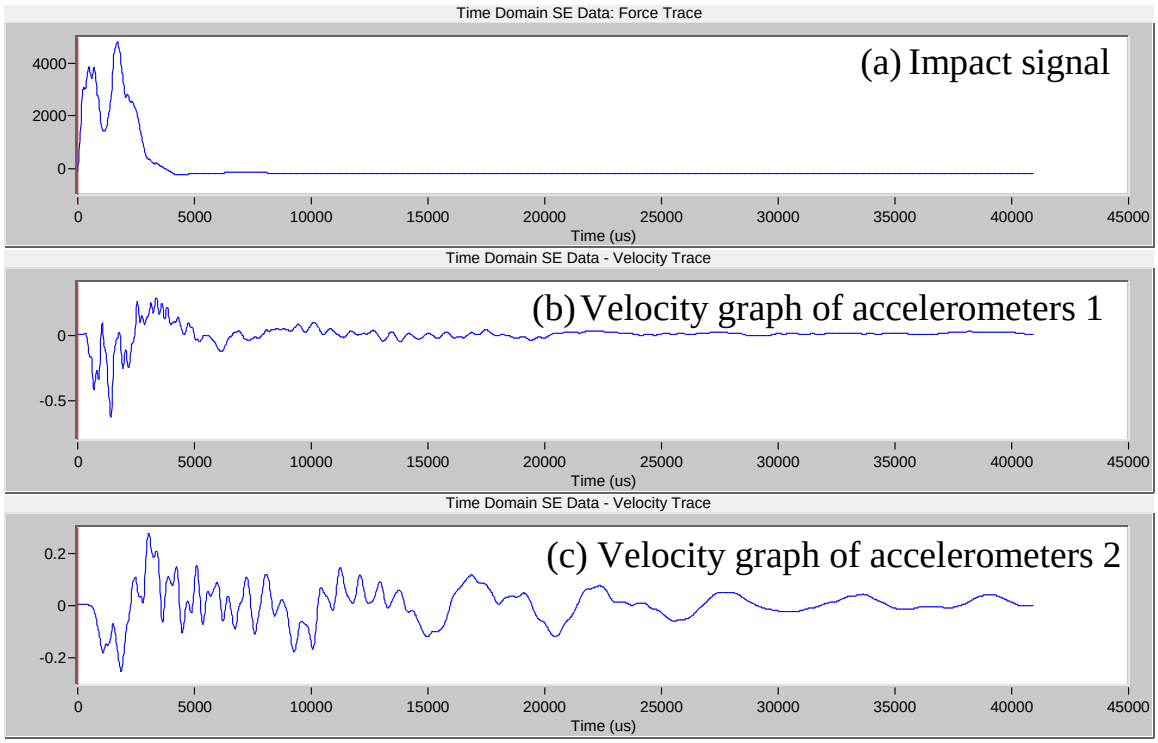

FIGURE 107 Impact Signal and Velocity Graphs using a Hard Tip

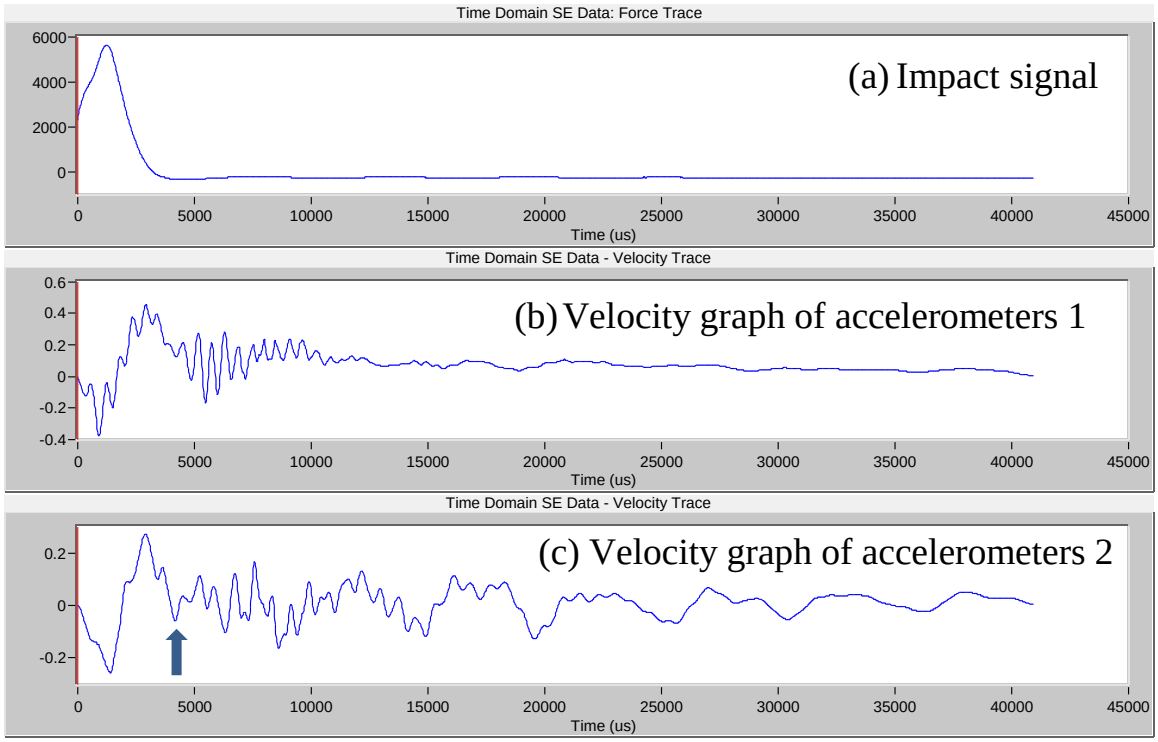

FIGURE 108 Impact Signal and Velocity Graphs Using a Medium-soft Tip

- Although striking on the wedge block produces horizontal compression wave as well as vertical compression wave that may complicate the velocity graphs, the increase of lateral compressive force should benefit the coupling between the block and the pile. The investigation showed that inclined hammer strikes produced similar results to those of vertical strikes on the cubic striking blocks. Multiple peaks in the hammer force history have also been found due to imperfect coupling in some cases.
- In general, all hammer tips produced good results when there was good coupling between the striking block and the pile. However, upward striking with hard hammer tip did not produce good velocity graphs (Tests 5, 9 and 11). Figure 109 shows three SE tests with three different hammer tips. As shown in Figure 109a, there are two echoes with similar magnitudes which made it difficult to select the correct echo. High frequency vibrations were seen in the velocity graph for hard tip but not for medium-hard and medium soft tips. The softer tips produced waves with lower frequencies that resulted in better data for this particular pile.

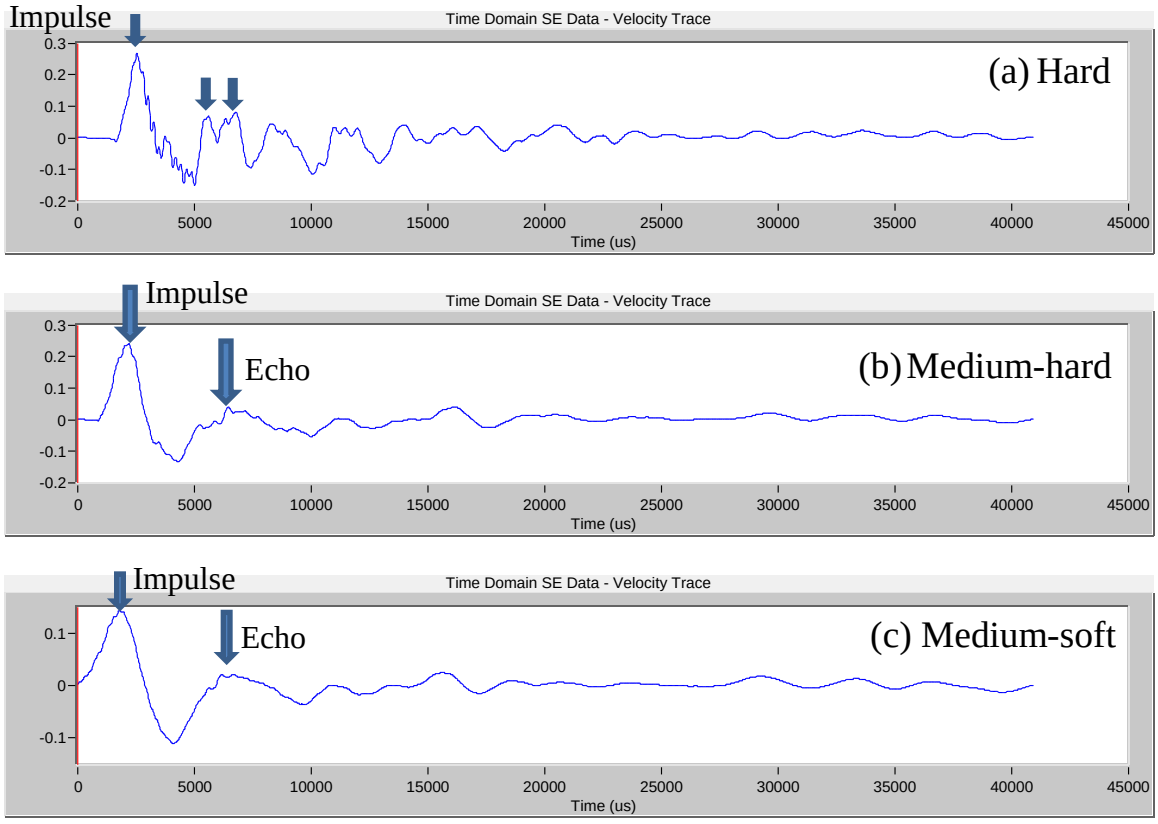

FIGURE 109 Velocity Graphs for Various Hammer Tips Conducted on Pile M-5

SE Tests on Piles M-7 Twenty-four SE tests were performed with two accelerometers attached to the side of the pile. Figure 110 shows the locations of the receivers for Pile M-7. Eight different scenarios were considered and each scenario was repeated three times. Different hammer tips including hard, medium-hard, medium-soft, and soft were utilized to perform the tests. The striking was applied on the top of the pile cap and on the cubic and wedge wooden blocks attached to the pile surface for striking. The specifications of the SE tests conducted on Pile M-7 are indicated in Table 29.

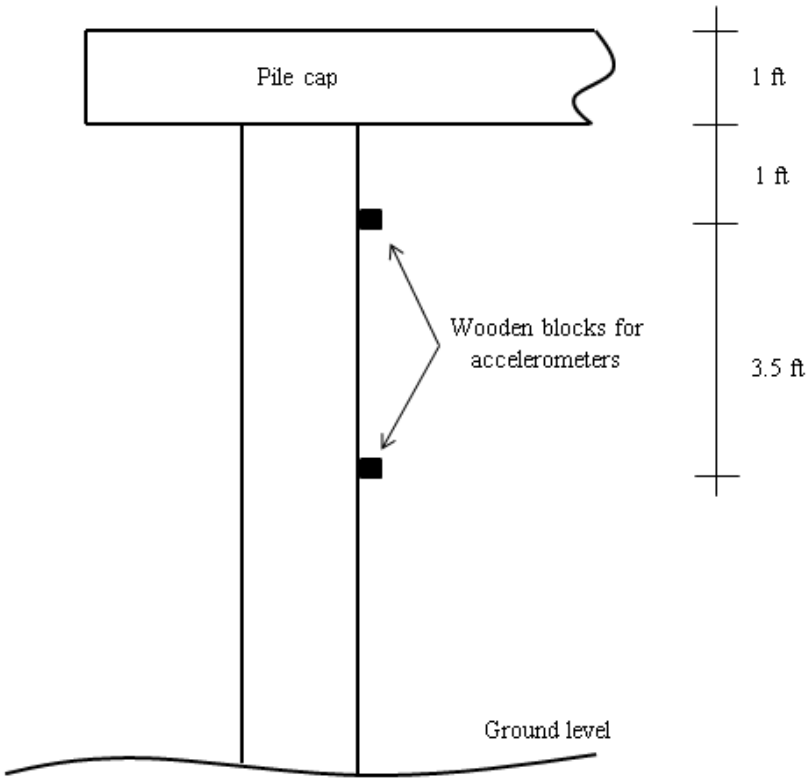

FIGURE 110 Locations of the Receivers Blocks on Pile M-7

The results of the SE tests on Pile M-7 obtained from both accelerometers are also shown in Table 29. This result is more consistent than those of Pile M-5 (see Table 28). First, striking on the pile cap directly above the pile produced excellent results. Second, there is no interference of reflections from superstructure. As shown in Figure 111, Pile M-7 is the exterior pile with only a pile cap above the pile. There is no superstructure above the pile cap. When the source is applied by upward striking at the pile cap, the generated up-going tension wave is reflected from the cap as a down-going compression wave. More complicated superstructures produce more complicated velocity graphs. This is the reason that the results of Pile M-5 is less consistent than Pile M-7. Once again, the results show that upward striking on pile cap next to the test pile is acceptable.

TABLE 29 Specifications and Results of SE Tests Conducted on Pile M-7.

Test No.	Hammer Tip	Striking Condition	L_t (ft) Obtained from Accelerometer 1	L_t (ft) Obtained from Accelerometer 2
1	Hard	Top of pile cap	22.5	24.4
2	Hard	Top of pile cap	27.2	29.9
3	Hard	Top of pile cap	24.7	27.5
4	Medium-hard	Top of pile cap	22.6	25.6
5	Medium-hard	Top of pile cap	22.7	26.2
6	Medium-hard	Top of pile cap	22.6	26.1
7	Medium-soft	Top of pile cap	23.0	26.2
8	Medium-soft	Top of pile cap	25.2	28.6
9	Medium-soft	Top of pile cap	23.2	27.4
10	Soft	Top of pile cap	23.8	27.8
11	Soft	Top of pile cap	24.8	28.3
12	Soft	Top of pile cap	24.7	28.1
13	Hard	Upward on pile cap	20.7	22.9
14	Hard	Upward on pile cap	21.1	24.6
15	Hard	Upward on pile cap	21.0	24.5
16	Medium-hard	Upward on pile cap	21.3	24.4
17	Medium-hard	Upward on pile cap	20.9	23.6
18	Medium-hard	Upward on pile cap	21.1	23.6
19	Medium-soft	Upward on pile cap	21.0	23.2
20	Medium-soft	Upward on pile cap	21.8	24.5
21	Medium-soft	Upward on pile cap	21.4	24.1
22	Soft	Upward on pile cap	21.3	22.0
23	Soft	Upward on pile cap	20.3	23.7
24	Soft	Upward on pile cap	20.6	22.8

FIGURE 111 Exterior Pile M-7 and the Pile Cap

SE Tests on Pile M-1 Twenty-eight SE tests have been performed on Pile M-1.The specifications of the tests are listed in Table 30. The accelerometers were placed at various locations. The SE setup for Pile M-1 is shown in Figure 112. Despite numerous attempts, none of the results could be used to determine the length of the pile.

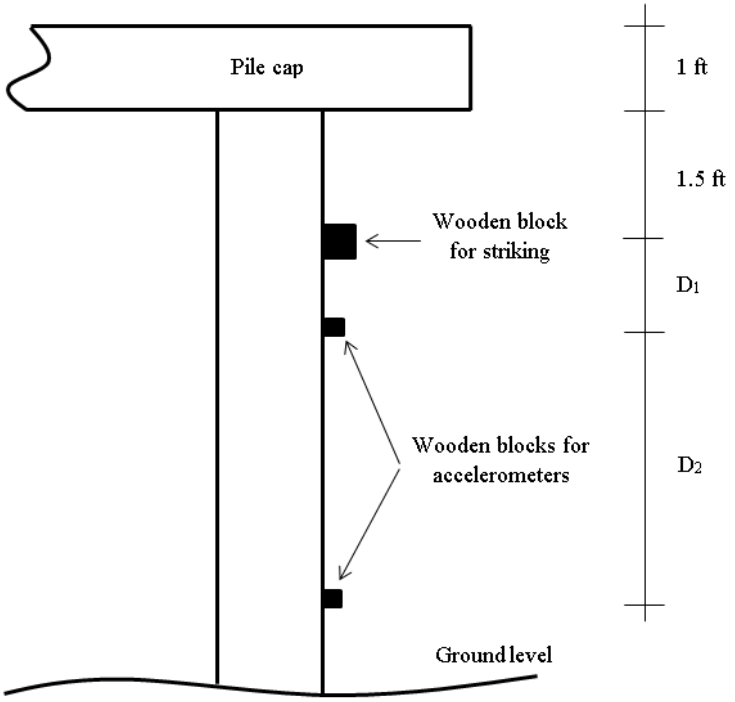

FIGURE 112 Locations of Source and Receivers blocks for Pile M-1

Although numerous SE tests with different striking conditions and hammer tips, placement of the receivers were carried out on Pile M-1, poor results were obtained. The echo from the pile toe could not be identified in the velocity graphs. We expected that either the presence of a big anomaly adjacent to ground level (such as a big internal crack) or the noise due to the running water (river current hits the pile constantly) hinders the determination of the echo from the pile toe. The velocity graphs received from the two sensors were very different and typical velocity graphs are shown in Figures 113 and 114. The arrows on the graphs of the Accelerometer 1 (closer to pile top) show a reflection from an impedance change but the echo did not appear in Accelerometer 2 (close to the ground level). Therefore, the echoes shown in Figures 113a and 114a are not considered as the echoes from the pile toe.

TABLE 30 Specifications of SE Tests Conducted on Pile M-1.

Test No.	Hammer Tip	Striking Condition	D_1 (ft)	D_2 (ft)
1	Hard	On block	1	6
2	Hard	On a nail of the bracing	1	6
3	Hard	Top of pile cap	1	6
4	Hard	Top of pile cap	1	6
5	Hard	Top of pile cap	2	5
6	Medium-hard	Top of pile cap	2	5
7	Medium-hard	Top of pile cap	2	5
8	Medium-hard	Top of pile cap	2	5
9	Medium-soft	Top of pile cap	2	5
10	Medium-soft	Top of pile cap	2	5
11	Medium-soft	Top of pile cap	2	5
12	Hard	Upward on pile cap	2	5
13	Hard	Upward on pile cap	2	5
14	Medium-soft	Upward on pile cap	2	5
15	Medium-soft	Upward on pile cap	2	5
16	Soft	Upward on pile cap	2	5
17	Soft	Upward on pile cap	2	5
18	Hard	On wedge	2	5
19	Hard	On wedge	2	5
20	Medium-hard	On wedge	2	5
21	Medium-hard	On wedge	2	5
22	Medium-hard	On wedge	2	5
23	Medium-soft	On wedge	2	5
24	Medium-soft	On wedge	2	5
25	Medium-soft	On wedge	2	5
26	Soft	On wedge	2	5
27	Soft	On wedge	2	5
28	Soft	On wedge	2	5

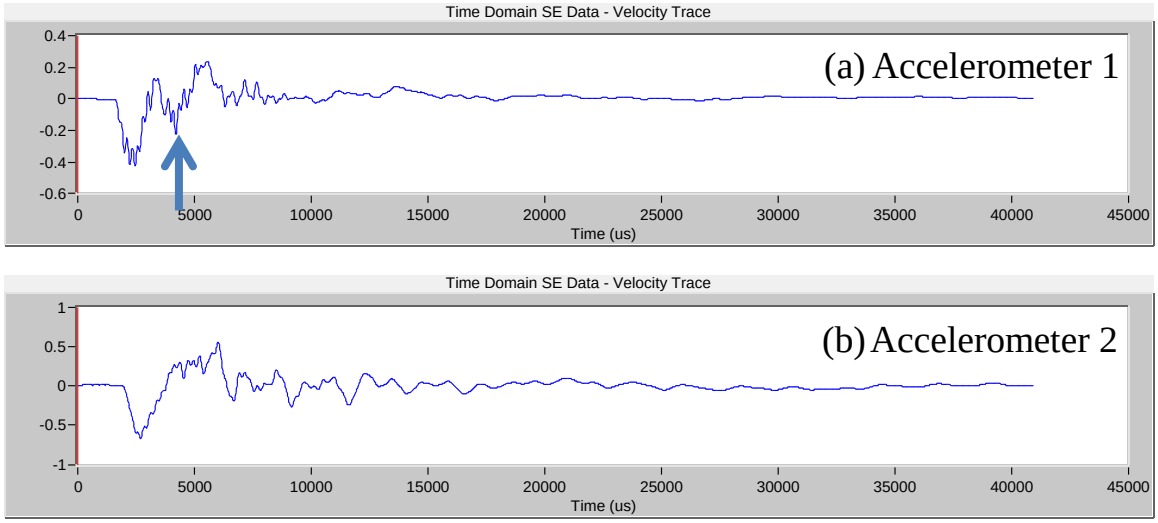

FIGURE 113 Velocity Graphs Obtained from Accelerometers 1 and 2 (Test 19)

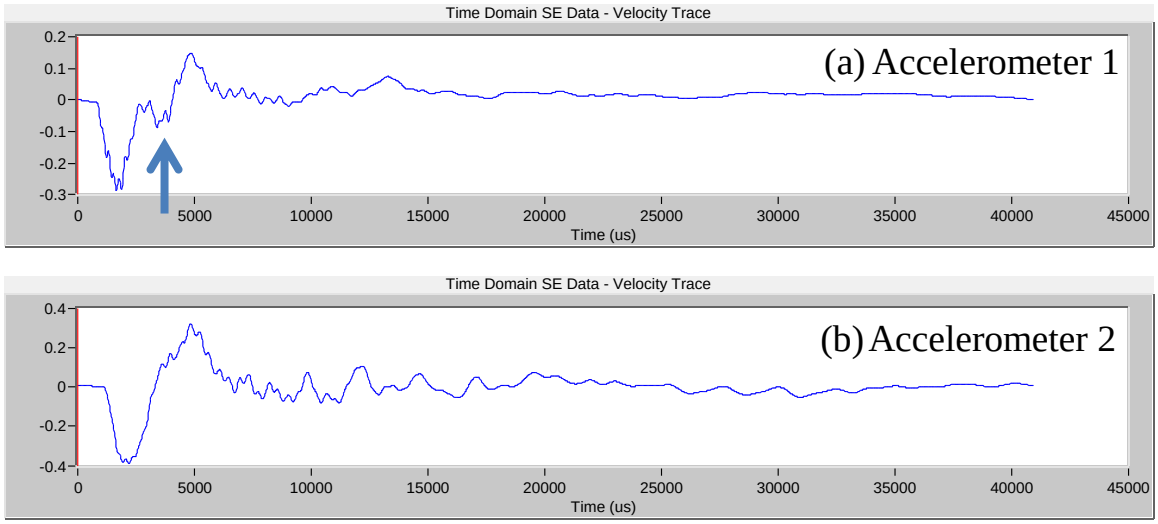

FIGURE 114 Velocity Graphs Obtained from Accelerometers 1 and 2 (Test 20)

Summary of Results of Bridge No. 1190 The results of all the tested piles are summarized in Table 31. The success rate of SE tests at this site is 87.5%.

TABLE 31 SE Tests Results for Piles of Bridge No. 1190.

Pile	Embedment Pile Length (ft)	Exposed Pile Length (ft)	Total Pile Length (ft)
B	15.1	5.3	20.4
E	15.7	4.6	20.3
1	15.5	7.4	22.9
8	13.9	6.1	20
10	15.3	7.7	23
M-1	-	-	-
M-5	18.4	11.5	29.9
M-7	11	11.5	22.5

2.1.4.4 Bridge No. 1676

Bridge No. 1676 is located 11 miles north of Socorro on I-25 Frontage Road (coordinates 34.211303, -106.921087). It is a 4-span bridge supported by square timber piles. The location and street view of the bridge are shown in Figures 115 and 116, respectively. The as-built foundation depth of this bridge was used to verify the results of SE/IR tests.

FIGURE 115 Location of Bridge No. 1676

FIGURE 116 Street View of Bridge No. 1676

The foundation plan and the investigated piles are indicated in Figure 117. SE tests were performed on three timber piles indicated in the figure. The SE tests were done with four different hammer tips including hard, medium-hard, medium-soft, and soft. Two accelerometers were attached to the side of the piles as shown in Figure 118. The wooden blocks were glued onto the pile surface.

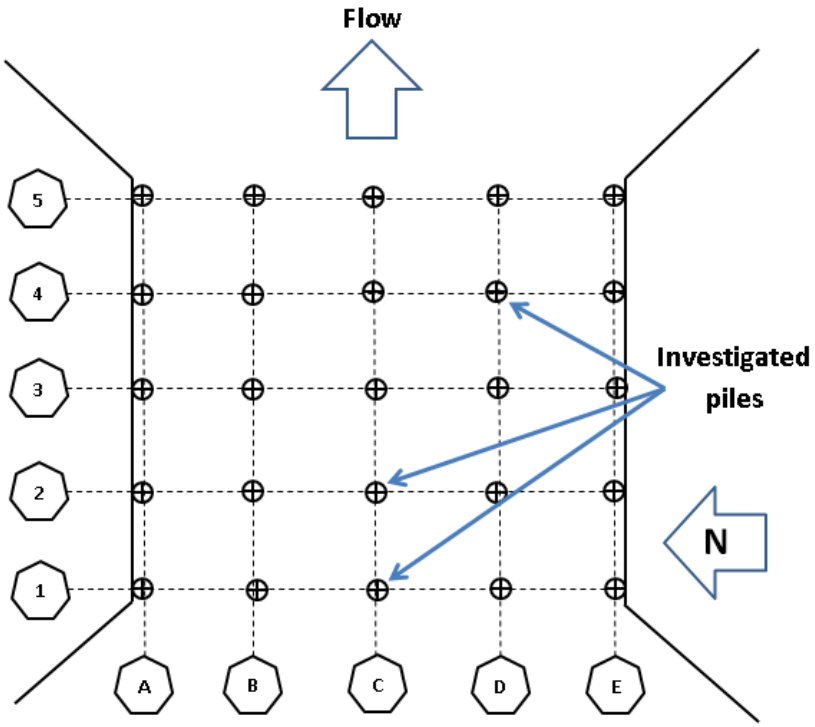

FIGURE 117 Foundation Plan and Investigated Piles of Bridge No. 1676

FIGURE 118 Accelerometers Attached onto a Pile

SE/IR Tests on Piles C-1 (SE Analysis) Eighteen SE/IR tests were performed on this pile. The source was applied by three different methods: downward striking at the top of the pile cap, upward striking at the pile cap near the pile, and inclined striking on a wooden wedge attached on the side of the pile. The source by inclined striking on a wedge wooden block was examined on this pile. The striking points (A and B), the locations of the wooden wedge and the accelerometers are shown in Figure 119. The location and the direction of hammer strikes of each test are indicated in Table 32.

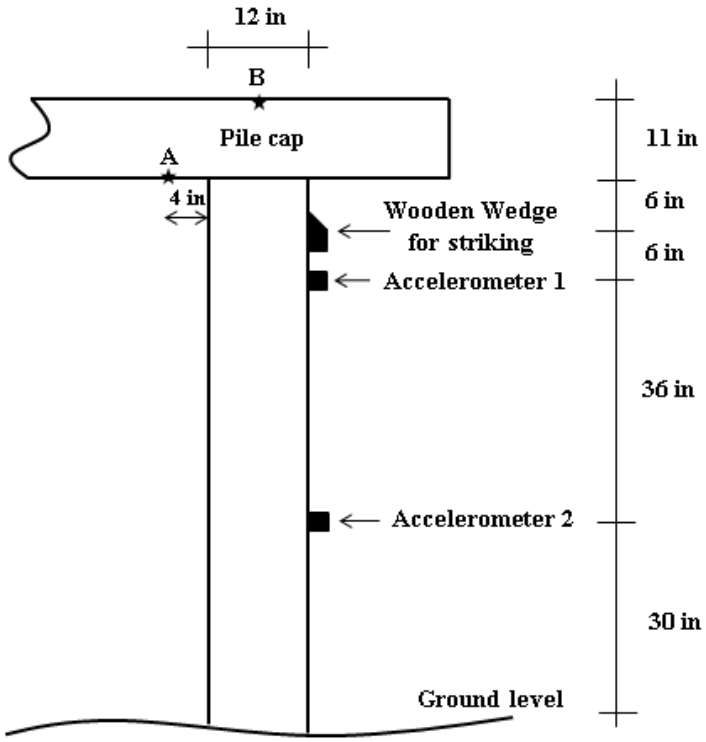

FIGURE 119 SE Setup for Pile C-1

Out of those eighteen SE tests, only the SE tests performed by striking on the pile cap above the pile produce useful velocity graphs. The other two striking methods did not produce good results. An example of useful velocity graph is shown in Figure 120. The impulse and the echo can be identified in the velocity graph (Test 4, Accelerometer 1). Δt is 4.56 ms. With the assumed velocity of 10,000 ft/s, the buried length is 22.8 ft and the length of the pile is 23.8 ft. Table 33 shows the pile lengths determined from the four successful SE tests. The average length of the pile is 24.4 ft.

Echoes could not be identified in the velocity graphs of the SE tests by upward striking at Point A (at the pile cap near the pile). It may be due the small energy of the down-going compressive wave along the pile such that the echo from the pile toe cannot be detected. The shape of the source signal when striking the wooden wedge showed multiple peaks. It indicated poor connection between the wedge and the pile. Very complicated vibration phenomenon was observed in the velocity graphs that made the echo determination difficult.

TABLE 32 Location and Direction of Hammer Strikes for Pile C-1.

Test No.	Hammer Tip	Striking Condition
1	Hard	Downward at B
2	Medium-hard	Downward at B
3	Med-soft	Downward at B
4	Soft	Downward at B
5	Hard	Upward at A
6	Hard	Upward at A
7	Hard	Upward at A
8	Hard	Upward at A
9	Medium-hard	Upward at A
10	Medium-soft	Upward at A
11	Soft	Upward at A
12	Soft	Upward at A
13	Hard	Inclined on wedge
14	Hard	Inclined on wedge
15	Hard	Inclined on wedge
16	Medium-hard	Inclined on wedge
17	Medium-soft	Inclined on wedge
18	Soft	Inclined on wedge

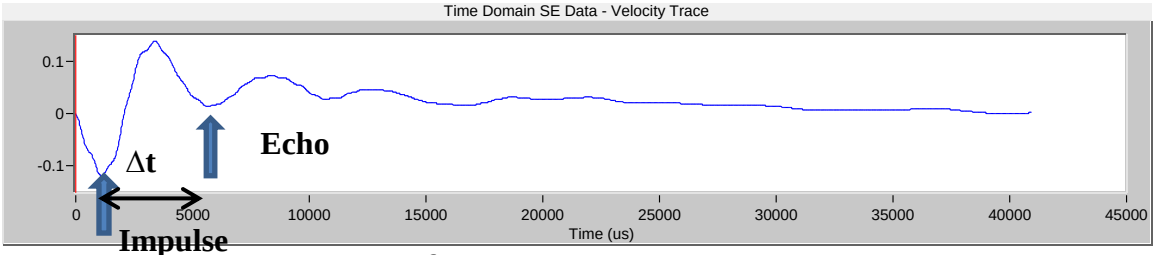

FIGURE 120 Velocity Graph of Test 4 Conducted on Pile C-1

TABLE 33 Calculated Pile Lengths of Pile C-1.

Test No.	Accelerometer 1		Accelerometer 2	
	Δt (μs)	L_t (ft)	Δt (μs)	L_t (ft)
1	4600	24	- *	-
2	4580	23.9	4380	25.9
3	4500	23.5	4020	24.1
4	4560	23.8	4320	25.6

SE/IR Tests on Piles C-1 (IR Analysis) IR analyses were carried out for the eighteen SE/IR tests mentioned previously. The first resonant frequencies and the estimated length of the pile for these eighteen tests are indicated in Table 34.

TABLE 34 First Resonant Frequencies of IR Analysis for Pile C-1.

Test No.	Accelerometer 1 (Hz)	Accelerometer 2 (Hz)
1	210	210
2	210	210
3	208	208
4	208	208
5	-	210
6	208	-
7	208	-
8	208	208
9	208	-
10	208	-
11	208	-
12	210	210
13	-	-
14	-	-
15	-	-
16	-	-
17	-	-
18	-	-

The pile length was estimated from the first resonant frequencies and the pile length was calculated:

$$L_t = \frac{v}{2 \times \Delta f}$$

Δf: First resonant frequency (Hz)

v: Assumed wave velocity = 10000 ft/s

The average pile lengths determined by IR analysis for the three source applications are listed in Table 35. Downward striking at Point *B* produced good estimation of pile length. The time domain analysis on the results of upward striking on Point *A* did not reveal the pile length. In contrast, IR analysis did produce a reasonable pile length (24 ft) from the data of Accelerometer 1 (closer to the pile top). The value is similar to 24.4 ft, the average pile length determined from SE analysis. We should try our best to place one accelerometer as close as to the pile top in SE/IR tests.

Poor results were obtained when the source was applied by striking the wedge. Thus, wooden wedge is not recommended as striking blocks.

TABLE 35 Average First Resonant Frequencies and Calculated Lengths of Pile C-1.

Striking Condition	Average Δf (Hz)	L_t (ft)
Downward at Point B	209	23.9
Upward at Point A	208.6	24
Inclined on wedge	-	-

SE/IR Tests on Pile C-2 (SE Analysis) Twelve SE/IR tests were conducted on Pile C-2 with different hammer tips. The source was created by downward striking on pile cap above the pile, downward striking on the pile cap near the pile, and upward striking on the pile cap near the pile. Figure 121 shows the source (Points A, B, and C) and receiver locations and Table 36 lists the specifications of these SE/IR tests.

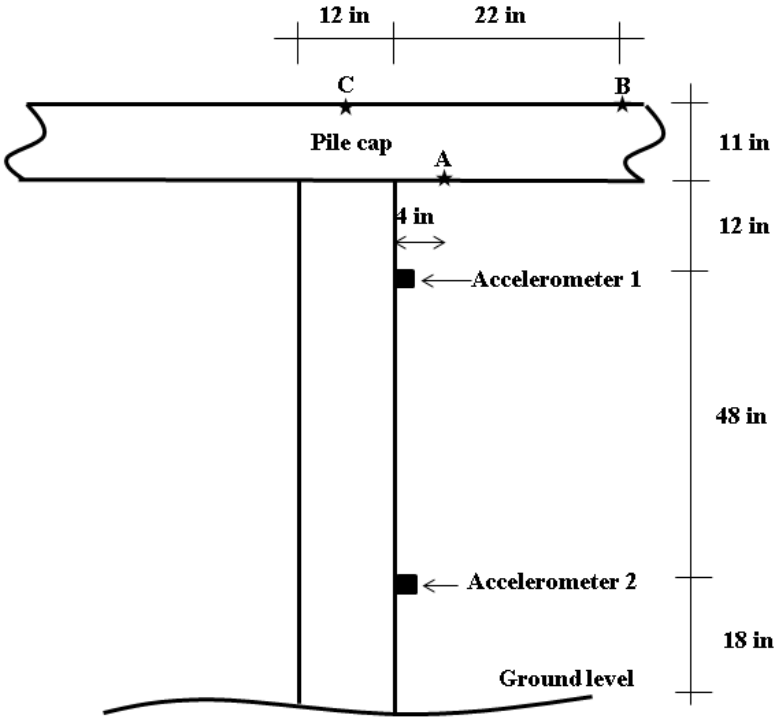

FIGURE 121 SE/IR Setup for Pile C-2

TABLE 36 Location and Direction of Hammer Strikes for Pile C-2.

Test No.	Hammer Tip	Location and Direction of Hammer Strike
1	Hard	Downward at C
2	Medium-hard	Downward at C
3	Medium-soft	Downward at C
4	Soft	Downward at C
5	Hard	Downward at B
6	Medium-hard	Downward at B
7	Medium-soft	Downward at B
8	Soft	Downward at B
9	Hard	Upward at A
10	Medium-hard	Upward at A
11	Medium-soft	Upward at A
12	Soft	Upward at A

When the impulse and echo were identified on the velocity graphs, the buried pile length and the total pile length were calculated. The calculated pile lengths from these SE/IR tests are indicated in Table 37. More successful SE tests were found when the striking point was closer to the pile. This is because more energy can be transmitted down the pile. If the impulse and echo were identified from the SE tests of different sources (Striking at Points A, B, or C), similar pile lengths were obtained.

TABLE 37 Calculated Pile Lengths of Pile C-2.

Test No.	Accelerometer 1		Accelerometer 2	
	Δt (μs)	L_t (ft)	Δt (μs)	L_t (ft)
1	-	-	-	-
2	-	-	3860	24.3
3	4520	23.6	4140	25.7
4	4980	25.9	4820	29.1
5	-	-	-	-
6	4540	23.7	3720	23.6
7	-	-	-	-
8	-	-	-	-
9	-	-	-	-
10	4320	22.6	3700	23.5
11	-	-	-	-
12	-	-	3860	24.3

The average length of each striking method was calculated and the result is presented in Table 38.

TABLE 38 Average Calculated Pile Lengths of Pile C-2.

Striking Condition	Average L_t (ft)
Downward at C	24.5
Downward at B	23.6
Upward at A	23.5

SE/IR Tests on Pile C-2 with IR analysis The IR Analysis were carried out for these twelve SE/IR tests. The success rate was low and the first resonant frequencies were identified for some tests as indicated in Table 39. The first frequency is equal to 210 Hz for Tests 2, 5, 6, and 7. The estimated pile length is 23.8 ft with an assumed wave velocity of 10,000 ft/s. For upward striking at A, IR analysis did not lead to pile length while SE analysis did. However, the overall success rate from IR analysis was unacceptable. Therefore, it is recommended that the IR analysis should be used as the secondary and SE analysis be considered as the primary analysis tool.

TABLE 39 First Resonant Frequencies (Hz) for Pile C-2.

Test No.	Accelerometer 1	Accelerometer 2
1	-	-
2	210	-
3	-	-
4	-	-
5	-	210
6	210	-
7	-	210
8	-	-
9	-	-
10	-	-
11	-	-
12	-	-

SE/IR Tests on Piles D-4 (SE Analysis) Twelve SE/IR tests were conducted on Pile D-4 with different hammer tips. Figure 122 shows the locations of the three sources (A, B, and C) and the locations of the two accelerometers. The longitudinal wave was created by striking downward at C, upward at A, and downward at B. The specifications of the SE/IR tests are indicated in Table 40.

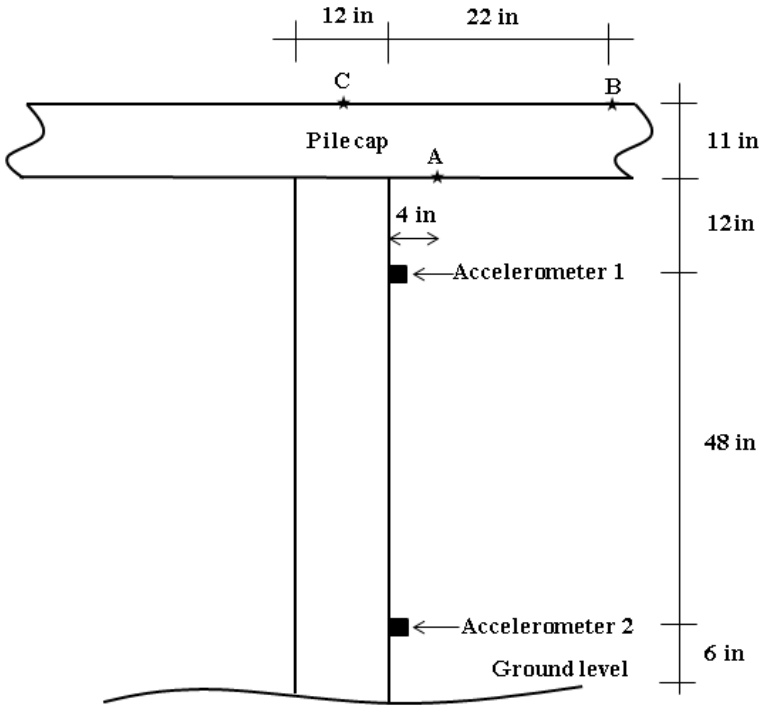

FIGURE 122 SE Setup for Pile D-4

TABLE 40 Location and Direction of Hammer Strikes for Pile D-4.

Test No.	Hammer Tip	Location and Direction of Hammer Strike
1	Hard	Downward at C
2	Medium-hard	Downward at C
3	Medium-soft	Downward at C
4	Soft	Downward at C
5	Hard	Upward at A
6	Medium-hard	Upward at A
7	Medium-soft	Upward at A
8	Soft	Upward at A
9	Hard	Downward at B
10	Medium-hard	Downward at B
11	Medium-soft	Downward at B
12	Soft	Downward at B

Table 41 shows the pile lengths calculated from these SE tests. For SE tests with clear impulse and echo in the velocity graphs, the lengths of the pile were calculated. The calculated pile lengths are indicated in Table 41.

TABLE 41 Calculated Pile Lengths of Pile D-4.

Test No.	Accelerometer 1		Accelerometer 2	
	Δt (μs)	L_t (ft)	Δt (μs)	L_t (ft)
1	-	-	4580	27.9
2	4420	23.1	-	-
3	4920	25.6	-	-
4	-	-	-	-
5	4280	22.4	-	-
6	4640	24.2	4600	28
7	4660	24.3	-	-
8	-	-	-	-
9	-	-	-	-
10	-	-	-	-
11	-	-	-	-
12	-	-	-	-

The success rate of downward striking at Point B (22 inches away from the test pile) is lower than the success rates of downward striking at Point C (above the pile) and upward striking at Point A (4 inches from the pile). Once again, the result indicated that the striking point should be as close to the pile as possible to guarantee the generation of waves with the greatest possible energy.

The average lengths for downward striking at C and upward striking at A are 25.5 and 24.7 ft, respectively.

SE/IR Tests on Piles D-4 (IR analysis) The IR analysis was carried out to supplement the SE analysis. The first resonant frequencies of all tests are indicated in Table 42. A single resonant frequency (208 Hz) was identified and the corresponding pile length is 24 ft. This value supported the finding obtained from the time domain analysis (23.1 to 28 ft).

TABLE 42 First Resonant Frequencies (Hz) for Pile D-4.

Test No.	Accelerometer 1	Accelerometer 2
1	208	208
2	208	208
3	208	208
4	208	208
5	-	208
6	208	208
7	208	208
8	208	208
9	-	-
10	208	208
11	208	208
12	208	208

Summary of SE/IR Results at Bridge No. 1676 The results of all test piles are summarized in Table 43. The error is less than 10% that is within the accuracy range of SE/IR tests. The success rate in determining the pile length is 100% at this site.

TABLE 43 SE Tests Results of Piles at Bridge No. 1676.

Pile	Embedment Pile Length (ft)	Exposed Pile Length (ft)	Total Pile Length (ft)	As-built Pile Length (ft)	Error(%)
C-1	17.6	6.5	24.1	23	4.8
C-2	17.3	6.5	23.8	23	3.5
D-4	18.9	5.5	24.4	23	6.1

2.1.4.5 Partially Dismantled Bridge near Route 419 (Bridge No. 6253)

The partially dismantled bridge (Bridge No. 6253) is located 64 miles east of Las Vegas. The bridge was used to be on Route 419 (coordinates 34.211303, -106.921087). Figure 123 shows the location of the bridge. Route 419 was realigned and the bridge was no longer in service. The superstructure of the bridge was removed when the research team arrived at the site. Only pile caps and round timber piles were presented as shown in Figure 124.

FIGURE 123 Location of the Partially Dismantled Bridge near Route 419

FIGURE 124 Photo of the Partially Dismantled Bridge near Route 419

This site was selected because the piles are going to be pulled out. The actual pile length finally become known which enables the research team to verify the results of nondestructive tests. SE/IR tests were conducted on five piles as shown in Figure 125. Since the findings were very similar to the conclusions of previous bridges on timber piles the results are not elaborated here. The results including the embedment pile lengths and the total pile lengths are listed in Table 44.

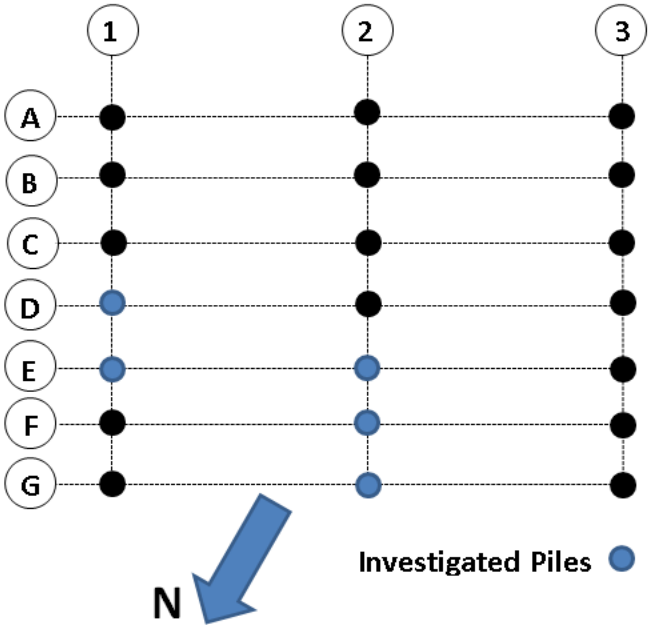

FIGURE 125 Investigated Piles of the Partially Dismantled Bridge near Route 419

TABLE 44 SE Tests Results of the Partially Dismantled Bridge near Route 419.

Pile	Embedment Pile Length (ft)	Exposed Pile Length (ft)	Total Pile Length (ft)
D-1	8.60	6.2	14.8
E-1	8.15	6.25	14.4
E-2	8.74	7.0	15.7
F-2	7.66	7.42	15.1
G-2	6.95	7.25	14.2

2.1.4.6 Bridge No. 7480

Bridge No. 7480 is located north of Shiprock, NM, on NM 491 crossing, over the Salt Creek. The coordinates of the bridge are 36.826389, -108.692500. Figures 126 and 127 show the location of the site and the street view of the bridge, respectively. The bridge is supported by 11 battered and 11 straight steel-H piles. The piles were extended from the bottom of the superstructure to the ground level, and continued under the ground surface to form the foundation.

FIGURE 126 Location of Bridge No. 7480


FIGURE 127 Street View of Bridge No. 7480

Although SE tests were found unsuitable for H-piles in the literature (*2, 19*), the research team also elected to conduct SE tests to explore the possibility of the piles depths detection by various test configurations.

Holes had been predrilled by NMDOT engineers. Metal blocks for striking and mounting accelerometer were attached onto the web of the H-pile with bolts. Two accelerometers were used. A nonconventional SE test setup is shown in Figure 128. The source (hammer striking) was between two accelerometers. Although numerous SE tests of different setups were performed on different piles, none of the results were successful.

FIGURE 128 SE Test Setup for a H-pile of Bridge No. 7480

Figure 129 shows a typical velocity graph obtained from a vertical striking on the metal block attached to the H-pile web. High frequency vibrations are evident in this figure. The high frequency response corresponds to the reflections from the boundaries of the steel cross section. When a strike is applied at the middle of the web, the wave travels horizontally as well as vertically through the thin-walled members, unlike circular (or square) solid piles in which most energy travels downward. The sensor picks up the reflected waves from the free boundaries, which in turn interfere with the expected reflected longitudinal wave from the pile bottom.

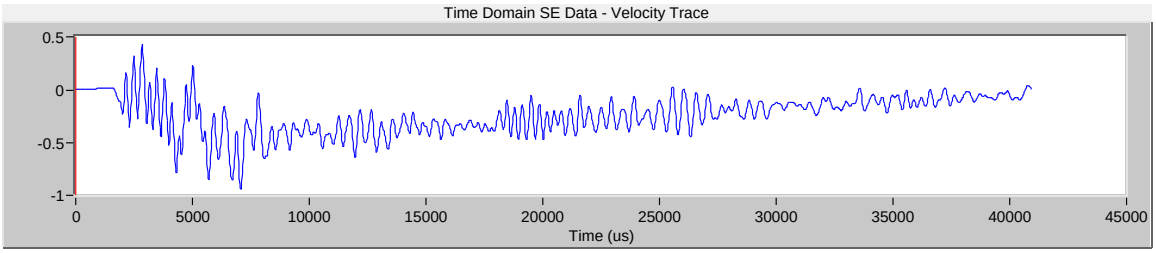

FIGURE 129 Velocity Time History Signal Obtained from Vertical Striking on a Metal Block Attached to a H-pile

Apart from the difficulties mentioned above, steel H-piles transmit a large portion of the wave energy into the surrounding soil due to their specific cross section configuration. Less energy is

transmitted to the pile bottom, which significantly decreases the amplitude of the echo from the pile toe.

2.1.4.7 Bridge No. 5899

In addition to the NDT tests performed on timber piles, the research team decided to conduct SE tests on concrete piers. Bridge No. 5899 in District 5 was selected for testing since there are three intermediate concrete piers. The bridge is located 66 miles north of Santa Fe on NM 111 crossing over the Rio Vallecitos as shown in Figure 130. The coordinates of the bridge are 36.49485, -106.1124972. The street and aerial views of the bridge are shown in Figure 131. The bridge is a 4-span concrete bridge supported by three intermediate concrete piers. The side view of one of the piers is indicated in Figure 132.

FIGURE 130 Location of Bridge No. 5899

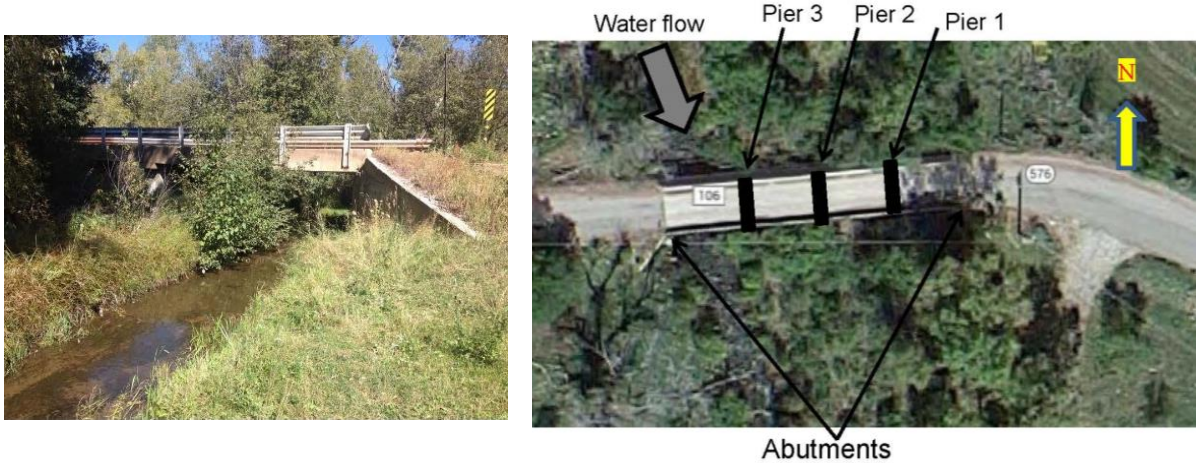

FIGURE 131 Street and Aerial Views of Bridge No. 5899

FIGURE 132 Side View of One of the Piers

SE tests were conducted on all three concrete piers. Figure 133 shows the schematic SE test setup for each pier. Alphabetical notations A-F designate various locations of the source and numeral notations 1-3 designate accelerometer locations. The distances d_1 and d_2 are shown in Table 45 for different piers.

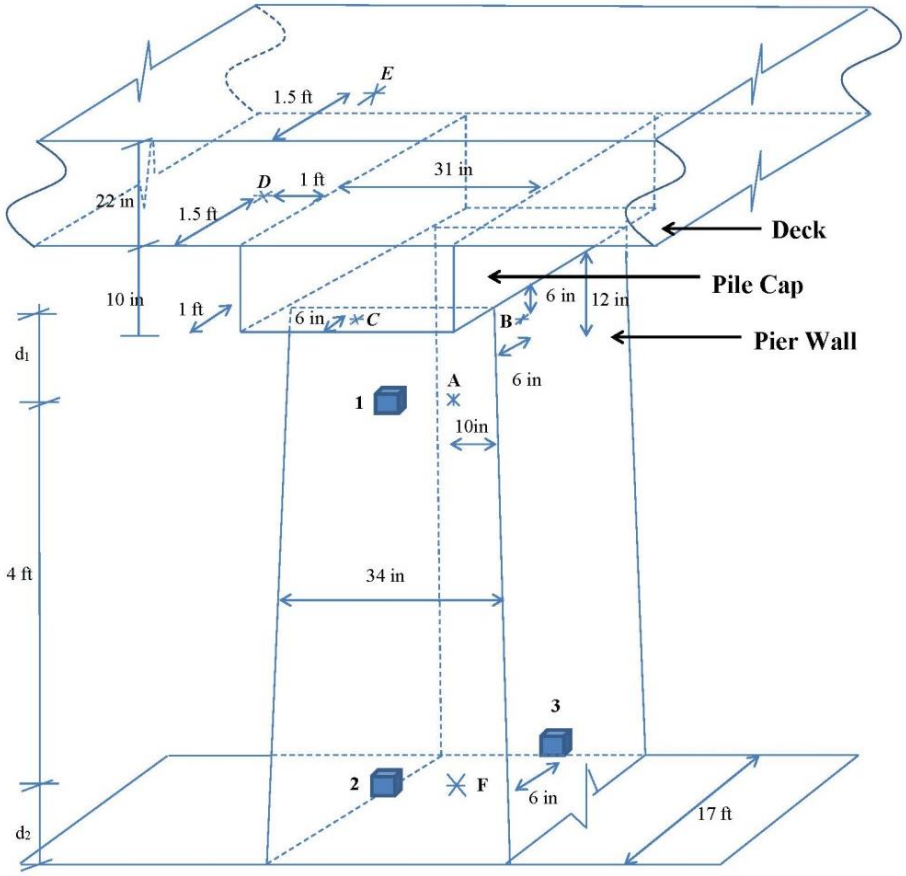

FIGURE 133 Schematic SE Test Setup for Each Pier

TABLE 45 Distances d_1 and d_2 for Sensor Placement on Each Pier Wall.

Pier 1		Pier 2				Pier 3	
North Side		South Side		North Side		North Side	
d_1 (in)	d_2 (in)	d_1 (in)	d_2 (in)	d_1 (in)	d_2 (in)	d_1 (in)	d_2 (in)
6	24	12	12	12	24	6	22

The SE tests were performed with two accelerometers attached vertically to the side of the test pier as shown in Figure 134. The accelerometers were vertically mounted on the wooden blocks glued onto the pier surface.

FIGURE 134 Attached Accelerometers on the Pier Side

Wave Velocity Measurement Before conducting SE tests to determine the buried lengths of the piers, the propagated wave velocity in the concrete pier was measured. Three horizontal strikes with hard hammer tip were applied at Point F (see Figure 133) and the time difference between the impulse and echo obtained from a horizontally placed accelerometer at Point 3 were measured. The generated wave from the horizontal strike reaches the accelerometer, reflects from the opposite side of the pier and arrives at the accelerometer again. Since the horizontal pier width is known, the wave velocity can be determined. The results are indicated in Table 46.

TABLE 46 Estimated Wave Velocities of the Concrete Pier.

Test No.	Δt (μs)	v (ft/s)
1	3,060	10,784
2	3,100	10,645
3	3,100	10,645

The average velocity (10,700 ft/s) was used to calculate the buried lengths of the piers for all SE tests conducted on the piers. For each SE test, the impulse and echo were sought in the velocity graphs and the Δt was used to determine the buried length.

SE tests on Pier 1 Fifteen SE tests were conducted on the north side of Pier 1. Three different hammer tips (hard, medium-hard, and medium-soft) and two striking directions (horizontal and vertical) were used. Table 47 shows the hammer tips and the striking locations and directions for each test. The locations can be found in Figure 133.

TABLE 47 Hammer Tips and Striking Locations and Directions for Testing at the North Side of Pier 1.

Test No.	Hammer Tip	Location (Direction) of Hammer Strike
1	Hard	A(horizontal)
2	Hard	A(horizontal)
3	Hard	A(horizontal)
4	Hard	B(horizontal)
5	Hard	B(horizontal)
6	Hard	B(horizontal)
7	Hard	E(vertical)
8	Hard	E(vertical)
9	Hard	E(vertical)
10	Medium-hard	E(vertical)
11	Medium-hard	E(vertical)
12	Medium-hard	E(vertical)
13	Medium-soft	E(vertical)
14	Medium-soft	E(vertical)
15	Medium-soft	E(vertical)

Table 48 shows the estimated lengths of the pier wall based on the SE results. The measured concrete wave velocity of 10700 ft/s was used to calculate the length of the pier wall. Horizontal striking did not produce useful results (echo from the bottom cannot be identified in the velocity graphs). Vertical striking generated good velocity graphs such that the echo from the bottom was identified easily. The average embedment depth of the pier wall is 22 ft and the height of the pier wall is 23.8 ft.

TABLE 48 Results of SE Tests Conducted at the North Side of Pier 1.

Test No.	Striking Direction	Accelerometer 1		Accelerometer 2	
		Δt (μs)	L_t (ft)	Δt (μs)	L_t (ft)
1	Horizontal	--	--	--	--
2	Horizontal	--	--	--	--
3	Horizontal	--	--	--	--
4	Horizontal	--	--	--	--
5	Horizontal	--	--	--	--
6	Horizontal	--	--	--	--
7	Vertical	4000	21.9	3220	21.7
8	Vertical	3900	21.4	3080	21.0
9	Vertical	--	--	3420	22.8
10	Vertical	4280	23.4	3340	22.4
11	Vertical	4200	23.0	3320	22.3
12	Vertical	4300	23.5	3360	22.5
13	Vertical	4420	24.1	3280	22.0
14	Vertical	4440	24.3	3140	21.3
15	Vertical	4000	21.9	3220	21.7

SE/IR Tests at South Side of Pier 2 by SE Analysis Twenty SE/IR tests were conducted at the south side of Pier 2. The source was applied on five different points with three different hammer tips. The strikes were the horizontal striking on the south (or west) side of the pier wall, upward striking on the pile cap (or on the bottom of the bridge deck), and vertical downward striking on the bridge deck above the pier wall. Figure 135 shows the application of upward striking on the pile cap and on the bottom surface of the bridge deck. Table 49 shows the used hammer tips and the location and direction of the hammer strike for each test at the south side of Pier 2. Table 50 shows the results of SE tests conducted at the south side of Pier 2. Similar to Pier 1, horizontal striking (Tests 1-3 and 9-11) did not produce useful data and consequently the pier length was not determined. The length of the pier was determined from SE tests of all vertical striking. The average length of Pier 2 at the south side is 26.8 ft.

TABLE 49 Hammer Tips, Location, and Direction of Hammer Strikes at the South Side of Pier 2.

Test No.	Hammer Tip	Location (Direction) of the Hammer Strike
1	Hard	A (Horizontal)
2	Hard	A (Horizontal)
3	Hard	A (Horizontal)
4	Hard	C (Vertical-upward)
5	Hard	C (Vertical-upward)
6	Hard	C (Vertical-upward)
7	Hard	D (Vertical-upward)
8	Hard	D (Vertical-upward)
9	Hard	B (Horizontal)
10	Hard	B (horizontal)
11	Hard	B (horizontal)
12	Hard	E (vertical)
13	Hard	E (vertical)
14	Hard	E (vertical)
15	Medium-hard	E (vertical)
16	Medium-hard	E (vertical)
17	Medium-hard	E (vertical)
18	Medium-soft	E (vertical)
19	Medium-soft	E (vertical)
20	Medium-soft	E (vertical)

FIGURE 135 Upward Striking on the Pile Cap and on the Bridge Deck

TABLE 50 Results of SE Tests Conducted at the South Side of Pier 2.

Test No.	Accelerometer 1		Accelerometer 2	
	Δt (μs)	L_t (ft)	Δt (μs)	L_t (ft)
1 ~ 3	--	--	--	--
4	--	--	4020	26.5
5	4,740	26.4	3880	25.8
6	-	-	4040	26.6
7	4,880	27.1	--	--
8	4,800	26.7	--	--
9 ~ 11	--	--	--	--
12	5,240	29.0	3660	24.6
13	5,220	28.9	3800	25.3
14	5,200	28.8	3800	25.3
15	5,020	27.9	3880	25.8
16	5,100	28.3	3720	24.9
17	5,100	28.3	3880	25.8
18	4,960	27.5	3960	26.2
19	5,020	27.9	4040	26.6
20	5,020	27.9	3880	25.8

SE/IR tests at South Side of Pier 2 by IR Analysis The IR analysis has been previously applied to SE/IR tests on timber piles. It was demonstrated that IR analysis may provide additional information on determining the length of the pile. When the impulse and echo are undistinguishable in the velocity graph of SE analysis, IR analysis may be able to provide a reasonable estimation regarding the buried depth by using the resonant frequencies. The resonant frequencies and corresponding calculated buried pier lengths at the south side of Pier 2 are indicated in Table 51. Similar to the SE analysis, horizontal striking (Tests 1-3 and 9-11) did not work either. Data of both accelerometers of all vertical striking produced useful and consistent results. The average height of Pier 2 at the south side is 24.5 ft. This value is less than the average height obtained from SE analysis (26.8 ft).

TABLE 51 Resonant Frequencies and Calculated Pier Lengths at the South Side of Pier 2.

Test No.	Accelerometer 1		Accelerometer 2	
	Δf (Hz)	L_t (ft)	Δf (Hz)	L_t (ft)
1 ~3	--	--	--	--
4	218	24.5	224	23.9
5	218	24.5	224	23.9
6	218	24.5	224	23.9
7	218	24.5	220	24.3
8	218	24.5	220	24.3
9 ~ 11	--	--	--	--
12	218	24.5	218	24.5
13	216	24.8	218	24.5
14	216	24.8	218	24.5
15	220	24.3	222	24.1
16	218	24.5	220	24.3
17	218	24.5	220	24.3
18	215	24.9	217	24.7
19	215	24.9	217	24.7
20	216	24.8	217	24.7

SE Tests at the North Side of Pier 2 Twelve SE tests were performed at the north side of Pier 2. Only hard hammer tip was used. The source was applied in four different ways as shown in Table 52. The results of the SE analysis are shown in Table 53.

TABLE 52 Hammer Tips, Location, and Direction of Hammer Strikes at the North Side of Pier 2.

Test No.	Location (Direction) of the Hammer Strike
1	A (Horizontal)
2	A (Horizontal)
3	A (Horizontal)
4	C (Vertical-upward)
5	C (Vertical-upward)
6	C (Vertical-upward)
7	D (Vertical-upward)
8	D (Vertical-upward)
9	D (Vertical-upward)
10	E (Vertical)
11	E (Vertical)
12	E (Vertical)

TABLE 53 Results of SE Tests Conducted at the North Side of Pier 2.

Test No.	Accelerometer 1		Accelerometer 2	
	Δt (μs)	L_t (ft)	Δt (μs)	L_t (ft)
1 ~ 3	--	--	--	--
4	--	--	5120	32.4
5	--	--	5120	32.4
6	--	--	5060	32.1
7	5940	32.8	5200	32.8
8	5540	30.6	5120	32.4
9	5800	32.0	5200	32.8
10	--	--	5160	32.6
11	--	--	5100	32.3
12	--	--	4860	31.0

Again, the results of horizontal striking did not work. Vertical striking produced good velocity graphs that can be used to determine the height of the pier. Examples of good SE velocity graphs (impulse and echo can be identified easily) for the downward and upward vertical strikes are shown in Figures 136 and 137 respectively. Comparing these two figures indicates the change of polarity for upward striking on the pile cap (or the deck) that generated tension wave.

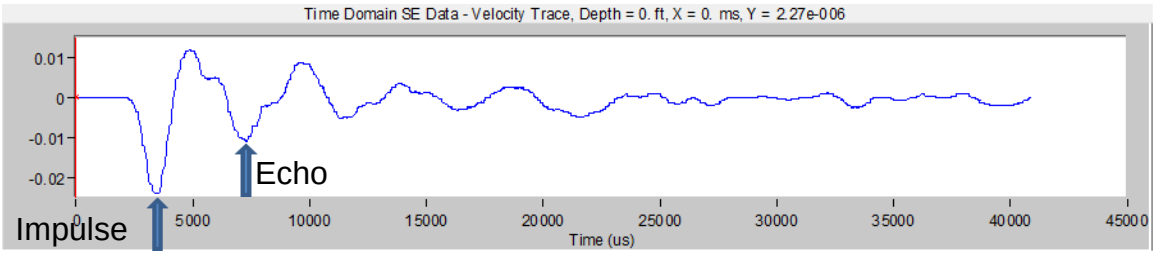

FIGURE 136 Typical Velocity Graph of Downward Striking at Point E

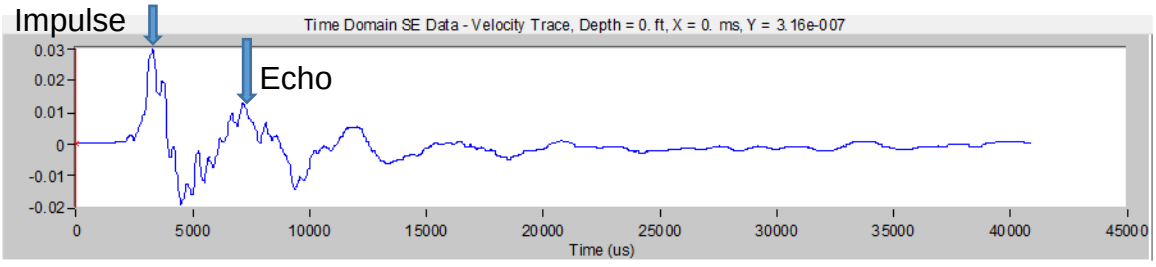

FIGURE 137 Typical Velocity Graph of Upward Vertically Striking at Point C

Table 54 shows the average buried depths of Pier 2 at south and north sides for different source applications. The NDT tests show that the embedment depth of pier at north side is 4.6 ft deeper than that of the south side. This may due to the existence of an abnormality at the south side that causes the impedance change.

TABLE 54 Average Buried Depths at the South and North Sides of Pier 2.

Input Method	South Side (ft)	North Side (ft)
Downward striking at E	20.9	25
Upward striking at C	20.3	25.7
Upward striking at D	20.9	25.1

SE/IR Tests on Pier 3 Fourteen SE tests were conducted at the north end of Pier 3 with the hard hammer tip. The source was applied in four different ways as indicated in Table 55.

TABLE 55 Direction and Location of Hammer Strike at the North Side of Pier 3.

Test No.	Location (Direction) of the Hammer Strike
1	A (Horizontal)
2	A (Horizontal)
3	A (Horizontal)
4	C (Vertical-upward)
5	C (Vertical-upward)
6	C (Vertical-upward)
7	D (Vertical-upward)
8	D (Vertical-upward)
9	D (Vertical-upward)
10	E (Vertical)
11	E (Vertical)
12	E (Vertical)
13	E (Vertical)
14	E (Vertical)

Table 56 shows the results of SE tests conducted at the north end of Pier 3. Some of the velocity graphs of Accelerometer 1 showed multiple echoes of similar magnitudes which made it difficult to determine the right echo from the toe. This was not expected since the accelerometer was close to the bridge deck. It was not due to the mounting or the malfunctioning of the accelerometer. Therefore, it is a good practice to use more than one accelerometer for SE/IR tests.

Table 57 lists the buried lengths and the total lengths of the pier at the north side using different striking methods. Consistent results were found and the average buried and total length are 16.3 ft and 23.5 ft respectively.

TABLE 56 Results of SE Tests Conducted at the North Side of Pier 3.

Test No.	Accelerometer 1			Accelerometer 2		
	Δt (μs)	L_t (ft)	L_b (ft)	Δt (μs)	L_t (ft)	L_b (ft)
1 ~ 3	--	--	--	--	--	--
4	4000	21.4	14.2	3540	24.3	17.1
5	4480	24.0	16.8	--	--	--
6	4220	23.9	16.7	3540	24.3	17.1
7	--	--	--	3300	23.0	15.8
8	--	--	--	--	--	--
9	3940	21.1	13.9	3600	24.6	17.4
10	--	--	--	3460	23.8	16.7
11	--	--	--	3480	24.0	16.8
12	--	--	--	3480	24.0	16.8
13	--	--	--	3500	24.1	16.9
14	--	--	--	3420	23.6	16.5

TABLE 57 Average Buried Lengths at the North Side of Pier 3.

Striking Method	Buried Length (ft)	Total Length (ft)
Downward striking at E	16.7	23.9
Upward striking at C	16.4	23.6
Upward striking at D	15.7	22.9

The SE tests data obtained at this bridge are consistent. The results showed that the source applied by horizontal striking was not working at all. Upward striking on the pile cap and the bridge deck generated acceptable results. Downward striking at the bridge deck above the pier was the best way to apply the source. Although the better location of the sensor is the one close to the top of the pier in general, bad results were obtained occasionally. The additional accelerometer provides the necessary redundancy. Otherwise, the SE test needs to be repeated by placing the accelerometer at a different location.

Summary of SE/IR Results on Bridge No. 5899 The test results are summarized in Table 58 and the success rate is 100% for this bridge.

TABLE 58 SE Tests Results for Piles of Bridge No. 5899.

Pier	Embedment Length of the Pier (ft)	Total Length of the Pier (ft)
1-(North Side)	16.0	22.6
2-(South Side)	20.9	27.2
2-(North Side)	25.0	32.8
3-(North Side)	16.7	23.7

2.1.5 Conclusions of SE/IR Tests

Numerous SE/IR tests have been conducted on a railway bridge and six highway bridges with known and unknown foundations depths. The lengths of the piles (piers) were determined using the velocity graphs obtained from the accelerometers for time domain and frequency domain analyses. Propagated wave velocity was determined when enough exposed length of the foundation was available. If not, the wave velocities were selected based on the pile condition observed in the field. In some cases, IR analyses were carried out to support and confirm the SE interpretations. Depending on the conditions of the foundations and superstructures, most tests were successful. Determination of the piles lengths was not viable in some SE/IR tests due to problems related to the method of applying the source, the location of the accelerometer, and other relevant factors that will be discussed here.

Initial testing procedures were developed and affecting factors were identified after the preliminary investigation of the columns at UNM. The selected bridges for the field tests made of various foundation materials (concrete, wood, and steel) with different geometries. Various SE/IR setups (source and receivers) were examined to identify major factors affecting the results. The conclusions of each bridge provided data leading to better understanding of those affecting factors. Then, the tests procedures were improved and modified. The conclusions inferred from field tests play a significant role in both conducting the tests and interpreting the data in the future.

Factors affecting the success of the SE/IR tests were scrutinized during the field tests. A successful SE test is the one in which the impulse and the echo from the pile bottom can be identified in the velocity graph with certainty. The effects of major factors such as striking specification, sensors location, hammer tips, environmental conditions, and pile condition are discussed

Method of Striking Depending on the accessibility of the pile top and the condition of the superstructure, we examined various impulse locations that are able to produce a longitudinal wave of enough energy along the test object. As shown in Figure 138 (similar to Figure 23), the impulse can be applied at Points A, B, C, and the striking block attached on the pile, as well as the top of the pile. The arrows indicate the direction of the striking.

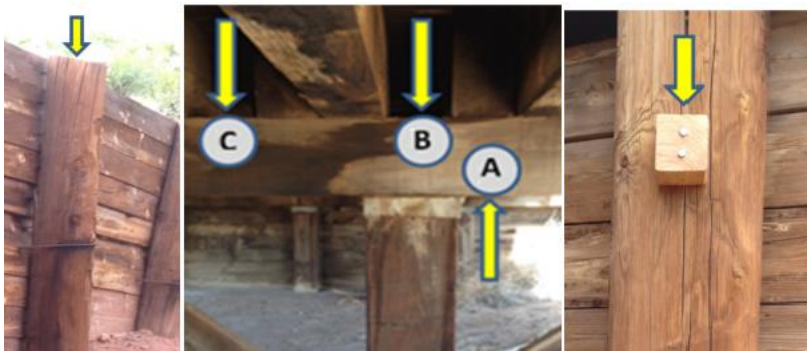

FIGURE 138 Proper Source Locations

Pile top striking This method can be used only when the pile top is accessible. The pile length was determined successfully in most of the cases. The impulses and echoes were clearly recognizable in the velocity graphs. Successful SE tests were obtained even for foundations for which only a small part of the pile top was exposed but large enough for a hammer strike.

Points B and C When the pile top is totally covered with the pile cap and superstructure, striking may be applied at Points B and C as indicated in Figure 138. However, we may only able to apply the impact by striking at Point C due to the location of girder in some cases. The success rate of SE/IR tests is lower than the pile top striking. Higher rate of successful SE tests has been observed at Point B than at Point C due to the greater distance between the striking point and the center of the pile. In addition, the calculated length is more consistent for striking at Point B than Point C. Therefore, Point B is preferable compared with Point C.

For reinforced concrete bridges, the longitudinal waves can be generated by striking at the top surface of the concrete bridge deck above the pier. However, the result depends on the impact energy. The impact energy should be great enough to assure the determination of the foundation depth.

If downward striking at Point C is used, the striking point should be as close to the pile center as possible to maximize the input energy.

Point A Upward striking on the bottom surface of the pile cap adjacent to the test pile can also be considered as an alternative means to generate the impulse source. The field study indicated that fewer successful SE tests were produced than striking at Point B since a stronger tensile wave together with a weaker reflected compression wave is transmitted down the pile rather than a stronger direct compression wave (striking at Point B).

Striking Block This method introduces additional uncertainty due to the problems related to the attachment of a striking block onto the pile surface. The impulse source is introduced by striking the block with a hammer. The field study indicated similar success rates for SE tests performed by striking at the wooden block and striking at Point A. The success rate was found to be much lower than striking at Point B.

Different methods of attaching the block onto the pile have been investigated. The block was mounted by nails (or screws), ties, and glue. Movement of the block was observed when the block was tied around the pile or was glued onto the pile by strong epoxy. Only secure attachment was found by mounting of the block by nails or screws. The striking block must be secured tightly onto the pile to restrict movement in order to produce good SE/IR results.

Blocks of different materials (aluminum and wood) and shapes (cube and wedge) have been tested. The aluminum block was specifically machined with a curved surface in order to provide a better contact with the side of the round piles. Table 59 shows the success rate of the SE tests in percentage performed by striking the block of different types.

TABLE 59 Success Rate of SE Tests for Different Striking Blocks.

Block Type	Aluminum Block	Wooden block	Wooden wedge
Success Rate (%)	23.3	56.8	35.7

As shown in Table 59, the success rate of using aluminum striking block is unsatisfied. The success rate is improved by using wooden blocks. The shape of the source signal for the aluminum block contained multiple peaks which was different from the typical hammer impulse on a rigid surface. The peaks may be due to either a momentary contact loss or multiple contacts between the block and the pile surface. Wedge blocks (the top surface is inclined) have been considered

although striking on wedge blocks produced a horizontal compression wave as well as a vertical compression wave. The study results showed that successful SE tests were produced by using the wedge blocks, however, more bad SE tests were found due to the imperfect coupling between the wedge block and the pile.

The problem of using striking blocks is mainly due to the appearance of multiple echoes in the velocity graphs which made the identification of the correct echo difficult.

Comparison of striking methods Table 60 lists the success rate of SE tests performed by different striking methods. Vertical downward striking on either the pile top or a point inside the projected pile cross section on pile cap top surface (Point B in Figure 138) transmits the most impulse energy directly to the pile, whereby the most consistent results have been obtained. Consequently, these two methods are the best to conduct SE/IR tests. If direct striking at the top of the pile is infeasible, striking on the top of the pile cap or upward striking on the bottom of the pile cap next to the pile (Points A or C in Figure 138) are alternative options. If none of these striking methods can be used, impulse source can be generated by striking on a wooden block that is tightly attached onto the pile. Striking the existing bolts or members that brace the pile sometimes produce successful SE tests.

It should be noted that each striking method will produce different levels of consistency depending on the strike quality, pile condition, and superstructure condition.

TABLE 60 Success Rate of SE Tests for Different Striking Methods.

Striking Point	Pile Top	Pile Top Edge	Pt. A	Pt. B	Pt. C	Striking Block
Success Rate (%)	83.3	52.4	54.1	81.3	37.5	56.3

Accelerometer Location If possible, the receiver should be placed at the top of the pile. Otherwise, the location should be selected such that the arrival time of the reflected upward wave from the pile bottom differs significantly from the reflected downward wave from the pile top. Since the pile length is not known repeating the test at a different sensor location is recommended when poor results are obtained.

As mentioned previously, when the sensor is placed too close to the striking point, the noise of high frequency was observed that significantly affected the identification of the echo in the velocity graph. The field tests indicated that successful SE tests were obtained when the accelerometer was placed 1-2 ft from the impulse source.

For the SE tests with two accelerometers, the inferred length of the pile was more consistent from the top accelerometer than the accelerometer mounted closer to the ground level, especially in the presence of running water. The accelerometer closer to the top of the pile is better because less complication from the reflections of both pile ends.

Hammer Tips The hard tip produced more successful SE tests than the other three softer tips. However, the benefit of using softer hammer tips was found occasionally. The velocity graphs of hard tip sometimes contained multiple echoes. The input signal of the hard tip contains waves of higher frequencies. The presence of such high frequencies were verified by numerical analysis. When closely spaced multiple valleys appear in the vicinity of the expected echo, using softer tips

may reveal the correct echo. When poor result of hard tip is observed, repeating the SE/IR test with a softer tip may overcome the difficulty.

Environmental and Foundation Conditions Environmental conditions may affect the SE/IR test results. In one of the investigated piles adjacent to water flow, the results of SE/IR tests were always bad although various setups were attempted. Successful tests were found on the next pile. It was expected that the noise due to the water flow (river current hit the pile) interfered with the SE tests. Other reasons might relate to the pile's condition such as rottenness or damage in the pile. The pile's condition has a huge effect on the clarity of signals. In one case, where there was a huge longitudinal crack in the pile, it was difficult to identify the correct echo because of the multiple wave reflections from the crack. When such abnormalities exist in piles, the actual depth of the foundation may not be determined by the SE/IR method.

Difficulties with Steel Piles Unsuccessful SE/IR tests were found for testing on a bridge supported by H-piles. High frequency vibrations were evident in the velocity graphs that corresponded to the reflections from the boundaries of the steel cross section. When a strike is applied at the middle of the web, the wave travels horizontally as well as vertically through the thin-walled members, unlike the results from a circular solid pile where most energy travels downward. The sensor picks up the reflected waves from the free boundaries, which in turn interfere with the expected reflected longitudinal waves from the pile bottom.

Apart from the difficulties mentioned above, steel H-piles transmit a large portion of the wave energy into the surrounding soil due to their specific cross section shape. Less energy is transmitted to the pile bottom, which significantly decreases the amplitude of the echo from the pile toe.

IR Analysis The IR analysis (based on the frequency content of the entire waveform) was carried out to complement the SE analysis. In some cases, IR analysis yielded the correct pile length while the echoes of SE tests could not be identified. It is recommended to perform an IR analysis when the SE data do not reveal the foundation depth. The field results indicated that the pile length determined by IR analysis was slightly different from those of obtained from SE tests, however, the calculated pile lengths from IR analysis were more consistent than those obtained from the SE tests. This might be due to the occasional wave interference of various frequencies which might hinder pinpointing the echo from the pile toe in the velocity graphs. The IR analysis isolates the effect of each frequency.

2.2 PARALLEL SEISMIC TESTS

PS tests can be used to determine the pile length for piles of all materials (timber, concrete, and steel). Also, the method can detect the pile length that is too long for being detected by SE/IR tests. Moreover, the PS method can be applied to detect the lengths of buried piles underneath a pile cap or a pier wall. The major disadvantage of the method is the requirement of drilling a borehole next to the pile with a depth deeper than the pile.

To study the applicability of the method on bridge foundations with different materials, both conventional and reverse test methods were used. Preliminary conventional PS tests were carried out to investigate the performance of the equipment on concrete short piers and to study the factors that affect PS tests results. Then, PS tests were performed on two bridge foundations made of steel H-piles and square timber piles. The as-built foundation depths are available at both sites. In addition to the conventional PS tests, the reverse PS test was performed on square timber piles of a bridge foundation. The reverse PS tests was accomplished with the purchased Geoprobe 7822DT drill rig and the results were compared to that obtained from the conventional PS tests.

2.2.1. PS Test Procedure

Before conducting a PS test, a borehole must be drilled next to the foundation. There are requirements for the preparation of the borehole:

- The borehole must align with the test pile.
- The depth of the borehole must be at least 15 ft deeper than the expected pile toe level.
- The hole should be bored as close as possible to the test pile (no more than 6 ft away from the pile).
- A 2-in PVC tube is prepared based on the depth of borehole and the bottom of the tube is caped.
- The PVC tube is inserted into the hole and the annular space between borehole and tube is grouted or filled with compacted soil.
- The PVC tube is filled with water.

The PS test is carried out in three steps: setup the hardware, data acquisition, and data processing.

2.2.1.1 Hardware Assemblage

Figure 139 shows the required equipment for conducting a PS test. The assembled equipment is shown in the figure. Engineers should follow the user manual of the equipment to assemble the device.

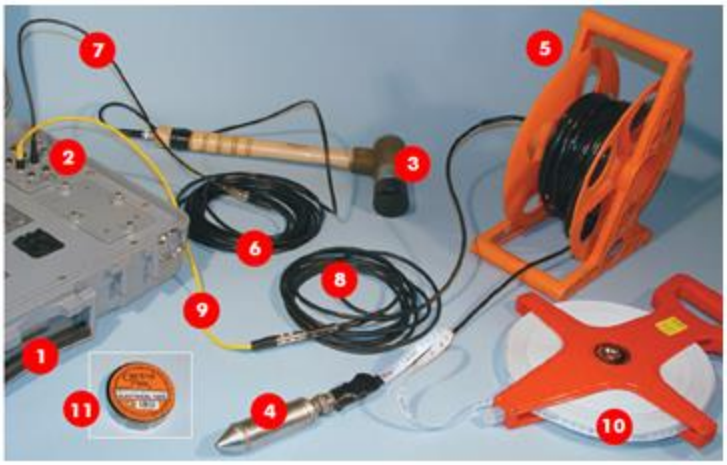

FIGURE 139 PS Equipment

2.2.1.2 PS Data Acquisition

The hydrophone is lowered towards the bottom of the PVC tube in an increment of either 1 ft or 2 ft. At each depth, the foundation is struck with a hammer and the software records and plots the signals of the hammer and hydrophone. The software WinGEO-T installed in the Olson Freedom Data PC has been used for data acquisition. A screen shot of the program including the obtained signals is shown in Figure 140.

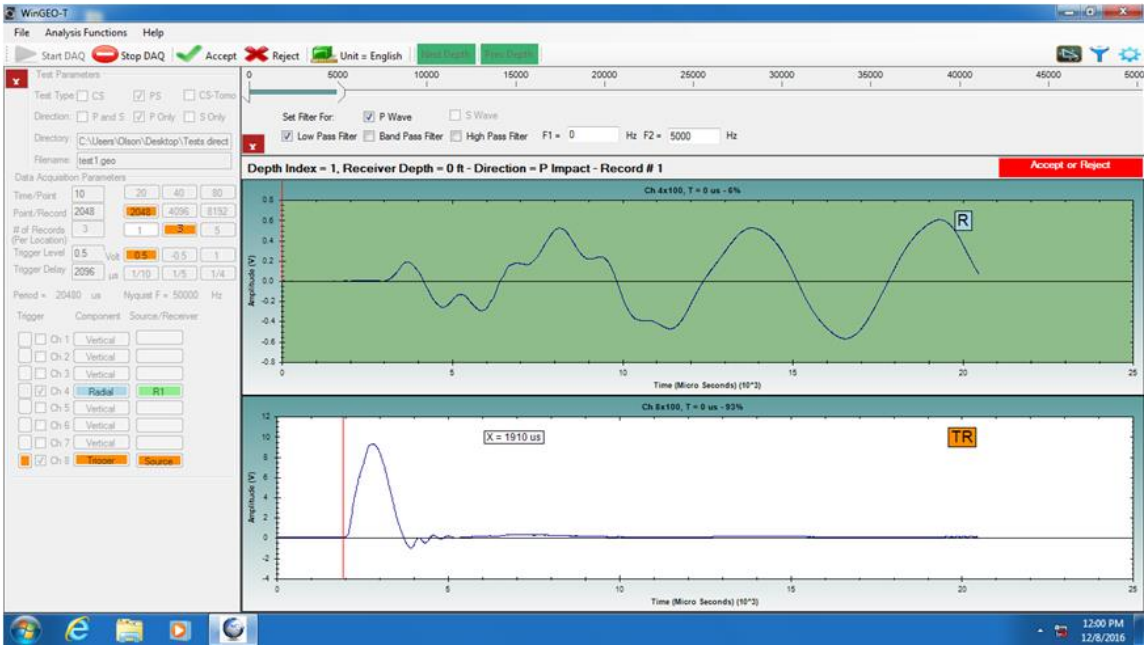

FIGURE 140 Screen Shot of Software WinGEO-T

2.2.1.3 Data Processing

After the data at each depth are gathered, the first arrival time corresponding to each depth can be determined from the velocity graph. Depending on the signal-to-noise ratio in the velocity graphs, the picking of the first arrival time may not be trivial. The correct pile length is determined if the first arrival times are picked correctly. A screen plot of a PS 'Stack Plot' of velocity graphs obtained from four consecutive depths is shown in Figure 141. The details of picking the arrival time and determining the pile toe will be discussed later.

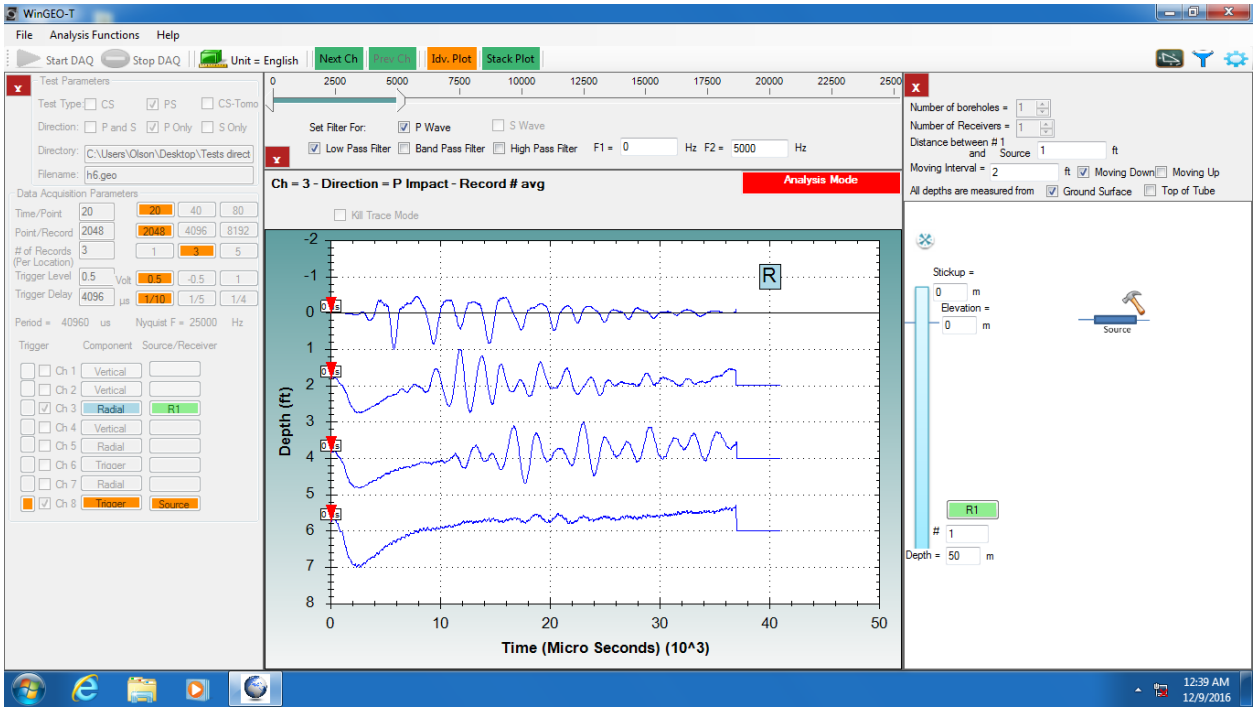

FIGURE 141 A Screen Shot of the Stack Plot with Four Consecutive Depths

2.2.2 Preliminary PS Tests

Initial PS tests were conducted at a test site off UNM campus to examine the capability of the equipment. The soil of the test site is silty clay with gravel. A 10-in diameter and 3-ft long reinforced concrete cylinder (pier) was installed at the test site. The PS test setup is shown in Figure 142. The depth of the concrete cylinder is 2 feet below ground. Four 2-in PVC pipes, each 5-ft in length, were installed at various distances from the center of the pile. The PVC pipes were then filled with water. PS tests were conducted by lowering a hydrophone into each of the pipes and impacting the center of the concrete pier with a hammer. The data were collected from each of the pipes at intervals of 1 foot starting at the ground level.

FIGURE 142 Configuration of the PS Testbed

Figure 143 shows the signal generated by the hammer. Figure 144 shows the received signals when the hydrophone is at the ground level and four feet below grade. The distance between the borehole and the concrete cylinder is 2 ft. Comparing Figures 144a and 144b, a delay in arrival time was observed as expected. Figure 144a shows a peak at 8 μs while Figure 144b shows a peak at 9 μs. The 1st valleys in Figures 144a and 144b were found at 11 μs and 13 μs, respectively.

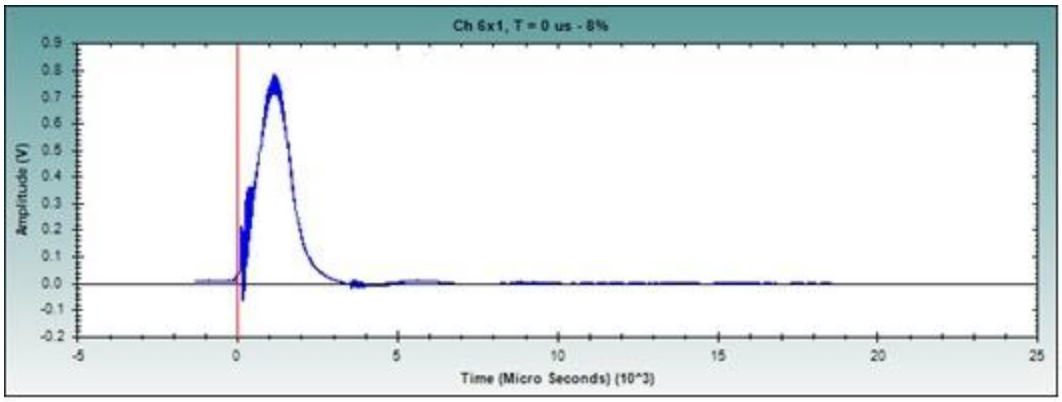

FIGURE 143 Duration and Amplitude of the Source Generated by a Hammer

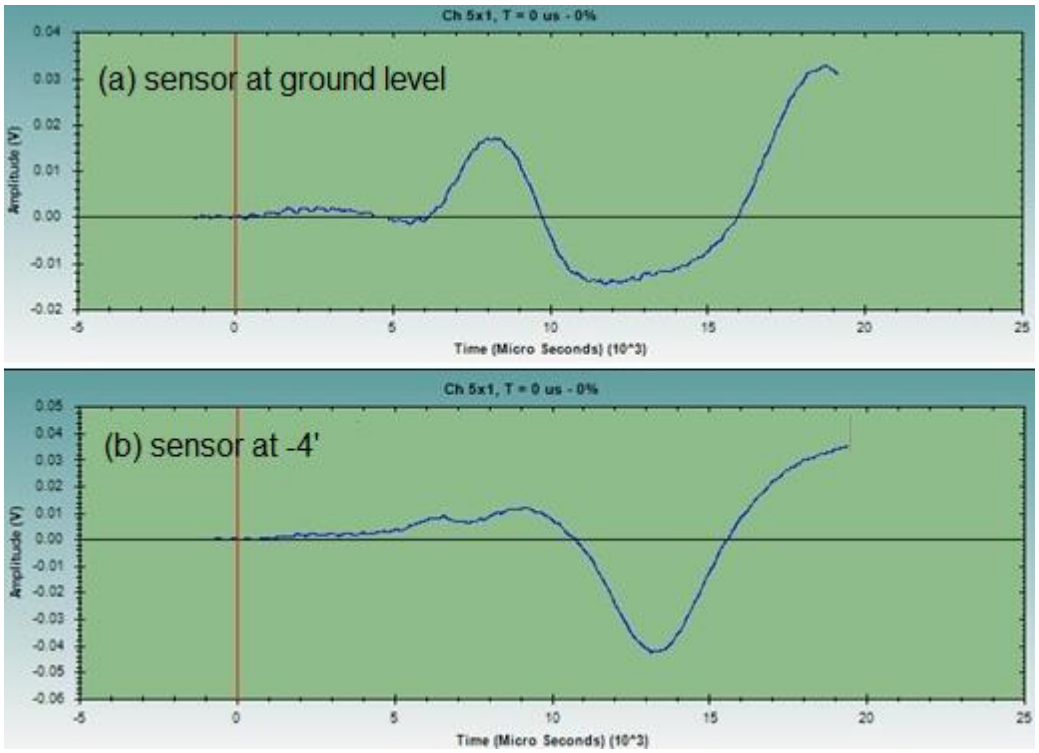

FIGURE 144 PS Data at Ground Level and at a Depth of 4 Feet

Assuming the typical wave velocities in concrete and in soil to be 12,000 ft./sec and 300 ft/sec respectively. The first arrival time should be 6.8 μs for the sound travels through 1 ft of concrete and 2 ft of soil for the sensor at the ground level. As shown in Figure 143, the peak of the input signal occurs at approximately 1 μs after impact. The 1st peak in Figure 144a is at 8 μs which is very close to the analytical value (7.8 = 6.8 + 1). The time taken for the wave to go through the concrete is insignificant compared to what it takes to go through the soil due to the much lower propagation speed in soil. When the sensor is 4 ft below ground, the analytical arrival time is 9.4 μs. There should be a delay of 1.6 μs. Figure 143 shows a delay of 1 and 2 μs based on the peaks and the valleys respectively. The result is in agreement with the theory.

PS tests were performed using other pipes (3, 4, and 5 ft from the source). For the PS test performed at the pipe placed at 3 ft from the source, the 1st peak and the 1st valley were at 10 and 13 μs respectively when the hydrophone was at the ground level. There was an additional 2 μs delay due to the additional one foot of soil in the wave path. Similar observations were found for the PS tests at the pipes 4 ft and 5 ft from the source.

The obtained waveform is always distorted when wave travels through various media. Therefore, interpreting the delay of less than 1 μs is unlikely to be accurate. This is likely to control the accuracy of PS tests.

The preliminary PS test results also indicated that the background noise affected the identification of the first arrival time of the wave. The good news is that the effect of the existing noise seems to decrease with depth. However, this finding may be inconclusive due to the limited depth of the PVC pipes.

2.2.3 Field PS Tests

PS tests were conducted on the foundations of Bridges Nos. 7480 and 1676. SE/IR tests have been conducted on these two bridges which were discussed previously. Bridge No. 7480 is supported by steel H-piles while Bridge No. 1676 is on timber piles. The results are presented according to the testing order at these two locations.

2.2.3.1 PS tests on Bridge No. 7480

Bridge No.7480 was selected by NMDOT as the first test site for conducting both PS and IF tests. The location of the site and the street view of the bridge can be found in Figures 126 and 127 respectively. The research team was only able to perform PS tests since the holes were bored at a distance greater than 18 in from the piles.

Eight test borings were drilled by Terracon. The borings are adjacent to the existing H-piles drilled to a depth ranging from about 25 to 40 ft below the ground surface. Figure 145 shows the plan view of the locations of boreholes related to the piles. Holes B-01 to B-04 are inclined. They are approximately parallel to the closest pile. Holes B-05 to B-08 are vertical.

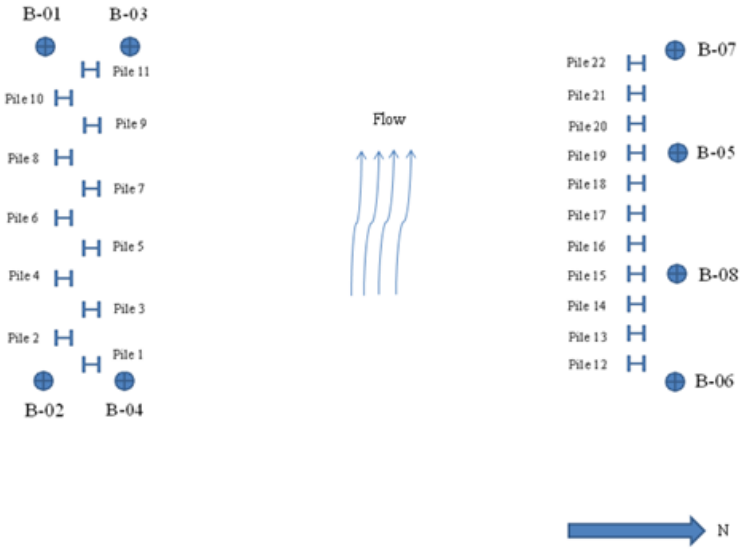

FIGURE 145 Foundation Configuration and Locations of Boreholes of Bridge No. 7480

Two-inch inner diameter PVC casings were placed in each boring with a water tight cap at the base and a removable cap at the top of the tube. The spacing between the PVC tube and the hole was backfilled with existing soil. Figure 146 shows a PVC pipe with its adjacent pile. Table 61 provides a summary of the depths for each borehole.

FIGURE 146 An Aligned PVC Pipe and the Adjacent Pile

TABLE 61 Boring Depths of the Holes.

Boring No.	Boring Depth (ft)
B-01	25
B-02	25
B-03	40
B-04	40
B-05	25
B-06	25
B-07	40
B-08	40

The contractor's report indicated three distinct soil layers at the site. The subsurface condition of the site is summarized in Table 62. The shale layer starts from a depth of 13~16 ft below grade. This layer is of interest since the as-built drawing indicates that the piles' tips were in the shale.

TABLE 62 Subsurface Condition at the Site.

Description	Approximate Depth to Bottom of Stratum (ft)	Material Encountered
Stratum 1	8 to 13	Sandy silt
Stratum 2	13 to 16	Clay, silt, sand and gravel content varied
Stratum 3	25 to 40 (termination of the borehole)	Shale bedrock

Difficulties at Site The original plan of the research team was to conduct PS tests at all borehole locations during the first visit. However, two problems were encountered at the site such that conducting PS tests at some holes were impossible. First, some PVC pipes (B-01, B-02, B-05 and B-08) were dry. A tentative PS test was conducted at one of the dry holes and the obtained poor result is shown in Figure 147. The hydrophone could not record good signals without the water coupling.

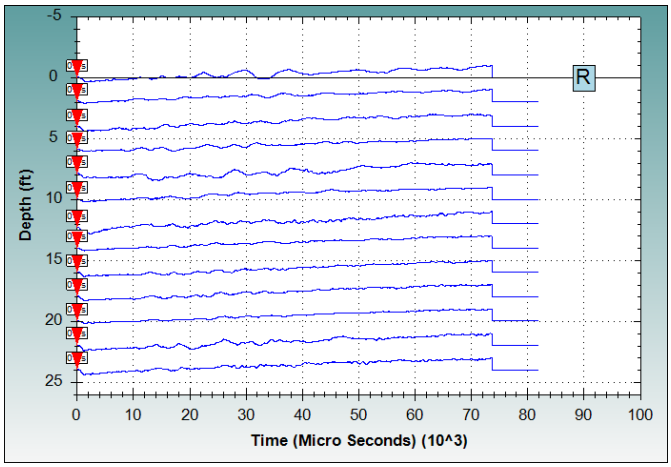

FIGURE 147 PS Test Result in a Dry Hole

The second problem was the damage of one installed PVC tube. As shown in Figure 148, the PVC pipe at B-06 was destroyed due to the movement of debris from flooding. Therefore, conducting PS test was also impossible at this borehole.

FIGURE 148 Destroyed Pipe (B-06)

Twenty PS tests were conducted during the second visit. The impulse was applied by striking the hammer vertically on the metal block that was attached on the web by bolts. Horizontal striking was applied on either the web or the flange. A hard hammer tip was used for Tests PS1 to PS19 while a medium-soft hammer tip was used in Test PS20. The strike direction, the borehole, and the borehole distance from the test pile are summarized in Table 63.

TABLE 63 Specifications of PS Tests.

Test	Pile	Strike Direction	Borehole	Borehole Distance (in)
PS1	1	Vertical	B-04	46
PS2	1	Vertical	B-04	46
PS3	1	Vertical	B-04	46
PS4	1	Vertical	B-04	46
PS5	2	Vertical	B-02	36
PS6	3	Vertical	B-04	136
PS7	10	Vertical	B-01	36
PS8	10	Horizontal (flange)	B-01	36
PS9	10	Horizontal (web)	B-01	36
PS10	11	Horizontal	B-03	72
PS11	11	Vertical	B-03	72
PS12	16	Vertical	B-07	153
PS13	16	Horizontal (flange)	B-07	153
PS14	19	Vertical	B-05	153
PS15	19	Horizontal (flange)	B-05	153
PS16	21	Horizontal (flange)	B-07	68
PS17	22	Vertical	B-07	36
PS18	22	Horizontal (flange)	B-07	36
PS19	22	Horizontal (web)	B-07	36
PS20	22	Vertical	B-07	36

Test Results for Pile 1 Four PS tests were carried out on Pile 1. The source was introduced by a vertical striking on an aluminum block which had been attached on the pile's web by bolts. The hydrophone was inserted in B-04 that was located at 4 ft from the test pile. A velocity time history obtained from the hydrophone is shown in Figure 149. The velocity time histories were recorded at intervals of 1 and 2 ft.

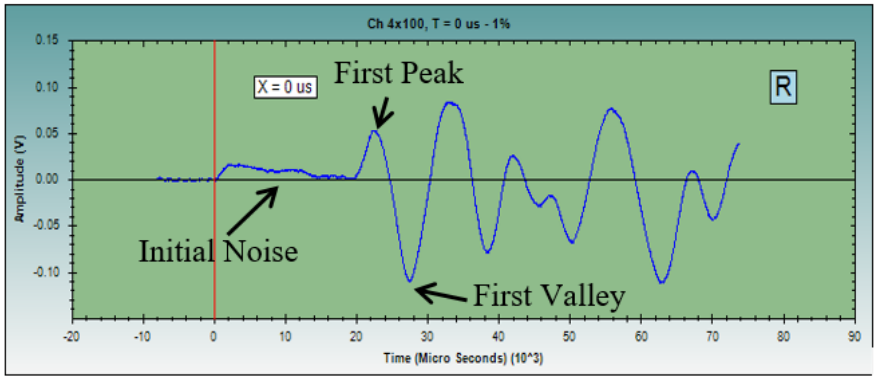

FIGURE 149 An Acceleration Time History Obtained from the Hydrophone

Because of the initial noise level shown in Figure 149, it is difficult to distinguish the arrival time of the first P-wave at some depths. For Test PS1, the first arrival times were plotted against depth in Figure 150. The figure shows three possible inflection points at three different depths below ground (8, 18, and 23 ft).

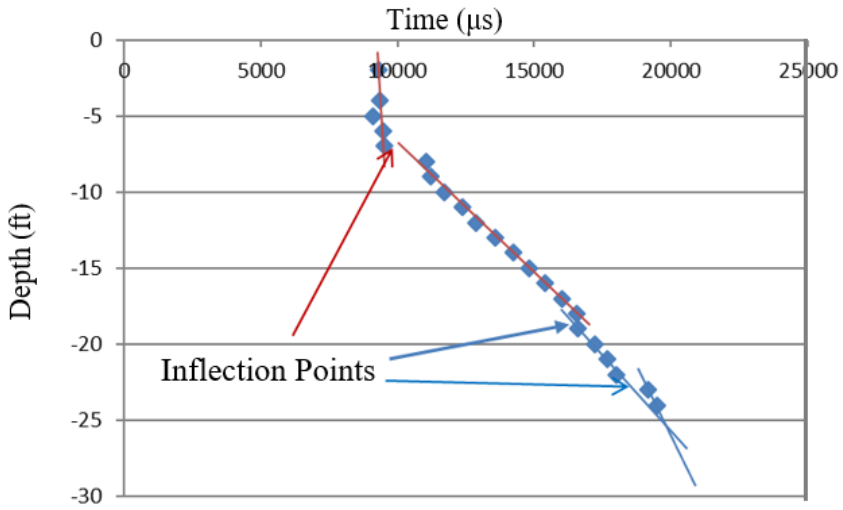

FIGURE 150 First Peak Versus Depth for Test PS1

The PS tests were repeated three more times. The results of Tests PS2, PS3, and PS4 are shown in Figures 151, 152, and 153, respectively. A first inflection point is recognizable at approximately 9 ft below the ground level for Tests PS2 and PS4 (see Figures 151 and 153). The second inflection points are at the depths of 20 and 18 ft for the Tests PS2 and PS4, respectively. In Test PS3 the first inflection point is at 8.5 ft and the second inflection point is at the depth of 22 ft (see Figure 152).

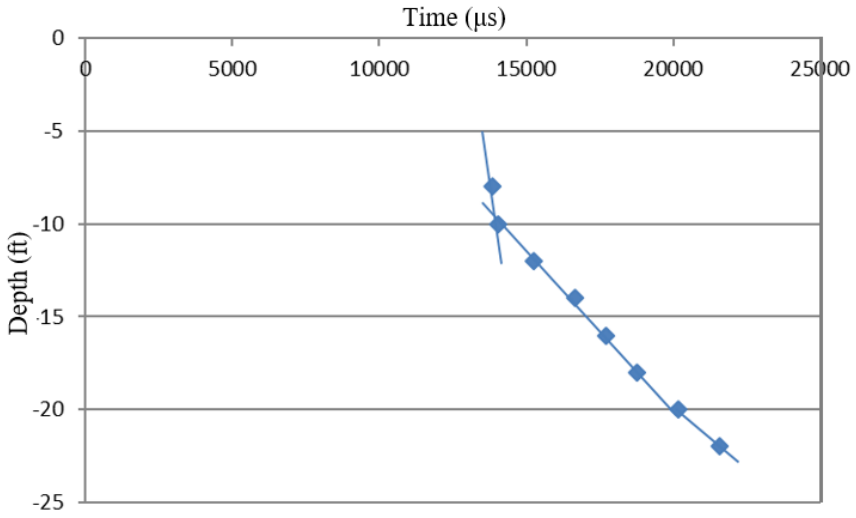

FIGURE 151 First Arrival Time Versus Depth (PS2)

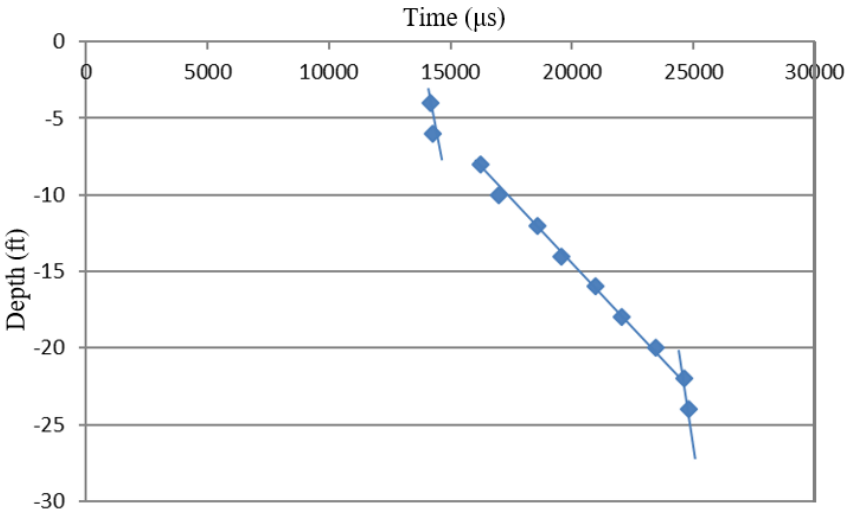

FIGURE 152 First Arrival Time Versus Depth (PS3)

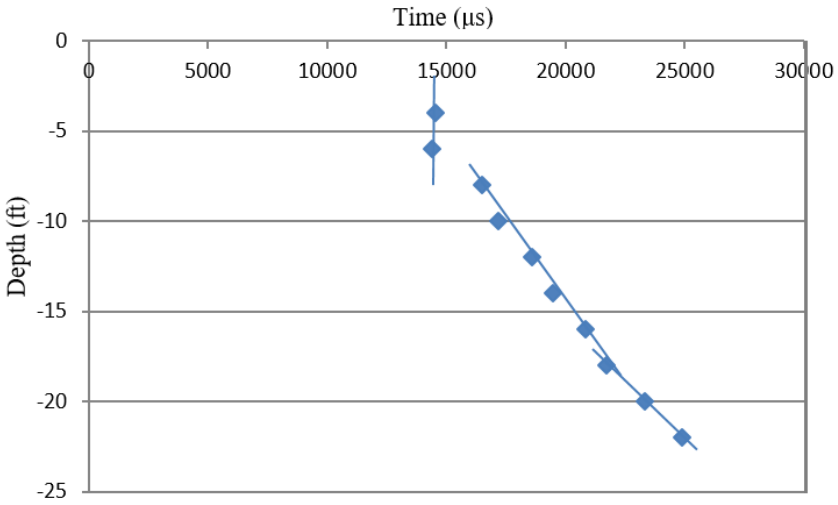

FIGURE 153 First Arrival Time Versus Depth (PS4)

It should be noted the first inflection point does not indicate the bottom of the pile. Unlike other states, unsaturated soils are common in New Mexico. The P-wave velocities usually increase with depth in non-saturated soils while the P-wave velocity in saturated soils is constant (5,000 ft/s). The increasing P-wave velocity with depth may affect the determination of the location of the pile tip. The inflection points within 18 ft below the ground level may indicate the soil layer interfaces. The second inflection points (between 18 and 22 ft) indicate the possible location of the pile's toe.

Test Result for Pile 2 A PS test was carried out on Pile 2. The hydrophone was at B-02. The source was applied by vertical striking with a hard tip hammer. The distance between the borehole and pile is 3 ft. Figure 154 shows the result of the PS5. Here the first inflection point seen at Pile 1 disappeared. This is a textbook PS test result. The inflection point is at the depth 22 ft which is the embedded pile depth.

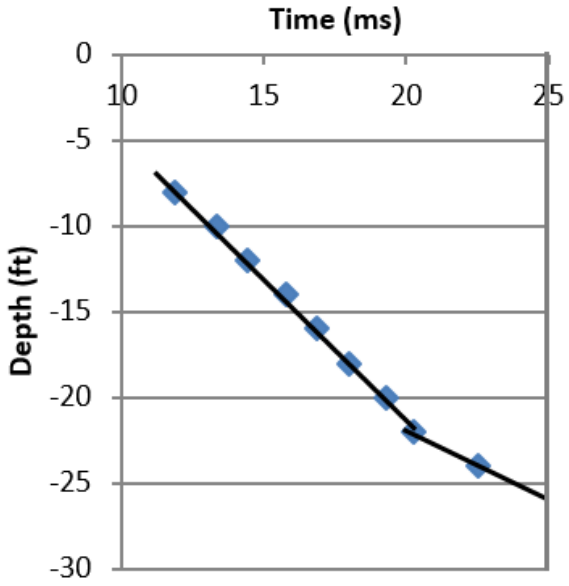

FIGURE 154 Result of Test PS5 on Pile 2

Test Results for Pile 3 A PS test was conducted on Pile 3 while B-04 was used as the location of the receiver. This borehole was installed for testing Pile 1. The distance between the pile and the borehole is 136 in which is significantly greater than the distances of previous tests. It was a wild attempt to see if meaningful results could be obtained with a great distance.

The signals were recorded at intervals of 2 ft while the hydrophone was lowering down during testing. The stacked graph is indicated in Figure 155. As expected, the distance between the source and the receiver was too great to provide useful information. Signals were very weak at shallow depths. The obvious valleys in the stacked graphs were not related to the P-wave.

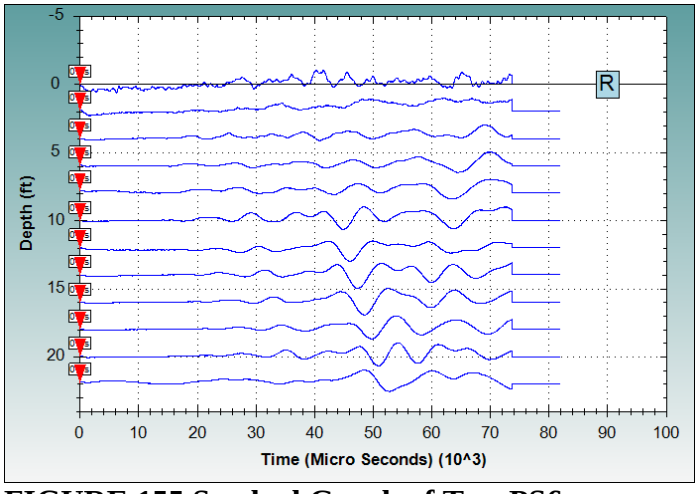

FIGURE 155 Stacked Graph of Test PS6

Test Results for Battered Pile 10 Three PS tests were conducted on Pile 10 to investigate the effect of striking direction on the obtained signal. The receiver was located at B-01. The distance between the source and receiver is 3 ft. The source was applied along three different directions

(vertical, horizontal strike at the flange, and horizontal strike at the web). When vertical striking was applied, a compression wave was generated at the striking point. In contrast, when the striking was horizontal, a shear wave was generated at the striking point. The generated wave travelled along the pile. When the traveling wave encountered an interface (a change of impedance), new compression waves and shear waves were generated and transmitted. For Test PS8, when the generated shear wave reached the ground level, a new compression wave will be developed at the soil-pile interface due to the direction of the particle movement. For Test PS9, compression wave will not be generated until the wave encounters a change in impedance.

The plots of arrival time versus depth are shown in Figure 156. Arrival times at shallow depths could not be determined due to strong initial noise. The arrival times at greater depths were identified with ease. The interface between the clay and the shale layers can be detected with the vertical striking (see Figure 156a) but not with the horizontal striking (see Figures 156b and 156c). The embedment depth of the pile was detected in all three tests. The estimated depths were determined as 24, 20, and 22 ft, respectively.

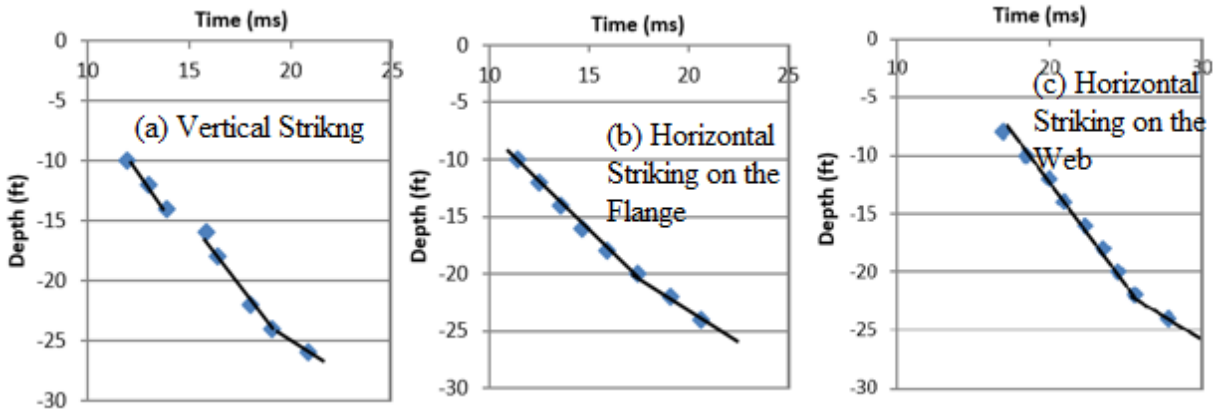

FIGURE 156 Result of Three PS Tests on Pile 10

Test Results for Pile 11 The effect of input source (horizontal and vertical strikes) was also examined on Pile 11. The source was applied by horizontal striking at the flange (Test PS10) and vertical striking (Test PS11). The distance between the pile and the borehole is 6 ft. The signals were recorded at intervals of 2 ft while the hydrophone lowered down the hole during testing. The results of Tests PS10 and PS11 are shown in Figures 161 and 162 respectively.

A first inflection point was determined at approximately 11 and 9 ft for horizontal and vertical striking respectively. The second inflection point at the depth of 21 ft was identified for Test PS10 but no inflection point was identified for Test PS11. This may be due to the traffic noise while conducting Test PS11. The first arrival times at depths between 19 and 23 ft were undistinguishable.

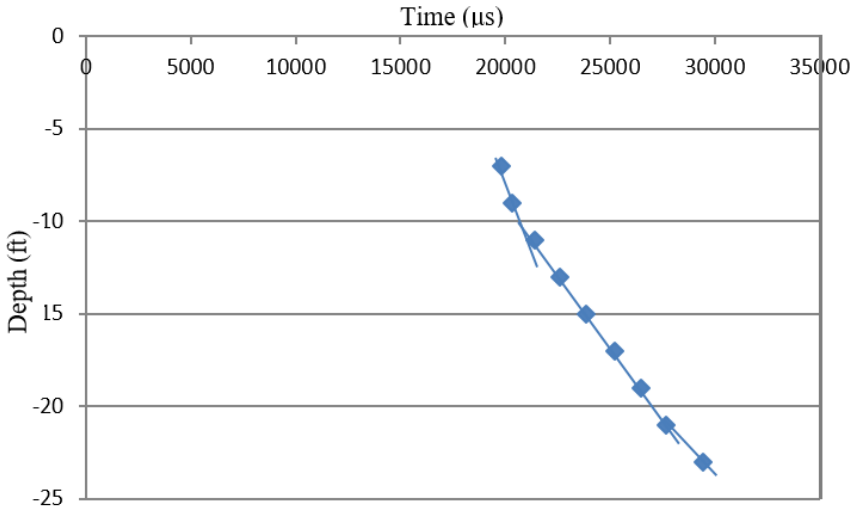

FIGURE 157 First Arrival Time Versus Depth (PS10)

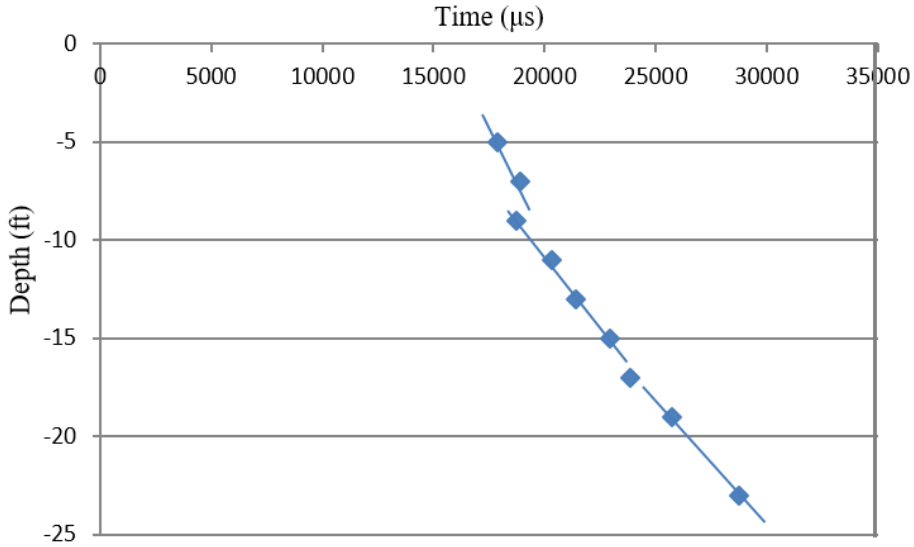

FIGURE 158 First Arrival Time Versus Depth (PS11)

Test Results for Piles 16 and 19 This was another wide attempt to see if PS tests work in greater distance between the source and receiver (12.7 ft). The source was applied on Piles 16 and 19 while the receiver was located at B-07 and B-05, respectively. The source was applied by vertical striking and horizontal striking on the flange for each pile. A total of four PS tests were conducted with a hard tip hammer.

The results of these four PS tests are shown in Figure 159. Due to the great distance between the source and receiver, neither vertical striking nor horizontal striking can produce useful results to determine the inflection point. The hammer could not produce strong enough wave to reach the receiver. There is a certain horizontal distance between the source and the receiver. Beyond which, meaningful PS tests cannot be obtained. The certain horizontal distance depends on the

strength of the input signal and soil condition. Our investigation showed that 12.7 ft was too far for our equipment to achieve interpretable results.

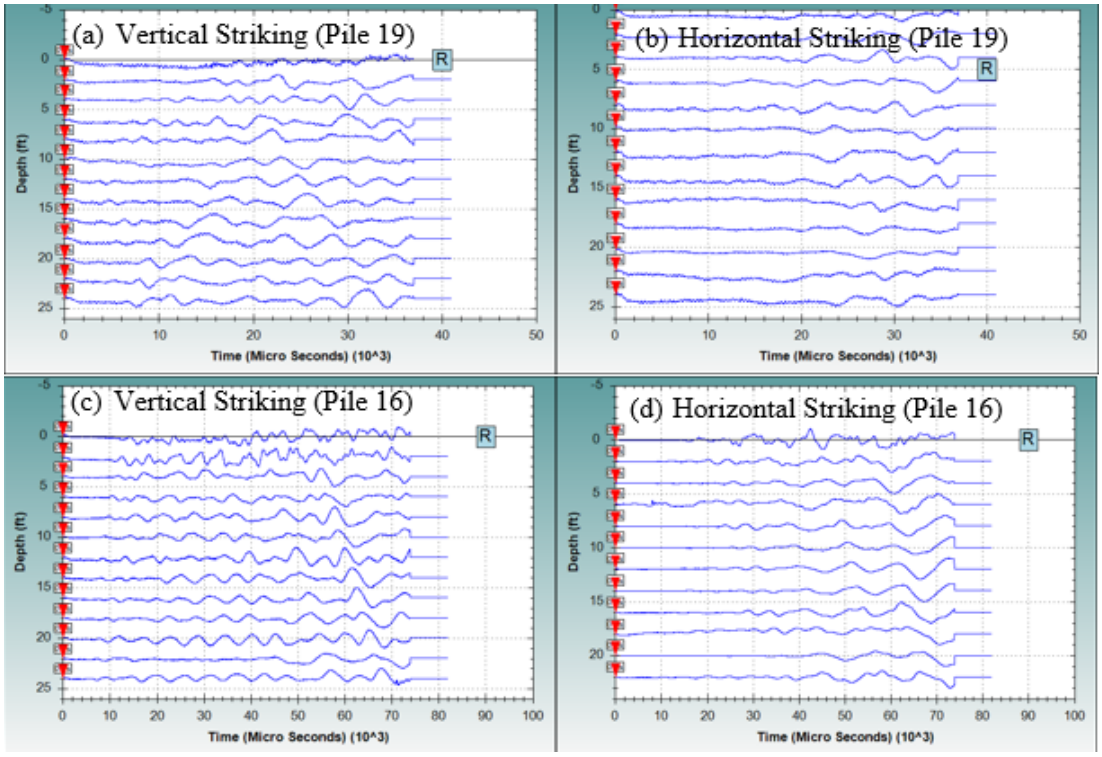

FIGURE 159 Stacked Graphs of PS Tests for Piles 16 and 19

Test Result for Pile 21 A PS test was conducted on Pile 21. The receiver was located at B-07. The distance between the source and receiver is 5.7 ft. The source was applied by horizontal striking on the flange with a hard tip. The result is shown in Figure 160. The inflection point was identified barely at a depth of 22 ft. More data points below 24 ft will be better to support the existence of an inflection point at 22 ft. The source to receiver distance of 5.7 ft produced good result.

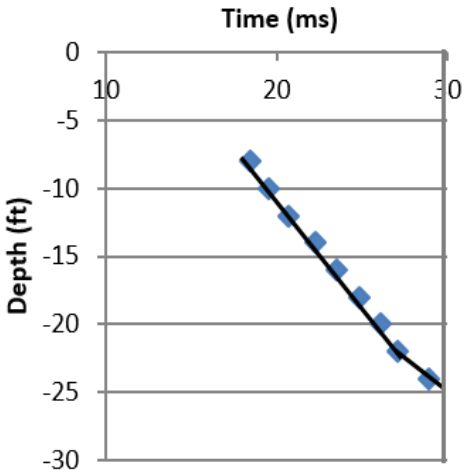

FIGURE 160 Result for Test PS16

Test Results for Pile 22 Four PS tests were conducted on Pile 22. The receiver was located at B-07. The distance between the pile (source) and the borehole (receiver) is 3 ft. The source was applied by vertical and horizontal striking (see Table 63). A hard tip hammer was used for Tests PS17 to PS19 while a medium-soft tip hammer was used in the last test (PS20) The stacked graphs of all four tests showed initial noise at depths less than 6 ft. With the presence of noise distinguishing the arrival time was difficult. Noise was reduced when the receiver (hydrophone) was at greater depths.

The effect of striking direction was examined by comparing the results of Tests PS17, PS18, and PS19 as shown in Figure 161.

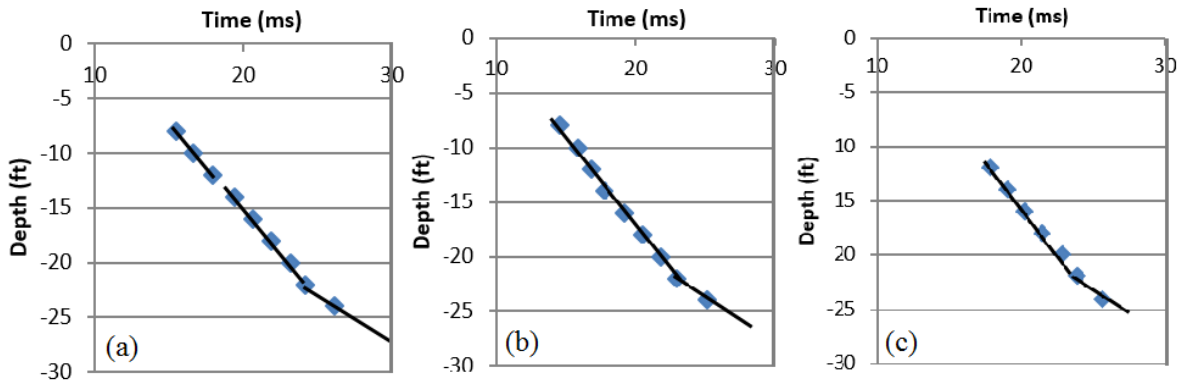

FIGURE 161 Results of Tests PS17, PS18, and PS19 (a) Vertical Striking, (b) Horizontal Striking on the Flange, (c) Horizontal Striking on the Web

The first possible inflection point was found at a depth of 13 ft. According to the soil profile of this site, the interface between the clay and shale layers is located about 13 ft below ground. This inflection point may be related to the interface. This first inflection point may not indicate the embedment depth of the foundation.

The second possible inflection point was at the depth of about 22 ft. This inflection point may indicate the location of the pile tip. The as-built drawing shows that the piles should be extended at least 5 ft into the shale layer. Therefore this inflection point is related to the embedment depth. Due to the limited depth of the installed PVC tubes, PS tests must stop at 25 ft. The clarity of this particular inflection point could be improved if the length of the PVC pipe were more than 25 ft.

Both vertical and horizontal striking produced signals strong enough to determine the embedment depth of the pile. Good signals were received by vertical striking and horizontal striking on the flange. Only fair result was obtained by horizontal striking on the web. Although horizontal striking can be used as a source, it is more desirable to generate a shear wave such that particle movement is parallel to the direction towards the receiver.

The result of Test PS20 with a softer hammer tip (medium-soft) is shown in Figure 162. Interpretation of the PS test was still possible although the received signals were not as well-defined as that produced by hard tip (see Figure 161a). Thus, it is better to use a hammer with hard tip to generate the wave (source).

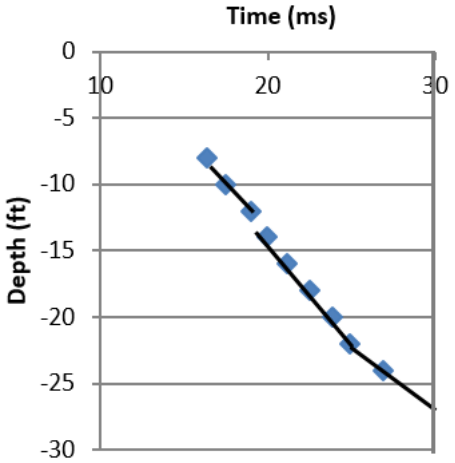

FIGURE 162 Result of Test PS20

Summary of Results of Bridge No. 7480 The results of PS tests conducted on H-piles are summarized in Table 64. The success rate is 77.8%. The success rate is close to 100% by ignoring the results of PS tests with the source to receiver distance greater than 6 ft.

TABLE 64 PS Tests Results of Bridge No. 7480.

Pile	Embedment Pile Length (ft)
1	21
2	22
3	20
10	22
11	19
16	-
19	-
21	22
22	22

Conclusions of PS tests on Steel H-Piles Based on the results of the PS tests conducted in the field following observations and conclusions were inferred:

- In the presence of ambient noise, determining the arrival time of the first P-wave from the velocity graphs was very difficult.
- The stacked graphs showed initial noise in the upper soil strata. The data at a depth less than 8 ft was questionable. However, the velocity graphs showed that the initial ambient noise reduces with depth.
- Both vertical and horizontal striking can be used as the source for PS tests. However, signal provided by horizontal striking seems to be less effective than that of vertical striking. It is preferable to select the direction of the horizontal striking such that the particle movement is in the direction towards the receiver.
- Layered soils introduced difficulties in the determination of pile tip. In some PS tests, an inflection point could be interpreted as the depth of the interface between the clay and shale layers.

- The strength of the signal reduced with the increase of the distance between the source and receiver. Good results were obtained when the distance was less than 6 ft for both straight and battered piles. When the distance was 12.7 ft poor results were obtained. Thus, a borehole should be drilled less than 6 ft from the test foundation (pile or pier) for future PS tests.

2.2.3.2 PS tests on Bridge No. 1676

Conventional PS tests were conducted on two timber piles at Bridge No. 1676. The location and foundation plan of the bridge are shown in Figures 115 and 117 respectively. The test piles were Pile B-1 and C-1. Two test borings were drilled adjacent to the timber piles by NMDOT using the Geoprobe 7822DT (purchased during this project). The plan view of the location of the boreholes is indicated in Figure 163. The low headroom drill rig and the drilling operation are shown in Figure 164.

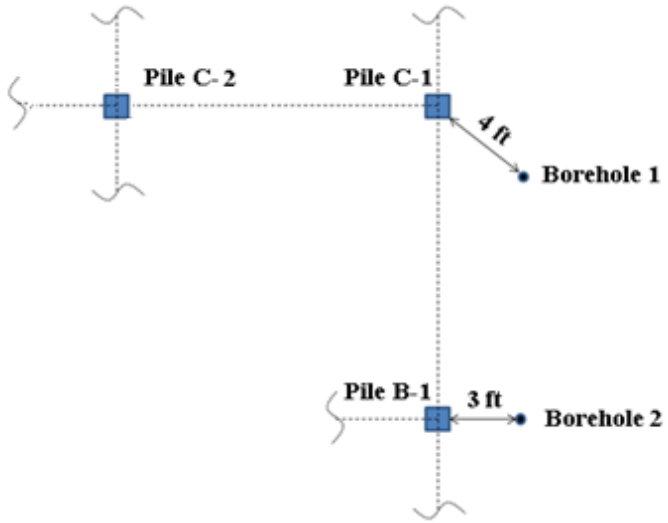

FIGURE 163 Plan View of Boreholes Locations

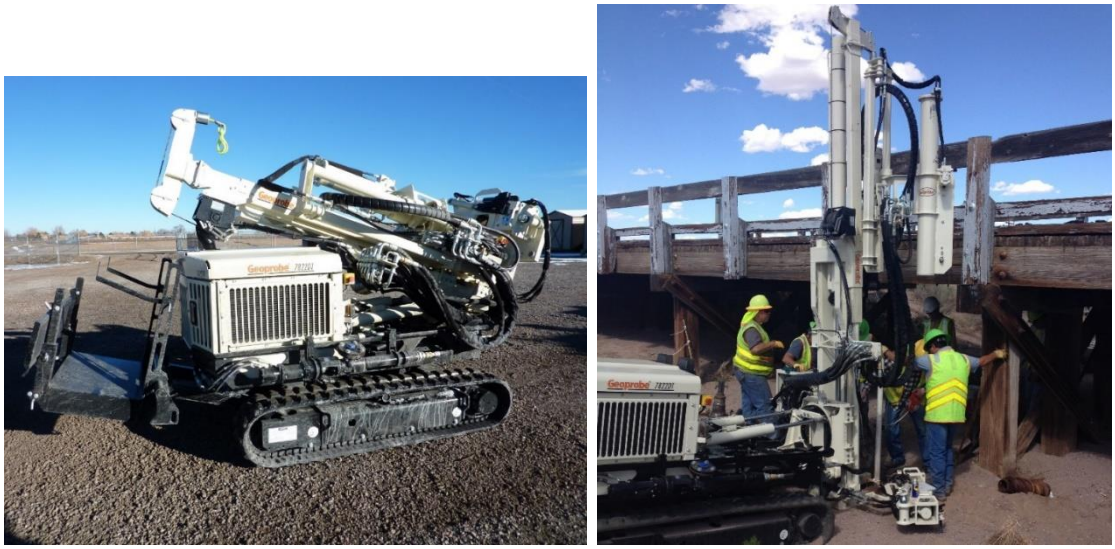

FIGURE 164 Geoprobe Model 7822DT- Low Headroom Drill Rig

The depths of boreholes 1 and 2 are 26 ft and 35 ft respectively. Two-inch inner diameter PVC casings were placed in each boring with a water tight cap at the base and a removable cap at the top. Native sandy soil was poured down into the hole to create a sand pack around the PVC tube.

Conventional PS tests were performed on Piles B-1 and C-1 while reverse PS tests were performed on Piles C-1 and C-2. In conventional PS tests, the source was at the pile and the receiver was at the borehole. In reverse PS tests, the source was at the borehole and the receiver was at the pile.

Conventional PS Test Results Nine PS tests were carried out on Piles B-1 and C-1 as shown in Table 65. In two tests, an 8-lb sledge hammer was used to impart greater impact energy into the pile. Hard tips were used for the regular hammer. The signals were recorded at an interval of 2 ft starting from the ground surface for Pile B-1. For Pile C-1, the signals were recorded starting 8 ft below the ground surface towards the PVC tube bottom with an interval of 1 ft.

TABLE 65 Specifications of PS Tests.

Test	Borehole	Pile	Striking Condition	Hammer
1	1	B-1	Vertical - Upward on pile cap	Regular
2	1	B-1	Vertical - Upward on pile cap	Regular
3	1	B-1	Vertical - Upward on pile cap	Regular
4	1	B-1	Vertical – Downward (inclined) on the connected bracing to the pile	Regular
5	1	B-1	Vertical - Upward on pile cap	8-lb Sledge hammer
6	1	B-1	Vertical - Upward on pile cap	8-lb Sledge hammer
7	2	C-1	Horizontal Striking on the side of the pile	Regular
8	2	C-1	Vertical - Downward on pile cap	Regular
9	2	C-1	Horizontal Striking on the side of the pile	Regular

Similar to the previous observation at Bridge No. 7480, noise affected the determination of the first arrival time at some depths. However, the noise was less intense at this site than that at Bridge No. 7480 due to zero traffic on the bridge during testing. Figure 165 shows the noise comparison between the data obtained at Bridges No. 7480 and 1676. The figure shows the significant effect of traffic noise on the PS tests results.

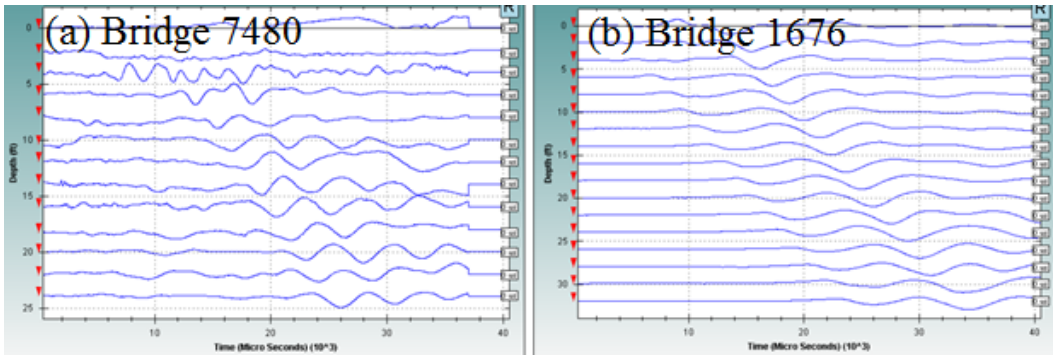

FIGURE 165 Stacked Graphs for Steel H-piles and for Wood Piles

Since the signals were generally greater than the noise at this bridge, the determination of first arrival times was not too difficult. First arrival times were determined by inspecting the background noise level in the received signals. The 'First arrival' was determined as the time when the signal begins to increase and consistently distinguish itself from the background noise level. Figure 166 shows the original and enlarged views of an obtained signal. The initial noise and the first arrival time are clearly identifiable in the enlarged view. The arrival times of the first P-wave were determined easily at greater depths since the ambient noise reduced with depth.

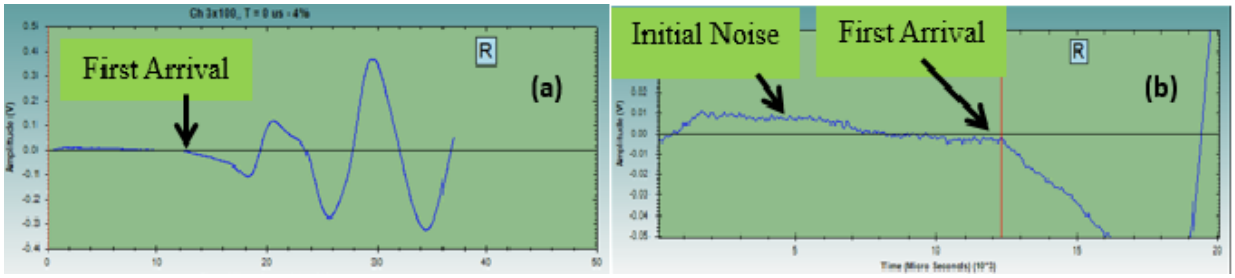

FIGURE 166 Examples of (a) Original View and (b) Enlarged View Showing the Initial Noise and First Arrival

After determining the arrival time at each depth, the arrival time versus depth was plotted for each PS test. The results of the PS tests are shown in Figures 167 to 175. Two appropriate straight lines were passed through the points and the intersection of the two lines indicated the location of the inflection point. Sometimes, identifying data points that belong to each line was based on engineering judgement. The straight lines in Figures 167 to 175 were introduced by linear curve fitting method with the selected data points.

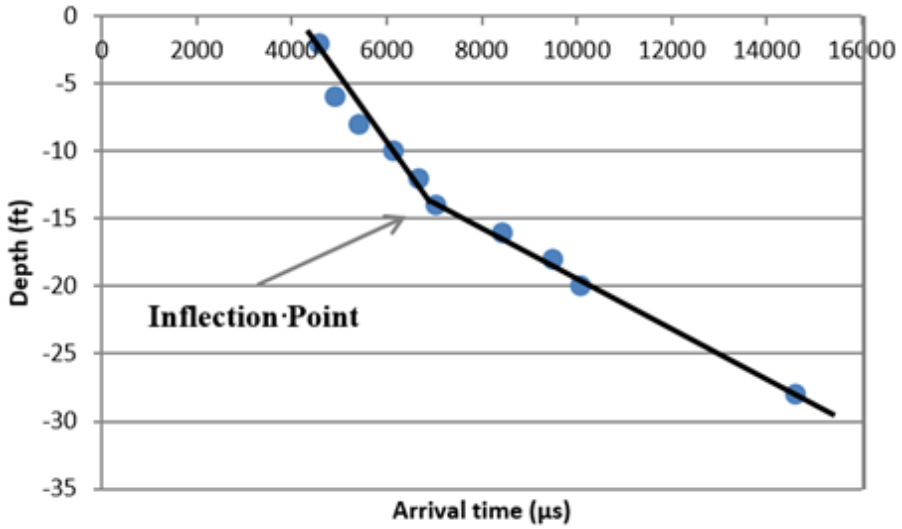

FIGURE 167 First Arrival Time Versus Depth (Test 1)

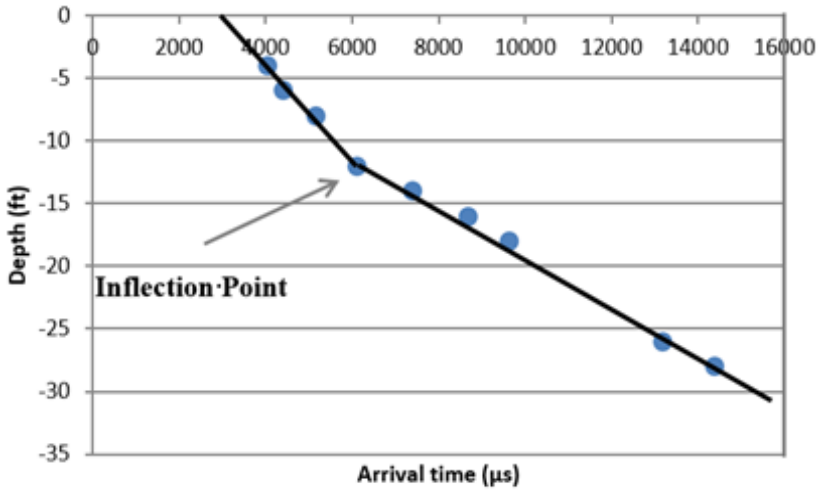

FIGURE 168 First Arrival Time Versus Depth (Test 2)

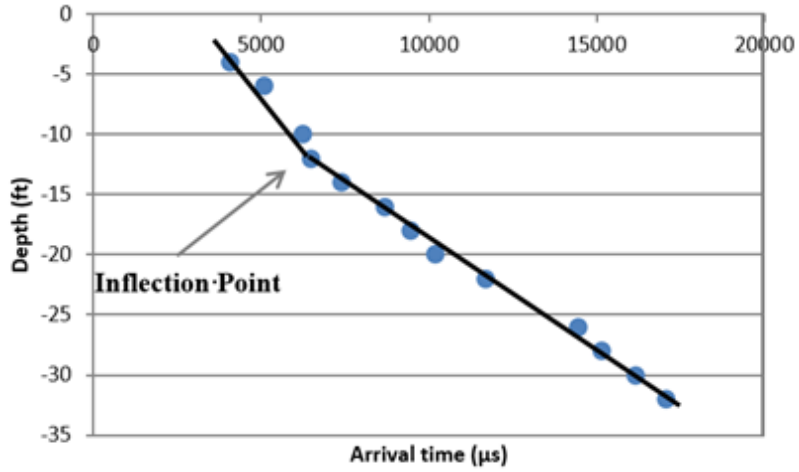

FIGURE 169 First Arrival Time Versus Depth (Test 3)

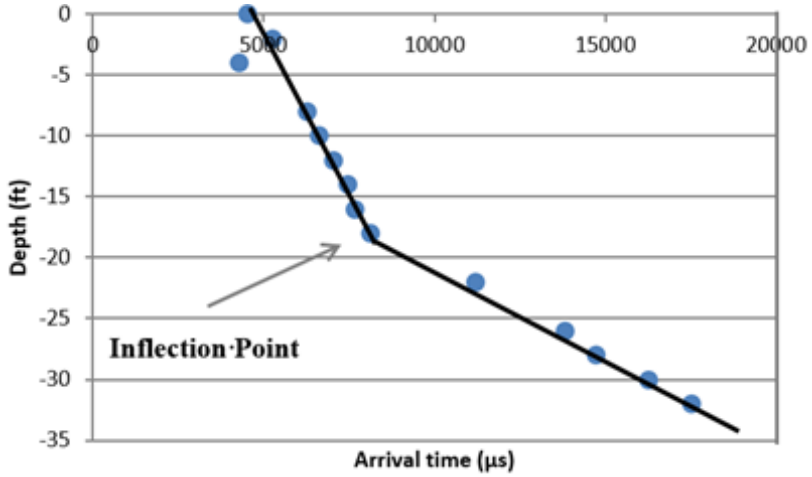

FIGURE 170 First Arrival Time Versus Depth (Test 4)

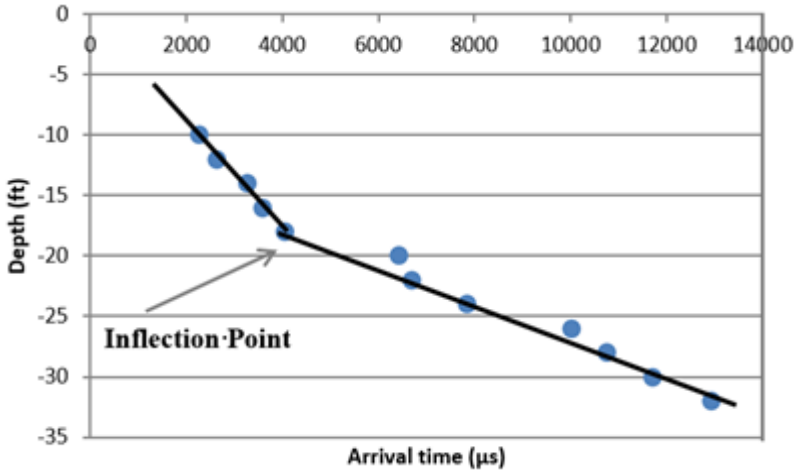

FIGURE 171 First Arrival Time Versus Depth (Test 5)

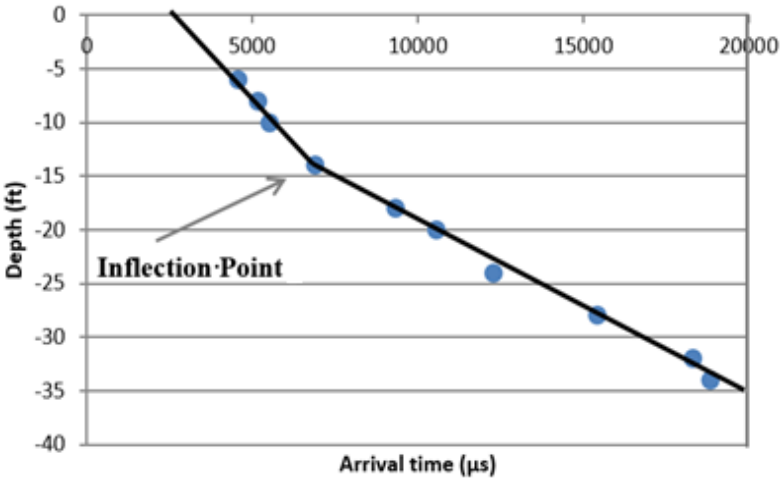

FIGURE 172 First Arrival Time Versus Depth (Test 6)

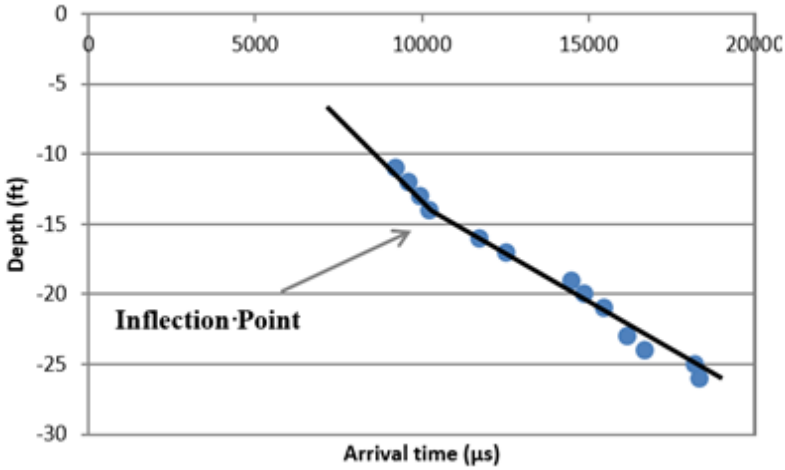

FIGURE 173 First Arrival Time Versus Depth (Test 7)

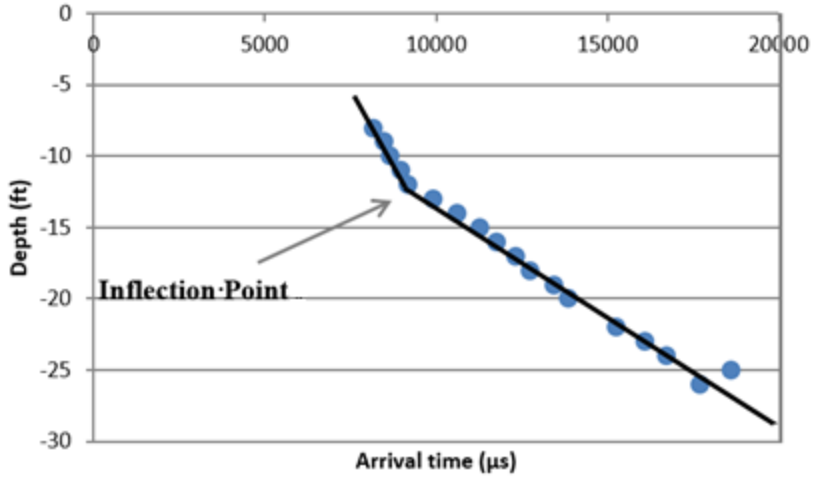

FIGURE 174 First Arrival Time Versus Depth (Test 8)

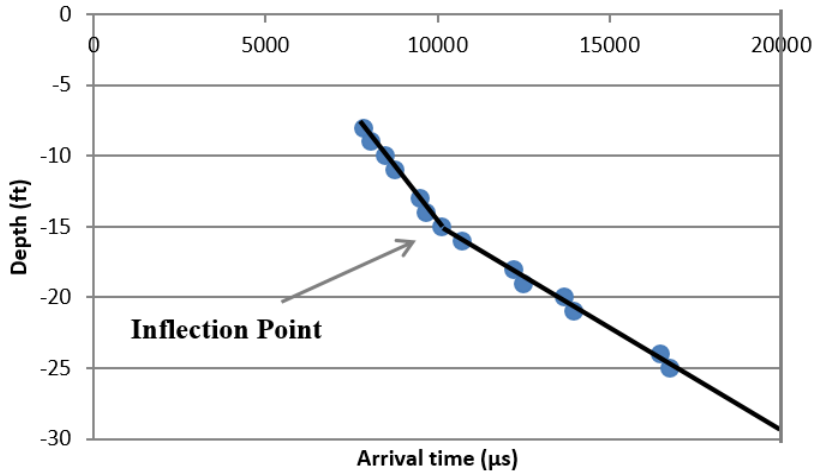

FIGURE 175 First Arrival Time Versus Depth (Test 9)

Comparing Figures 168 and 171, using an 8-lb sledge hammer did not show any improvement at this site. Applying upward striking with a regular hammer was much easier than the sledge hammer.

The depths of the inflection points for PS tests conducted on Piles B-1 and C-1 are shown in Tables 66 and 67 respectively.

TABLE 66 Depths of the Inflection Points for Pile B-1.

Test	Striking Method	Inflection Point Depth (ft)
1	Vertical - Upward on pile cap	14
2	Vertical - Upward on pile cap	12
3	Vertical - Upward on pile cap	12
4	Vertical – Downward (inclined) on the connected bracing to the pile	18
5	Vertical - Upward on pile cap	18
6	Vertical - Upward on pile cap	14

TABLE 67 Depths of the Inflection Points for Pile C-1.

Test	Striking method	Inflection point depth (ft)
7	Horizontal striking on the side of the pile	14
8	Vertical - Downward on pile cap	12
9	Horizontal striking on the side of the pile	15

Summary of Results Table 68 lists the range of estimated length of piles, the average value, and the value from the as-built drawings. The average pile lengths are comparable to the as-built pile length. It is difficult to determine the true errors since the actual pile length may be different from the as-built value.

TABLE 68 The Range of Estimated Pile Length, Average and Known Pile Lengths.

Pile	Range of Pile Length (ft)	Average Pile Length (ft)	As-built Pile Length (ft)
B-1	18 - 24	20.7	23
C-1	18 - 21	19.7	23

Conclusions of Conventional PS Tests at Bridge No. 1676 Based on the PS test results the following conclusions were inferred:

- Determination of first arrival time was much easier without the traffic noise.
- Accurate arrival time determination required more detailed consideration of the background noise.
- The calculated pile lengths were similar but shorter than the as-built pile length.
- Both regular and sledge hammers produced acceptable results.
- Both vertical and horizontal striking generated acceptable results, however, vertical striking produced clearer inflection points.

Reverse PS Tests Two reverse PS test were conducted on two timber piles of Bridge No. 1676 during drilling the boreholes. The advantage of the reverse PS test is that no pre-knowledge of the pile depth is needed since drilling can be continued until the inflection point is identified. Moreover, multiple piles can be tested simultaneously using one borehole.

In this method, the hollow stem auger was advanced to a desired depth. A standard split-spoon sampler was inserted through the hollow stem of the auger column towards the bottom of the hole. The source for PS testing was created by striking the top of the drill rod. The receiver (accelerometer) was mounted on the test pile using wooden blocks. Figure 176 shows the reverse PS setup for Piles C-1 and C-2 at Bridge No. 1676. The propagated wave traveled through the rod, soil, and pile, and finally was received by the sensors. The procedure was repeated at various depths.

The obtained signals were stacked together for Piles C-1 and C-2 as shown in Figure 177. Very noisy signals were observed compared with the results of conventional PS tests (see Figure 165b). Since the Pile C-1 is closer to the source than Pile C-2, the signals arrived earlier at Pile C-1 than Pile C-2. Due to the noise level, it was very difficult to pinpoint the arrival times at most depths.

Thus, we do not have enough conclusive data for the determination of the inflection point. The ambient noise was more intense on the ground than at greater depths.

Another way to conduct PS tests without drilling a borehole is the use of a seismic cone as the receiver. This method can be explored in the future. The disadvantage of this method is that the PS test cannot be repeated at previous depths after the advancement of the cone due to the disturbance of the surrounding soil.

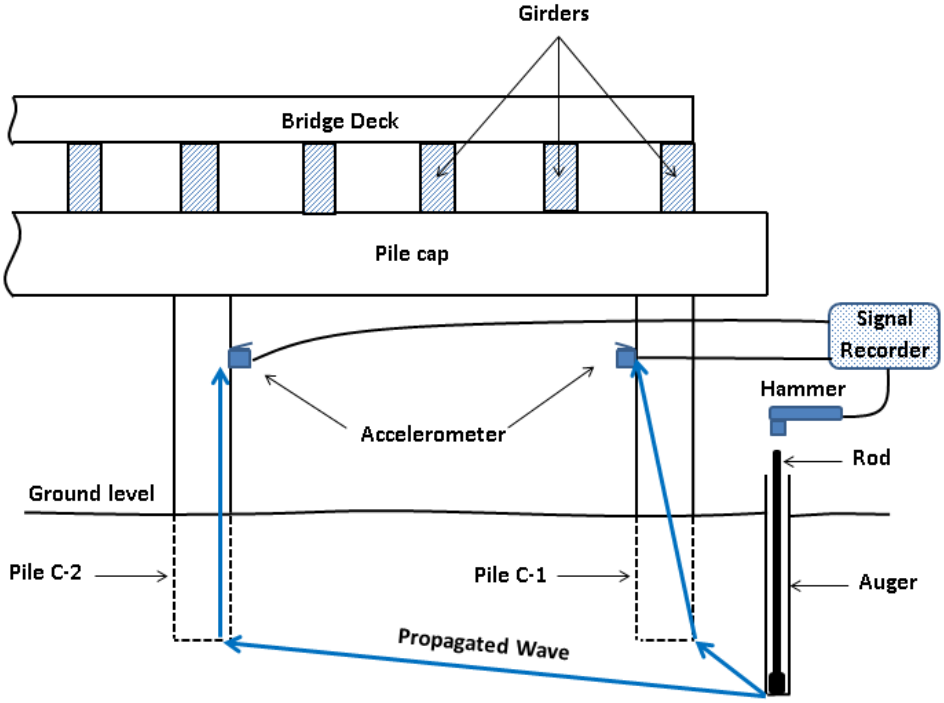

FIGURE 176 Reverse PS Setup for Piles C-1 and C-2 of Bridge No. 1676

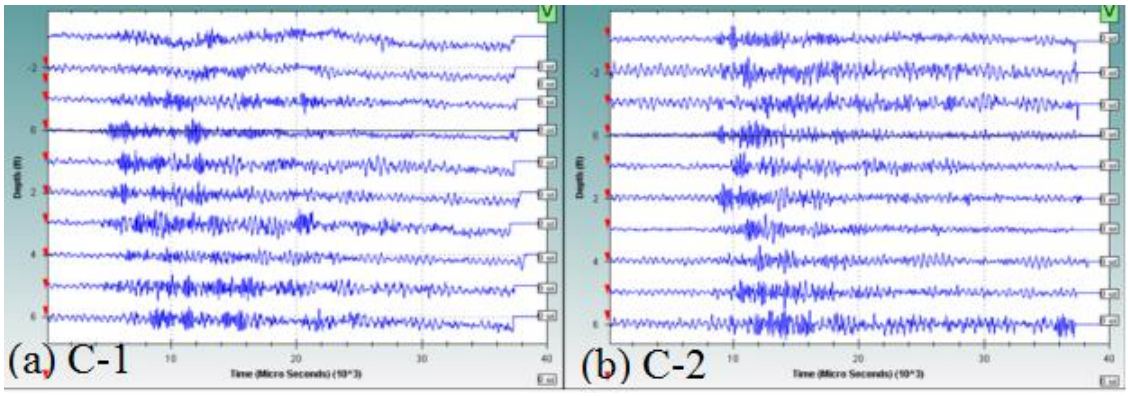

FIGURE 177 Stacked Graphs for Piles C-1 and C-2

2.2.4 Conclusions of PS Tests

PS tests have been carried out on bridges supported by timber and steel piles. Both conventional and reverse PS tests were performed. The source was applied in testing the steel piles by either vertical striking on an aluminum block attached to the H-pile web or horizontal striking on the piles. Vertical striking on the pile cap and horizontal striking on the pile were applied by both regular and sledge hammers on the bridge supported by timber piles. Reverse PS tests were also conducted on the bridge with timber piles. The conventional PS tests were successful but the reverse PS tests did not yield good data due to the ambient noise. Therefore, the following conclusions are from the conventional PS tests only.

The first arrival times were determined by inspecting the background noise level in the signals prior to arrival of any sound wave from the source. The first arrival time was determined as the time when the signal begins to increase and consistently distinguish itself from the background noise level. The PS tests showed that determining the arrival time of the first P-wave objectively is a challenge depending on the level of ambient noise. The arrival time of the first P-wave was determined easily at greater depths since the ambient noise reduced with depth.

Both vertical and horizontal striking generated good signals although the signals provided by vertical striking were generally clearer than those of horizontal striking.

The field study also showed the effect of the distance between the borehole and the test pile. Good results were obtained when the distance between the source and receiver was less than or equal to 4 ft. PS tests did not work when the distance between the source and receiver was greater than 6 ft. Other researchers recommended that the borehole should be no more than 6 ft from the pile. Therefore, it is suggested that the borehole should be installed less than 6 ft from the test pile.

2.3 INDUCTION FIELD METHOD

IF tests are the best NDT method for detecting the depth of steel piles. In addition, IF tests are not affected by bridge vibration.

Two testbeds were constructed to examine the capability of the equipment and to investigate various aspects of IF tests. The findings were useful for conducting IF tests in the field on foundations containing metal (steel and reinforced concrete foundations). The first testbed contained a metal I-beam placed horizontally in a wooden box full of soil. The box was filled with sand (or clay) and IF tests were conducted with the Probe placed inside the pipes at various locations. The second testbed was created off UNM campus. To conduct the desired PS tests, a reinforced concrete pier and four PVC tubes at various distances from the pier were installed. IF tests were also performed to examine the effect of the distance between the pier and the tube.

The original plan of IF field tests included performing IF tests at Bridge No. 7480. IF tests were not conducted on the bridge since the distance between the boreholes and the test piles were greater than 1.5 ft which is beyond the capability of the equipment.

2.3.1 IF Test Procedure

Before conducting IF tests, a borehole must be drilled next to the test pile. There are requirements for the preparation of the borehole:

- The borehole must align with the test pile.
- The depth of the borehole must be at least 10 ft deeper than the expected pile toe level.
- The hole should be bored as close as possible to the test pile (no more than 1.5 ft away from the pile).
- 2-in PVC tube is installed to keep the borehole from caving.
- The space between the borehole and the tube is filled with soil.

Similar to the PS tests, an IF test is carried out in three steps including hardware setup, data acquisition, and data processing.

2.3.1.1 IF Hardware Setup

Figure 178 shows the correct assembly of the Length Inductive Test Equipment (LITE) for IF tests. The equipment includes battery, signal conditioning box, multimeter, and the Probe (induction sensor). The details of the signal conditioning box are shown in Figure 179.

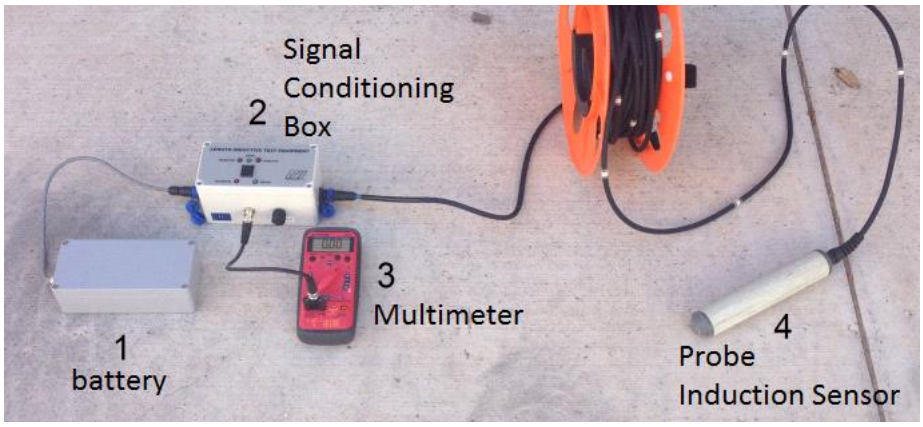

FIGURE 178 Length Inductive Test Equipment (LITE) for IF tests

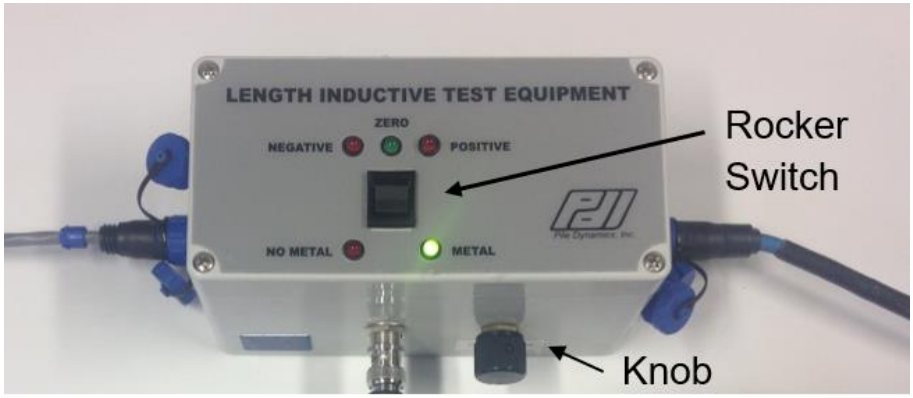

FIGURE 179 Details of Signal Conditioning Box

2.3.1.2 IF Data Acqisition

Calibrate the system before conducting IF tests. The calibration should follow these steps.

1) Assemble the components as shown in Figure 178.
2) Set the Multimeter to "20V" in the DC.
3) Set the reference point
   - Place the Probe in a location such that there is no metal object within 3 ft.
   - Push down the rocker switch until one of the three lights (negative/zero/positive) illuminates.
   - Turn the knob until the green light (middle one) is on and the voltage is approximately *2.5 V*.
4) Push down the rocker until either NO METAL or METAL illuminates.
5) Bring the Probe in contact with a metal object, the Multimeter should show a reading close to 5.04 V. If the readout is still less than 3V, the battery is low, either the Multimeter or the Signal Conditioning Box is defective.

The Multimeter should display a voltage between 2.5 V and 5.04 V. The voltage will be 2.5 V when there is no metal object within a distance of 2 ft from the Probe. The voltage should increase when moving the Probe closer to a metal object.

After calibration, following steps should be carried out to perform an IF test:

1) Insert the Probe into the previously installed PVC tube.
2) If the first reading remains 2.5 V, the distance between the hole and the metal in the pile is greater than 18 inches, or there is no metal in the foundation.
3) Lower the Probe in 1-ft increment and record the voltage at every foot till the bottom of the hole.

A successful IF test (the pile length is determined) should show a drop of voltage before the Probe touches the bottom of the hole. An example of a successful IF test is shown in Figure 180.

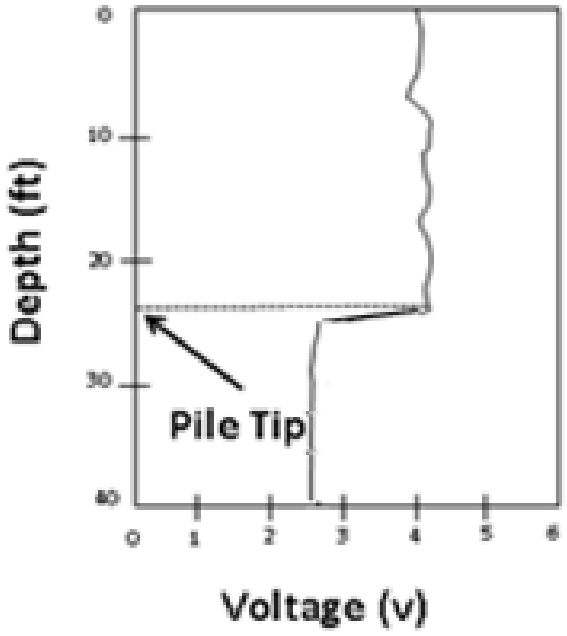

FIGURE 180 A Successful IF Test Result

2.3.2 IF Testing: Testbed at UNM

The first testbed contained a metal I-beam placed horizontally in a wooden box full of soil as shown in Figure 181. A metal beam buried in a wood box filled with soil was a suitable prototype of a real steel foundation of a bridge. The dimensions of the wooden box were 12 ft × 4 ft × 18 in. The I-beam was 5 ft long, 12 in depth and an 8 in flange width. The preliminary tests were supposed to be conducted in the structural lab at UNM. However, during conducting the IF tests in the structural lab, it was revealed that the test could not be conducted on the concrete floor due to the presence of steel reinforcement. The testbed was therefore moved outdoor on an asphalt paved driveway as shown in Figure 181. Before recording the data, three PVC tubes were placed horizontally at a distance of 1, 1.5 and 2 ft respectively from the steel beam.

FIGURE 181 Test Configuration with Steel Beam and Wooden Box

2.3.2.1 IF Results in Air

The steel beam was placed in the box vertically and horizontally and the IF tests were conducted. The Length Induction Test Equipment (LITE) was assembled as shown in Figure 178. The system was calibrated and the Probe was then inserted into each of the PVC tubes. Data were recorded at 80 points as shown in Figures 182 and 183. The corresponding results are indicated in Tables 69 and 70. The initial voltage was 2.55 v. This implies that the voltage will be greater than 2.55 when there is metal object nearby. The italicized values in the tables designate the locations where metal was detected. The results show that the distance between the Probe and the metal beam should be limited to 18 in for the possibility of metal detection.

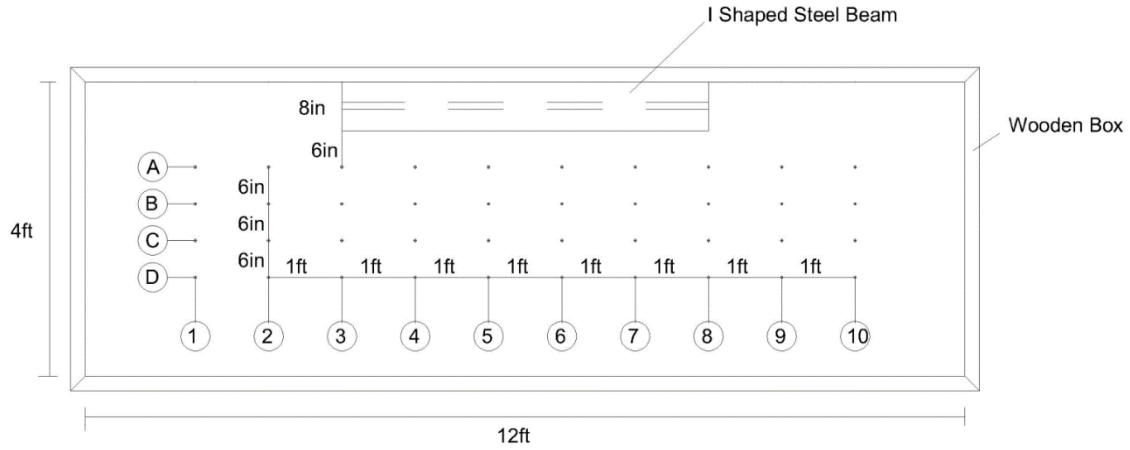

FIGURE 182 Test Locations with Beam in the 1st Configuration

TABLE 69 Test Results (Locations Correspond to Figure 182).

	1	2	3	4	5	6	7	8	9	10
A	2.45	*2.97*	*5.04*	*5.04*	*5.04*	*5.04*	*5.04*	*5.04*	*2.74*	2.45
B	2.55	*2.69*	*3.59*	*4.37*	*4.21*	*4.12*	*4.12*	*3.3*	*2.67*	2.53
C	2.4	2.4	2.62	*2.72*	*2.77*	*2.64*	*2.64*	2.55	2.47	2.42
D	2.6	2.6	2.62	2.62	2.61	2.6	2.6	2.57	2.56	2.55

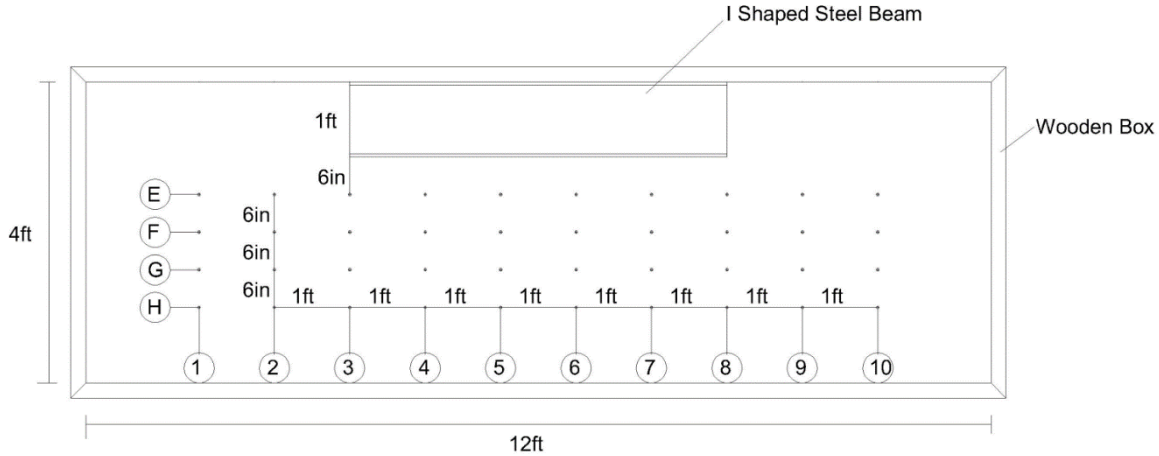

FIGURE 183 Test Locations with Beam in the 2nd Configuration

TABLE 70 Test Results (Locations Correspond to Figure 183).

	1	2	3	4	5	6	7	8	9	10
E	2.43	*2.96*	*5.04*	*5.04*	*5.04*	*5.04*	*5.04*	*5.04*	*2.89*	2.45
F	2.4	2.55	*3.48*	*4.46*	*4.84*	*4.74*	*4.88*	*3.79*	2.54	2.4
G	2.36	2.39	2.56	*2.7*	*2.78*	*2.84*	*2.76*	2.55	2.43	2.35
H	2.37	2.39	2.5	2.46	2.48	2.53	2.46	2.42	2.42	2.37

2.3.2.2 IF Results in Sand

In the next step, we investigated the effect of sand on IF test results. Two PVC tubes were placed horizontally at distances of 12 in and 18 in from the edge of the steel beam. The box was filled with sand at two different moisture contents. The tests were conducted with the Probe running inside the pipes at various locations. The results are shown in Tables 71 and 72 for sand at 4% moisture content and saturated sand, respectively.

TABLE 71 IF Test Results for Sand with 4% Moisture Content.

	1	2	3	4	5	6	7	8	9	10
B	*3.08*	*3.39*	*5.04*	*5.04*	*5.04*	*5.04*	*5.04*	*5.04*	*3.86*	*3.10*
C	*3.08*	*3.20*	*3.29*	*3.41*	*3.56*	*3.63*	*3.62*	*3.52*	*3.38*	*3.18*

TABLE 72 IF Test Results for Saturated Sand.

	1	2	3	4	5	6	7	8	9	10
B	*3.17*	*3.75*	*5.04*	*5.04*	*5.04*	*5.04*	*5.04*	*5.04*	*5.04*	*3.23*
C	*3.06*	*3.22*	*3.36*	*3.43*	*3.53*	*3.56*	*3.51*	*3.37*	*3.20*	*3.00*

The readings in Tables 71 and 72 are significantly higher than those in Tables 69 and 70. The presence of soil mineralization enhances the recognition of metal objects. The results of Tables 69 and 70 indicated that the steel beam cannot be clearly detected at a distance of 18 in while there is no soil in the box. However, with the presence of sand, the beam was clearly detectable at 18 in. Therefore, the borehole should be constructed within 18 in from the pile in the field. Comparing Tables 71 and 72, soil moisture content has no effect on IF tests.

2.3.2.3 IF Results in Clay

In the final step, the box was filled with clay and the IF tests were repeated. The measurement of voltages at the 20 recording points is shown in Table 73.

TABLE 73 Measurements at Points on Axes B and C with the Presence of Clay.

	1	2	3	4	5	6	7	8	9	10
B	2.98	*3.05*	*3.99*	*5.04*	*5.04*	*5.04*	*5.04*	*4.41*	*3.13*	2.68
C	2.91	2.95	*3.04*	*3.18*	*3.22*	*3.28*	*3.22*	*3.12*	2.91	2.69

By comparing the data from Tables 71 and 73, it was realized that there was a slight difference between the results of clayey and sandy soils; the clay was a slightly worse media for detecting the steel beam than the sand (voltages in row C are slightly lower than those in Table 71). However, the beam was clearly detectable at a distance of 18 in with the presence of clay.

2.3.3 IF testing: Testbed off Campus

In order to determine if an induction-based nondestructive method would be successful in locating the bottom of a reinforced concrete pier, a particular test site was established. The test site was the same as the one used for PS test presented previously.

A three-foot deep by one-foot diameter hole was excavated. A four-foot long, one-foot diameter reinforced concrete pier was cast in place at the test site. The pier was reinforced with 5-#5 vertical rebar and #3 ties at 6 in, as shown in Figure 184. There was 3 in clear cover to the outside of the #3 ties. Three two-inch diameter holes were then bored 6-ft into the ground. The boreholes run parallel to the concrete pier located distances of 6, 12, and 18 in from the outside edge of the pier as can be seen in Figure 185. A 2-in diameter PVC pipe was inserted in the holes to a depth of 3 ft below the bottom of the pier as shown in Figure 186. The LITE was assembled and calibrated. The Probe was inserted into the tube and the voltage readings were recorded at 1 ft intervals. The results are shown in Table 74.

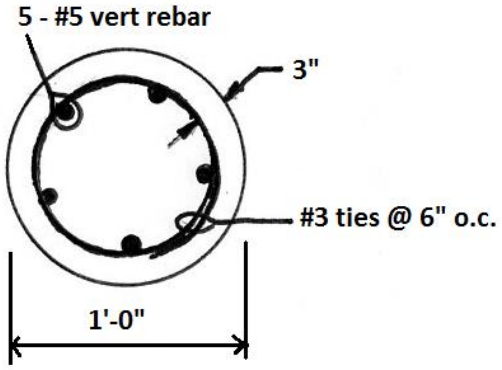

FIGURE 184 The 1-ft Reinforced Concrete Pier

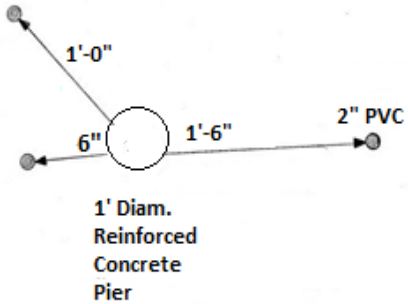

FIGURE 185 Layout of the Concrete Pier and Boreholes

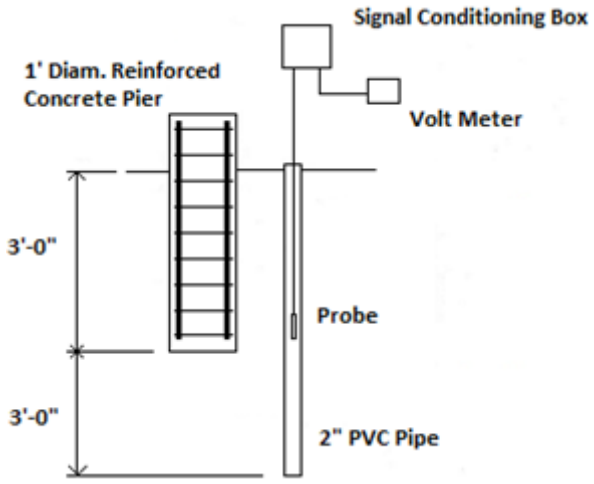

FIGURE 186 Schematics of the Reinforced Concrete Pier and the IF Test

TABLE 74 Voltage Readings Recorded at Each Borehole Location.

Depth (ft)	Borehole @ 6”	Borehole @ 12”	Borehole @ 18”
0	5.01 V	5.04 V	3.95 V
1	5.01 V	5.04 V	3.92 V
2	5.04 V	5.04 V	3.45 V
3	5.04 V	5.01 V	3.42 V
4	3.59 V	3.62 V	2.65 V
5	2.56 V	2.75 V	2.50 V
6	2.50 V	2.50 V	2.50 V

The results show that the IF method could determine the depth of a reinforced concrete pier. It can determine the pier depth to an accuracy of approximately 6 in. It is also noted that while the bottom of the pier can be easily determined at a borehole distance of 6 and 12 in, when this distance is 18 inches the results become less conclusive.

2.3.4 Conclusion of IF Testing

Although IF field tests could not be performed in this project, two proper testbeds were constructed to investigate various aspects of IF tests. The findings were valuable and provided guidelines to perform IF tests on steel and reinforced concrete foundations.

The first testbed contained a metal I-beam placed horizontally in a wooden box full of soil. The box was filled with sand (or clay) and IF tests were conducted with the Probe placed inside the

PVC tubes at various locations. IF tests were also performed on a reinforced concrete pier to study the performance of IF tests on reinforced concrete foundations.

The IF tests conducted at UNM indicated that the soil type affected the quality of detection. It was easier to detect the I-beam in sand than in clay although the beam could be detected in both types of soil at a distance less than 18 in. The results also showed that the moisture content of soils had no effect on the IF tests.

IF tests performed on the reinforced concrete cylinder located off campus showed that the IF method could be used effectively for determining the depth of a reinforced concrete pier. An accuracy level of approximately 6 in was obtained. The method worked at a borehole distance of 6 in and 12 in from the test pier. When the distance between the pier and the hole increased to 18 in or more, the results were less conclusive. It might be due to the location of the rebar that are 3 in from the pier surface. Therefore, the bore hole for IF tests must be drilled closer than 18 in in order to detect the reinforced concrete foundation.

IF tests can be used to detect steel and reinforced concrete foundations. For steel foundations a borehole must be drilled within 18 inches from the test object. For reinforced concrete piers, a borehole must be drilled closer than 16 inches for a typical 2 in cover of concrete.

2.4 FINITE ELEMENT SIMULATIONS

Finite Element Modeling (FEM) was used to provide insight on the physical results of SE tests. Finite element simulations of 1D wave propagation in square-section timber piles and 3D wave propagation in concrete pier walls were carried out using ABAQUS. The lengths of the timber piles and pier walls were calculated based on the acceleration (or velocity) responses at different nodes in the models. The effect of input signal shape, the method of impulse application, and the location of sensor were investigated on timber piles. The effect of pier width, hammer tip type, the reflection from the deck, and the direction of striking were examined on models of pier walls. The effect of the material damping was also considered in the analysis. Rayleigh damping coefficients were taken into account based on the foundation resonant frequencies (*41*). In addition to the individual pier wall, a more complicated foundation comprising a pier wall and a pile was investigated.

2.4.1. Wave Propagation in Piles and Columns

In this section, proper FEM models were developed for better understanding of the wave propagation in the wood column at UNM and the timber piles of the Santo Domingo Bridge (see Table 4). Numerical wave propagation simulations were carried out. The lengths of piles were calculated based on the acceleration and velocity response at a node (the location of a sensor). The effect of the shape of the input signal on the result of SE tests was investigated. No artificial damping was applied in the FEM simulations. The element type is C3D8R (8-node linear brick, reduced integration, hourglass control).

2.4.1.1 Models of UNM Wood Column

Two FEM models have been developed. The first one is an individual wood column whereas the second is a wood column with a foundation as shown in Figures 187 and 188 respectively.

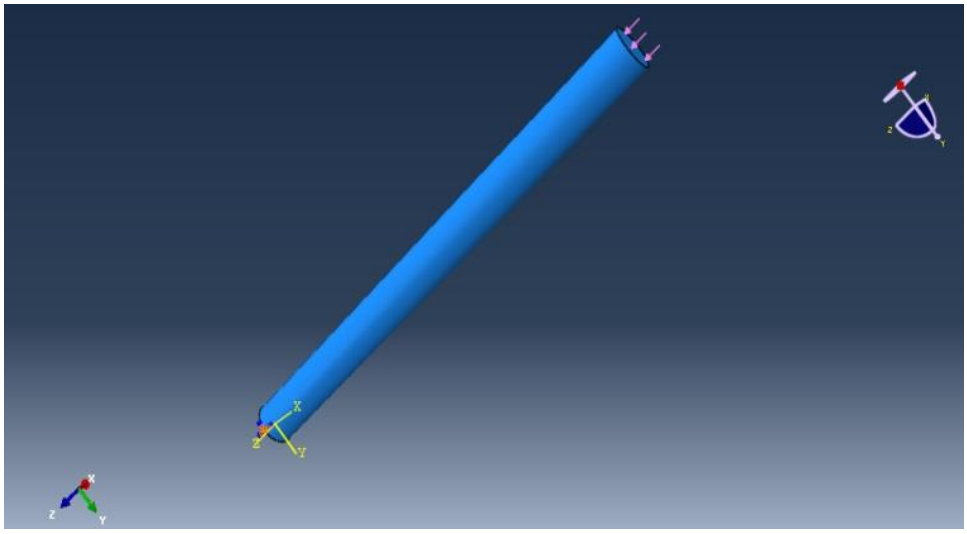

FIGURE 187 A FEM Model of a Wood Column

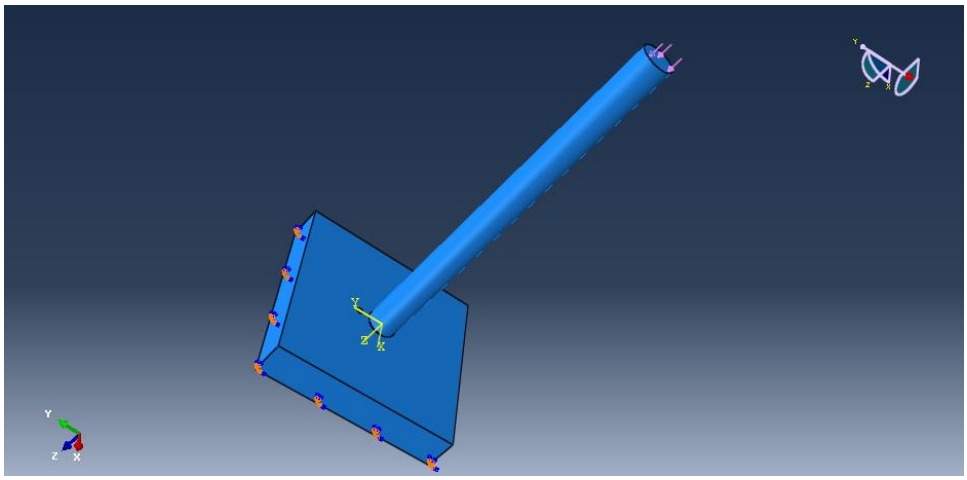

FIGURE 188 A FEM Model of a Wood Column with Foundation

2.4.1.2 Individual Wood Column

The length and diameter of the wood column used in the FEM analysis are 3 m and 0.24 m respectively. The modulus of elastic (E) and the Poisson ratio (ν) of wood are 10 GPa and 0.1 respectively. The density (ρ) is 500 kg/m^3. The P-wave velocity is:

$$\text{P-wave velocity} = \sqrt{\frac{E}{\rho}} = \sqrt{\frac{10000000000}{500}} = 4470\ m/s$$

The impulse, a uniform pressure, was applied at the top surface of the column as shown in Figure 187. The bottom of the pile was free. The waveform of the impulse has a rectangular shape with a duration of 2 ms. This duration is similar to those observed in physical SE tests.

The impulse (wave) traveled through the column and reflected from any changes in impedance along the pile. Figure 189 shows a snap shot of the stress distribution along the column.

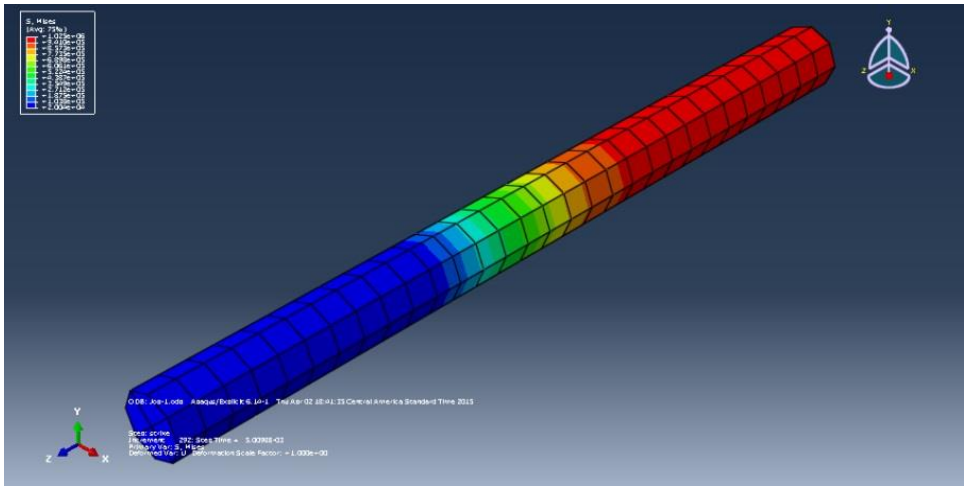

FIGURE 189 Snap Shot of the Distribution of Stresses along the Column

The responses of acceleration and velocity at a node 0.1 m below the top of the column are indicated in Figure 190. In SE tests, accelerometers or geophones record acceleration velocity time histories respectively.

Unlike the physical SE tests, there is no energy dissipation (zero damping) in this FEM model. More wave reflections are shown in the figure. Since the model contains a free end, the polarity of the reflected wave will change (incoming compression wave becomes outgoing tension wave). The time difference between two consecutive positive peaks (or negative valleys) corresponds to twice the length of the pile. The acceleration and velocity have 90 degrees phase difference. Maximum acceleration occurs at zero velocity. The arrows in the figure show the moments of zero velocity at the targeted node. Δt (the difference between impulse and echo) was determined from two consecutive zeros (1.34 ms) to avoid the polarity change because of the free surface. The length of the column is calculated as:

$$L = v \times \Delta t = \frac{1}{2} \times 1.34 \times 10^{-3} \times 4470 = 3 \text{ m}$$

The calculated length is in accordance with the actual length (3 - 0.1 = 2.9 m) of the column.

Three other different input signals (triangular, trapezoidal, and sinusoidal impulses) were also used. Figure 191 shows the responses of the acceleration and velocity for trapezoidal, sinusoidal, and triangular impulses. The reflections can be identified clearly in these figures. The time differences between the impulses and echoes are the same as that obtained with rectangular impulse. Therefore, the shape of the impulse does not affect the determination of Δt.

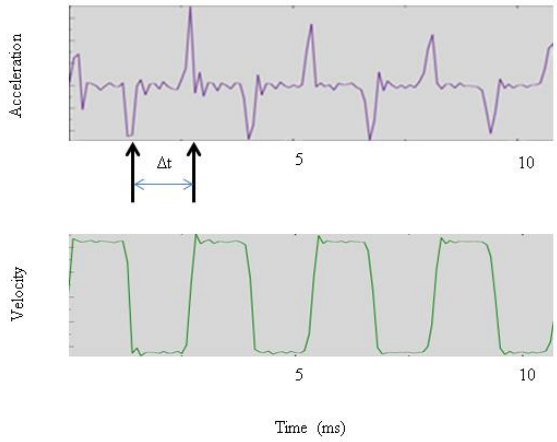

FIGURE 190 Acceleration and Velocity Time Histories

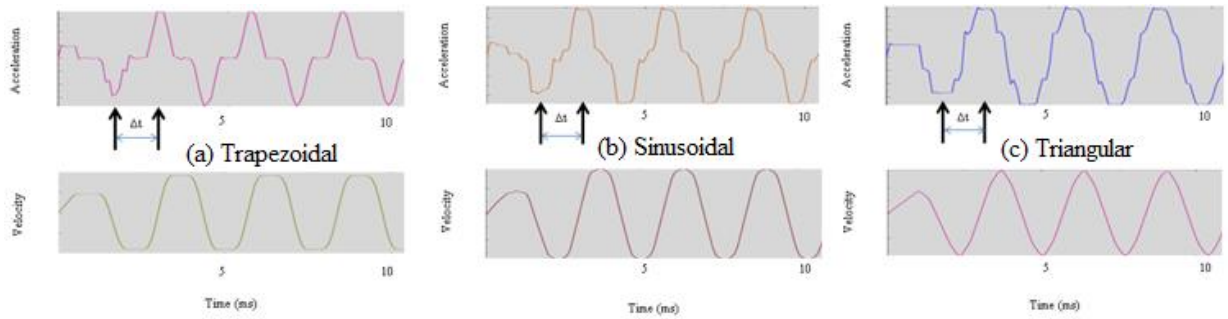

FIGURE 191 Acceleration and Velocity Time Histories for Different Input Signals

In physical SE tests a hammer applies a load on a small area rather than uniformly across the cross section of a pile. As shown in Figure 192, impulse of a rectangular waveform was applied on a 2-in diameter circle. It is to mimic the non-uniformity of stress wave across the cross-sectional area at the striking point in the physical SE tests.

The result is shown in Figure 193. The general response is similar to the model in which the load was applied on the whole area of the column's top (see Figure 190). Δt is still 1.34 ms. However, a second peak with great magnitude was shown in the acceleration graph that was not observed in Figure 190. If these two peaks (first and second) are very similar in magnitude, determining Δt will be difficult based on the acceleration response.

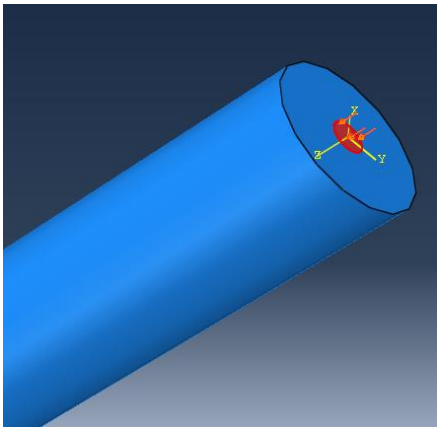

FIGURE 192 Input Signal is Applied on Limited Area

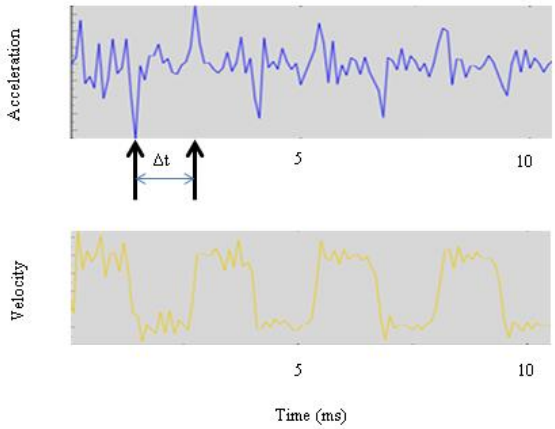

FIGURE 193 Result of Input on a Limited Area

Wood Column with Foundation A concrete foundation (1.5×1.5×0.3 m) attached to the wood column is simulated. The concrete's properties are: E = 20 GPa, ρ = 2400 kg/m^3, υ = 0.2. Figure 194 shows the model with the snap shot of the stress distribution.

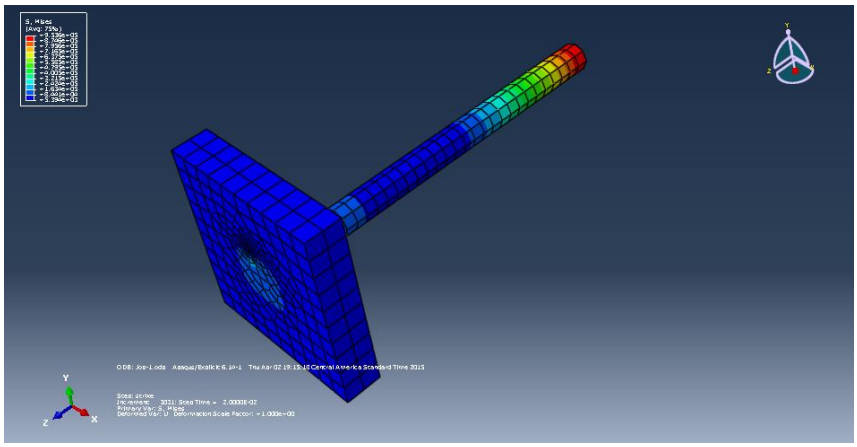

FIGURE 194 Distribution of Stresses along the Column with Foundation at a Moment

Rectangular and triangular impulses were applied. The acceleration and velocity graphs for the rectangular and triangular impulses are shown in Figure 195.

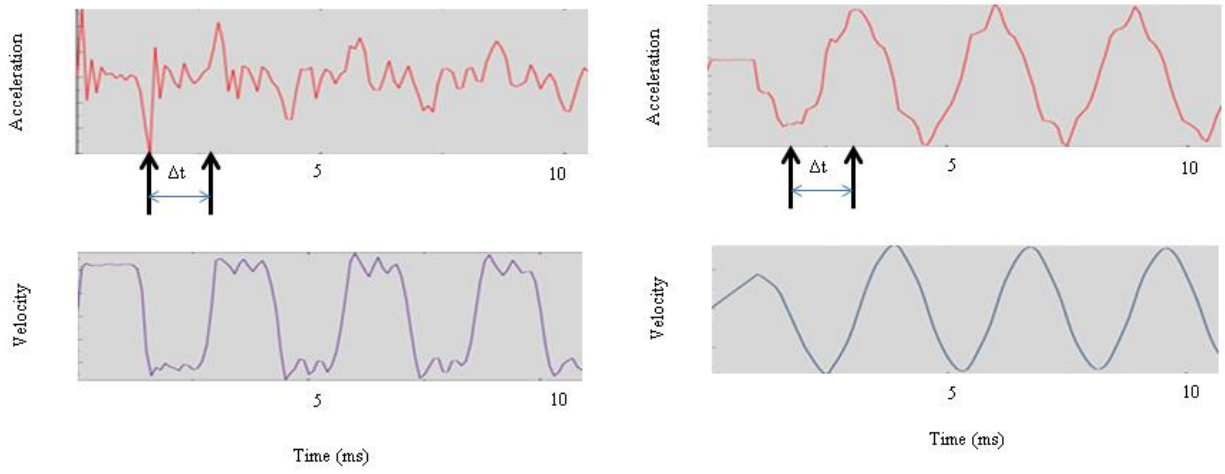

(a) Rectangular Input Signal (b) Triangular Input Signal

FIGURE 195 Results of Rectangular and Triangular Input Signals

Wave reflection can be seen in these figures. The interpretation of Δt is easier for triangular input signal than for rectangular signal. The length of the column is estimated as:

$$L = v \times \Delta t = \frac{1}{2} \times 1.44 \times 10^{-3} \times 4470 = 3.2 \text{ m}$$

This calculated length is similar to the actual length (3 + 0.3 - 0.1 = 3.2 m).

2.4.1.3 Santo Domingo Bridge

SE tests have been performed on the timber piles at the Santo Domingo Bridge. Finite Element models were used to simulate these SE tests. The initial inputs for one of the bridge piles are:

Length = 9 m

Diameter = 0.33 m

E = 10 GPa

ρ = 700 kg/m^3

υ = 0.1

P-wave velocity = $\sqrt{\frac{10000000000}{700}} = 3780\ m/s$

The surrounding soil was not included in this numerical model. Only a simple FEM model of the pile was created. A snap shot of the stress distribution is shown in Figure 196.

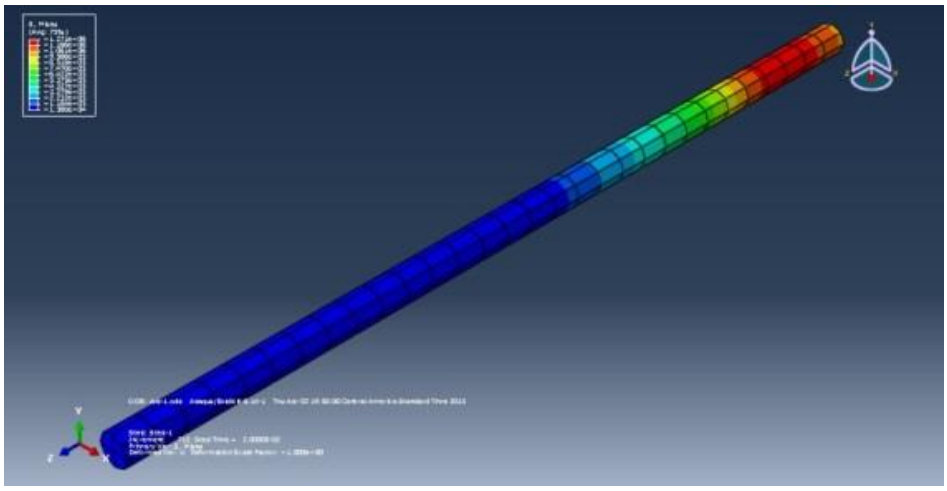

FIGURE 196 Snap Shot of the Distribution of Stresses of a Model of the Santo Domingo's Pile

Different forms of impulses were applied at the top of the pile. The graphs of the acceleration and velocity time histories for rectangular, triangular, trapezoidal, and sinusoidal impulses are shown in Figure 197. They are the obtained response at a node located 0.3 m below the top of the pile.

Wave reflections are recognizable from these graphs. The Δt (time difference between the impulse and echo) is 4.7 ms and the pile length is calculated as:

$L = \frac{1}{2} \times v \times \Delta t = \frac{1}{2} \times 4.7 \times 10^{-3} \times 3780 = 8.9$ m

The calculated length is in accordance with the actual length (9 - 0.3 = 8.7 m) of the pile.

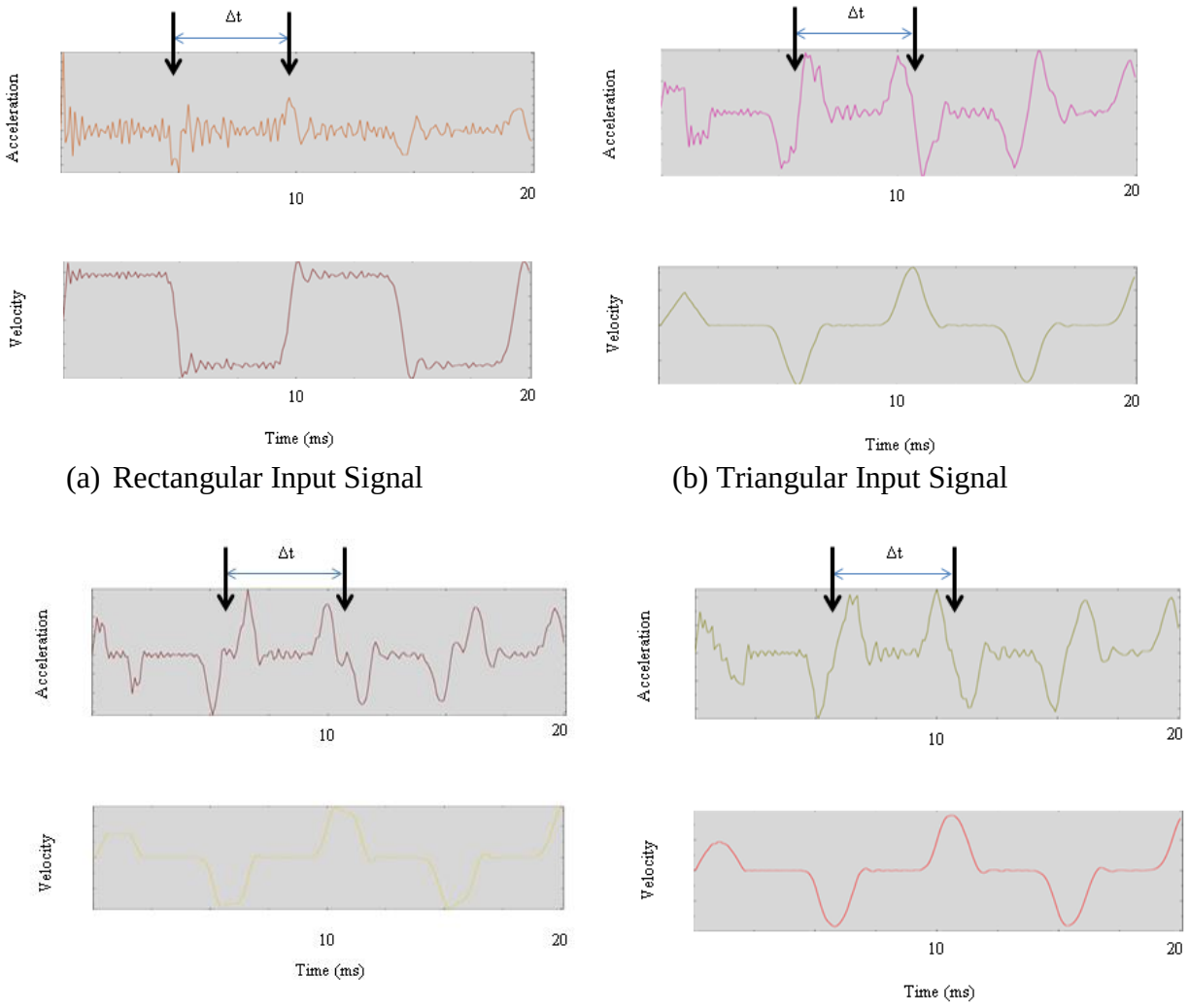

(a) Rectangular Input Signal (b) Triangular Input Signal

(c) Trapezoidal Input Signal (d) Sinusoidal Input Signal

FIGURE 197 Results of Input Signals of Different Shapes

2.4.1.4 Waveform Analysis of Piles

A 5.5 m timber pile of with a diameter of 0.24 m was modeled in ABAQUS. The material properties are: elastic modulus = 9.5MPa, density = 700Kg/m^3, Poisson's ratio = 0.08. The corresponding wave velocity is 3,684 m/s and the wave takes 1.5 ms to travel the 5.5 m pile consequently.

Figure 198 shows one end of the FEM model. Figure 199 shows the result of the acceleration at the node shown in Figure 198. Note that the reflections from the end of the column arrived every 3 ms in the absence of any damping as expected.

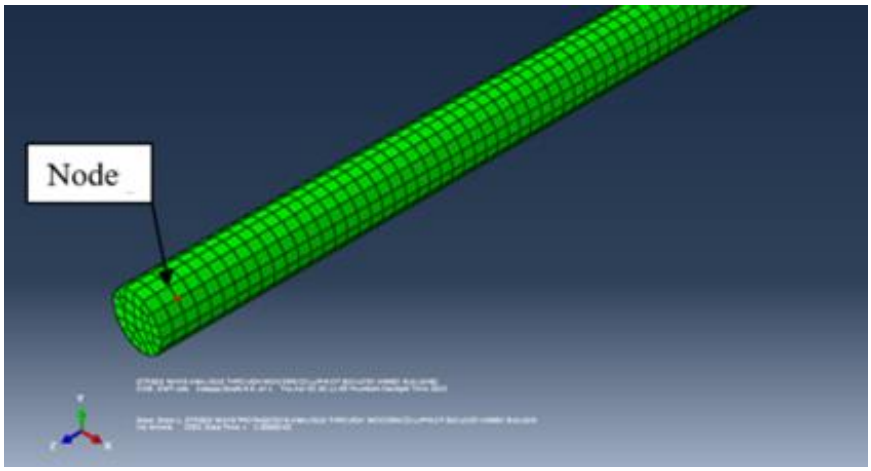

FIGURE 198 FEM Mesh of Wood Column

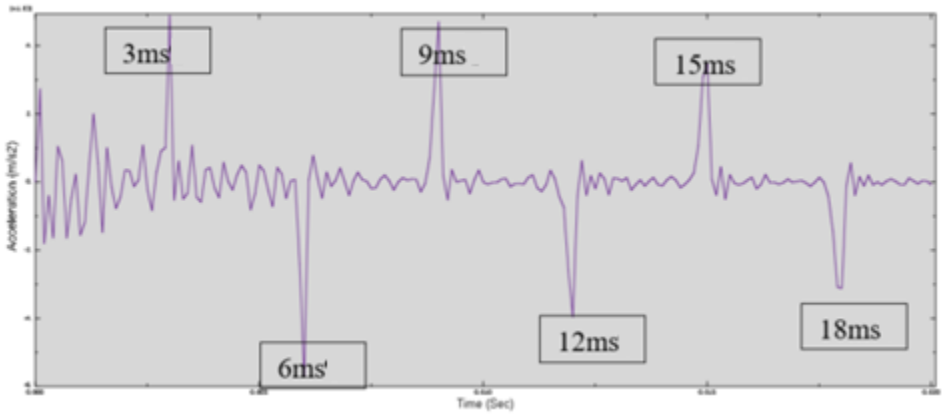

FIGURE 199 Acceleration at a Node Close to the End of the Column

Figure 199 shows that the waveform was inverted each time it hit the end. At a fixed boundary a compression wave is reflected back as a compression wave (no phase change), while at the free end (left end near the node) it is converted to a tension wave. A tension wave is converted to a compression wave upon hitting the free end. Therefore, the sign of the incident wave changes as it reflected from the free end of the pile. On the other hand, the sign of the reflected wave is the same as the incident wave at the fixed end. This is why two valleys in the waveform acquired from field tests provide the complete travel time for reflection from the bottom of the pile.

The actual waveform detected in field tests is subjected to damping inherent in the wood and surrounding material which absorbs the wave energy. The acceleration at the node mentioned in the previous section is shown in Figure 200. The damping coefficients are α=0.002 and β=0.0002 corresponding to the Rayleigh damping equation shown below.

$$[C] = \alpha [M] + \beta [K]$$

Note that in the presence of damping, the reflections arrive at the same time as shown in Figure 199, but the high-frequency content of the acceleration was removed and the amplitude decays over time similar to the field test results. The initial impulse (at time 0) is more evident. Compression force applied towards the right produces negative acceleration because the positive axis in our reference frame is pointing towards the left.

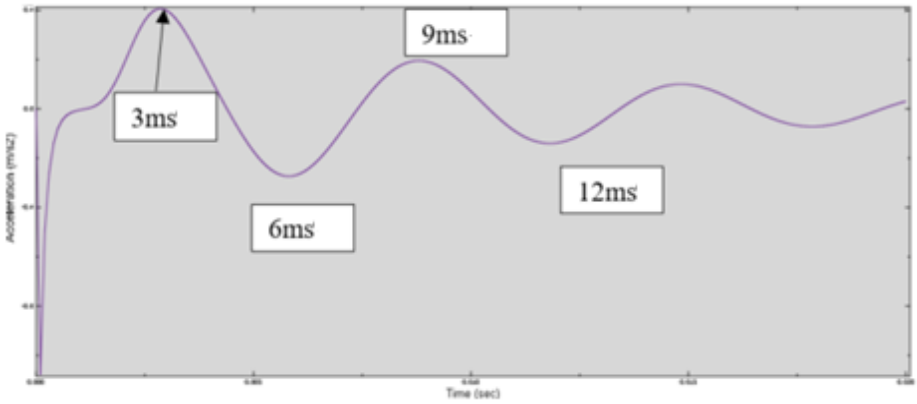

FIGURE 200 Acceleration at Node Close to the End with Rayleigh Damping

Figure 201 shows a more complex waveform that was seen when the accelerometer was mounted farther from one end. The reflections arriving from both ends made the analysis more difficult.

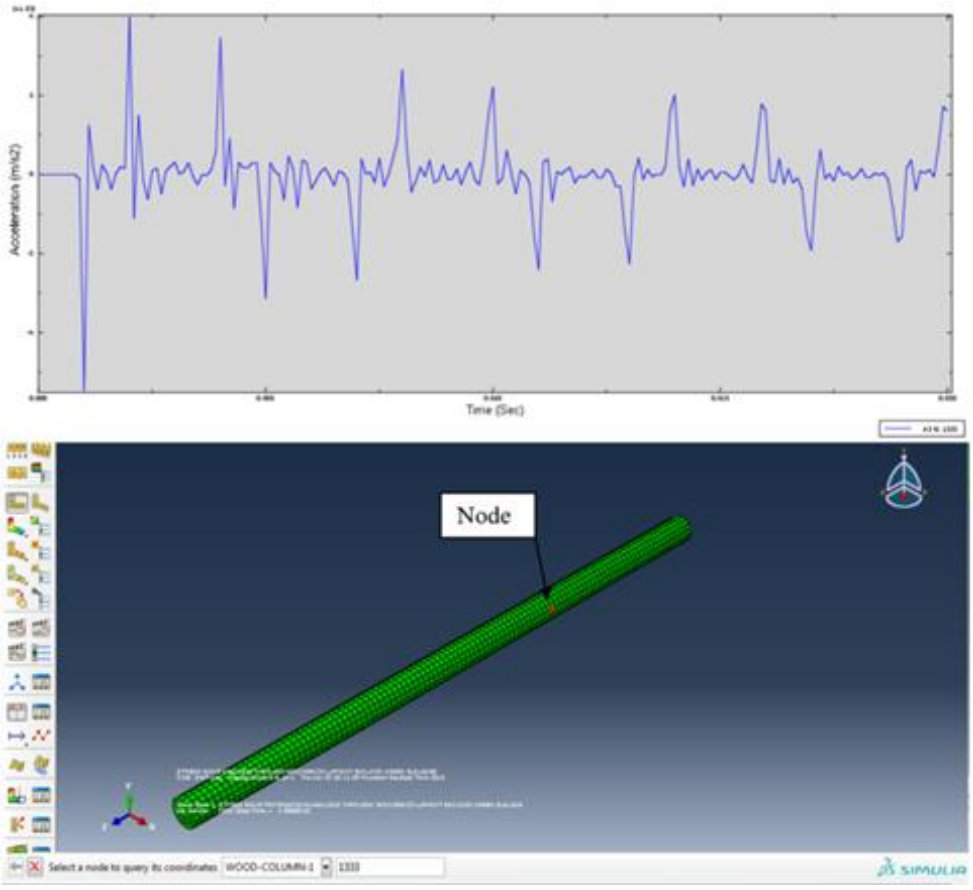

FIGURE 201 Acceleration at a Node 1/3 Length of the Pile from the Right End

2.4.2. Wave Propagation in Pier Walls without Damping

2.4.2.1 Wave Propagation in Pier Walls

In this section the wave propagation inside a 3-D pier wall was investigated. To do so, a concrete pier wall similar to the Pier 3 of Bridge No. 5899 was modeled in ABAQUS. The effects of hammer tip and the reflection from the deck on the received signals were examined.

The calculated height of Pier 3 was 23 ft (7m) from field SE tests results. The same height was used in the numerical model. The properties of the material and loading information are listed in Table 75. The assumed wave velocity (3261 m/s) is the same as that obtained in the field. The corresponding modulus of elasticity is calculated as:

$$E = \rho v^2 = 2400 \times 3261^2 = 25.52\ GPa$$

TABLE 75 Input Parameters of the Finite Element Simulations.

V (wave velocity)	3261 m/s
E (modulus of elasticity)	25.52 GPa
ρ (density)	2400 kg/m^3
ν (Poisson's ratio)	0.2
Impulse amplitude	1 MPa
Impulse shape	Parabola
Impulse duration	1.2 ms
Simulation time duration	20 ms
Elements type	C3D8R (8-node linear brick)
Approximate mesh dimensions	0.2 m

No damping is considered in the numerical models and the effect of damping will be considered later.

2.4.2.2 Effect of Pier Wall Width

Since the wave propagation in a pier wall may be different from that of a long slender pile, the results obtained from pier wall models with different widths were compared with the result of a long slender pile of the same height. The cross section and the side view of the selected pier wall are shown in Figure 202. Hereafter Nodes A and B assumed to be approximately coinciding with the Accelerometers 1 and 2 in the field tests respectively. The locations of Nodes A and B were two inches below the actual locations of Accelerometers 1 and 2 respectively, however the discrepancy is negligible compared with the height of the models.

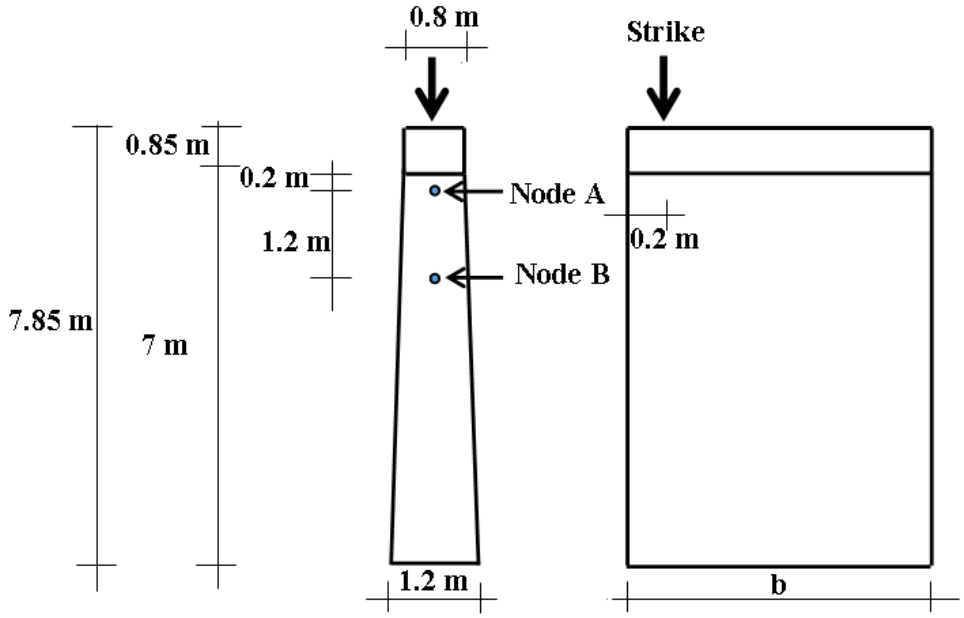

FIGURE 202 Cross Section and Side View of the Pier Wall

M1 is a finite element model of a square section pier (0.4 m x 0.4 m) with a length of 7.85 m. M2 to M6 are the models shown in Figure 202 of different widths (b). The width of each model is listed in Table 76. Model M6 has the same dimensions as the Pier 3 of Bridge No 5899.

TABLE 76 Widths of the Pier in Models M2 to M6.

Model	Width(m)
M2	0.4
M3	0.8
M4	1.7
M5	3.5
M6	5.2

A typical velocity graph obtained at Node A is shown in Figure 203. The unit of the velocity in this figure is m/s. Figure 204 shows the comparison of the velocity graphs of all models (M2 ~ M6). A total duration of 7 ms is shown here for clarity.

The degree of preciseness of determining Δt decreases with the increase of width *b*. The calculated length (6.2 m) is slightly less than the actual length in model M6 (6.8 m). The error is within the tolerance of SE tests (10%). The width of the pier slightly affects the estimation of the height of the pier in the numerical models.

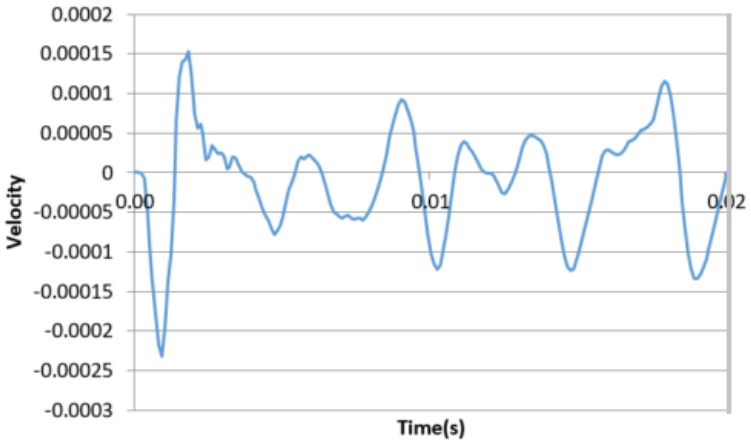

FIGURE 203 Velocity Graphs Obtained at Node A (b = 5.2 m)

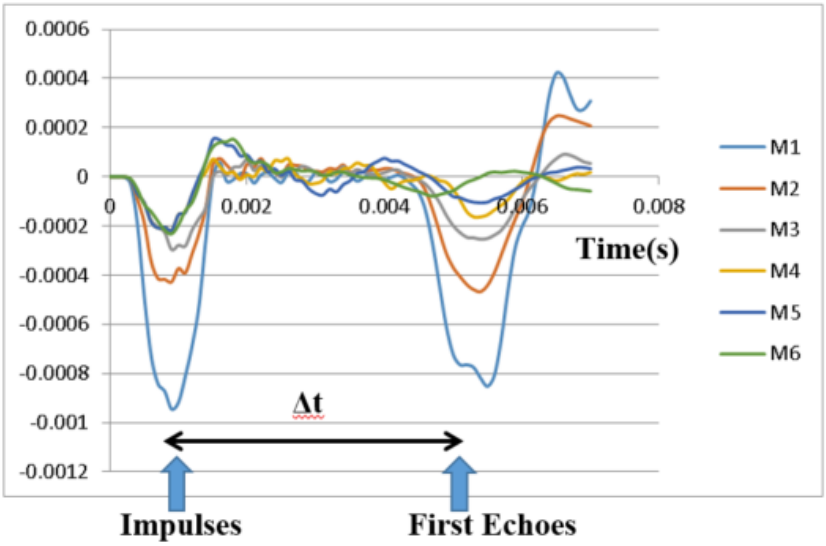

FIGURE 204 Impulses and the First Echoes of Models M1 to M6

2.4.2.3 Effect of Hammer Tip

Different hammer tips (hard, medium-hard, and medium-soft) have been used on the pier in the field. It was decided to investigate the effect of hammer tip by using different impulse time durations. A FEM model of Pier 3 including the pier wall, the pile cap and a 2-ft deck was developed and the dimensions are shown in Figure 205.

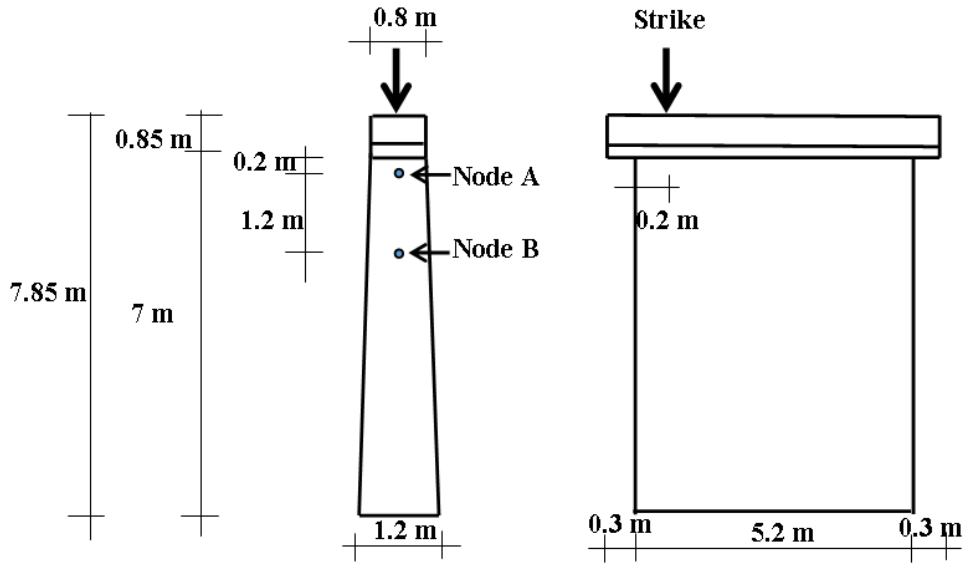

FIGURE 205 Dimensions of the Numerical Model and the Locations of the Source and Receiver

Three hammer tips and their corresponding impulse time durations are indicated in Table 77 for the three models (M7~M9). The velocity graphs of Models M7 to M9 at Nodes A and B are shown in Figures 206 and 207 respectively. The impulses and echoes can be identified for all models. The calculated heights based on the velocity graphs at Nodes A and B are indicated in Table 78. L_{tr} is the calculated length from Δt and L_a is the actual distance from the node to the pier bottom. The results are acceptable at Node A for different hammer tips. However, greater errors were found at Node B for medium-hard and medium-soft tips. The effect of hammer tip depends on the location of the sensors.

TABLE 77 Impulse Time Durations and Corresponding Hammer Tips (M7~M9).

Model	Hammer Tip Type	Impulse Time duration (ms)
M7	Hard	1.2
M8	Medium-hard	2.4
M9	Medium-soft	3.6

TABLE 78 Calculated Nodes A and B Heights for Different Hammer Tips.

Hammer Tip	Node A				Node B			
	Δt (ms)	L_{tr} (m)	L_a (m)	Error (%)	Δt (ms)	L_{tr} (m)	L_a (m)	Error (%)
Hard	4	6.52	6.85	-4.8	3.4	5.54	5.65	-1.9
Medium-hard	4.4	7.17	6.85	4.7	3.9	6.36	5.65	12.5
Medium-Soft	4.3	7.01	6.85	2.4	3.9	6.36	5.65	12.5

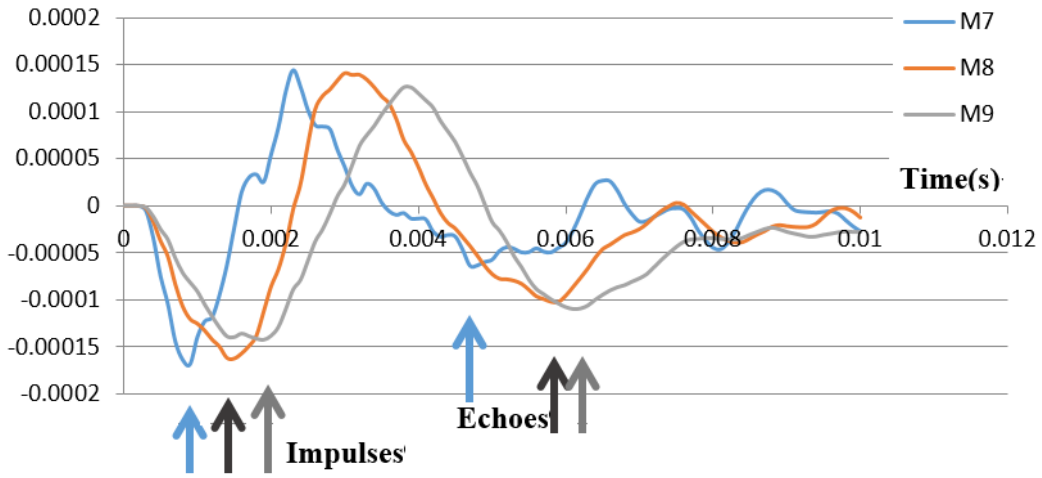

FIGURE 206 Velocity Graphs of Models M7 to M9 Obtained at Node A

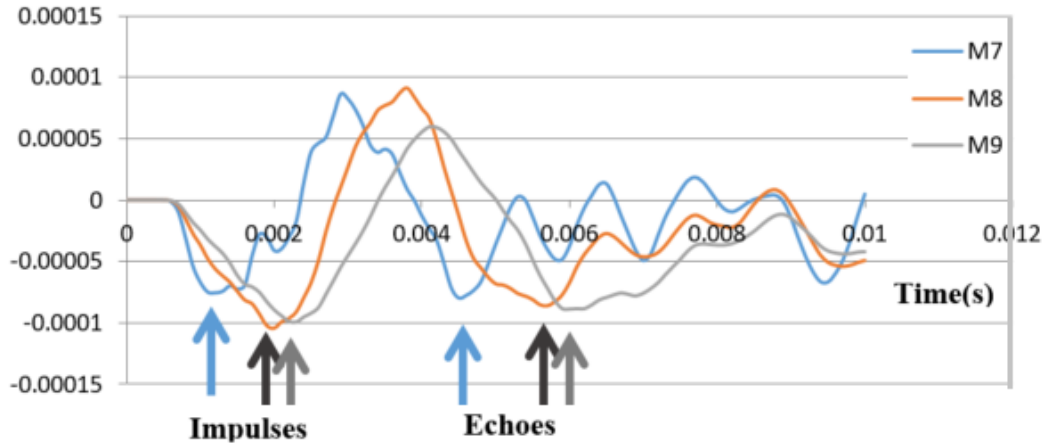

FIGURE 207 Velocity Graphs of Models M7 to M9 Obtained at Node B

2.4.2.4 Effect of Deck Reflection

The effect of reflection from the end of the deck was investigated by varying the deck dimension. The cross section and side view of the model are indicated in Figure 208.

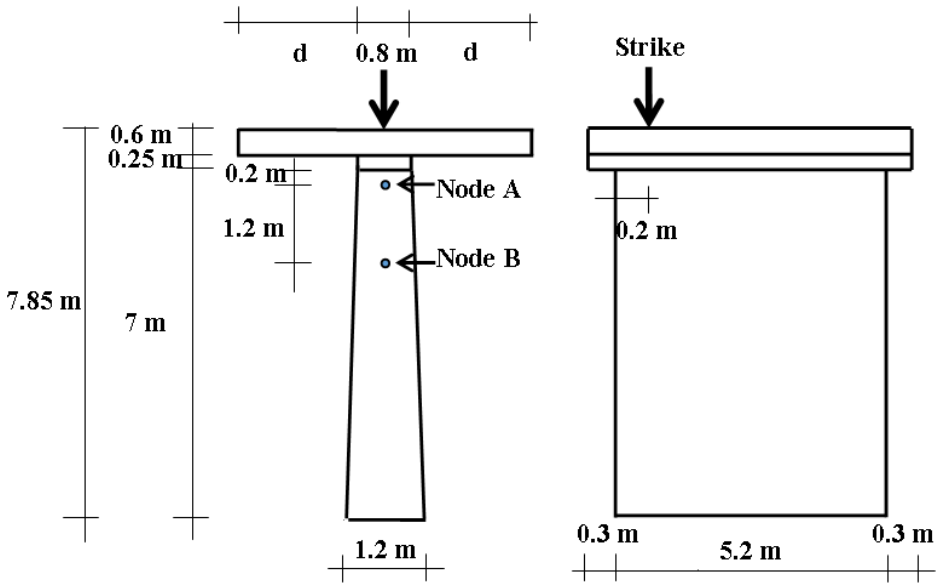

FIGURE 208 Cross Section and Side View of a Model with Deck

Finite element analyses on models with different deck widths (d) were performed where d is listed in Table 79.

TABLE 79 Deck Widths for FEM Models M10 to M12.

Model	d (m)
M10	13
M11	10
M12	7

A typical velocity graph obtained at Node A is shown in Figure 209. Figure 210 shows the velocity graphs of these three models. The impulses and echoes are the same for different widths of deck (see Points I and E on Figure 210). Δt = 4.1 ms corresponds to a length of 6.69 m which is very close to the actual height of Node A (6.8m). Therefore, there is no deck effect.

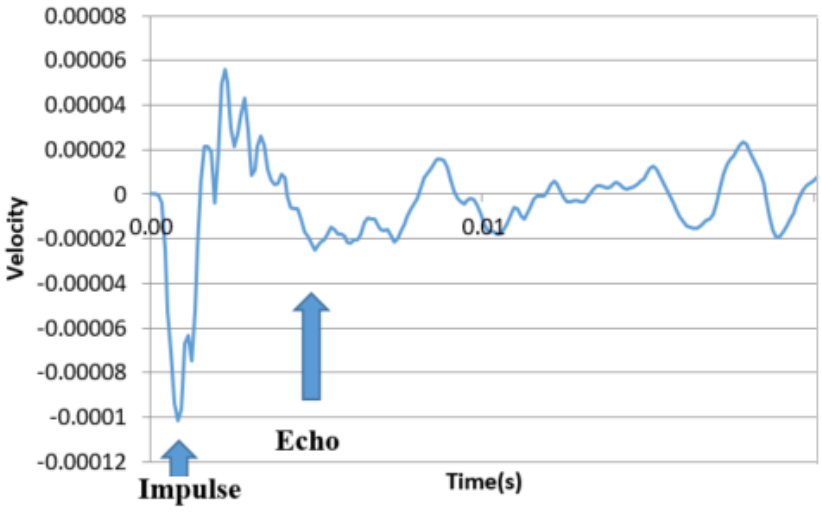

FIGURE 209 Velocity Graph Obtained in Node A (d = 10 m)

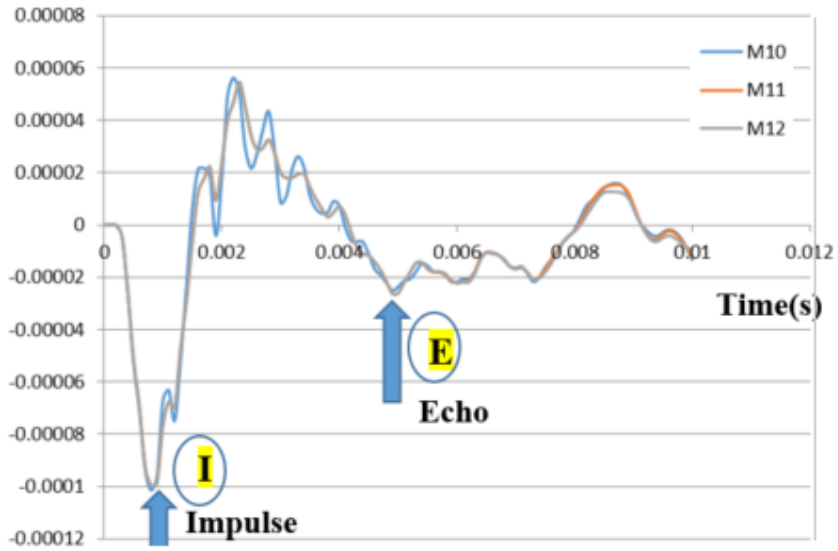

FIGURE 210 Velocity Graphs Obtained at Node A (M10 to M12)

2.4.2.5 Effect of Upward Striking

Upward striking on the pile cap and on the bridge deck were simulated with the numerical model shown in Figure 208 (d = 7 m). The velocity graphs obtained at Node A by striking on the pile cap and deck are shown in Figures 211 and 212, respectively. The impulses and echoes were identified with ease for upward striking at the pile cap and deck. The calculated heights are very close to the actual height and listed in Table 80. Therefore, both upward striking on the pile cap and on the bridge deck are acceptable alternative source to determine the height of the pier wall when the top of the deck is inaccessible.

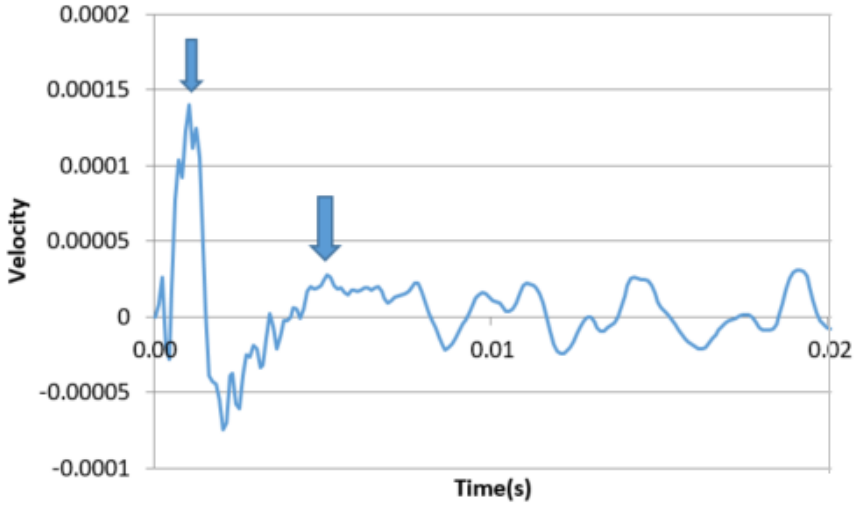

FIGURE 211 Velocity Graphs Obtained from Upward Striking at the Pile Cap

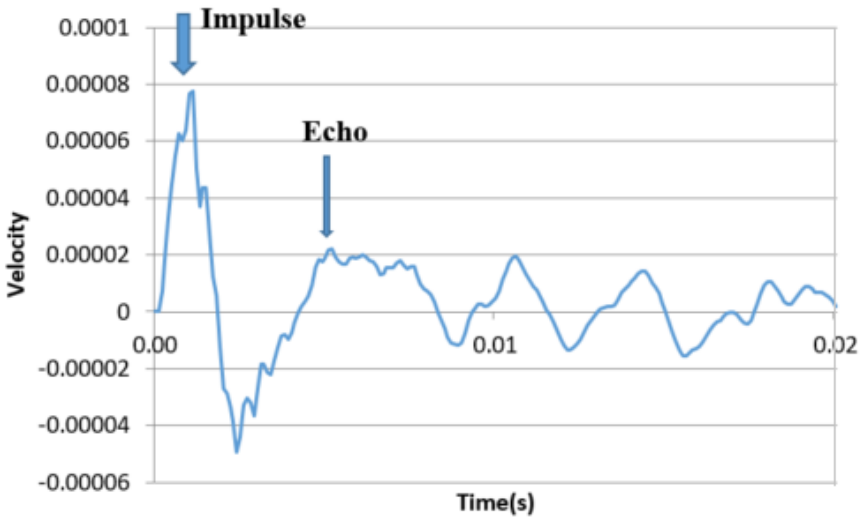

FIGURE 212 Velocity Graphs Obtained from Upward Striking at the Bridge Deck

TABLE 80 Calculated Heights for Upward Striking.

Striking Location	Δt (ms)	L_{tr} (m)	L_a (m)	Error (%)
Pile cap	4	6.52	6.8	-4.1
Bridge deck	4	6.52	6.8	-4.1

2.4.2.6 Summary of FEM Study of Pier Walls without Damping

The time difference between the impulse and echo did not change significantly with different widths of the pier wall. Similar numerical results were found for all hammer tips when the receiver was close to the top of the pier. For the deck width greater than 7 m, the reflections from the end of the deck did not affect the signals. Since the calculated heights obtained from the upward striking were similar to the actual height, applying upward striking on the pile cap or on the bridge deck is good alternative to determine the height of the pier walls while the top of the deck is inaccessible.

2.4.3. Wave Propagation in Pier Walls with Damping

In section 2.4.2.1, a concrete pier wall similar to the Pier 3 of the Bridge No. 5899 was modeled using ABAQUS. The effects of pier width, hammer contact time, deck ends reflections and upward striking on the pier cap and bridge deck were investigated in the absence of energy dissipation. In this section, the effect of aforementioned factors were investigated again with material damping.

Since the actual dynamic behavior of a pier wall depends on damping, the effect of damping on the obtained signals should be considered. In this study, only the effect of foundation material damping was considered in the analysis. Rayleigh damping coefficients $\alpha = 1.25$ and $\beta = 0.00022$ were taken into account based on the pier wall resonant frequencies [*41*].

2.4.3.1 Effect of Pier Wall Width

In this section, the effect of material damping on received signals was examined. The velocity graphs obtained at Node A for Models M2 and M9 for undamped and damped cases are depicted in Figures 213 and 214 respectively. In Model M2 (pier width = 0.4 m), the echo is clearly visible in both undamped and damped cases. The effect of damping is insignificant. Model M9 is an example of cases with the width greater than 5.2 m. In the undamped model, multiple echoes are shown in the vicinity of the expected echo. With the presence of damping, high frequency fluctuations around the echo have been eliminated and the echo point is detectable. The advantage of the presence of material damping in the data interpretation is evident.

The measured heights based on the velocity graphs at nodes A and B in Models M2 to M9 for both undamped and damped cases are shown in Tables 81 and 82 respectively. The actual height of the pier is also shown in these two tables. The echoes in the velocity graphs at Node B cannot be determined in undamped models when the width is greater than 1.4 m. However, in all the models, the echoes become visible with material damping. The errors are greater at Node B than at Node A when the width is greater than 1.7 m.

The presence of high frequency vibrations near the echo makes interpretation difficult or impossible when there is no energy dissipation. FEM results showed that the presence of material damping divulges the echoes from the pier bottom by removing high frequency vibrations near the echo. Since the pier wall material possesses damping, the undamped cases will never happen in reality.

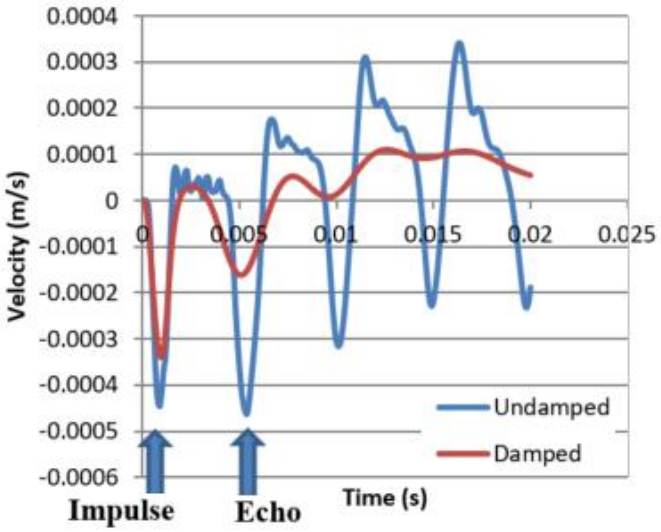

FIGURE 213 Velocity Graph of Undamped and Damped Model M2 at Node A

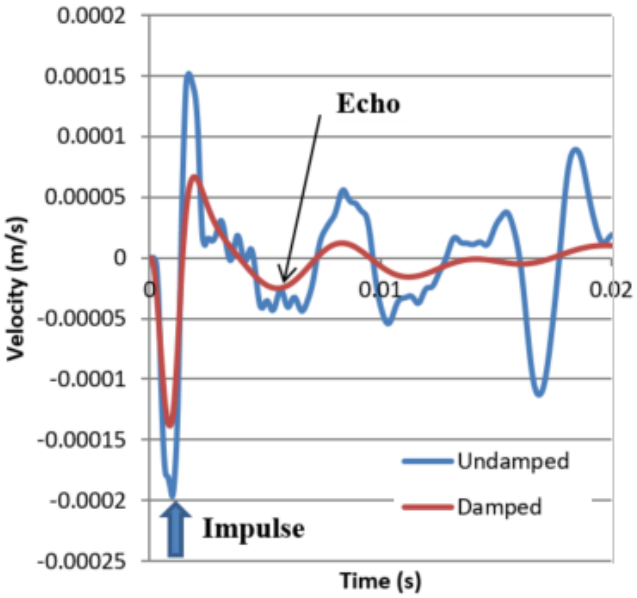

FIGURE 214 Velocity Graph of Undamped and Damped Model M9 at Node A

TABLE 81 Measured and Actual Heights of Node A in Models M2 to M9.

Model	Node A							
	Undamped				Damped			
	Δt (sec)	L_{tr} (m)	L_a (m)	Error %	Δt (sec)	L_{tr} (m)	L_a (m)	Error %
M2	0.0044	7.17	6.80	5.5	0.0039	6.36	6.80	-6.5
M3	0.0042	6.85	6.80	0.7	0.0039	6.36	6.80	-6.5
M4	0.0045	7.34	6.80	7.9	0.0043	7.01	6.80	3.1
M5	0.0045	7.34	6.80	7.9	0.0043	7.01	6.80	3.1
M6	0.0038	6.20	6.80	-8.9	0.004	6.52	6.80	-4.1
M7	Not Clear	-	6.80	-	0.0046	7.50	6.80	10.3
M8	Not Clear		6.80	-	0.0045	7.34	6.80	7.9
M9	Not Clear	-	6.80	-	0.004	6.52	6.80	-4.1

TABLE 82 Measured and Actual Heights of Node B in Models M2 to M9.

Model	Node B							
	Undamped				Damped			
	Δt (sec)	L_{tr} (m)	L_a (m)	Error %	Δt (sec)	L_{tr} (m)	L_a (m)	Error %
M2	0.0034	5.54	5.60	-1.0	0.0034	5.54	5.60	-1.0
M3	0.0035	5.71	5.60	1.9	0.0034	5.54	5.60	-1.0
M4	Not Clear	-	5.60	-	0.0038	6.20	5.60	10.6
M5	Not Clear	-	5.60	-	0.004	6.52	5.60	16.5
M6	Not Clear	-	5.60	-	0.0037	6.03	5.60	7.7
M7	Not Clear	-	5.60	-	0.0044	7.17	5.60	28.1
M8	Not Clear	-	5.60	-	0.0042	6.85	5.60	22.3
M9	Not Clear	-	5.60	-	0.0039	6.36	5.60	13.6

2.4.3.2 Effect of Hammer Tip

The FEM model of a pier wall with a width of 5.2 m (see Figure 208) and material damping was analyzed with different hammer tips. The hammer tips and the corresponding impulse contact durations are shown in Table 83.

TABLE 83 Hammer Tips and the Corresponding Impulse Contact Durations of Three Models.

Model	Hammer Tip Type	Impulse Time Duration (ms)
M6	Hard	1.2
M6-1	Medium-hard	2.4
M6-2	Medium-soft	3.6

The impulses and echoes are recognizable for all three models. The calculated heights based on the Δt obtained at Nodes A and B are listed in Table 84. When the contact time increases, the error becomes greater at both Nodes A and B. In addition, the errors at Node B are greater than Node A. Therefore, it is recommended to use a hammer with hard tip and place the sensors as close as possible to the top of the pier wall to achieve more successful SE tests.

TABLE 84 Calculated Heights of Nodes A and B for Damped Models.

Model	Node A				Node B			
	Δt (sec)	L_{tr} (m)	L_a (m)	Error %	Δt (sec)	L_{tr} (m)	L_a (m)	Error %
M6	0.0041	6.69	6.80	-1.7	0.0038	6.20	5.60	10.6
M6-1	0.0043	7.01	6.80	3.1	0.004	6.52	5.60	16.5
M6-2	0.0048	7.83	6.80	15.1	0.0043	7.01	5.60	25.2

2.4.3.3 Effect of Deck Reflection

The effect of the deck width was investigated by varying the deck dimension in the finite element models. The cross section and side view of the FEM model are depicted in Figure 215.

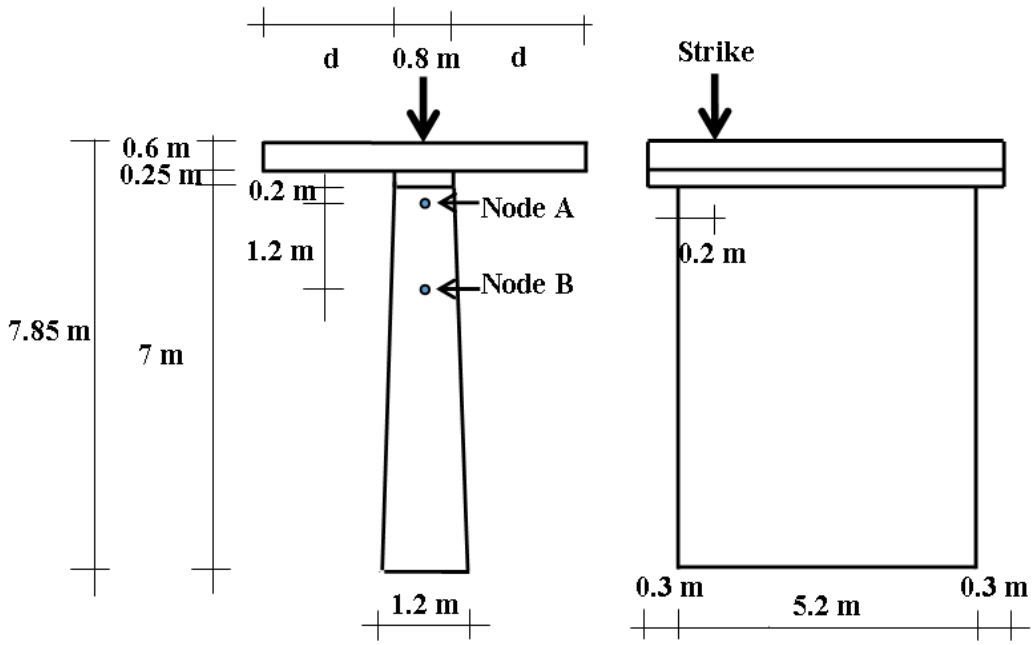

FIGURE 215 Cross Section and Side View of the Models with Bridge Deck

Finite element analyses on models with three different deck widths (d = 6, 8, 12 m) were performed. The corresponding deck widths of these models are listed in Table 85.

TABLE 85 FEM Models of Various Deck Widths.

Model	d (m)
M10	6
M11	8
M12	12

The velocity graphs of above-mentioned undamped and damped models at Nodes A and B are plotted together in Figures 216 and 217 respectively. These graphs show that the impulse and echo are the same for models with the widths of 6, 8 and 12 m (see Points I and E on Figures 216 and 217). The calculated heights based on the Δt at Nodes A and B are shown in Table 86. Considering the echoes at Point E, the calculated lengths are very close to the actual lengths from the pier bottom to Nodes A and B in the undamped models. The error is less than 2%. However, the errors are large for the damped models.

Since the deck ends of Pier 3 in the field were located farther than 6 m, no deck effect is expected on the signals obtained from Accelerometers 1 and 2. However the errors become greater especially in Node B.

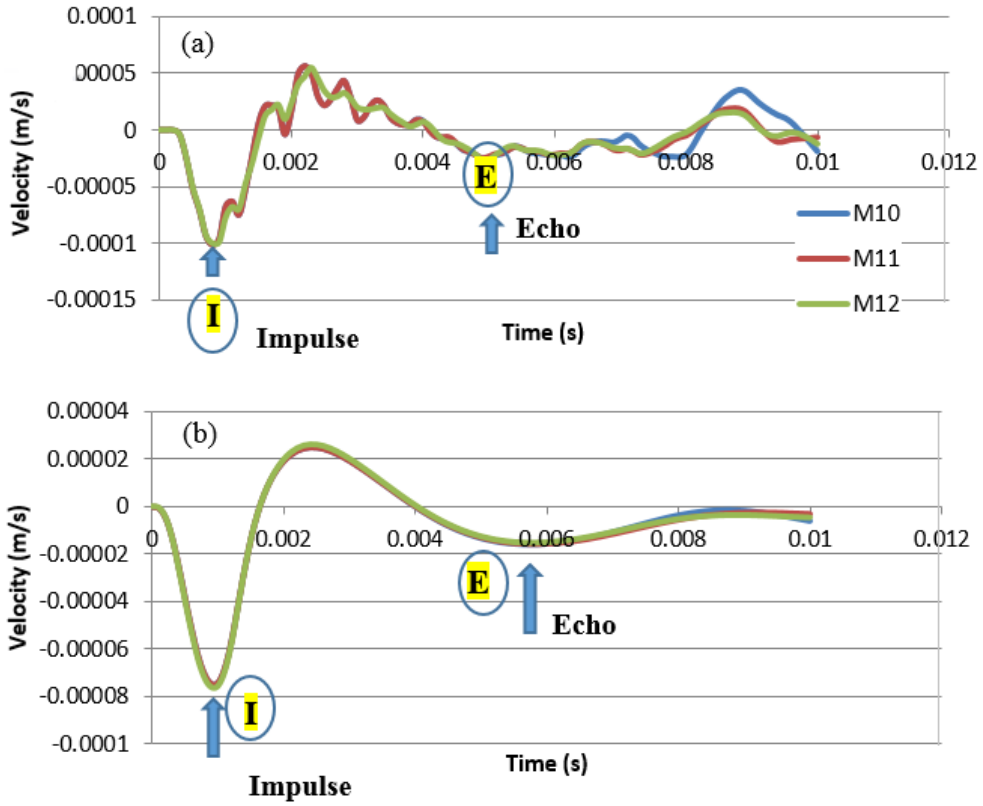

FIGURE 216 Velocity Graphs Obtained at Node A (Models M10 to M12) (a) Undamped Models (b) Damped Models

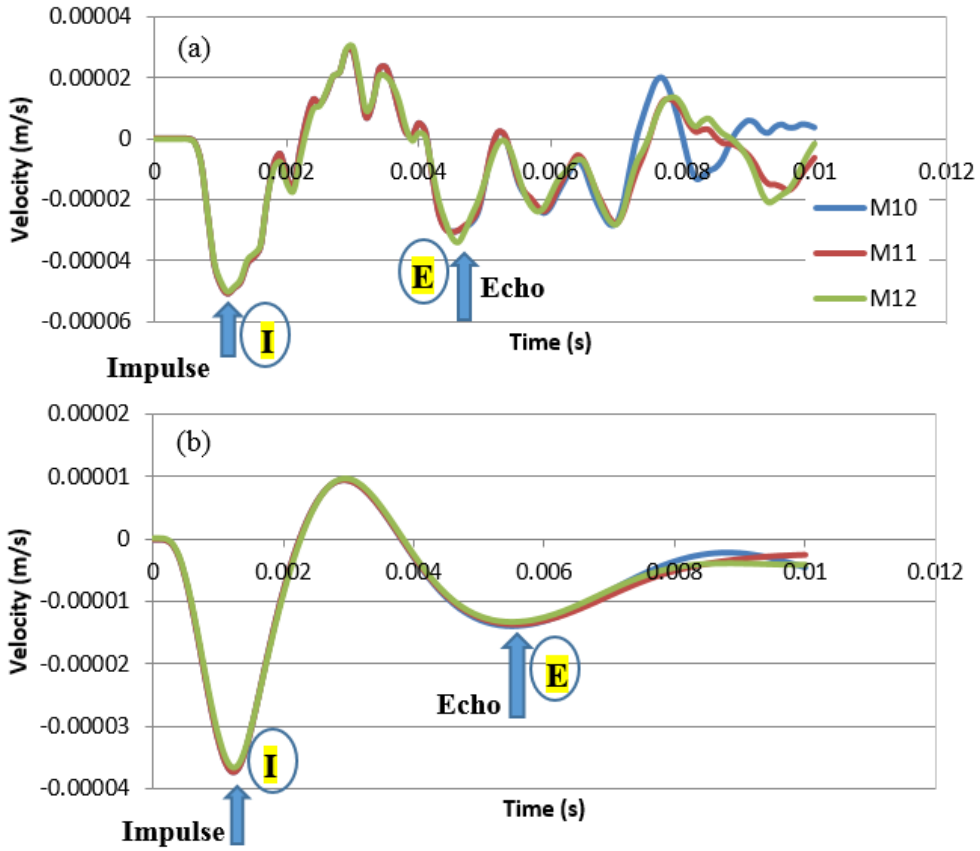

FIGURE 217 Velocity Graphs Obtained at Node B (Models M10 to M12) (a) Undamped Models (b) Damped Models

TABLE 86 Calculated Heights Corresponding to Nodes A and B in Models M10 to M12.

Node	Undamped				Damped			
	Δt (sec)	L_{tr} (m)	L_a (m)	Error %	Δt(sec)	L_{tr} (m)	L_a (m)	Error %
A	0.0041	6.69	6.80	-1.7	0.0047	7.66	6.80	12.7
B	0.0034	5.54	5.60	-1.0	0.0042	6.85	5.60	22.3

2.4.3.4 Effect of Upward Striking

Upward striking on the pile cap and bridge deck were simulated in the numerical model shown in Figure 215 (d = 7m). In Model M13 an upward strike on pier cap at Point C was applied, whereas the strike was applied at Point D in Model M14 (see Figure 133). The velocity graphs of undamped and damped models obtained at Nodes A and B in Models M13 and M14 are shown in Figures 218 and 219, respectively. Although impulses and echoes can be identified for both upward striking methods, the first echoes are less distinguishable at Node A for the undamped model. This may be due to the reflections from the deck and pier cap that contaminate the result since Node A is closer to the deck. The echo becomes more distinct with the presence of damping. The calculated heights of Nodes A and B are listed in Tables 87 and 88 respectively. Similar to the previous findings, errors are greater when the sensor is farther away from the top of the pier.

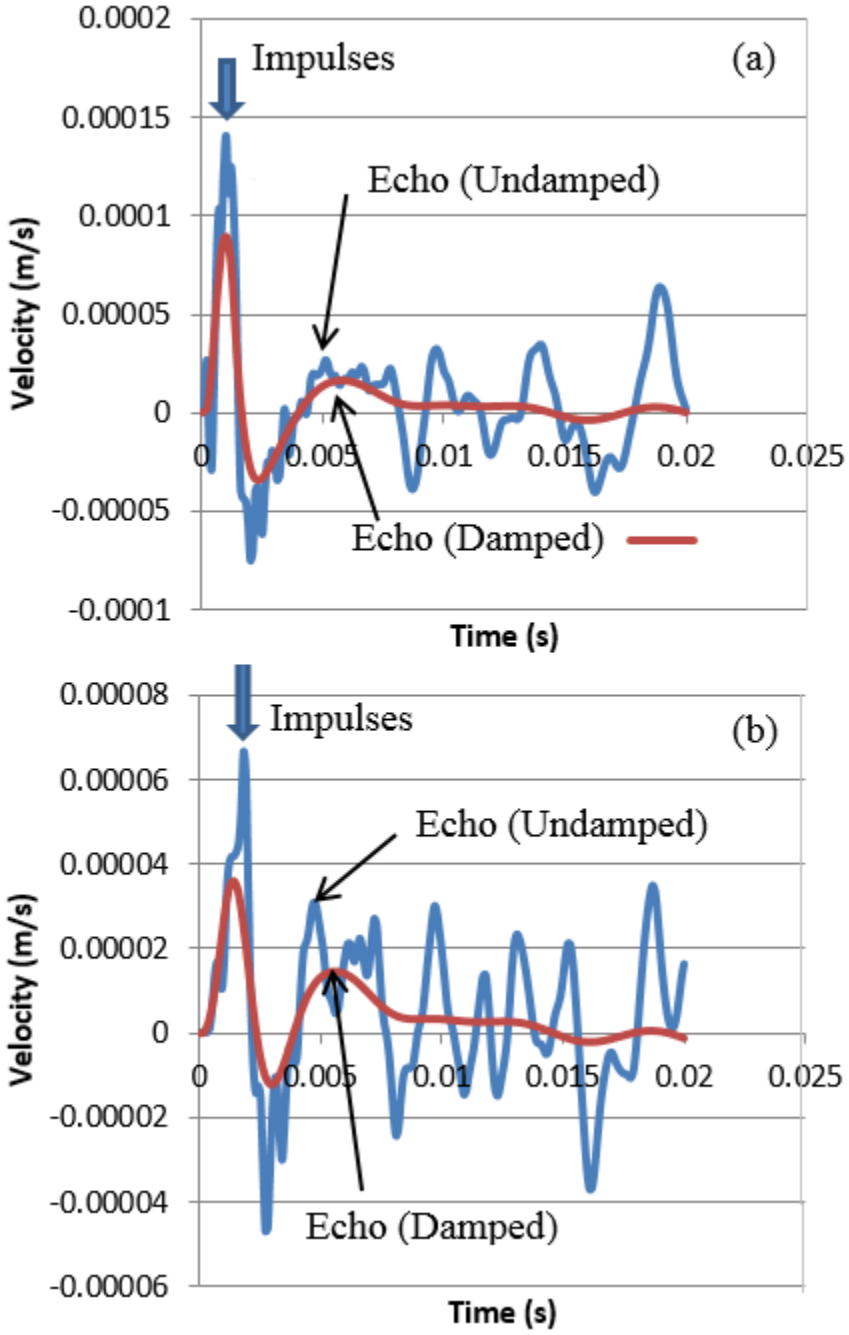

FIGURE 218 Velocity Graphs of Undamped and Damped Models Obtained at (a) Node A and (b) Node B from Upward Striking on the Pier Cap (M13)

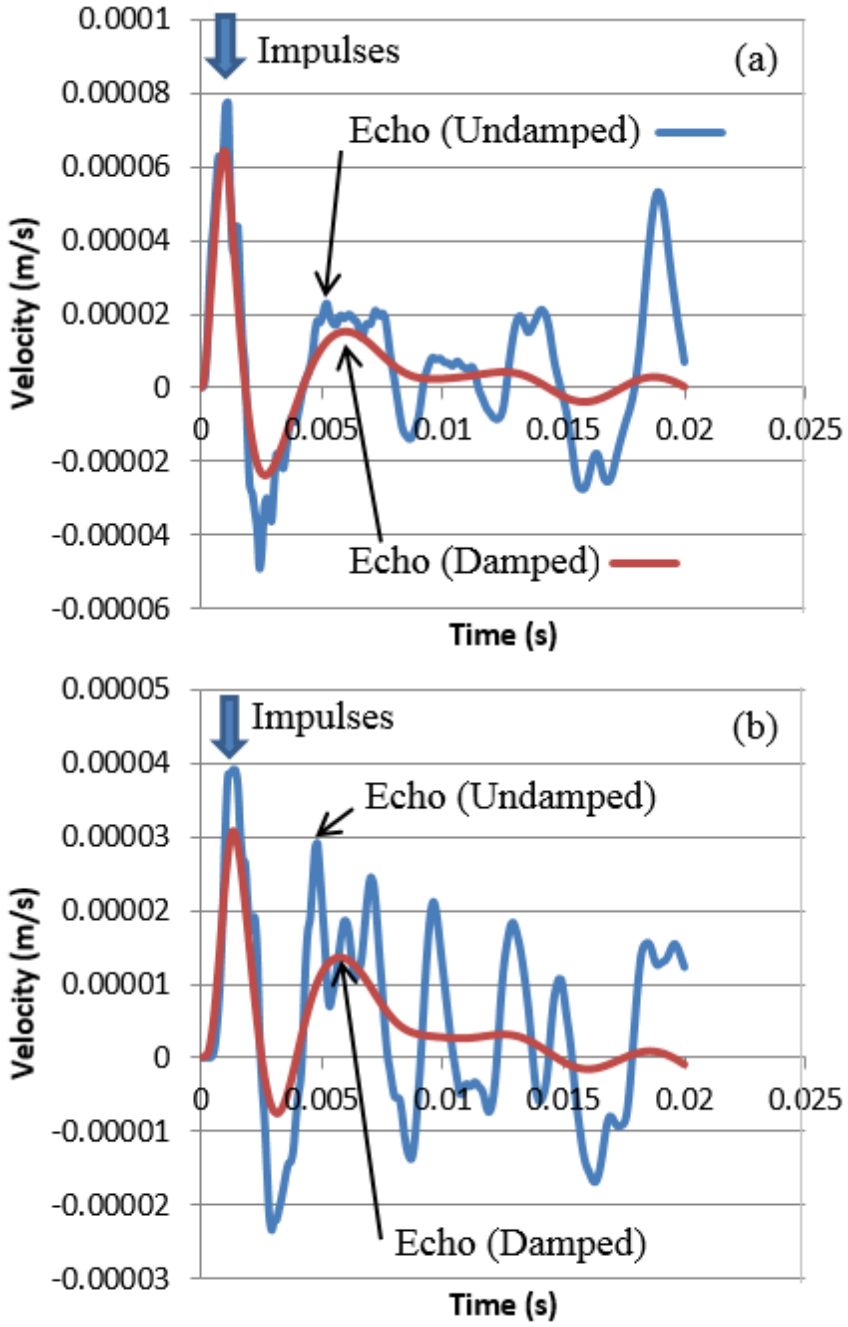

FIGURE 219 Velocity Graphs of Undamped and Damped Models Obtained at (a) Node A and (b) Node B from Upward Striking on the Pier Cap (M14)

TABLE 87 Calculated Heights for Upward Striking at Node A in Models M13 and M14.

Model	Node A							
	Undamped				Damped			
	Δt (sec)	L_{tr} (m)	L_a (m)	Error %	Δt (sec)	L_{tr} (m)	L_a (m)	Error %
M13	0.0041	6.69	6.80	-1.7	0.0046	7.50	6.80	10.3
M14	0.0042	6.85	6.80	0.7	0.0048	7.83	6.80	15.1

TABLE 88 Calculated Heights for Upward Striking at Node B in Models M13 and M14.

Model	Node B							
	Undamped				Damped			
	Δt (sec)	L_{tr} (m)	L_a (m)	Error %	Δt (sec)	L_{tr} (m)	L_a (m)	Error %
M13	0.0029	4.73	5.60	-15.6	0.004	6.52	5.60	16.5
M14	0.0035	5.71	5.60	1.9	0.0043	7.01	5.60	25.2

2.4.4 Complicated Foundations Comprising Pier Walls and Piles

Many bridges are supported by complicated foundations composed of a pier wall and piles or a buried pile cap and piles as shown in Figure 220. Since the piles are buried, the source and receiver of SE method can only be placed on the exposed pier wall or the superstructure. When the wave travels down the pier wall, two waves (a reflected and a transmitted wave) will be generated at the interface between the pier wall and pile due to the change of impedance. The transmitted wave travels down the pile and reflects back from the pile toe. That upward reflected wave will generate two waves at the interface again. The effect of the interface is similar to damping in terms of the reduction in the wave energy. Thus, it makes echo identification difficult unless the energy is large enough. It will be valuable to study numerically whether SE tests can be used to detect the pile length in such complicated foundations.

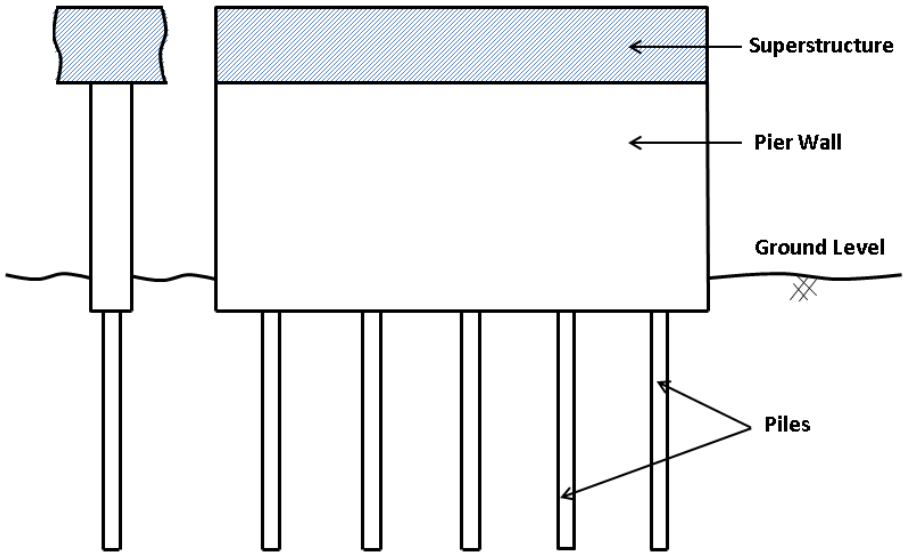

FIGURE 220 Bridge Foundation Comprising a Pier Wall and Multiple Piles

This type of study was not found in the literature. The applicability of the SE method on this type of foundation was investigated by finite element analysis. Figure 221 shows a FEM model of a pier wall (3.3 ft tall and 50 ft wide) supported by a pile of 20 ft.

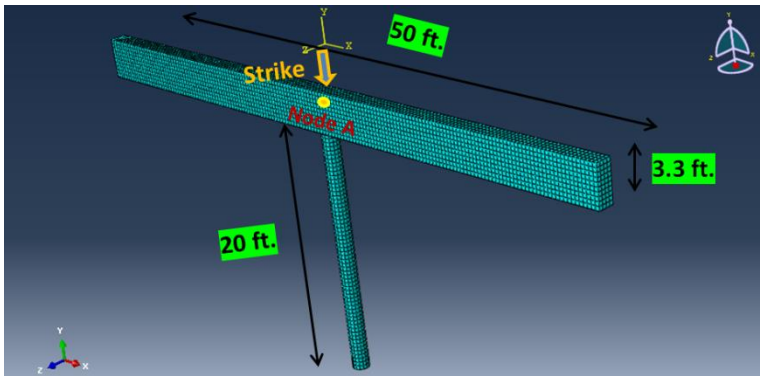

FIGURE 221 A FEM model of a Pier Wall Supported by a Pile

The impulse source was applied at the top of the pier wall and the receiver was placed at Node A in the pier wall. Figure 222 shows the velocity graph obtained at Node A. Upon applying the impulse, consecutive reflections from the pier bottom were recorded at Node A. The orange arrows indicate the reflections from the pier bottom. The blue arrow shows the reflection from the pile toe. The energy transmitted through the pile is great enough such that the echo from the pile toe can be detected in this configuration.

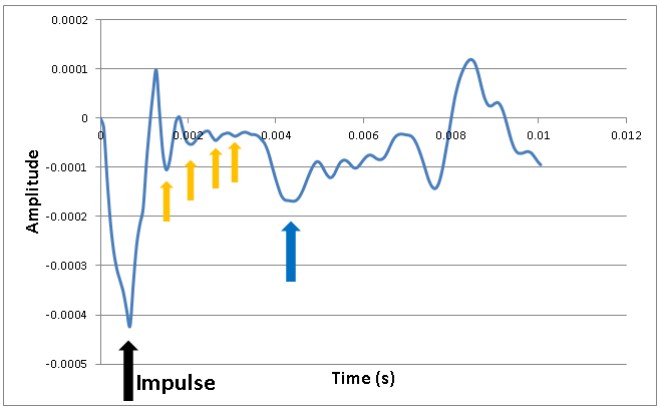

FIGURE 222 Velocity Time-amplitude Signal Recorded at Node A (Pier Height = 3.3 ft)

When the pier height is more than 4 ft, the pile toe reflection cannot be detected. An example of the velocity graph of a pier wall with a height of 10 ft is shown in Figure 223. The graph clearly shows the consecutive reflections from the pier bottom (orange arrows) but not the reflection from the pile toe. Our investigation revealed that if the height of the pier wall was less than 4 ft, the pile toe could be determined by the SE method. This observation is based on a FEM model in the absence of damping. In a real world situation, the damping of the surrounding soil will reduce the amplitude of the reflected wave significantly. Therefore, the SE method may be able to detect the pile length beneath a pier wall with a thickness less than 4 ft. This explains the unsuccessful SE tests reported by Olson (*2*) for the cases of shallow foundations with piles underneath.

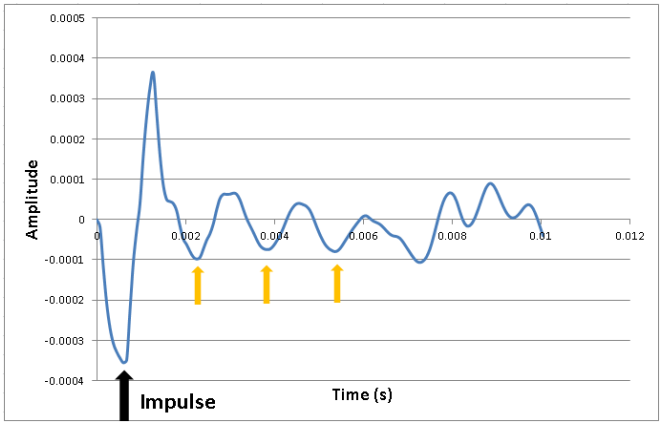

FIGURE 223 Velocity Time-amplitude Signal Recorded at Node A (Pier Height = 10 ft)

2.4.5 Conclusions of FEM Simulations

2.4.5.1 Wood Columns

1D wave propagation in piles was modeled as the first step of the numerical investigation. Impulses of different shapes were imparted, and acceleration and velocity were obtained at different nodes. The lengths of the piles were calculated based on the velocity-time histories. Foundation material (bedrock and soft soils) affects the polarity of the reflected waves from the pile toe.

The actual waveform detected from field tests depends on the intrinsic damping in the pile and the radial damping through the surrounding soils. The FEM results indicated that damping reduced the high-frequency content in the velocity-time history, and the amplitude decayed over time. This is consistent with the test results obtained in the field.

The FEM analysis indicated a more complex waveform when the accelerometer was mounted farther from the top of the pile. This is due to the interference of the reflected waves from both ends. This also explains why inconsistent results happened more often at the accelerometer placed far away from the top of the pile.

2.4.5.2 Concrete Pier Walls

A concrete pier wall similar to one of the pier walls of Bridge No. 5899 (see Table 4) was modeled by 3D-FEM. The effects of pier width, hammer tip type, the reflections from the deck, and upward striking on the received signals were examined. The effect of the material damping on the signals was also investigated. The summary of the findings is presented here.

Wave Propagation The results obtained from 3D simulations showed that the 1D equation was applicable in the determination of the buried length of a pier wall. The time differences between the impulse and echo did not fluctuate significantly with the change of the width of the pier wall.

Material Damping The FEM results showed that the presence of material damping made the interpretation easier due to the removal of high frequency contents near the expected echo in the velocity graph. When there was no damping, multiple peaks and valleys occurred in the vicinity of the expected echo point, which made determining the echo very difficult. However, damping

reduces the energy of the reflected wave, which may be detrimental in detecting the echo from the pile toe.

Hammer Tip Type Although good results were found for all hammer tips (rendering different impulse time durations in the simulations), accuracy decreased as contact time increased. Hard tip is recommended. This finding has also been confirmed from field observation.

Deck Reflections FEM analysis showed that the width of the deck may not affect the determination of height of the pier. Based on the FEM findings, there should not be any effect of deck reflections on the SE/IR test result since the widths of the decks of Bridge No. 5899 are wide enough.

Upward Striking on Pile Cap and Bridge Deck The calculated pier wall height obtained from upward striking was similar to the height obtained from downward striking. When the top of the deck is inaccessible, upward striking on pile cap is a good alternative source application.

Complicated Foundations Comprising Pier Walls and Piles The results of FEM analysis showed that, if the height of the pier wall was less than 4 ft, the pile toe could be determined by the SE method in the absence of damping. However, in real bridge foundations, the damping of the surrounding soil will reduce the amplitude of the reflected wave significantly. Therefore, the SE method may be able to detect the pile length of a pier wall with a thickness less than 4 ft. This explains the unsuccessful SE tests reported in the literature for the cases of shallow foundations supported by piles.

2.5 WAVEFORM INVERSION

The investigation reported herein implemented to clarify the waveform inversion method and its applicability to reveal some aspects of wave propagation in foundations. One of the Santo Domingo Bridge piles was simulated. The impulse created by the hammer is f(t). The impulse shape and duration was in accordance with the actual hammer impulse obtained from the field data. The resulting output at the sensor, s(t), can be obtained as the result of the convolution integral involving the input f(t) and the structure's impulse response g(t) as given in Eq. 5.

$$s(t) = \int_0^t f(\tau)g(t-\tau)\delta\tau \tag{5}$$

Figure 224 depicts the impulse response function g(t) at an accelerometer mounted closely at the end of a simulated pile while Figure 225 shows the impulse response function when the accelerometer was mounted at ¼ length from the pile top. The reflections from the pile are shown clearly in both figures, however, for the accelerometer mounted farther from the top, the impulse response contains more peaks that correspond to the wave arriving from the pile's top and bottom.

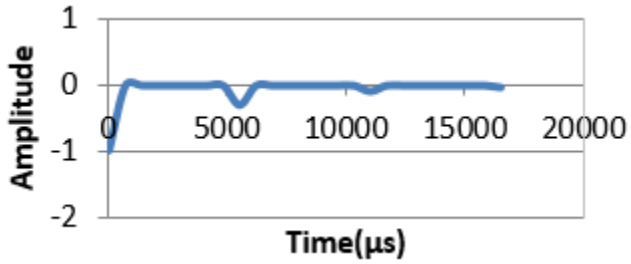

FIGURE 224 The Impulse Response Function at an Accelerometer Mounted Close to End of a Pile

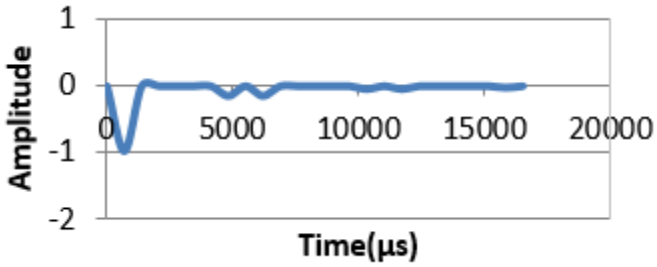

FIGURE 225 The Impulse Response Function at an Accelerometer Mounted at ¼ Length from the Top of a Pile

Velocity graphs (sensor data) were obtained by convolution of the hammer input f(t) and the impulse response function g(t). Figure 226 shows the results of two convolution integrals and a field test. Figure 226a is the result of the sensor located near the top of the pile which is comparable to the field result (Figure 226b) shown in Figure 58. For the sensor located ¼ length from the pile top, the convolution result of the input f(t) with the impulse response functions in Figure 225 is shown in Figure 226c. The time difference between the two dotted lines is less than that shown in Figure 226a. Reflection times are different due to the location of the sensor. Note that the individual reflections from the two ends evident in the impulse response (Figure 228) are depleted in the sensor result (Figure 226c) due to the long duration of the impulse (2.75 ms).

.

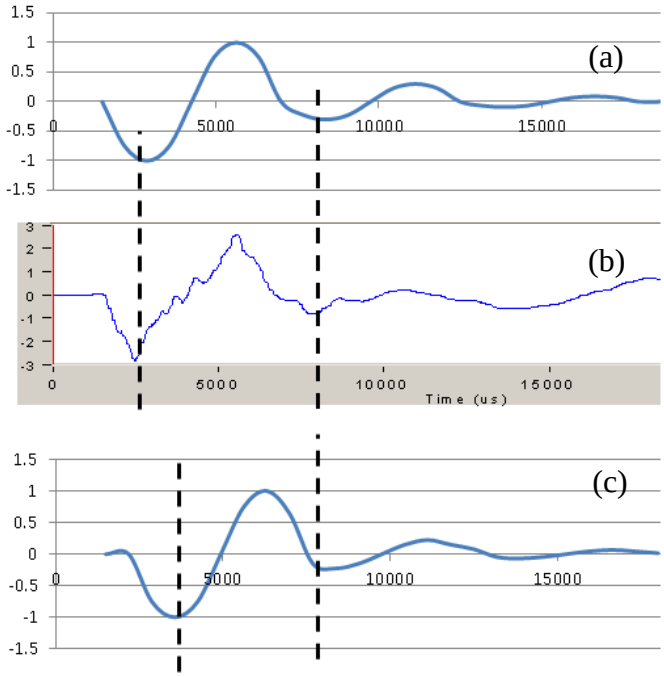

FIGURE 226 (a) Predicted Output from Convolution of Impulse Response at a Sensor Close to the Pile Top, (b) Field Test Data from a Sensor Mounted Close to Top of a Pile of Santo Domingo Bridge (c) Predicted Sensor Output from Convolution of Impulse Response at a Sensor ¼ Length away from the Pile Top

3. CONCLUSIONS

The SE/IR and PS methods have been investigated and utilized to determine the length of piles and the height of pier walls. Before performing the field tests, preliminary tests were conducted in a controlled environment to investigate various variables that affected the selected nondestructive tests. Field tests were performed with specific details to obtain the best possible results. The preliminary tests yielded valuable knowledge in the testing procedures for conducting SE/IR, PS, and IF tests. The results obtained from the FEM simulations were used to understand the 1D and 3D wave propagation in piles and pier walls. Valuable indications in both performing the nondestructive tests and interpreting the tests results were obtained from the FEM simulations and waveform inversion. The NDT methodology was then validated by performing SE/IR and PS tests on two bridges with as-built drawings.

The SE/IR results showed that the obtained signal was affected by various factors such as hammer tip type, striking method, pile and superstructure conditions and environmental conditions. Unfavorable reflections from discontinuities along the pile such as cracks, voids, variations in foundation material and layered soils could influence the SE/IR results. Different suggestions on the striking method, the source and sensor locations, and other pertinent factors were offered. These suggestions have been validated by the success and failure of SE/IR tests in the field on piles and pier walls. When the expected echo based on the time domain analysis is doubtful, IR analysis may be able to estimate the foundation depth. Although SE/IR tests led to successful tests on timber and concrete foundations, unsuccessful SE tests were found for steel H-piles. Therefore, the SE/IR method is recommended for the determination of the embedment of piles composed of concrete and wood but not steel.

PS tests were conducted successfully on the timber and steel piles. The results indicated that there was no effect on the characteristics of source (vertical, horizontal and even inclined striking on any appropriate parts of the structure). To pinpoint the first arrival time may be difficult due to ambient noise sometimes. The ambient noise level decreased with depth.

Although field IF tests could not be performed in this project due to the difficulty of drilling a borehole within 18 inches to the foundation, successful IF tests are expected if the distance between the steel pile and the borehole is less than 18 inches as demonstrated through the tests performed on the testbed.

The procedures manual developed in this project should assist NMDOT engineers to select NDT methods and for the best practice of solving problems related to unknown bridge foundations. Special care should be paid on the data interpretation of SE/IR and PS tests since the accuracy of the interpretation are affected by many factors.

THIS PAGE LEFT INTENTIONALLY BLANK

4. REFERENCES

1. Federal Highway Administration and Florida Department of Transportation (2010). "Unknown Foundation Bridges Pilot Study," NCHRP Web-only document107. http://www.fdot.gov/maintenance/STR/IN/Unknown_Foundations_Pilot_Study_02-26-10.pdf
2. Olson L. D. and Aouad, M. F. (2001). "Unknown Subsurface Bridge Foundation Testing," NCHRP 21-5(2) Final Report, TRB, Washington DC.
3. Parker, G., Toro-Escobar, C. M. and Voigt, R. L. (1998). Countermeasures to protect bridge piers from scour, SAFL Project Report 433, 1998, Vols. 1 (27 p) and 2 (360 p).
4. Olson, L.D., Jalinoos, F., and Aouad, M.F. (1996). "NCHRP Research Results Digest 213: Nondestructive Testing of Unknown Subsurface Bridge Foundations, Results of NCHRP Project E 21-5", Transportation Research Board, National Research Council, Washington, DC.
5. Stein, S. and Sedmera, K. (2006). "Risk-based management guidelines for scour at bridges with unknown foundation, NCHRP 24-25, Web-only Document-107. http://www.trb.org/Publications/Blurbs/157792.aspx.
6. Nichols, S. (2009) "Overview—Assessment of bridges with unknown foundations," FHWA Unknown Foundation Webinar 1, ⟨http://www.fhwa.dot.gov/unknown foundations⟩ (Jan. 13, 2010).
7. Rivers, B., and Nurmi, C. (2009). "Categorization, thresholds, and prioritization," Assessment of Bridges with Unknown Foundations, FHWA Unknown Foundation Webinar 2, ⟨http://www.fhwa.dot.gov/unknownfoundations⟩ (Jan. 13, 2010).
8. Rivers, B. (2009). "Positive discovery and inference." Assessment of Bridges with Unknown Foundations," FHWA Unknown Foundation Webinar 3, http://www.fhwa.dot.gov/ unknown foundations⟩ (Jan. 13,2010).
9. Nurmi, C. (2009). "Plans of action and management systems for bridges coded 'U'," Assessment of Bridges with Unknown Foundations, FHWA Unknown Foundation Webinar 4, ⟨http://www.fhwa.dot.gov/unknownfoundations⟩ (Jan. 13, 2010).
10. Washer, G. A. (1997). "Developments for the Nondestructive evaluation of highways bridges in the United States," Proc. Non-Destructive Testing in Civil Engineering, (NDT-CE '97) Liverpool, UK, Vol. 2, 543-552
11. Aouad, M. F. and Olson, L.D., (1996). "Nondestructive Evaluation of Bridge Foundations," in "Structural Materials Technology and NDT Conference", ed. Stolarski and Hartbower, San Diego, CA, Technomic Publishing, ISBN# 1-56676-424-6, 293-298.
12. Hertlein, B. and Davis, A. (2006). Nondestructive Testing of Deep Foundations, John Wiley & Sons, p.265. http://www.wiley.com/WileyCDA/WileyTitle/productCd-0470848502.html
13. Davis, A.G. (1995). "Nondestructive Evaluation of Existing Deep Foundations," ASCE Journal of the Performance of Constructed Facilities, 9, 57-74.
14. Nash, D. (2010). "Unknown Foundations Investigations: The Experiences of the LA DOTD," 35th Southwest Geotechnical Engineers Conference, Baton Rouge, LA.
15. Chakraborty, S. and Brown, D. A. (1997) "Evaluation of Unknown Pile Length under Existing Bridges in Alabama," IR-97-05, p. 122.
16. Robinson, B. and Webster, S. (2008). "Successful Testing for Unknown Bridge Foundations," Fifth Highway Geophysics – NDE Conference, 101-110.

17. NCDOT Geotechnical Engineering Unit. (2010). "Unknown Bridge Foundation Process," Internal flowchart developed for NCDOT's Unknown Foundation Program. North Carolina Department of Transportation, Raleigh, NC.
18. Gucunski, N., Imani, A., Romero, F., Nazarian, S., Yuan, D., Wiggenhauser, H., Shokouhi, P., Taffe, A., and Kutrubes, D. (2013). Nondestructive Testing to Identify Concrete Bridge Deck Deterioration, National Academies Press, p. 85.
19. Hossain, M., Khan, M., Hossain, J., Kibria, G., and Taufiq, T. (2013). "Evaluation of Unknown Foundation Depth Using Different NDT Methods," Journal of Performance of Constructed Facilities, 27(2), 209-214.
20. Terracon (2011). http://ds.terracon.com/2011/09/state-of-the-art-deep-foundation-testing/
21. Finno, R.J. and Gassman, S.L. (1998). "Impulse Response Evaluation of Drilled Shafts." Journal of Geotechnical and Geoenvironmental Engineering, 124(10), 965-975.
22. Yin, J., and Liu, M. (1999). "Assessment of Pile Integrity by Low-Strain Stress Wave Method", HKIE Transactions, 6:1, 42-49.
23. Kim, D.S. and Kim H.W., (2003). "Effects of Surrounding Soil Stiffness and Shaft Length in the Impact-Echo Test of Drilled Shaft." KSCE Journal of Civil Engineering, 7(6), 755-762.
24. Ni, S., Lehmann, L., Charng J., Lo, K. (2006). Low-Strain Integrity Testing of Drilled Piles with High Slenderness Ratio", Computers and geotechnics, 33, 283-293.
25. Ni, S.-H., Huang, Y.-H., Lo, K.-F., and Charng, J.-J. (2011). "Estimating the Flaw Size in Drilled Shafts Using an Impulse Response Method," KSCE Journal of Civil Engineering, 15(7):1197-1207.
26. Rausche, F., Shen, R.K., and Likins, G. (1991). "A Comparison of pulse echo and transient response pile integrity test methods," Transportation Research Board, Annual Meeting, January 1991, Washington, D.C.
27. Jozi, B., Dackermann, U., Braun R., Li, J., and Samali, B. (2014). "Application and Improvement of Conventional Stress -Wave- Based Non-Destructive Testing Methods for the Condition Assessment of In -Service Timber Utility Poles" 23rd Austrasian Conference on the Mechanics of Structures and Materials (ACMSM23), Byron Bay, Australia, December 9-12.
28. Ding, X.M., Liu, H.L., and Zhang, B. (2011). "High-frequency interference in low strain integrity testing of large-diameter pipe piles," Sci. China Sci. Tech. , 54(2), 420-430.
29. Huang, Y., Ni, S., Lo, K., Charng, J. (2010) "Assessment of Identifiable Defect Size in a Drilled Shaft Using Sonic Echo Method: Numerical Simulation", Computers and Geotechnics, 37, 757-768.
30. Yu, C., and Liao, S. (2006). "Theoretical Basis and Numerical Simulation of Impedance Log Test for Evaluating the Integrity of Columns And Piles", Can. Geotech. J., 43, 1238-1248.
31. Davis, A., and Dunn, C., (1974). "From the Theory to Field Experience with the Non-Destructive Vibrations Testing of Piles", Proc. Instn. Civ. Engrs, Part 2, 57, December, 571-593.
32. Lo, K.F., S.H., Ni, S.H., Huang, Y.H., and Zhou X.M. (2009). "Measurement of Unknown Bridge Foundation Depth by Parallel Seismic Method." Experimental Techniques 33(1), 23-27.
33. Turner, M.J. (1997). Integrity Testing in Piling Practice, Ciria Report 144. London.
34. Liao, S.-T., Tong, J.-H, Chen, C.-H. and Wu, T.-T. (2006). "Numerical simulation and experimental study of Parallel Seismic test for piles," International Journal of Solids and Structures 43(7), 2279–2298.

35. Sack, D., Slaughter, S., and Olson, L. (2004). “Combined Measurement of Unknown Foundation Depths and Soil Properties with Nondestructive Evaluation Methods”, DOI: http://dx.doi.org/10.3141/1868-08.
36. Olson, L. (2010). “Condition Assessment of Unknown Foundations”, 35th SW Geotechnical Engineers Conference, April 26-29, Baton Rouge, LA.
37. Lu, Z., Wang, Z., and Liu, D.J. (2013). “A study on the application of the parallel seismic method in pile testing,” Soil Dynamics and Earthquake Engineering 55(12), 255–262.
38. Standard Test Method for Low Strain Impact Integrity Testing of Deep Foundations (2013), https://www.astm.org/Standards/D5882.htm
39. Eshaghi, S., Dashti, H., Shahverdi, M., (2012). “Evaluation of Internal Cracks and Collapse in Poplar Wood (Populus nigra) during a Conventional Drying Process with Ultrasonic Inspection”, Not Sci. Biol., 4(2), 141-145.
40. http://www.engineeringtoolbox.com/sound-speed-solids-d_713.html
41. Spears, R.E. and Jensen, S.R. (2009). “Approach for Selection of Rayleigh Damping Parameters Used for Time History Analysis,” ASME Pressure Vessels and Piping Division Conference, July 26-30, Prague, Czech Republic.

THIS PAGE LEFT INTENTIONALLY BLANK

APPENDICES

APPENDIX A: DATABASE OF BRIDGES WITH UNKNOWN FOUNDATIONS IN NEW MEXICO

BRIDGE_ ID	FACILITY	MILEP OST	LOCATION	FEATINT	SERVTYP UND (NBI #42B)	SCOUR CRIT (NBI #113)	Foundation Material	Foundation Design	Foundation Depths (ft)	Method used to determine depths	Foundation Notes
							concrete, steel, timber, masonry, concrete filled pipe,	Spread footing, driven piles, drilled shafts, …	length from pile cap or pier cap, describe in foundation notes.	SE, IR, PS, IF, exploratory, ….	All and any relevant foundation information
166	49-033	0.1	0.15 MI E OF JCT NM-41	GALISTEO RIVER	5	U					
310	39-0334	0.0	0.01 MI E OF JCT US 64/84	UNNAMED WATERWAY	5	U					
312	NM-162	0.8	0.8 MI N OF JCT US-64	RITO DE TIERRA AMARILLA	5	U	Concrete	wing wall	10.2~10.8	SE	
397	NM-50	1.0	1.02 MI EAST JCT I-25	UNNAMED WATERWAY	5	U					
851	NM-434	0.2	0.1 MI N OF NM-518/MORA	MORA RIVER	5	U					
997	47-B28A	0.3	0.3 MI E OF I-25 FRNTG RD	TRES HERMANOS CREEK	5	U					
1043	37-C020	0.0	10.6 MI E OF US-66	UNNAMED WATERWAY	5	U					
1059	NM-21	5.1	5.1 MI SOUTH JCT US 64	URRACA CREEK	5	U					
1104	NM-456	2.8	12.3 MI E OF JCT NM-370	CIMARRON RIVER	5	U					
1191	NM-21	2.7	12.8 MI S OF JCT US-64	MORAS CREEK	5	U					
1192	NM-21	3.3	13.3 MI S OF JCT US-64	LA MAQUINA CREEK	5	U					
1550	FL-5663	0.7	0.1 MI N OF INDEPENDENCE	PAJARITO ARROYO	5	U					
1757	FR-4102	1.6	4.4 MI E OF GUADALUPE C/L	ARROYO DE LAS PALOMAS	5	U					
1758	FR-4102	2.4	5.3 MI E QUAY/QUADALUPE	UNNAMED WATERWAY	5	U					
1873	NM-35	5.1	5.1 MI N OF JCT NM-152	WILLOW SPRING CANYON	5	U	Timber	Driven piles			
1876	NM-35	8.5	8.6 MI N OF JCT NM-152	UNNAMED WATERWAY	5	U	Timber	Driven piles			
1916	15-524	0.0	1.4 MI W OF US62/CARLSBAD	SOUTHERN CANAL	5	U					
2368	NM-158	0.5	0.5 MI NE OF JCT NM-185	LEASBURG CANAL	5	U					
2371	FL-5724	0.0	0.6 M N OF US-380 ON LEA	NORTH SPRING RIVER	5	U					

BRIDGE_ID	FACILITY	MILEPOST	LOCATION	FEATINT	SERVTYPUND (NBI #42B)	SCOURCRIT (NBI #113)	Foundation Material	Foundation Design	Foundation Depths (ft)	Method used to determine depths	Foundation Notes
							concrete, steel, timber, masonry, concrete filled pipe,	Spread footing, driven piles, drilled shafts, …	length from pile cap or pier cap, describe in foundation notes.	SE, IR, PS, IF, exploratory, ….	All and any relevant foundation information
2388	NM-320	0.6	0.6 MI E OF JCT NM-185	IRRIGATION CANAL	5	U					
2391	FL-5818	0.0	50' N OF 7TH STREET	SPRING RIVER	5	U					
2861	FL-5724	0.0	0.7 M S JCT US-380/ROSWEL	HONDO RIVER	5	U					
3121	45-3000	4.0	4.10 WEST OF JCT US 550	UNNAMED WATERWAY	5	U	Steel	Driven piles			
3303	NM-304	15.9	9.2 MI N OF JCT US-60	SAN JUAN CANAL	5	U					
3372	IRR/NM-602	0.1	30.6 MI S OF I-40	RIO PESCADO	5	U					
3382	45-Z003	3.8	3.8 MI N OF JCT NM 516	BOHANAN ARROYO	5	U					
3961	NM-104	54.8	18.5 MI SE OF JCT NM-419	LITTLE CUERVO CREEK	5	U					
4063	49-Z001	0.0	DEFOURI & ALAMEDA ST/SF	SANTA FE RIVER	5	U					
4069	NM-344	13.3	13.3 MI N OF I-40	CANADA DE LAS NORRIAS	5	U	Timber	Driven piles	9.5~26.4	SE	
4075	FL-5784	0.3	DELGADO ST/ALAMEDA/ SF	SANTA FE RIVER	5	U					
4076	FL-4805	0.0	JCT ALAMEDA & DELGADO	ARROYO SAIZ	5	U					
4186	NM-400	10.2	0.3 MI S OF JCT I-40	RIO PUERCO	5	U					
4187	NM-400	7.3	3.2 MI S OF JCT I-40	UNNAMED WATERWAY	5	U					
4231	31-003A	0.3	0.2 MI N OF NM-118/GALLUP	RIO PUERCO	5	U					
4263	13-C052	0.0	5.3 M N OF US-70/FAIRACRE	RIO GRANDE	5	U					
4264	NM-154	1.7	1.7 MI E OF NM-185/HATCH	RIO GRANDE	5	U					
4283	NM-226	0.9	0.9 MI E OF JCT NM-28	RIO GRANDE	5	U					
4551	NM-189	0.9	0.9 MI E OF JCT NM-28	RIO GRANDE	5	U					

BRIDGE_ID	FACILITY	MILEPOST	LOCATION	FEATINT	SERVTYPUND (NBI #42B)	SCOURCRIT (NBI #113)	Foundation Material	Foundation Design	Foundation Depths (ft)	Method used to determine depths	Foundation Notes
							concrete, steel, timber, masonry, concrete filled pipe,	Spread footing, driven piles, drilled shafts, …	length from pile cap or pier cap, describe in foundation notes.	SE, IR, PS, IF, exploratory, ….	All and any relevant foundation information
4920	NM-456	24.3	24.3 MI NE OF JCT NM-325	CIMARRON RIVER	5	U					
4984	NM-97	7.6	7.6 MI NE OF NM-161/NM-97	MORA RIVER	5	U					
5074	NM-126	0.9	0.9 MI SE JCT US 550/CUBA	RITO LECHE	5	U					
5223	NM-119	3.9	3.9 MI W OF JCT US-84	UNNAMED WATERWAY	5	U					
5296	NM-186	0.7	0.7 MI E OF JCT NM-28	LA UNION MAIN CANAL	5	U					
5299	NM-419	7.2	7.1 MI NE OF NM-104	UNNAMED WATERWAY	5	U					
5472	NM-436	3.5	0.1 MI W OF JCT NM-187	GARFIELD CANAL	5	U					
5474	NM-58	4.8	4.8 MI E OF JCT US-64	IRRIGATION CANAL	5	U					
5489	FL-4266	0.0	0.3 Mi N US-285/Carlsbad	Pecos River	5	U					
5527	NM-503	14.3	0.29 MI S OF JCT NM-76	RIO QUEMADO	5	U	Steel pipe?	Driven piles			
5548	NM-337	10.1	19.3 M S JCT I-40/NM337	CHILILI CREEK	5	U					
5591	NM-24	33.9	15.7 Mi S Jct US82/Dunken	Unnamed Waterway	5	U					
5863	IRR/US-64	14.0	7.9 MI W OF JCT US-491	SHIPROCK WASH	5	U	Concrete				
5893	NM-126	15.5	15.4 MI E OF JCT US-550	RITO PENA NEGRAS	5	U	Concrete	wing wall	6.8~8.8	SE	
5898	NM-126	27.7	11.0 MI W OF JCT NM-4	RIO CEBOLLA	5	U					
5899	NM-576	0.1	0.15 MI W NM 111 @ 14.2	VALLECITOS RIVER	5	U	Concrete	Pier wall	10.6~15.4, 22~33	SE	
5912	NM-485	0.1	0.05 MI W OF JCT NM-4	JEMEZ CREEK	5	U					
5917	NM-165	9.7	9.7 M E Jct I-25/NM-165	LAS HUERTAS CREEK	5	U					
5966	NM-419	10.5	10.5 MI N OF NM-104	UNNAMED WATERWAY	5	U					

BRIDGE_ID	FACILITY	MILEPOST	LOCATION	FEATINT	SERVTYPUND (NBI #42B)	SCOURCRIT (NBI #113)	Foundation Material	Foundation Design	Foundation Depths (ft)	Method used to determine depths	Foundation Notes
							concrete, steel, timber, masonry, concrete filled pipe,	Spread footing, driven piles, drilled shafts, …	length from pile cap or pier cap, describe in foundation notes.	SE, IR, PS, IF, exploratory, ….	All and any relevant foundation information
5969	NM-204	4.1	4.1 MI W OF US-64	UNNAMED WATERWAY	5	U					
6052	NM-73	1.6	1.60 MI S OF JCT NM-75	RIO SANTA BARBARA	5	U					
6090	FL-5722	0.0	0.2 MI S OF US-380/ROSWEL	HONDO RIVER	5	U					
6091	FL-5722	0.0	0.6 MI N OF US-380/ROSWEL	NORTH SPRING RIVER	5	U					
6094	FL-4267 WBL	0.0	1.1 MI W JCT US285/MERMOD	SOUTHERN CANAL	5	U					
6095	FL-4268	0.0	1ST & CHURCH ST/CARLSBAD	SOUTHERN CANAL	5	U					
6199	NM-574	0.3	0.3 MI E OF JCT NM 170	LA PLATA RIVER	5	U					
6257	NM-419	17.5	17.5 MI N OF NM-104	UNNAMED WATERWAY	5	U					
6266	NM-456	17.9	27.7 M NE OF JCT US-64/87	UNNAMED WATERWAY	5	U					
6299	NM-370	44.1	3.9 MI S OF JCT NM-456	TRAVESSER CREEK	5	U					
6342	FL-5661	0.2	0.1 MI N OF VALENCIA ST	ARROYO HERMANOS	5	U					
6587	NM-456	14.2	23.5 MI NE JCT US-64/87	IRRIGATION CANAL	5	U					
6658	NM-592	0.4	0.4 MI E OF JCT SFCR 73	UNNAMED WATERWAY	5	U					
6659	NM-592	1.5	1.5 MI E OF JCT SFCR 73	UNNAMED WATERWAY	5	U	Timber	Driven piles	6.6~11.6	SE	
6682	C.R. 07-A007	0.0	0.5 MI E OF I-25/ MAXWELL	CANADIAN RIVER	5	U					
6922	NM-104	39.0	7.1 MI W OF JCT NM-419	UNNAMED WATERWAY	5	U	Timber	Driven piles	7.6~23.4; 20~22	SE	
6931	FL-4807	1.4	PASEO DEL PERALTA/ALAMEDA	SANTA FE RIVER	5	U					
6944	FL-4777	0.6	GUADALUPE ST/ALAMEDA/SF	SANTA FE RIVER	5	U					
6945	FL-4797	0.8	SANDOVAL & ALAMEDA	SANTA FE RIVER	5	U					

BRIDGE_ID	FACILITY	MILEPOST	LOCATION	FEATINT	SERVTYPUND (NBI #42B)	SCOURCRIT (NBI #113)	Foundation Material	Foundation Design	Foundation Depths (ft)	Method used to determine depths	Foundation Notes
							concrete, steel, timber, masonry, concrete filled pipe,	Spread footing, driven piles, drilled shafts, …	length from pile cap or pier cap, describe in foundation notes.	SE, IR, PS, IF, exploratory, ….	All and any relevant foundation information
7052	FL-4920	0.0	1.2 MI N 1st/Alamogordo	MCKINLEY DITCH	5	U					
7281	NM-434	19.2	19.3 MI N OF NM-518/MORA	COYOTE CREEK	5	U					
7282	NM-434	19.4	19.4 MI N OF NM-518/MORA	COYOTE CREEK	5	U					
7284	NM-434	20.5	20.5 MI N OF NM-518/MORA	COYOTE CREEK	5	U					
7346	NM-562	14.0	14.0 MI W OF JCT NM-402	GARCIA CREEK	5	U					
7478	NM-72	6.9	5.9 MI E OF I-25/RATON	UNNAMED WATERWAY	5	U					
7481	NM-304	1.8	4.7 Mi S of US-60/NM-304	Salas Arroyo	5	U	Timber	Driven piles	6.2~17.3	SE	
7521	FL-5787	0.1	NM 475 & SAN FRANCISCO ST	ARROYO DE LAS MASCARAS	5	U					
7524	NM-570	0.2	0.20 N OF JCT NM-68/PILAR	RITO CIENEQUILLA	5	U					
7536	NM-161	7.7	7.7 MI SE OF JCT NM-518	MORA RIVER	5	U	Concrete	Pier wall	13.5~14.5	SE	
7546	First Street	0.5	0.1 MI N OF SUGARITE ST	RATON CREEK	5	U					
7619	NM-503	11.3	3.7 MI N OF JCT NM-520	RIO DE MEDIO	5	U	Concrete	Pier wall	7.1~9.2	SE	
7628	NM-313	13.0	4.7 Mi N of Jct US-550	Las Huertas Creek	5	U	Timber	Driven piles	7.1~18.9	SE	
7629	17-B019	0.0	0.3 MI E OF JCT NM-61	UNNAMED WATERWAY	5	U					
7651	NM-370	2.3	2.4 MI N OF JCT US-64/87	RABBIT EAR CREEK	5	U					
7661	NM-283	13.7	13.7 MI W OF JCT I-25	TECOLOTE CREEK	5	U					
7673	37-QR-AR	0.0	1.8 MI S JCT NM-104	UNNAMED WATERWAY	5	U					
7681	37-QRAK	0.0	2.1 MI W OF JCT NM-278	IRRIGATION CANAL	5	U					
7715	13-Z018	0.0	0.3 M E JCT NM154/NM140	UNNAMED WATERWAY	5	U					

BRIDGE_ID	FACILITY	MILEPOST	LOCATION	FEATINT	SERVTYPUND (NBI #42B)	SCOURCRIT (NBI #113)	Foundation Material	Foundation Design	Foundation Depths (ft)	Method used to determine depths	Foundation Notes
							concrete, steel, timber, masonry, concrete filled pipe,	Spread footing, driven piles, drilled shafts, …	length from pile cap or pier cap, describe in foundation notes.	SE, IR, PS, IF, exploratory, ….	All and any relevant foundation information
7720	13-Z022	0.0	.5 MI W OF NM187@MP 9.85	GARFIELD CANAL	5	U					
7721	13-E393	0.0	.55 MI S OF NM140@MP 0.8	UNNAMED WATERWAY	5	U					
7733	07-A020	0.0	1.2 MI N OF JCT NM-555	UNNAMED WATERWAY	5	U					
7743	07-A011	0.0	6 MI S JCT I-25/US-64	CHICORICO CREEK	5	U					
7746	NM-161	1.9	1.9 MI E OF JCT NM-518	CEBOLLA CREEK	5	U					
7753	55-B005	0.0	1.0 MI W NM 522 @ MM 6.9	RIO HONDO	5	U					
7755	55-B002	0.0	0.3 MI W OF JCT NM-522	RIO HONDO	5	U					
7759	55-046	0.0	0.9 MI E OF NM 75 & NM 76	RIO SANTA BARBARA	5	U					
7760	55-Z023	0.0	0.30 MI E OF NM-76	RIO SANTA BARBARA	5	U					
7767	55-0306	0.0	0.40 MI S OF JCT NM-196	RIO COSTILLA	5	U					
7774	55-Z082	0.0	EAST OF NM-68/RNCHO TAOS	RIO GRANDE DE RANCHO	5	U					
7776	55-0172	0.0	0.5 MI W US-64 @ MP-253.4	RIO PUEBLO DE TAOS	5	U					
7781	55-0117	0.0	0.1 MI S NM-240/RANCHOS	RIO GRANDE DE RANCHO	5	U					
7784	05-0049	0.0	4.7 M N JCT NM-2 @ DEXTER	HAGERMAN CANAL	5	U					
7785	53-3058	0.0	3.5 M N JCT NM-2 @ DEXTER	HAGERMAN CANAL	5	U					
7787	05-1227	0.0	5.1 E/1.7 M S OF US70/285	HAGERMAN CANAL	5	U					
7793	(CRD-70	0.0	.9 S & .2 W OF NM2/DEXTER	HAGERMAN CANAL	5	U					
7794	05-0049	0.0	2.45 M N JCT NM-2/NM-339	HAGERMAN CANAL	5	U					
7795	05-1229	0.0	5 E US-70/285 2.5 S US380	HAGERMAN CANAL	5	U					

BRIDGE_ID	FACILITY	MILEPOST	LOCATION	FEATINT	SERVTYPUND (NBI #42B)	SCOURCRIT (NBI #113)	Foundation Material	Foundation Design	Foundation Depths (ft)	Method used to determine depths	Foundation Notes
							concrete, steel, timber, masonry, concrete filled pipe,	Spread footing, driven piles, drilled shafts, …	length from pile cap or pier cap, describe in foundation notes.	SE, IR, PS, IF, exploratory, ….	All and any relevant foundation information
7817	05-0184	0.0	3 M S & 2.7 M W US-70/285	RIO HONDO	5	U					
7823	05-Z009	0.0	2.3 S & .3 W OF NM2/D	HAGERMAN CANAL	5	U					
7825	05-023	0.0	0.2 M S OF US-82 @MP 44.7	RIO PENASCO	5	U					
7861	39-Z083	0.0	0.8 MI S NM 76 @ MP 11.4	RIO QUEMADO	5	U					
7874	13-0000	0.0	0.2 MILES ON FRANKLIN ST.	COLORADO DRAIN	5	U					
7883	49-072A	0.0	E OF NM 590 @ MM 4.10	BIG CREEK	5	U					
7894	31-Z001	0.0	1.2 MI W OF MCK CO RD-1	UNNAMED WATERWAY	5	U					
7897	05-0301	0.0	2 MI E OF NM-2/DEXTER	PECOS RIVER	5	U					
8003	17-6001	0.0	5.8 MI W US-180 @MP-131.3	SAN VICENTE ARROYO	5	U					
8012	FL-4750	0.5	JCT DELGADO/PALACE AVE	SAIZ ARROYO	5	U					
8021	27-B009	0.0	0.3 MI W OF US-70 @MP-274	RUIDOSO RIVER	5	U					
8039	59-B034	0.0	0.2 M S NM-456 @ MP 10.1	DRY CIMARRON RIVER	5	U					
8042	FL-4385	0.2	0.2 MI N MAIN ST/FARMINGT	GLADE ARROYO	5	U					
8052	43-Z001	0.0	2.1 MI N OF JCT US 550	UNNAMED WATERWAY	5	U					
8056	43-S007	0.0	2.0 Mi N of Ojo Encino Rd	PENISTAJA ARROYO	5	U					
8062	43-Z001	0.0	0.5 M S MISSION RD/TORREO	CANON MEDIO	5	U					
8063	43-Z001	0.0	0.1 MI S OF JCT NM-197	VICENTE ARROYO	5	U					
8071	43-OS39	0.0	0.1 MI E NM-4 @ MP-20.2	JEMEZ CREEK	5	U					
8081	31-0004	0.0	North of NM-118 @MP6.8	UNNAMED WATERWAY	5	U					

BRIDGE_ID	FACILITY	MILEPOST	LOCATION	FEATINT	SERVTYPUND (NBI #42B)	SCOURCRIT (NBI #113)	Foundation Material	Foundation Design	Foundation Depths (ft)	Method used to determine depths	Foundation Notes
							concrete, steel, timber, masonry, concrete filled pipe,	Spread footing, driven piles, drilled shafts, …	length from pile cap or pier cap, describe in foundation notes.	SE, IR, PS, IF, exploratory, ….	All and any relevant foundation information
8087	31-Z001	0.4	0.4 MI N OF NM-53/RAMAH	CEBOLLA CREEK	5	U					
8092	31-MC13	0.0	0.4 MI E US-491 @ MP-9.7	UNNAMED WATERWAY	5	U					
8097	31-MC43	0.0	0.99 MI W OF NM566 MP 3.1	UNNAMED WATERWAY	5	U					
8111	45-3500	0.3	0.3 MI S NM 516	FLORA VISTA ARROYO	5	U					
8113	45-6675	0.0	1.2 MI S US-64 @ MP-39.8	SAN JUAN RIVER	5	U					
8115	45-4599	0.2	0.23 M N US64 & SJCR4599	IRRIGATION DITCH	5	U					
8118	45-4450	4.0	4.0 Mi S of US-64 @ MP-75	LARGO CANYON	5	U					
8127	45Z013	0.0	1.8 MI NE of NM @ MP 5.9	IRRIGATION DITCH	5	U					
8130	45-5500	0.0	0.80 MI S OF JCT US 64	SAN JUAN RIVER	5	U					
8153	03-A011	2.5	2.6 M E Arizona St line	LARGO DRAIN	5	U					
8193	FL-5277	0.0	1.1 MI WEST JCT US-285	SOUTHERN CANAL	5	U					
8213	47-B43B	0.0	1.8 MI N OF I-25 FRTG RD	PECOS RIVER	5	U					
8216	47-B41D	0.0	0.3 MI S OF I-25 FRNTG RD	SAN JOSE ARROYO	5	U					
8222	47-004	0.0	0.1 MI W OF NM-94 @MP-3.9	UNNAMED WATERWAY	5	U					
8224	47-0C23	0.9	1.8 MI N OF I-25 FRNTG RD	PECOS ARROYO	5	U					
8225	47-A19A	0.0	2.2 MI W OF JCT NM-283	TECOLOTE CREEK	5	U					
8247	45-Z003	0.5	10.5 N of Jct NM516/CR290	COX CANYON	5	U					
8256	FL-5270	0.0	1.1M W JCT 285-MERMOD ST.	SOUTHERN CANAL	5	U					
8295	33-C013	0.0	.73 MI NE OF JCT NM-161	MORA RIVER	5	U					

BRIDGE_ID	FACILITY	MILEPOST	LOCATION	FEATINT	SERVTYPUND (NBI #42B)	SCOURCRIT (NBI #113)	Foundation Material	Foundation Design	Foundation Depths (ft)	Method used to determine depths	Foundation Notes
							concrete, steel, timber, masonry, concrete filled pipe,	Spread footing, driven piles, drilled shafts, …	length from pile cap or pier cap, describe in foundation notes.	SE, IR, PS, IF, exploratory, ….	All and any relevant foundation information
8297	19-040U	0.0	9.7 M N JCT I40 @ MP 267	ARROYO DE LAS CANOVAS	5	U					
8299	33-Z000	0.0	.5 MI N OF NM-121@ MP 0.2	MORA RIVER	5	U					
8300	33-B028	4.1	4.1 M SW NM-518/CLEVELAND	RIO DE CASA	5	U					
8358	FL-4750	0.8	JCT PALACE & ALAMEDA	SANTA FE RIVER	5	U					
8359	FL-4805	3.1	JCT ALAMEDA/CAMINO CABRA	SANTA FE RIVER	5	U					
8369	39-0070	0.0	2.40 MI S NM-580 & NM	RIO DE PENASCO	5	U					
8370	39-0065	0.0	0.25 MI N JCT NM75/DIXON	RIO DE PENASCO	5	U					
8372	47-A04A	0.0	.67 MI W JCT NM-94 @ 3.9	CANADA DEL ROCIO	5	U					
8380	55-057	0.0	0.23 MI South JCT NM-75	RIO LUCIO	5	U					
8382	Ave	1.5	0.12 MI N. OF JCT NM-329	LA MANTECA ARROYO	5	U					
8387	49-Z006	0.0	0.7 M S OF NM 76 & CR 94	SANTA CRUZ RIVER	5	U					
8388	FL-5765	2.1	CERRO GORDO & UPPER CANYO	SANTA FE RIVER	5	U					
8412	15-0658	0.0	.6 S & 1.6 W JCT 62-2	HACKBERRY DRAW	5	U					
8419	35-D012	0.0	AT JCT NM-521 @ WEED	AGUA CHIQUITA	5	U					
8420	05-1175	0.0	5.0 MI E OF JCT NM-256	HAGERMAN CANAL	5	U					
8434	27-E008	0.0	3.82 MI E OF US70 @MP-278	RUIDOSO RIVER	5	U					
8435	27-E010	0.0	4.51 M W US-70/380	RIO RUIDOSO	5	U					
8444	15-0704	0.0	.5 miles South on Tidwell	SOUTHERN CANAL	5	U					
8445	47-C53B	0.0	15.7 MI NE OF NM-104	UNNAMED WATERWAY	5	U					

BRIDGE_ID	FACILITY	MILEPOST	LOCATION	FEATINT	SERVTYPUND (NBI #42B)	SCOURCRIT (NBI #113)	Foundation Material	Foundation Design	Foundation Depths (ft)	Method used to determine depths	Foundation Notes
							concrete, steel, timber, masonry, concrete filled pipe,	Spread footing, driven piles, drilled shafts, …	length from pile cap or pier cap, describe in foundation notes.	SE, IR, PS, IF, exploratory, ….	All and any relevant foundation information
8501	17-C071	0.0	0.35 MI E US-180 @ MP79.0	DUCK CREEK	5	U					
8511	31-001	0.0	2.78 MI N OF JCT NM-118	DEFIANCE DRAW	5	U					
8514	QR-AH	0.0	1.7 MI S OF US-54@ MM311.	IRRIGATION CANAL	5	U					
8515	37-QR63	0.0	0.5 MI W OF JCT CR-A021	BLUE HOLE CREEK	5	U					
8516	15-0701	0.0	0.3 M S OF US285 @MP 30.1	SOUTHERN CANAL	5	U					
8517	33-B028	0.0	3.4 M SW NM-518/CLEVELAND	RIO LA CASA	5	U					
8518	33-B028	3.3	3.3 M SW NM-518/CLEVELAND	RIO LA CASA	5	U					
8519	33-B028	1.7	2.8 M SW NM-518/CLEVELAND	RIO LA CASA	5	U					
8520	47-Z024	0.0	0.15 M SE OF I-25 FRTG RD	UNNAMED WATERWAY	5	U					
8521	19-002Q	0.0	1.5 MI W US-84 @ MP-27.8	UNNAMED WATERWAY	5	U					
8522	33-A040	0.0	0.9 M W JCT NM434 @MP14.3	UNNAMED WATERWAY	5	U					
8523	07-A007	0.0	16.1 MI E OF I-25/MAXWELL	UNNAMED WATERWAY	5	U					
8524	07-A007	0.0	13.2 MI E OF I-25/MAXWELL	UNNAMED WATERWAY	5	U					
8525	07-A007	0.0	10.9 MI E OF I-25/MAXWELL	UNNAMED WATERWAY	5	U					
8526	07-A007	0.0	15.1 MI E OF I-25/MAXWELL	UNNAMED WATERWAY	5	U					
8527	33-Z000	0.0	0.06 MI E OF JCT NM-518	MORA RIVER	5	U					
8529	31-Z019	0.0	17.92 M W NM-197 @TORREON	NORTH FORK/CHICO ARROYO	5	U					
8531	33-060C	0.0	0.50 MI N OF JCT NM-518	MORA RIVER	5	U					
8532	55-0206	0.0	0.3 MI S OF NM-522/QUESTA	RED RIVER	5	U					

BRIDGE_ID	FACILITY	MILEPOST	LOCATION	FEATINT	SERVTYPUND (NBI #42B)	SCOURCRIT (NBI #113)	Foundation Material	Foundation Design	Foundation Depths (ft)	Method used to determine depths	Foundation Notes
							concrete, steel, timber, masonry, concrete filled pipe,	Spread footing, driven piles, drilled shafts, …	length from pile cap or pier cap, describe in foundation notes.	SE, IR, PS, IF, exploratory, ….	All and any relevant foundation information
8551	15-0706	0.0	2.9 MI S OF US-285@ OTIS	SOUTHERN CANAL	5	U					
8556	39-0379	0.0	26.4 MI S OF US 64/BLANCO	LARGO CANYON	5	U					
8560	19-Z003	0.0	9.5 MI S OF I-40/MILAGRO	ARROYO PINTADA	5	U					
8566	43-Z001	0.0	0.1 MI NW OF JCT NM-4	JEMEZ RIVER	5	U					
8567	43-Z001	0.0	20.7 MI. S.of US 550	CHICO ARROYO	5	U					
8578	47-B43B	0.0	5.2 MI N OF I-25 FRNTG RD	COW CREEK	5	U					
8584	05-Z014	0.0	1.5 S OF US-82 AT MP 77.2	PENASCO RIVER	5	U					
8588	FL-4166	0.0	0.6 MI S OF US-82/ARTESIA	EAGLE DRAW	5	U					
8590	47-A11E	0.0	3.9 MI N OF MILLS/8TH ST	STORRIE LAKE CANAL	5	U					
8591	19-03BA	0.0	0.48 MI NW OF JCT NM-91	UNNAMED WATERWAY	5	U					
8599	39-0194	3.0	3.0 MI S OF NM 96	CANONES CREEK	5	U					
8608	43-Z009	0.0	0.1 MI N NM-197 IN CUBA	RITO LECHE	5	U					
8609	55-Z015	0.0	0.5 MI S OF NM-38 @MP-0.6	RED RIVER	5	U					
8613	55-A083	0.0	0.05 MI S OF JCT US-64	RIO FERNANDO DE TAOS	5	U					
8614	55-042	0.2	0.20 MI S OF JCT NM-73	SANTA BARBARA RIVER	5	U					
8615	55-045	0.1	0.1 MI S OF JCT NM-75	SANTA BARBARA RIVER	5	U					
8616	55-0073	71.1	0.4 MI S OF NM-518/TALPA	RIO GRANDE DE RANCHOS	5	U					
8631	11-C001	0.0	1.32 MI E OF S END NM-272	TAIBAN CREEK	5	U					
8649	17-Z000	0.0	3.2 MI NE NM90/BRKN-ARROW	SAN VICENTE ARROYO	5	U					

BRIDGE_ID	FACILITY	MILEPOST	LOCATION	FEATINT	SERVTYPUND (NBI #42B)	SCOURCRIT (NBI #113)	Foundation Material	Foundation Design	Foundation Depths (ft)	Method used to determine depths	Foundation Notes
							concrete, steel, timber, masonry, concrete filled pipe,	Spread footing, driven piles, drilled shafts, …	length from pile cap or pier cap, describe in foundation notes.	SE, IR, PS, IF, exploratory, ….	All and any relevant foundation information
8651	49-088D	4.3	0.5 Miles South of NM-76	SANTA CRUZ RIVER	5	U					
8656	55-0108	0.1	0.7 MI N JCT NM-68/NM-570	RIO GRANDE RIVER	5	U					
8658	NM-516	1.5	2.15 MI N JCT US64/NM-516	NORTH FARMINGTON DITCH	5	U					
8672	55-0114	0.0	0.05 MI WEST JCT NM-240	RIO GRANDE DE RANCHOS	5	U					
8676	17-3069	0.0	0.1 M E NM35/LAKE ROBERT	SAPILLO CREEK	5	U					
8677	17-Z011	1.7	21.7 M N JCT US-70/NM-464	GILA RIVER	5	U					
8679	49-0088	0.0	0.05 MI S OF JCT NM 76	SANTA CRUZ RIVER	5	U					
8681	39-Z443	0.0	U.S.285/Colo CR C	LOS PINOS RIVER	5	U					
8682	05-1166	0.0	2.6 M E LIN CL/2 M S US70	HONDO RIVER	5	U					
8690	33-B017	0.0	0.1 MI N NM-518 @CLEVELND	MORA RIVER	5	U					
8751	FL-4189	0.2	MCCOY AVENUE IN AZTEC	HAMPTON ARROYO	5	U					
8760	35-A059	0.0	0.5 M N JCT NM-545/LA LUZ	LA LUZ CANYON	5	U					
8762	35-E038	0.0	4.83 MI SW OF NM-24/PINON	BONITA DRAW	5	U					
8764	39-Z012	7.6	13.75 MI N OF JCT NM68/76	RIO GRANDE	5	U					
8772	17-3068	0.0	0.06 MI S OF JCT NM-35	GRIGGS CANYON	5	U					
8779	27-E003	0.0	0.2 MI E OF US-70 @MP-273	RUIDOSO RIVER	5	U					
8783	31-0004	0.0	5.7 MI N OF JCT NM-118	UNNAMED WATERWAY	5	U					
8785	31-0030	0.0	1.2 M SE AZTEC/BASILIO DR	PERETTI CANYON	5	U					
8786	31-0030	0.0	1.6 M SE AZTEC/BASILIO DR	PERETTI CANYON	5	U					

BRIDGE_ID	FACILITY	MILEPOST	LOCATION	FEATINT	SERVTYPUND (NBI #42B)	SCOURCRIT (NBI #113)	Foundation Material	Foundation Design	Foundation Depths (ft)	Method used to determine depths	Foundation Notes
							concrete, steel, timber, masonry, concrete filled pipe,	Spread footing, driven piles, drilled shafts, …	length from pile cap or pier cap, describe in foundation notes.	SE, IR, PS, IF, exploratory, ….	All and any relevant foundation information
8787	FL-5562	0.3	0.2 MI W OF LOOP-15/VEGAS	GALLINAS RIVER	5	U					
8788	27-B018	0.0	0.25 MI S US-70 @MP-284.3	RUIDOSO RIVER	5	U					
8791	33-7000	0.0	0.1 MI E OF NM-434/MP17.6	COYOTE CREEK	5	U					
8803	45-7900	0.0	8.6 MI S OF JCT US 550	ESCAVADA WASH	5	U					
8815	27-B022	0.0	250' W US-380 @ MP-150.1	BONITO CREEK	5	U					
8862	31-0027	0.0	2.7 MI NE OF NM 118	UNNAMED WATERWAY	5	U					
8863	31-Z001	0.0	0.4 MI E NM-566 @ MP-0.35	UNNAMED WATERWAY	5	U					
8864	31-0010	7.9	7.9 MI E NM-602 @ MP-18.3	BREAD SPRINGS WASH	5	U					
8865	31-0027	0.0	4.2 MI N OF I-40, MM 44.7	UNNAMED WATERWAY	5	U					
8866	31-0003	0.0	3.0 MI W US-491 @ MP-15.4	DEER SPRINGS WASH	5	U					
8867	31-Z001	0.0	2.8 MI W US-491 @ MP-17.9	MEXICAN SPR WASH	5	U					
8869	31-Z055	0.0	1.49 MI E US-491 @ MP-9.7	DYE BRUSH WASH	5	U					
8870	31-0009	0.0	2.3 MI W US-491 @ MP-5.35	DEATH WASH	5	U					
8872	31-Z017	0.0	1.1 mi. No. of W. Maloney	UNNAMED WATERWAY	5	U					
8877	IRR/CR-10	0.0	1.3 MI E NM-602 @ MP-22.9	BREAD SPRINGS WASH	5	U					
8895	FL-5785	0.2	JCT VIANSON/SIRINGO ROAD	SIRINGO DRAINAGE	5	U					
8905	31-0049	2.7	0.9 MI N OF N 11-49	RIO PUERCO	5	U					
8912	31-MC37	0.0	E OF US-491 @ MP-15.2	FIGUREDO WASH	5	U					
8918	33-A027	0.0	0.1 MI NW OF NM-518	MORA RIVER	5	U					

BRIDGE_ ID	FACILITY	MILEP OST	LOCATION	FEATINT	SERVTYP UND (NBI #42B)	SCOUR CRIT (NBI #113)	Foundation Material	Foundation Design	Foundation Depths (ft)	Method used to determine depths	Foundation Notes
							concrete, steel, timber, masonry, concrete filled pipe,	Spread footing, driven piles, drilled shafts, …	length from pile cap or pier cap, describe in foundation notes.	SE, IR, PS, IF, exploratory, ….	All and any relevant foundation information
8971	07-Z000	0.0	0.5 MI S OF NM-72	RATON CREEK	5	U					
8982	31-Z034	0.0	3.6 MI W NM-602 @ MP-18.6	UNNAMED WATERWAY	5	U					
8983	31-0077	0.0	5.6 MI W OF NM-566 MP-5.6	UNNAMED WATERWAY	5	U					
9005	43-0124	0.0	0.05 W OF NM-126 @ MP-38	RIO SAN ANTONIO	5	U					
9012	39-0194	0.9	0.9 MI E OF NM-96	CANONES CREEK	5	U					
9024	31-0032	0.0	.96 M S NM118/PORT ENTRY	SALT WATER WASH	5	U					
9048	FL-5732	1.2	0.1 MI E OF CAMINO CABRA	ARROYO MORAS	5	U					
9077	FL-5701	0.0	JCT MISSOURI & 9TH ST	SPRING RIVER	5	U					
9088	FL-4710	0.0	800' S OF COLLEGE BLVD	SPRING RIVER	5	U					
9122	FL-5815	0.0	100'N JCT RICHARDSON&10TH	SPRING RIVER	5	U					
9129	FL-5710	0.0	150' W JCT US-285 & ALB.	HONDO RIVER	5	U					
9133	31-0002	0.0	1.37 M W. NM602 @ MM25.56	BREAD SPRINGS WASH	5	U					
9202	FL-5815	0.0	300' N S. RICHARSON/BLAND	RIO HONDO	5	U					
9405	FL-4804	0.3	W ALAMEDA & CAMINO ALIRE	SANTA FE RIVER	5	U					
9499	39-0353	0.0	0.05 M S JCT US-64/CR-356	AMARGO CREEK	5	U					
9547	15-0741	0.0	4.75 Mi E Jct US 285	Pecos River	5	U					
9583	Escondido	0.0	.3 mi NE US 64 in Chama	CHAMITA RIVER	5	U					
10023	31-0049	0.0	8.3 MI N OF NM-566	RIO PUERCO OF THE WEST	5	U					
10028	31-050	0.0	6.6 Mi E NM 400/Co Rd 50	UNNAMED WATERWAY	5	U					

APPENDIX B QUESTIONNAIRE TO STATE DEPARTMENTS OF TRANSPORTATION

1. Does your agency currently use a nondestructive testing (NDT) method to estimate the depth and/or other characteristics of bridge foundations with unknown foundations?

2. If yes, which method(s) is/are used in your state (i.e. sonic echo/impulse response, parallel seismic, induction field, etc.) for this purpose? If your state DOT uses more than one method for different types of bridge materials, geometry or other factors, please provide a copy of the testing manual or other documentation that describes which method is used under which conditions. Please provide current specifications and practices regarding NDT testing reliability, information storage, maintenance cost, data processing, and interpretation, if possible.

3. Has your state tried other NDT methods to identify the depth or condition of unknown bridge foundations and opted against using them? Which methods? Why did your state decide against using them?

4. Which unit in your agency is responsible for NDT testing of bridges with unknown foundations? Is the testing performed by agency staff or by contractors? If by agency staff, what is the technical background of in-house personnel responsible for performing the testing? If by contractors, what is the average cost per structure when performed by contractors?

5. How many bridges in your state have been identified as having unknown foundations?

New Mexico Department of Transportation
RESEARCH BUREAU
7500B Pan American Freeway NE
PO Box 94690
Albuquerque, NM 87199-4690
Tel: (505) 798-6730